Universiteit Antwerpen

Faculty of Pharmaceutical, Biomedical and Veterinary Sciences

Multimodal approach to unravel network disturbances and compensatory mechanisms during pre- and early-plaque stages of Alzheimer's Disease

Dissertation to obtain the degree of Doctor in Biomedical Sciences at the University of Antwerp, to be defended by

Monica van den Berg

Supervisor:

Prof. Dr. Marleen Verhoye

Antwerpen, 2023

Multimodal approach to unravel network disturbances and compensatory mechanisms during pre-and early-plaque stages of Alzheimer's disease

Multimodale benadering om netwerkverstoringen en compensatiemechanismen te ontrafelen tijdens de pre- en vroege-plaque stadia van de ziekte van Alzheimer

This PhD project was funded by the Research Foundation Flanders, Belgium (FWO, project Nr FWO-G048917N and FWO-G045420N) and Stichting Alzheimer Onderzoek, Belgium (SAO) (SAO-FRA-20180003).

Cover illustration: Sam de Waegenaere and Monica van den Berg, using Midjourney
Printing and design: Monica van den Berg and Natacha Hoevenaegel, Nieuwe Mediadienst, Universiteit van Antwerpen

Members of the Jury

Prof. dr. Marleen Verhoye – Promotor

Bio-Imaging Lab, Department of Biomedical Sciences, Faculty of Pharmaceutical, Biomedical and Veterinary Sciences, University of Antwerp, Belgium

Prof. dr. Ir. Peter Delputte – Chair of the internal thesis committee

Laboratory for Microbiology, Parasitology and Hygiene (LMPH), Department of Biomedical Sciences, Faculty of Pharmaceutical, Biomedical and Veterinary Sciences, University of Antwerp, Belgium

dr. Ir. Arjan den Dekker – Member of the internal thesis committee

Imec - Vision Lab, Department of Physics, Faculty of Sciences, University of Antwerp, Belgium

Prof. dr. Sebastiaan Engelborghs – Internal member of the jury

Neurology Department, Universitair Ziekenhuis Brussel

Experimentele Neurobiologie Groep (ENU), Department of Biomedical Sciences, Faculty of Pharmaceutical, Biomedical and Veterinary Sciences, University of Antwerp, Belgium

Prof. dr. Tommas Ellender – Internal member of the jury

Neuronal Circuit Research, Experimental Neurobiology Unit (ENU), Department of Biomedical Sciences, Faculty of Pharmaceutical, Biomedical and Veterinary Sciences, University of Antwerp, Belgium

dr. Valerio Zerbi – External member of the jury

Research and Teaching Associate, Zerbi Group, EPF (École Polytechnique Fédérale de Lausanne), Switzerland

Prof. dr. Gilles Vandewalle – External member of the jury

GIGA-Cyclotron Research Centre-In Vivo Imaging, Université de Liège, Belgium

Table of Contents

Summary

Due to the aging world population, the number of people that are suffering from Alzheimer´s Disease (AD), a severe neurodegenerative disorder leading to dementia, is expected to dramatically increase, putting a large economic and societal burden. In AD, an accumulation of both toxic amyloid-beta (Aβ) aggregates and neurofibrillary tau tangles disrupts neuronal function, leading to severe cognitive deficits and behavioral alterations, which eventually results in the need for 24-hour care. AD is characterized by a long preclinical phase, where the progressive accumulation of Aβ and tau interferes with synaptic function and network activity, without causing cognitive symptoms. Moreover, recent studies have demonstrated that synaptic dysfunction, induced by soluble Aβ monomers and oligomers, already occurs before Aβ-plaques are present in the brain. Network alterations resulting from these synaptic changes can be reliably detected with methods as resting-state functional MRI. In addition, early network imbalance has been demonstrated to drive disease progression in AD. Methods which could reliably detect this synaptic dysfunction, such as resting state functional MRI, might be valuable biomarkers for AD. Therefore, researchers hypothesize that restoration of the network imbalance at early stages of the disease could slow down or stop the disease progression of AD. However, insights into the disease mechanisms underlying presymptomatic network dysfunction are still lacking. Investigation of network dysfunction during different behavioral states could provide valuable insights into which neuronal systems are affected at the presymptomatic stages of disease. And maybe in the future, by targeting these affected systems, an effective disease-modifying treatment could be developed. In this thesis we aimed to **evaluate if whole brain network activity and hippocampal oscillatory activity is altered at pre- and early-plaque stages of AD and how this is linked to histopathological AD-related alterations and behavioral disturbances.** For this purpose, we used a multimodal approach where we obtained results from resting state functional MRI, *in vivo* hippocampal measurements of neuronal activity in freely behaving animals and ex vivo histological

analysis. We investigated pre- and early-plaque stages of AD, using the TgF344-AD rat model, which displays all phenotypical hallmarks of AD.

First, we investigated how spatial and temporal properties of recurrent patterns of brain activity are altered in TgF344-AD rats, by using resting state functional MRI and quasi-periodic pattern analysis. We observed that during the pre-plaque stage, before Aβ-plaques and tau accumulations are present in the brain, large differences in spatial activation occur in the TgF344-AD rats compared to wild-type littermates. A decreased co-activation between several regions of the default mode-like network (DMLN) and the basal forebrain (BFB) was observed, suggesting a disconnection between the subcortical and cortical areas of the DMLN in TgF344-AD rats. In addition, we observed that activity within the BFB preceded the activity in regions of the DMLN in wildtype littermates, but not in TgF344-AD rats, suggesting altered basal forebrain function at the pre-plaque stage. Interestingly, these changes in network activity coincided with increased astrocyte abundance limited to several nuclei of the BFB in TgF344-AD rats, suggesting an important role of BFB neuroinflammation on whole-brain network activity. During the early-plaque phase, spatial and temporal properties of quasi-periodic patterns in TgF344-AD rats were more similar to wild-type littermates, and the astrogliosis in the basal forebrain was diminished. These findings suggest that compensatory mechanisms are at play during the early-plaque phase, which partially restore the network imbalance observed at the pre-plaque stage.

Secondly, we investigated how neuronal activity within the hippocampus, a region important for learning and memory, was altered during these presymptomatic stages of AD. We evaluated circadian rhythmicity, sleep architecture and hippocampal function during the pre- and early-plaque stages of AD in TgF344-AD rats. During the pre-plaque stage, we have observed decreased REM bout length, suggestive of REM sleep fragmentation in TgF344-AD rats. In addition, several electrophysiological correlates of memory function, such as the power of gamma oscillations and theta-gamma coupling, were found to be altered in TgF344-AD rats. Interestingly, during the early-plaque phase we observed a partial functional recovery of hippocampal oscillations and REM bout length in TgF344-AD rats, which coincided with an increase in the number of cholinergic

synapses in several hippocampal regions. The partial recovery of hippocampal function and behavior suggests that the cholinergic sprouting which originates from the BFB could be an important compensatory mechanism during the early-plaque stage of AD. In a next study we further validated that hippocampal function during the pre-plaque stage was altered while animals are awake and exploring a novel environment. We observed altered hippocampal oscillatory activity at the pre-plaque stage, which coincided with increased anxiety in TgF344-AD rats compared to wild-type littermates.

Thirdly, we aimed to investigate the effects of modulating cholinergic signaling on the functional connectivity in whole-brain networks. We observed that activation of cholinergic neurons in the nucleus basalis of Meynert, one of the cholinergic regions affected in AD, induced a decrease in functional connectivity in the DMLN, clearly demonstrating the importance of BFB cholinergic signaling in the modulation/regulation of the DMLN. Moreover, it provides important evidence that chemogenetic tools could be a method to selectively activate specific neuronal populations, to counteract network imbalances during early stages of AD and thereby altering the disease course of AD.

In conclusion, the results presented in this thesis demonstrate that during pre-plaque stages of AD, alterations in network function and hippocampal function can be observed in TgF344-AD rats, which are associated with soluble Aβ pathology, astrogliosis in the BFB and impaired BFB function. Moreover, cholinergic compensatory mechanisms are at play during the early-plaque stage, which partially recover hippocampal network activity and whole-brain network activity in TgF344-AD rats. Finally, the results of this thesis suggest that activation of cholinergic neurons in the nucleus basalis of Meynert using chemogenetic tools could be a valuable technique to counteract network imbalances during the presymptomatic stages of AD.

Samenvatting

Door de vergrijzing van de bevolking zal het aantal mensen dat lijdt aan de ziekte van Alzheimer (AD) in de toekomst drastisch toenemen. AD is een ernstige neurodegeneratieve aandoening die leidt tot dementie. Dementie wordt gekenmerkt door cognitieve- en gedragsproblemen die ertoe zullen leiden dat personen niet meer voor zichzelf kunnen zorgen en professionele 24-uurs zorg nodig hebben, wat een grote economische en maatschappelijke last met zich meebrengt.

In AD is er een opstapeling van toxische amyloïde-beta (Aβ)-aggregaten en neurofibrillaire tau-kluwen in de hersenen, die de normale neuronale functie ernstig verstoren. De ziekte wordt gekenmerkt door een lange preklinische fase, waarin de progressieve accumulatie van Aβ en tau de synaptische functie en netwerkactiviteit verstoort, zonder symptomen te veroorzaken. Recente studies hebben aangetoond dat deze synaptische disfunctie, geïnduceerd door oplosbare Aβ-monomeren en -oligomeren, al optreedt voordat er Aβ-plaques in de hersenen aanwezig zijn. Methoden die deze synaptische disfunctie op betrouwbare wijze kunnen detecteren, zoals resting-state functionele MRI (rsfMRI), kunnen waardevolle biomarkers zijn voor AD. Bovendien is aangetoond dat de disbalans in netwerkactiviteit, veroorzaakt door synaptische disfunctie, het ziekteproces versnelt. Onderzoekers vermoeden dat het herstellen van de balans in netwerkactiviteit tijdens vroege stadia van AD het ziekteverloop zou kunnen vertragen of zelfs stoppen. Echter, de ziektemechanismen die aan de basis liggen van deze presymptomatische netwerkdisfunctie zijn nog niet bekend. Onderzoek om te achterhalen welke neuronale systemen zijn aangetast in de presymptomatische stadia van de ziekte is noodzakelijk en zou in de toekomst kunnen leiden tot nieuwe therapeutische behandelingen.

De hippocampus is een gebied in de hersenen dat belangrijk is voor hetgeheugen. Wanneer men wakker is, zorgt de hippocampus ervoor dat nieuwe herinneringen aangemaakt worden. Tijdens slaap worden deze nieuwe herinneringen versterkt of verzwakt, een proces dat geheugenconsolidatie wordt genoemd. Beschadiging van de netwerken in de hippocampus leidt tot geheugenaandoeningen, zoals die aanwezig zijn

bij personen die lijden aan AD. De hippocampus is een van de eerste hersenregio's die aangetast zijn in AD, waardoor geheugenproblemen hier de eerste kenmerken van zijn. Het is echter nog niet bekend hoe de netwerkfunctie in de hippocampus is aangetast tijdens vroege stadia van de ziekte.

In dit proefschrift onderzochten we hoe de activiteit van verschillende hersennetwerken en de neuronale activiteit in de hippocampus verandert in pre- en vroege-plaquestadia. Daarnaast onderzochten we hoe deze veranderingen verband houden met histopathologische AD-gerelateerde veranderingen en gedragsveranderingen. Daarvoor hebben we een multimodale benadering gebruikt waarbij we rsfMRI, *in vivo* metingen van neuronale activiteit in de hippocampus in wakkere en slapende dieren en ex vivo histologische analyse combineerden. De focus lag hierbij op de pre- en vroege-plaquestadia van AD, die overeenkomen met de presymptomatische stadia van AD. Hiervoor gebruikten we het TgF344-AD rattenmodel, dat alle ziektekenmerken van AD vertoont.

Ten eerste hebben we onderzocht hoe spatiale en temporele eigenschappen van terugkerende patronen van hersenactiviteit veranderd zijn in TgF344-AD ratten, door gebruik te maken van rsfMRI en de analyse van quasi-periodieke patronen van hersenactiviteit. We hebben aangetoond dat tijdens het pre-plaquestadium, voordat Aβ-plaques en tau-accumulaties in de hersenen aanwezig zijn, grote verschillen in spatiale activatie optreden bij de TgF344-AD ratten. Er werd een verminderde co-activatie waargenomen tussen verschillende regio's van het default mode-like network (DMLN) en de basale voorhersenen, wat duidt op een ontkoppeling tussen de subcorticale en corticale regio's van het DMLN in TgF344-AD ratten. Bovendien hebben we waargenomen dat activiteit in de basale voorhersenen voorafgaat aan de activiteit in regio's van het DMLN in gezonde ratten, maar dat dit niet het geval is in TgF344-AD ratten. Dit duidt op een veranderde functie van de basale voorhersenen in het pre-plaquestadium. Deze veranderingen in netwerkactiviteit vielen samen met een verhoogd aantal astrocyten in verschillende nuclei van de basale voorhersenen in TgF344-AD ratten. Dit leidde tot het vermoeden dat neuro-inflammatie van de basale voorhersenen een belangrijke invloed heeft op de netwerkactiviteit van het hele brein.

In de vroege-plaquefase observeerden we dat de quasi-periodieke patronen in TgF344-AD ratten meer leken op die van gezonde ratten. Dit suggereert dat er een herstel van de netwerkactiviteit optreedt tijdens het vroege-plaquestadium. Daarnaast was de astrogliose in de basale voorhersenen afwezig tijdens dit ziektestadium. Deze bevindingen suggereren dat compensatiemechanismen een rol spelen in de vroege-plaquefase, waardoor de disbalans in netwerkactiviteit die tijdens de pre-plaquefase aanwezig was, gedeeltelijk hersteld werd.

Ten tweede onderzochten we hoe neuronale activiteit in de hippocampus veranderd is tijdens deze presymptomatische stadia van AD in wakkere en slapende dieren. Daarvoor onderzochten we het circadiaans ritme, de slaaparchitectuur en de hippocampale functie tijdens de pre- en vroege-plaquestadia van AD in TgF344-AD ratten. Tijdens de pre-plaquefase observeerden we kortere REM-episodes in TgF344-AD ratten, wat wijst op REM-slaapfragmentatie. Bovendien bleken verschillende elektrofysiologische kenmerken van geheugen, zoals de amplitude van gamma-oscillaties en theta-gamma-koppeling, veranderd te zijn in TgF344-AD ratten. Tijdens de vroege-plaquefase zagen we een gedeeltelijk herstel van de hippocampale oscillaties en de lengte van REM-episodes in TgF344-AD ratten. Daarbij zagen we een toename van het aantal cholinerge synapsen in verschillende gebieden van de hippocampus tijdens de vroege-plaquefase in de TgF344-AD ratten. Het gedeeltelijke herstel van de hippocampale functie en het slaapgedrag suggereert dat de verhoogde densiteit van cholinerge uitlopers, die afkomstig zijn van cholinerge neuronen in de basale voorhersenen, een belangrijk compensatiemechanisme is tijdens het vroege-plaquestadium van AD. In een volgende studie hebben we verder gevalideerd dat de functie van de hippocampus tijdens de pre-plaquefase is veranderd terwijl dieren wakker zijn en een nieuwe omgeving verkennen. Ook hier observeerden we veranderde neuronale oscillaties in de hippocampus tijdens het pre-plaquestadium. Deze bevindingen suggereerden dat de geheugenfunctie van de hippocampus ook in wakkere TgF344-AD ratten was aangetast. De open field test, een gedragstest die gebruikt wordt om onderzoekend gedrag en ruimtelijk geheugen te testen, toonde een verhoogde angst aan in TgF344-AD ratten.

Ten derde onderzochten we de effecten van het moduleren van de activiteit van cholinerge neuronen in de basale voorhersenen, op de connectiviteit in verschillende hersennetwerken. We toonden aan dat activatie van cholinerge neuronen in de nucleus basalis van Meynert, een van de cholinerge regio's die al vroeg in AD is aangetast, leidt tot een afname van functionele connectiviteit in het DMLN. Deze resultaten toonden duidelijk het belang aan van cholinerge modulatie in de regulatie van hersennetwerken. Bovendien leveren deze resultaten belangrijk bewijs op dat chemogenetische stimulatie, waarbij selectief specifieke neuronale populaties geactiveerd kunnen worden, gebruikt kan worden om de netwerkfunctie tijdens vroege stadia van AD te herstellen.

Ten slotte tonen de resultaten gepresenteerd in dit proefschrift aan dat tijdens de pre-plaquestadia van AD, veranderingen in netwerkfunctie en hippocampale functie kunnen worden waargenomen bij TgF344-AD ratten met behulp van rsfMRI en elektrofysiologie. Deze veranderingen zijn geassocieerd met oplosbare Aβ-pathologie, astrogliose in de basale voorhersenen en een veranderde functie van de basale voorhersenen. Bovendien spelen cholinerge compensatiemechanismen een rol tijdens het vroege-plaquestadium, die de functie van de hippocampus en de netwerkfunctie van het hele brein gedeeltelijk herstellen bij TgF344-AD ratten. Ten slotte suggereren de resultaten van dit proefschrift dat de chemogenetische activatie van cholinerge neuronen in de nucleus basalis van Meynert een waardevolle techniek zou kunnen zijn om netwerkfunctie te herstellen tijdens de pre-symptomatische stadia van AD.

List of abbreviations

5-HT	Serotonin
A1	Primary auditory cortex
ACh	Acetylcholine
AD	Alzheimer's Disease
ADHD	Attention deficit hyperactivity disorder
ag	Angular gyrus
aMPFC	Anterior medial prefrontal cortex
Amy	Amygdala
ANOVA	Analysis of variance
AP	Anterioposterior
APP	Amyloid precursor protein
Au	Auditory cortex
Aβ	Amyloid-beta
Aβ-plaques	Amyloid-beta plaques
BFB	Basal forebrain
BFCS	Basal forebrain cholinergic system
BOLD	Blood oxygenation level dependent
CA	Cornu Ammonis
CAP	Coactivation pattern
CBF	Cerebral blood flow
CG	Cingulate cortex
ChAT	Choline acetyl transferase
CLI	Connectivity Laterality Index
CNO	Clozapine-N-oxide
CO	Cerebral Organoid
CPu	Caudate Putamen
Cre	Cre-recombinase
CSF	Cerebrospinal fluid
DA	Dopamine
DBS	Deep brain stimulation
deoxyHb	Deoxygenated hemoglobin
DG	Dentate gyrus
DMLN	Default mode-like network
DMN	Default mode network
DREADDs	Designer receptors exclusively activated by designer drugs
DV	Dorsoventral

EEG	Electro encephalography
ELI	Expression Laterality Index
ELISA	Enzyme-linked immunoassay
EMG	Electro-myography
Ent	Entorhinal cortex
EPI	Echoplanar imaging
EPSP	Excitatory postsynaptic potential
fALFF	Fractional amplitude of low frequency fluctuations
FC	Functional Connectivity
FDR	False discovery rate
Foi	Frequencies of interest
FOV	Field of view
FrA	Frontal association cortex
GABA	Gamma-amino-butyric acid
GFAP	Glial fibrillary acidic protein
HC	Hippocampus
HDB	Horizontal diagonal band of Broca
HF+	Hippocampal formation
HFO	High frequency oscillations
Iba-1	Ionized calcium-binding adaptor molecule 1
ICA	Independent component analysis
ifg	Inferior frontal gyrus
IL	Infralimbic cortex
infs	intermediate frontal sulcus
Ins	Insular cortex
IPSP	Inhibitory postsynaptic potential
IQR	Inter-Quartile range
L	Limbic
lAu/TeA	Left auditory cortex and temporary association cortex
LCN	Lateral cortical network
LFF	Low frequency fluctuations
LFP	Local field potentials
LH	Lateral hypothalamus
lHC	Left hippocampus
LMM	Linear mixed model
lOFC	Left orbitofrontal cortex
lPPC	Left parietal cortex
LTC	Lateral temporal cortex

lV2	Left secondary visual cortex
M1	Primary motor cortex
M2	Secondary motor cortex
MCI	Mild cognitive impairment
MEG	Magneto-Encephalography
mENT	Medial Entorhinal cortex
mfg	Middle frontal gyrus
MI	Modulation index
ML	Mediolateral
MS	Medial Septum
ms	Millisecond
mtc	Middle temporal cortex
NA	Noradrenaline
nACC	Nucleus Accumbens
NBM	Nucleus Basalis of Meynert
NE	Norepinephrine
NFT	Neurofibrillary tangles
NREM	Non-rapid eye movement
OFC	Orbitofrontal cortex
oxyHb	Oxygenated hemoglobin
PAC	Phase-amplitude coupling
PBS	Phosphate buffered saline
PCA	Principal component analysis
PCC	Posterior cingulate cortex
PET	Positron emission tomography
Pf	Prefrontal
PHC	Parahippocampus
phf	Para-hippocampal formation
piPL	Posterior inferior parietal lobule
Pir	Piriform cortex
pmc	Posteromedial cortex
PrL	Prelimbic cortex
ps	Principal sulcus
PSD	Power spectral density
PSF	Peak spectral frequency
pTau	hyperphosphorylated Tau
PtPD	Parietal cortex
Pyr	Pyramidal layer

QPP	Quasi-periodic pattern
rAu/TeA	Right auditory cortex and temporary association cortex
REM	Rapid eye movement
RF	Reticular formation
rHip	Right hippocampus
rOFC	Right orbitofrontal cortex
ROI	Region of interest
rPPC	Right parietal cortex
rQPP	Representative quasi-periodic pattern
RSC	Retrosplenial cortex
rsfMRI	Resting state functional MRI
RSNs	Resting state networks
rV2	Right secondary visual cortex
S1	Primary somatosensory cortex
S2	Secondary somatosensory cortex
SBA	Seed-based analysis
SCD	Subjective cognitive decline
SEM	Standard error of mean
sfg	Superior frontal gyrus
SI	Substantia Innominate
SLD	Sublaterodorsal nucleus
SS	Somatosensory cortex
STC	Sliding template correlation
SWA	Sliding window analysis
SWR	Sharp-wave ripple
SWS	Slow wave sleep
Tau	Tubulin associated protein
TBS	Tris buffered saline
TE	Echo-time
TempP	Temporal cortex
Tg	Transgenic
TMN	Tuberomammillary nucleus
tPAC	Time-resolved phase amplitude coupling
TPJ	Temporoparietal junction
TPN	Task positive network
TR	Repetition time
TST	Total sleep time
vAChT	Vesicular Acetylcholine transporter

VC	Visual cortex
vGAT	Vesicular GABA transporter
vGLUT	Vesicular Glutamate transporter
vlPAG	Ventrolateral peri-aquaductal grey
VLPO	Ventrolateral preoptic area
vMPFC	Ventral medial prefrontal cortex
vmpfc	Ventromedial prefrontal cortex
WI	Wake immobility
ws	Window size
WT	Wild-type
Z	Zeitgeber

1. General Introduction

1.1 What is Alzheimer's Disease?

According to the World Health Organization, approximately 55 million people are suffering from dementia today. Dementia is a debilitating neurological syndrome characterized by cognitive deficits, behavioral changes and functional impairments which have a large impact on daily life activities and human wellbeing. Due to the aging world population, this number is expected to increase to 78 million people suffering from dementia in 2030. In 2019, the estimated global societal cost of dementia was $1.3 trillion, demonstrating the large economic burden of dementia on society (Brayne & Miller, 2017). Currently, disease modifying therapies are still lacking. Alzheimer's disease (AD) is one of the major causes of dementia, accounting for approximately 60-70% of all dementia cases. Alzheimer's disease is characterized by the progressive accumulation of two toxic protein aggregates in the brain, the extracellular amyloid-beta (Aβ) plaques and intracellular neurofibrillary tangles (NFT), which lead to neuroinflammation, neuronal loss and dementia.

Aβ is the product of proteolytic cleavage of the amyloid precursor protein (APP), a transmembrane protein which is thought to have important functions in cell signaling, neurite growth, synapse formation, synaptic function and synaptic plasticity (Muller, Deller, & Korte, 2017). APP can be cleaved by α-secretase and γ-secretase, the so-called non-amyloidogenic pathway, resulting in the production of non-pathological fragments. In addition, APP can be processed by β-secretase and γ-secretase through the amyloidogenic pathway, resulting in the neurotoxic $A\beta_{1\text{-}40}$ and $A\beta_{1\text{-}42}$. Both amyloidogenic APP products have an increased tendency to aggregate and are the main components of the Aβ-plaques observed in AD patients (O'Brien & Wong, 2011).

The second neuropathological hallmark of AD are the NFT's which consist of hyperphosphorylated tubulin associated unit proteins (Tau). Tau proteins are a group of

six protein isoforms that are produced by splicing of the microtubule-associated protein tau. These proteins are part of the healthy cytoskeleton and have an important role in stabilizing microtubules in the axons. The function of tau is regulated by phosphorylation. Tau in a low phosphorylated state, as is observed in healthy adults, is necessary for stabilization of microtubules. However, in AD, hyperphosphorylation of tau (pTau) occurs, leading to aggregation of pTau into NFT's (Y. Wang & Mandelkow, 2016).

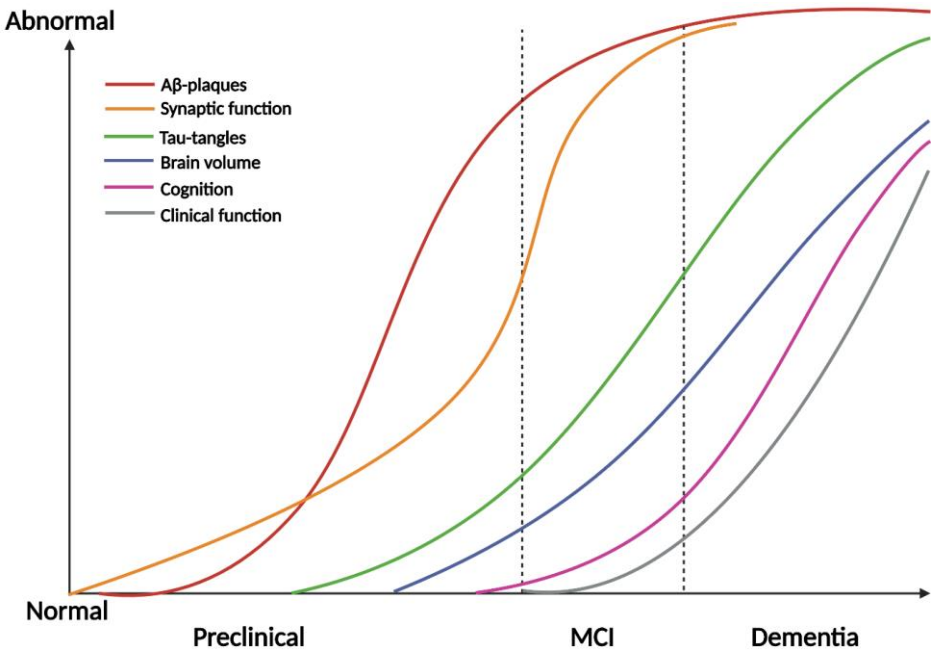

Figure 1-1: Dynamic biomarkers change from normal to abnormal across the continuum of AD. Aβ is identified by amyloid PET and/or cerebrospinal fluid (CSF) measurements and starts to accumulate decades before the onset of symptoms. Synaptic dysfunction can already be detected before Aβ-plaques are accumulating in the brain, as indicated by the dashed line. CSF biomarkers for tauopathy become abnormal at a later preclinical phase, together with brain atrophy, just before cognitive symptoms arise. Figure adapted from (Sperling et al., 2011).

The pathophysiological changes in AD start decades prior to clinical manifestations of the disease, limiting the ability to define AD purely on its clinical presentation. AD is

considered as a continuum of pathophysiological and clinical representations, which describes several phases of the disease: preclinical AD, subjective cognitive decline (SCD), mild cognitive impairment (MCI) and AD related dementia (Aisen et al., 2017)(Figure 1-1). The MCI stage is considered as the first symptomatic stage, when cognitive deterioration is observable, which does not interfere with daily activities. People with SCD are individuals who experience a deterioration in cognitive performance, which is not detected through neuropsychological evaluation and therefore, does not meet the criterium for MCI. But as studies have demonstrated that there is a higher prevalence of positive biomarkers for Aβ and neurodegeneration, SCD is categorized as an early preclinical phase of AD (Studart & Nitrini, 2016). During the dementia phase, the cognitive and behavioral problems interfere with daily activities, eventually resulting in the need for 24-hour care. Currently AD is diagnosed at the MCI or the dementia phase, based on the presence of cognitive deterioration in the absence of other physiological diseases. However, figure 1-1 demonstrates that irreversible damage has already been inflicted to the brain at the MCI stage (Aisen et al., 2017).

Despite decades of research, the exact cause of AD is still unknown, however, several hypotheses have been proposed. One important hypothesis is the amyloid cascade hypothesis, which is based on the fact that Aβ accumulation is the first detectable neuropathological event in the brain of AD patients. The amyloid cascade hypothesis states that the abnormal accumulation of pathological Aβ induces tau hyperphosphorylation, neuroinflammation, synaptic dysfunction, neuronal loss, and cognitive and behavioral deficits (Tolar, Abushakra, & Sabbagh, 2020). This hypothesis led to the development of disease modifying treatments targeting Aβ plaques, which unfortunately, showed mixed results with lack of therapeutic efficacy being the main problem. One possible explanation for this is that these approaches were applied too late in the disease progression of AD, when extensive damage is already inflicted to the brain (Anderson, Hadjichrysanthou, Evans, & Wong, 2017; Tolar et al., 2020). A large-scale phase 3 clinical trial which tested a monoclonal antibody against Aβ-plaques did show promising results, as the treated patients demonstrated a slower cognitive decline

then the untreated patients. However, severe side effects were observed, such as brain hemorrhages, leading to the death of already three patients (Dhadda et al., 2022; Mahase, 2023; Mead & Fox, 2023; Sabbagh & van Dyck, 2023). This failure again demonstrates the need for novel therapeutic targets to slow down or halt disease progression. Several studies have demonstrated that soluble Aβ (sAβ) alters neurotransmission and causes disturbances in networks before the formation of Aβ-plaques (Busche & Konnerth, 2015). Moreover, sAβ monomers and oligomers have been demonstrated to induce neuronal hyperexcitability by increasing glutamatergic- and decreasing GABAergic neurotransmission (Hector & Brouillette, 2020). The neuronal hyperexcitability perturbs normal network function before cognitive symptoms become apparent. Moreover, this increased neuronal activity further increases the production and excretion of sAβ, and therefore, drives disease progression (Bi, Wen, Wu, & Shen, 2020; Styr & Slutsky, 2018). **Methods to detect network disruptions caused by early synaptic dysfunction at pre-plaque stages of AD could be valuable to allow diagnosis and intervention during the presymptomatic phase of AD. Moreover, unraveling the disease mechanisms underlying the altered network activity could provide promising therapeutic targets which might alter disease progression.**

1.1.1 Modeling Alzheimer's disease *in vitro*

Although *in vivo* studies of AD provide some understanding of important pathological mechanisms, findings from these studies have not yielded the specific target to develop a successful therapy to treat AD. This shows the importance of the development of systems that recapitulate human-specific features of AD (Fig 1-2). The development of human-induced pluripotent stem cell-derived neurons offers the opportunity to study neuropathological mechanisms of AD in patient-derived tissue cultures (Mungenast, Siegert, & Tsai, 2016; Slanzi, Iannoto, Rossi, Zenaro, & Constantin, 2020). Neuronal cultures grown from patients with familial AD, carrying mutations in key genes of AD, recapitulate important AD pathologies, including Aβ pathology, p-tau accumulation, and neuronal hyperactivity. These 2D models have revealed several pathological mechanisms of AD (Mungenast et al., 2016). However, these neuronal cultures suffer

from several drawbacks, including the inability to reproduce all disease hallmarks, no replication of age-dependent pathogenic events and a lack of supporting glial cells such as astrocytes, which play an important role in AD (Bubnys & Tsai, 2022; Slanzi et al., 2020).

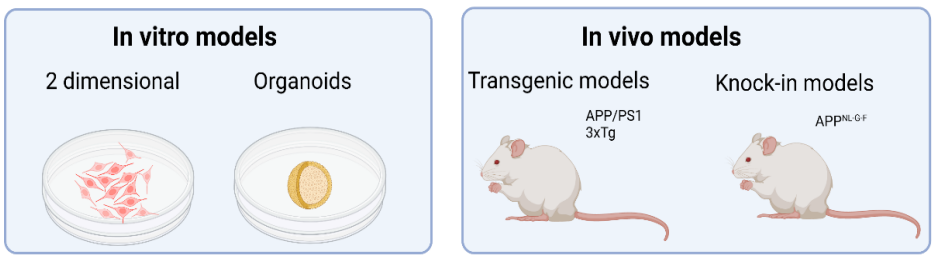

Figure 1-2: *In vitro* and *in vivo* models of AD. *In vitro* models of AD are 2 dimensional neuronal cultures originating from pluripotent stem cells and organoids. *In vivo* models are either transgenic models, which bear human AD related mutations or knock-in models, where the mouse APP gene is humanized, resulting in amyloidosis.

These limitations have encouraged the development of three-dimensional models of AD, of which the cerebral organoids (COs) are the latest discovery (Bubnys & Tsai, 2022; Venkataraman, Fair, McElroy, Hester, & Fu, 2022). These organoids offer several advantages compared to 2D neuronal cultures and *in vivo* models. The COs consist of different cell populations, such as astrocytes, oligodendrocytes and even vasculature, resulting in a spatial organization which resembles the fetal neocortex. Moreover, functional synapses are present, and the neurons display periods of coordinated firing, suggestive of the presence of neuronal networks. In addition, compared to 2D *in vitro* models, the gene expression of the cells in a CO more closely resemble the *in vivo* conditions. These organoids are ideal for high throughput assays for drug discovery. But most importantly, COs offer one major advantage. Because mice don't develop AD, most models rely on non-physiological protein overexpression or induction of multiple human mutations, resulting in an AD-like pathology. Because COs are derived directly from AD patients, they may develop AD pathology which represents a more physiological disease stage (Bubnys & Tsai, 2022). However, COs still have several limitations such as immaturity of the neurons, the difference in cellular composition from *in vivo* situation

and a lack of mature neuronal networks. In addition, COs do not mimic all the neuropathological hallmarks of AD. Apart from the limitations, COs do offer the possibility to answer research questions related to disease onset, propagation and spread of AD proteins, investigating cellular vulnerability in AD and identification of biomarkers based on transcriptomics and genomics, as patient-derived cells will provide insights in how the genetic landscape contributes to the pathogenesis of AD (Bubnys & Tsai, 2022; Venkataraman et al., 2022).

1.1.2 Animal models of AD

Animal models have been extensively used to investigate the neuropathological mechanisms of AD and to develop new techniques to detect AD at earlier stages of the disease. The main advantage of animal models with regard to humans is the possibility to investigate very early stages of AD, before cognitive symptoms are present. Moreover, animal models offer the opportunity to follow up disease progression over a relatively short time span. In addition, animal experiments allow (pharmacological) manipulations aiming to elucidate disease mechanisms and/or to follow up treatment effects. The majority of AD models are mouse models which carry genetic mutations known to cause familial AD in humans. To date, the majority of the experimental models are animal models, which consist mostly of transgenic mice that express human genes that result in the formation of amyloid plaques (human APP gene alone or in combination with human PSEN1 gene) and/or neurofibrillary tangles (expression of human MAPT gene) (Myers & McGonigle, 2019). These mouse models display an age-dependent amyloidosis and/or tauopathy, based on the inserted genes and mutations. Moreover, neuroinflammatory responses such as microgliosis and astrogliosis are present in these animal models. A more recent group of animal models are knock-in or knock-out models. These models are generated by humanizing mouse Aβ and knocking in specific familial AD mutations, instead of inserting human Aβ in the mouse genome. These mice are considered to be a more physiological model of AD as they are designed to avoid the confounding effects of APP over-expression present in all other transgenic mouse models. However, similar to the transgenic models are knock-in mice models of

familial AD and not sporadic AD (Drummond & Wisniewski, 2017; Jankowsky & Zheng, 2017).

One major disadvantage of the current mouse models is that none of them replicates the entire human AD pathology, but usually only display specific aspects of the disease, limiting the translation to humans. Several clinical trials assessing potential novel treatments, which were shown to be beneficial in mice, have failed in humans, demonstrating the importance to develop new translational animal models in order to bridge this gap between preclinical and clinical research. Taking this into account, rats are a promising preclinical model as they are evolutionarily closer to humans, especially reflected in their genetic and physiological traits (Do Carmo & Cuello, 2013; Jacob & Kwitek, 2002). One important difference regarding mice and rats is that rats express the full tau proteome, consisting of six isoforms, similar to humans, whereas mice only express three tau isoforms (Hanes et al., 2009; McMillan et al., 2008). Rats exhibit more complex behavioural phenotypes and are of larger size, which makes them a better suited model to study.

Several AD rat models recapitulate some of the hallmarks for AD, but fail to present all human AD hallmarks, such as the McGill-R-Thy1-APP rat model, which demonstrates amyloid pathology in the absence of tauopathy and neuronal loss. The recently developed TgF344-AD rat model (R. M. Cohen et al., 2013), is a promising AD model as it recapitulates all human pathological hallmarks of AD, including amyloidosis, tauopathy, synaptic dysfunction, neuronal loss, and cognitive deficits (R. M. Cohen et al., 2013). Numerous studies have been performed to characterize the AD pathology in these TgF344-AD rats, to disentangle disease mechanisms and to investigate the effect of therapeutic strategies (Figure 1-3). Most of the studies have been performed at the start of Aβ plaque deposition, which starts around 6 months of age (R. M. Cohen et al., 2013). Interestingly, at 6 months of age, pTau accumulations were observed in the locus coeruleus (LC), which is also the first region affected by tauopathy in human AD (Rorabaugh et al., 2017). This tauopathy shows seeding-like spreading to the hippocampal circuit and medial entorhinal cortex, similar as in humans (Braak & Braak,

1991). Even more interesting is the fact that it's the rat tau protein that spontaneously starts to hyperphosphorylate, similar to the spontaneous hyperphosphorylation of tau (pTau) observed in humans, further demonstrating the high translational value of these rats. The early accumulation of pTau has been demonstrated to alter noradrenergic signalling. Researchers observed decreased noradrenergic innervation in the hippocampus of TgF344-AD rats starting from 6 months of age, which led to a B-adrenergic receptor function-induced hyperexcitability in the hippocampus (A. M. Goodman, Langner, Jackson, Alex, & McMahon, 2021; Smith, Goodman, & McMahon, 2022). Impaired spatial memory has been observed at 4 months of age, while other studies report memory deficits starting from 6 months of age (Berkowitz, Harvey, Drake, Thompson, & Clark, 2018; Fowler et al., 2022; Proskauer Pena et al., 2021). TgF344-AD rats further demonstrate increased anxiety from 4 months onward and alterations in sleep at 17 months of age, suggesting that AD related behavioural changes are also present in this model throughout different disease stages (Kreuzer et al., 2020; Pentkowski et al., 2018; Sare et al., 2020). In addition to the classical AD-like features, further research has demonstrated synaptic dysfunction leading to impaired neuroplasticity in the hippocampal circuit starting from 6 months of age (Bazzigaluppi et al., 2018; Ratner et al., 2021; Smith & McMahon, 2018; Stoiljkovic, Kelley, Stutz, Horvath, & Hajos, 2019), and alterations in whole brain connectivity were observed from 5 months onward (Anckaerts et al., 2019; Tudela, Munoz-Moreno, Sala-Llonch, Lopez-Gil, & Soria, 2019). Moreover, neurovascular dysfunction has been observed between 9-10 months of age (Joo et al., 2017). These observations demonstrate that the **TgF344-AD rat model is highly promising in being a translational model for AD, since it recapitulates almost all human-like AD hallmarks.**

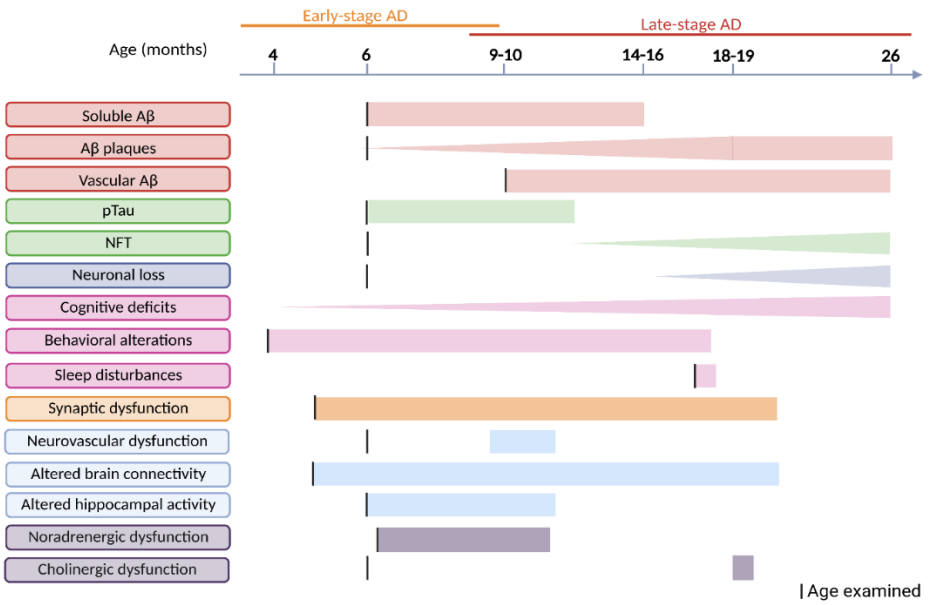

Figure 1-3: Overview of AD pathology in the TgF344-AD rat model. This figure is based on results reported in (Anckaerts et al., 2019; Bazzigaluppi et al., 2018; Berkowitz et al., 2018; Bernaud et al., 2022; Chaney et al., 2021; R. M. Cohen et al., 2013; Fowler et al., 2022; A. M. Goodman et al., 2021; Joo et al., 2017; Kreuzer et al., 2020; Pentkowski et al., 2018; Pentkowski, Bouquin, Maestas-Olguin, Villasenor, & Clark, 2022; Rorabaugh et al., 2017; Sare et al., 2020; Smith et al., 2022; Smith & McMahon, 2018; Stoiljkovic et al., 2019; Tudela et al., 2019)

1.2 *In vivo* magnetic resonance imaging (MRI) to study networks in the brain at rest

The human brain is a complex network of interconnected brain regions, where each network has a unique connectivity pattern, allowing regions to have specific roles in a variety of brain functions. For example, some brain regions collectively increase their activity during periods of rest, while another set of brain regions increase their activity during cognitive tasks. Disturbances in the functional integrity of networks or changes in the interaction between different networks have been linked with several brain disorders. Decades of research have focused on understanding how functionally connected neuronal systems are responsible for various cognitive functions and unravelling the specific roles of different brain regions during different behaviors.

Box 1-1: Magnetic resonance imaging (MRI)

The MRI signal originates from the hydrogen nucleus, the most abundant element in our body, which contains one proton, spins around its own axis creating a magnetic momentum (μ). The direction of the momentum of spins is random under normal circumstances (1). However, when a magnetic field is applied (B_0) to the hydrogen spins, the spins will be restricted in a spin-up or spin-down state along the magnetic field (2). The spins will precess additionally around the magnetic field B_0 with a frequency (w_0) proportional to the magnetic field strength. The majority of spins will be in the spin up state, creating a netto longitudinal magnetization (M_z). Next, a radiofrequency (RF) pulse is applied to the spins, which changes the distribution of the equilibrium of the spins and bring the proton spins in phase, which will cause the M_z component to be rotated, creating a transversal M_{xy} component (4). The precessing of ions (M_{xy}) induces magnetic flux which will be detected by the receive RF coil. Over time, the spins will dephase and fall back to their equilibrium state due to two relaxation processes (5, 6). The relaxation process is dependent on the physical and chemical features of the surrounding tissue (7). Therefore, relaxation can be divided into T1 relaxation, or spin-lattice relaxation and T2 relaxation, so-called spin-spin relaxation. T1 relaxation reflects the mobility of the surrounding molecules of the spins, which absorb the energy of the proton spin, enabling it to return to equilibrium. T2 relaxation is independent on T1 relaxation and occurs at the same time. Spin-spin interactions cause non-stationary variations in the magnetic field, resulting in the spins to sligtly shift their phases, resulting in a decay of M_{xy}. In addition, inhomogeneties of the B_0 field also influence the decay of M_{xy}, which is characterized by the T2* relaxation time. Those three types of relaxation are dependent on the biochemical environment and therefore provide tissue specific MRI contrast.

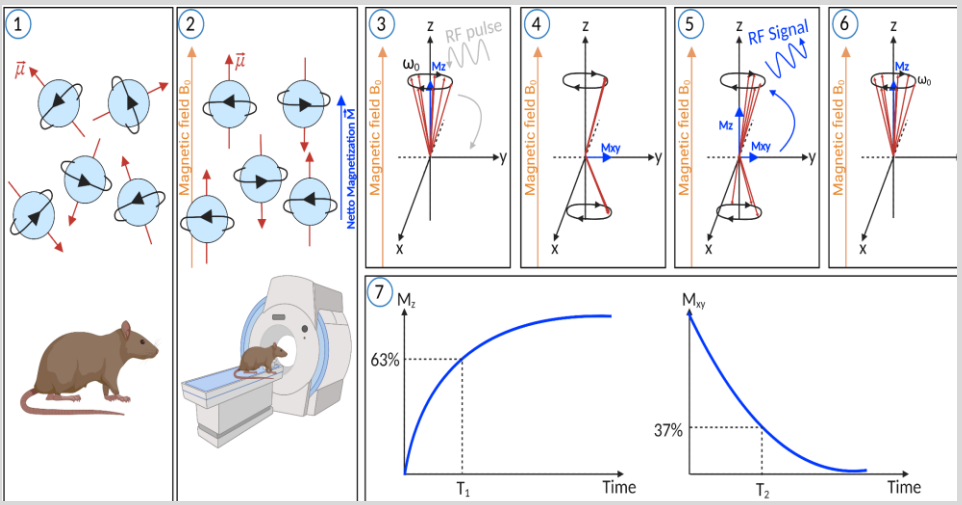

Magnetic Resonance Imaging (MRI) is a noninvasive imaging technique which uses a magnetic field to investigate structural and functional properties of the body. The principles behind MRI are described in box 1-1. Several MRI techniques are used in neuroscience which provide insights on for example anatomical differences, blood flow, molecular composition and brain activity (functional MRI – fMRI). The first functional studies were aiming to reveal the brains' functional organization by mapping the regional activation during specific tasks. This has led to the discovery of a set of brain regions of which the activity increased while the subject was involved in externally oriented attention demanding tasks. This network was named task positive network (TPN). The human TPN includes cortical regions which are consistently activated during directed attention and have also been termed the dorsal attention network: the intraparietal sulcus and the frontal eye fields. In addition, the TPN includes regions which are activated during various cognitive tasks and include the dorsal, lateral, and ventral prefrontal regions, insular cortices, and the supplementary motor area.

Besides the observations of several brain regions which increased their activity upon cognition, researchers discovered several brain regions that were consistently deactivated during various cognitive tasks (Gusnard, Akbudak, Shulman, & Raichle, 2001; Raichle et al., 2001). Moreover, they observed that the magnitude of decrease was proportional to the difficulty of the task, the higher the attentional demand, the stronger the decrease in those brain regions (Mayer, Roebroeck, Maurer, & Linden, 2010). Upon termination of the task, the activity within these regions increased, suggesting that these regions are highly active during periods of rest (Raichle et al., 2001). This network was named the default-mode network (DMN) and includes the medial prefrontal cortex, anterior and posterior cingulate cortex, lateral parietal cortex, inferior temporal cortex and hippocampal formation (Fox et al., 2005; Raichle, 2015) (Figure 1-4A). The DMN has been shown to be activated during internally directed mental processes, such as mind wandering, self-referential thoughts, recall of past episodes and thinking about the future. Earlier works have analyzed this network as a single large-scale system, however, given the different cognitive functions within the

DMN, studies have divided the network into a midline core, the anterior DMN or dorsal medial prefrontal cortex system and the posterior DMN or medial temporal lobe subsystem (Andrews-Hanna, Reidler, Sepulcre, Poulin, & Buckner, 2010) (Figure 1-4B). The medial temporal lobe subsystem of the DMN is associated with memory related internal mental processes, whereas the dorsal medial prefrontal system is closely related to self-referential thoughts and social cognitive processes (Andrews-Hanna, Reidler, Sepulcre, et al., 2010). Collectively, these findings suggest an antagonistic relationship between the DMN, involved in internally oriented mental processes, and the TPN, activated during externally oriented attention demanding tasks. However, the mechanisms by which these two networks are modulated still remain elusive.

Spatially and functionally homologous networks have been observed in different species, such as monkeys, mice, and rats (Gozzi & Schwarz, 2016; Liska, Galbusera, Schwarz, & Gozzi, 2015; Lu et al., 2012; Vincent et al., 2007). The main nodes of the lateral cortical network (LCN), the rodent homolog of the TPN, consist of the frontal association cortex, somatosensory cortices, motor cortices and insular cortices (Gozzi & Schwarz, 2016; Liska et al., 2015) (Figure 1-4A). The default mode-like network (DMLN), which is the rodent analog of the DMN consists of the cingulate cortex, retrosplenial cortex, orbitofrontal cortices, limbic cortices, temporal cortex/auditory association cortex, visual cortex, and dorsal hippocampus (Gozzi & Schwarz, 2016) (Figure 1-4A). Interestingly, the DMLN in rodents can be compartmentalized in an anterior and posterior DMLN, based on cognitive functions, similar to the human DMN (Figure 1-4B) (Liska et al., 2015). The high intraspecies homology of the networks supports the value of investigating network dynamics in rodents.

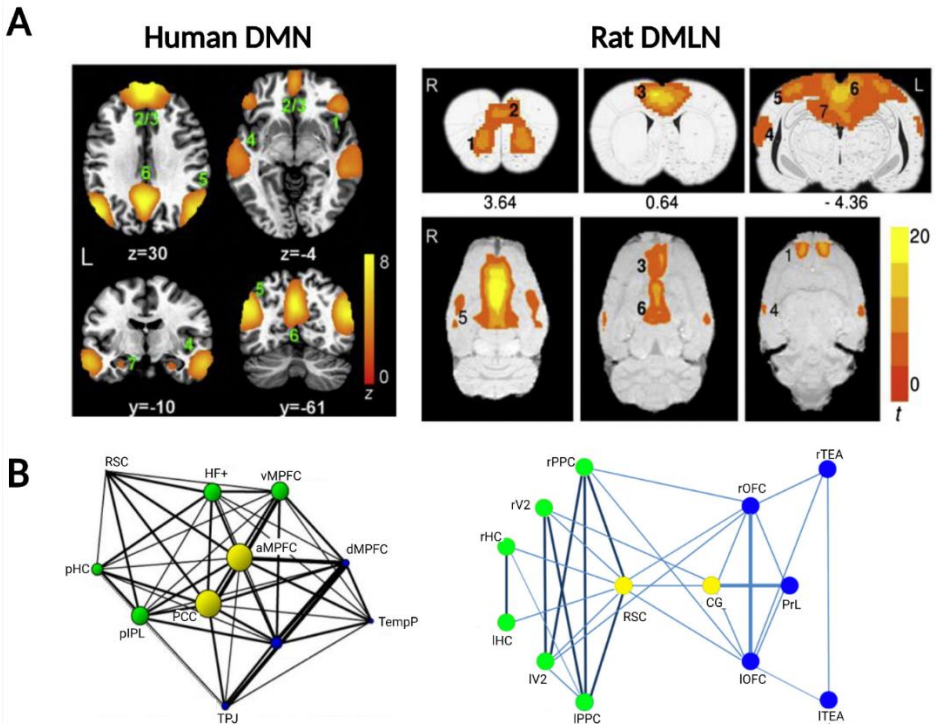

Figure 1-4: Comparison between DMN and DMLN in the human and rodent brain, respectively. A) The rodent default-mode like network (DMLN) consists of anatomically homological regions similar to the human default mode network (DMN). B) Both the human DMN and rodent DMLN can be compartmentalized into different subnetworks, based on cognitive functions. Figure adapted from (Andrews-Hanna, Reidler, Sepulcre, et al., 2010; Gozzi & Schwarz, 2016; Liska et al., 2015)

These findings inspired researchers to examine if regions belonging to the aforementioned networks were functionally connected in the absence of a task using resting state functional MRI (rsfMRI). Several studies have demonstrated that spontaneous BOLD activation patterns within regions belonging to specific networks, such as the DMN, were highly correlated at rest and were therefore functionally connected also during rest (Fox et al., 2005; Fransson, 2006; Greicius, Krasnow, Reiss, & Menon, 2003; Greicius & Menon, 2004). Interestingly, the connectivity between regions of these so-called resting-state networks and the interaction between networks has been demonstrated to be altered in various neurological disorders. Numerous clinical

rsfMRI studies have detected FC alterations in patients with MCI and AD-related dementia, as well as in animal models of AD. Aberrations in FC were mainly observed in the DMN and have been linked to cognitive and behavioral performance (Anckaerts et al., 2019; Herdick et al., 2020; Latif-Hernandez et al., 2019; Pan et al., 2017; Shah et al., 2013; Shah et al., 2016; van Harten et al., 2018; Y. Xie et al., 2019). **Network disturbances caused by synaptic dysfunction are hypothesized to arise very early in AD, therefore, rsfMRI would be an interesting tool to develop non-invasive biomarkers for AD.**

1.2.1 Resting state functional MRI

Resting state functional MRI is a non-invasive technique, used to measure neuronal activity represented as coupling between neuronal activity, energy demand and cerebral blood flow, *i.e.,* neurovascular coupling. This technique detects local changes in blood oxygenation levels by using the blood oxygenation level dependent (BOLD) signal (Figure 1-5). The BOLD signal is based on differences in magnetic properties of oxyhemoglobin (oxyHb) and de-oxyhemoglobin (deoxyHb). DeoxyHb is paramagnetic due to its unpaired electron, which will distort the local magnetic field B_0, inducing faster dephasing and reducing the T2* signal. OxyHb on the other hand is diamagnetic and therefore will not alter the B_0. Thus, higher concentrations of oxyHb will result in an increased T2* signal, because of slower dephasing. Based on this endogenous contrast mechanism, spontaneous activation of neuronal populations can be investigated. When neurons are active, their demand for glucose and oxygen increases. This initiates a metabolic signaling cascade which induces vasodilation, hence an increased local cerebral blood flow (CBF). This vascular response overcompensates the metabolic O2 demand, resulting in an increased oxyHb/deoxyHb ratio, resulting in less inhomogeneities of B_0. As a result, the T2(*) BOLD signal intensity within these activated regions will increase.

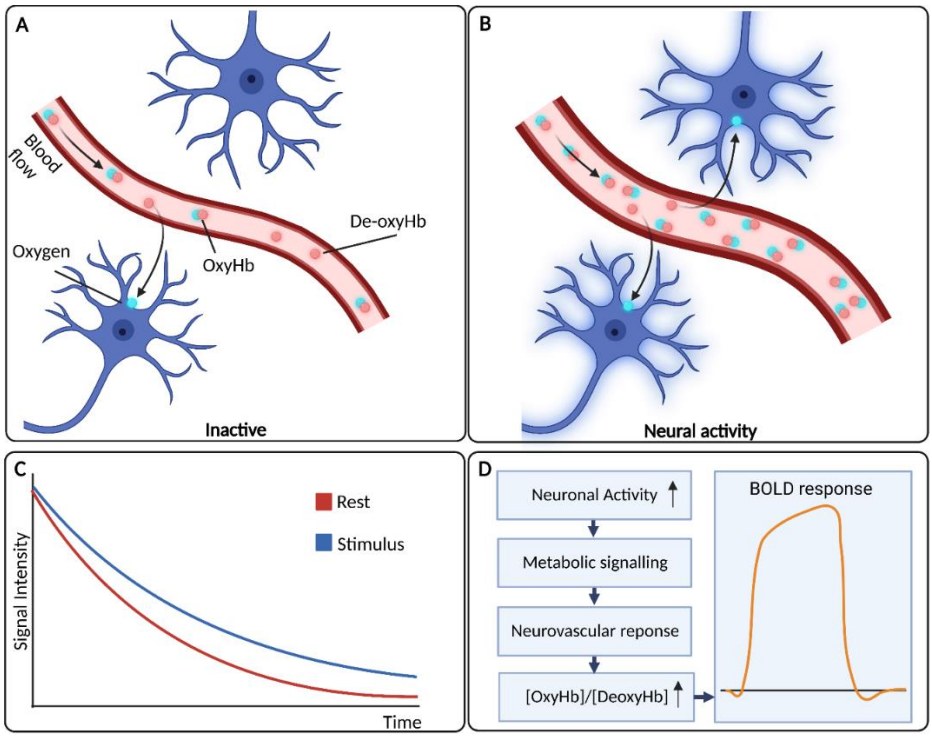

Figure 1-5: Principle of the BOLD response. A. In rest, blood supply to neurons contains a limited amount of oxygen. B. Upon neuronal activation, the hemodynamic response will result in an increased ratio of OxyHb/DeoxyHb. C. The increased ratio of OxyHb/DeoxyHb upon activation reduce the distortion of the magnetic field, resulting in an increased T2* relaxation time and thus higher signal intensity in the activated region (blue curve). D. Schematic overview of the hemodynamic response and neurovascular coupling, on which BOLD fMRI measurements are based.

Spontaneous neuronal activity during rest can be observed as fluctuations of the BOLD signal in the low frequency range (0.01-0.2 Hz), the so-called low frequency fluctuations (LFF). These resting state LFF can be measured using T2* weighted echo planar imaging (EPI). This MRI sequence allows the acquisition of whole brain images in 2 seconds. Images are continuously acquired for a period of usually 10 minutes, resulting in a series of images from which the time courses or temporal BOLD fluctuations can be obtained (Figure 1-6). The temporal correlation of BOLD time series across spatially remote brain regions is an indication of the level of functional connectivity (FC) between those brain

regions. Regions which demonstrate a high similarity in BOLD time course, thus a high FC, can be clustered to form resting state networks such as the DMN and TPN.

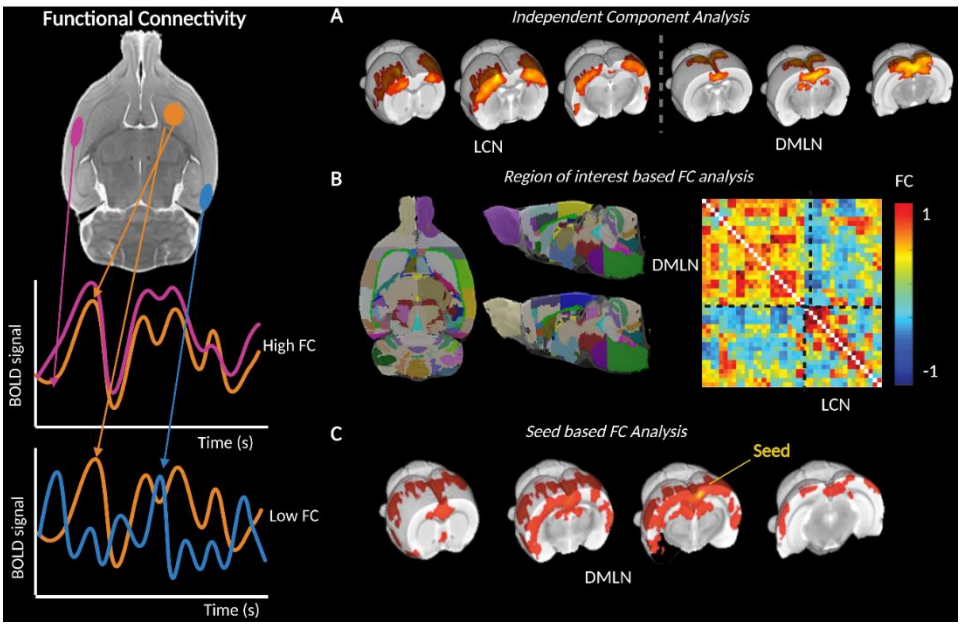

Figure 1-6: Functional connectivity analysis of rsfMRI data. The obtained BOLD time series show spontaneous fluctuations over time. The temporal correlation between these fluctuations of different regions is referred to as functional connectivity (FC). Functional connectivity can be assessed using different techniques, such as independent component analysis (A), region of interest-based FC matrix in which the color represent the strength of functional connectivity between pair of regions (B), and seed-based FC analysis (example given for a seed in the retrosplenial cortex) demonstrating in yellow-red voxels for which the BOLD timecourse is significant correlated with the seed-specific BOLD timecourse.(C).

Preprocessing of the resting state data consists of various steps such as spatial normalization, spatial smoothing, and temporal filtering in the LFF range. Processing of rsfMRI data to evaluate FC can include a variety of methods (Figure 1-6) of which the most popular approaches are independent component analysis (ICA), region-of-interest (ROI) based FC analysis and seed-based FC analysis (SBA). ICA is a data-driven approach to evaluate FC, where the data is decomposed into a set of maximally independent time

courses and associated spatial maps which describe temporal and spatial characteristics of distinct resting state components. The main advantage of ICA is that it is free of any a priori assumption or potential user-biased seed selection (Figure 1-6A). In contrast, ROI-based FC analysis and SBA do require selection of a set of ROIs or seed regions. In a ROI based FC analysis, an average BOLD time course is extracted from all voxels within a ROI and FC between other ROI time courses is calculated using a Pearson correlation, resulting in a ROI based FC matrix (Figure 1-6B). In a seed-based FC analysis, the BOLD signal of all voxels from a region of interest, called the seed region, are averaged, to give a seed-specific BOLD time course which is then compared to the BOLD timecourse of each other voxel in the brain. This will result in a seed-specific FC map which shows the voxels for which the BOLD timecourse is significantly correlated to the averaged BOLD timecourse of the seed region (Figure 1-6C). Dependent on the research question, the SBA can be performed for different seeds.

RsfMRI has been used to investigate how regional connectivity within networks is altered in AD and how these alterations are linked with cognitive deficits associated with AD. Numerous studies have investigated brain connectivity in patients with MCI, severe dementia, and cognitively healthy individuals at risk of dementia, for example people with commonly known genetic risk factors such as APOE4. Current evidence demonstrates alterations in FC, mainly within the DMN across the spectrum of AD stages (Badhwar et al., 2017; Brier, Thomas, & Ances, 2014; Krajcovicova, Marecek, Mikl, & Rektorova, 2014; Sheline et al., 2010). Several studies have reported an initial increase in FC in the hippocampus and posterior DMN, followed by a continuous decline in posterior DMN connectivity. A similar pattern was observed in the anterior DMN, where an initial increase in FC was observed in the anterior DMN, followed by a decreased FC at later stages of AD. Moreover, a progressively decreased FC between anterior and posterior DMN has been observed across the AD spectrum. (Hafkemeijer et al., 2017; Jalilianhasanpour, Beheshtian, Sherbaf, Sahraian, & Sair, 2019). Interestingly, several studies have demonstrated that alterations in DMN connectivity correlate with clinical symptom severity (Jalilianhasanpour et al., 2019).

Despite all the efforts to unravel network dysfunction in AD, the disease mechanisms underlying the alterations in FC are still largely unknown. Moreover, the majority of the studies are performed during symptomatic stages of AD, when advanced pathology is already present in the brain. This is the main reason for the limited knowledge about disease mechanisms of early network dysfunction in AD. Investigating network dysfunction in animal models for AD using rsfMRI offers the advantage to further disentangle the neuropathological mechanisms of AD at different stages of the disease, including the presymptomatic, pre-plaque stages of AD. Several studies have observed aberrant FC within the DMLN and hippocampus at different stages of AD, similar as is observed in humans, even before amyloid deposits were present in the brain (Latif-Hernandez et al., 2019; Shah et al., 2013; Shah et al., 2018; Shah et al., 2016). Moreover, alterations in FC have been linked to cognitive deficits and altered synaptic transmission in several mouse models for AD (Ben-Nejma et al., 2019; Shah et al., 2018; Stargardt, Swaab, & Bossers, 2015). Interestingly, preclinical MRI studies observed increased FC within the hippocampal network and DMLN, before Aβ-plaques were observed in the brain, confirming that network activity is altered prior to the accumulation of Aβ-plaques (Ben-Nejma et al., 2019; Latif-Hernandez et al., 2019; Shah et al., 2018; Shah et al., 2016).

1.2.2 Dynamic analyses methods for rsfMRI data

The results of aforementioned studies are highly promising towards the development of rsfMRI biomarkers for AD and rsfMRI has proven to be a powerful tool to study brain functional connectivity, but it has not reached its full potential. Several downsides to rsfMRI include low reproducibility, large variability between results and low specificity of the results, meaning that, for example, different neurological diseases demonstrate similar decreases in FC, limiting the diagnostic use of these FC changes. All rsfMRI studies described earlier have used analysis strategies that assume that FC is stationary across the duration of an entire scan session, because the relationship between two given brain regions is calculated from their entire time series. This results in a single value to

describe the interaction between two brain regions. The brain's functional organization is however dynamic, with brain regions interacting across multiple time scales. Ignoring this can potentially results in the loss of relevant information. The recent advances in the fMRI field towards dynamic (d)rsfMRI confirmed that when the dynamics of FC are taken into account, fundamental new insights into macroscale neural processes are uncovered (X. Liu, Zhang, Chang, & Duyn, 2018; Majeed, Magnuson, & Keilholz, 2009; Moguilner et al., 2021).

The most often used strategy is the sliding window analysis (SWA), which investigates FC within short time window that is shifted across all images across time. In SWA, a correlation value between two regions is calculated for each window, resulting in time-varying correlation between the regions. This could, for example, demonstrate short instances of high FC, which would not be detected using static FC across the complete time course. SWA analysis can be used to detect transient patterns of connectivity, so-called connectivity states. Parameters of these states, such as dwell time, which is the duration of a certain state, and frequency of occurrence, have been shown to be altered in various neurological disorders (Billings et al., 2017; Y. Du, Fu, & Calhoun, 2018; Shakil, Lee, & Keilholz, 2016). Aforementioned results indicate that sliding window correlations and/or connectivity states are a promising tool to investigate brain network activity at shorter timescales. However, several limitations should be considered, such as defining the appropriate window size to reduce noise without losing the ability to detect potentially relevant transient effects (Y. Du et al., 2018; Hutchison et al., 2013).

Researchers hypothesized that the dynamic connectivity states reflect short-lasting patterns of co-activations and/or co-deactivations between different brain areas. Co-activation patterns (CAPs) are an example of patterns of brain activity that can be extracted from the dynamical analysis of rsfMRI data using k-means clustering over all BOLD images based on the spatial dissimilarity of the whole-brain activation pattern of each frame (Figure 1-7) (Gutierrez-Barragan, Basson, Panzeri, & Gozzi, 2019; X. Liu et al., 2018). These CAPs represent BOLD-based transient brain states that are obtained at a

single time frame resolution (i.e., at every measured fMRI volume). CAPs demonstrate the co(de)activation between several regions and for example show the anticorrelated activity between the DMN and TPN (Figure 1-7). Several properties of these CAPs, such as the magnitude of spatial BOLD activity and occurrence of a certain CAP, have been shown to be altered at late stages of AD in the APP/PS1 mouse model of AD (Adhikari et al. 2020) .

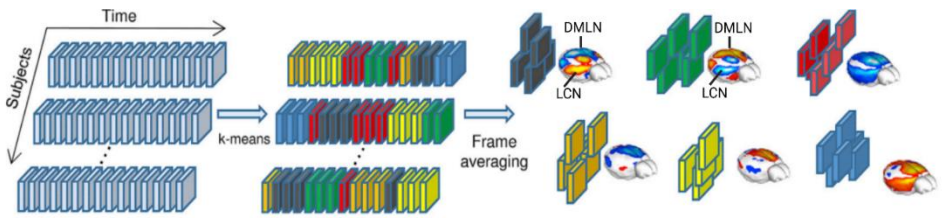

Figure 1-7: Co-activation patterns (CAP). K-means clustering is performed based on the spatial dissimilarity of the whole-brain activation pattern of each frame. The BOLD images in a cluster are then averaged to create a CAP.

The observation that network states can be captured at very short time scales has led researchers to question whether sequences of BOLD volumes, where BOLD activity propagates across regions, are present in rsfMRI data. Spatiotemporal patterns of BOLD activity have been observed in mice, rats, monkeys, and humans using a pattern finding algorithm (Abbas, Belloy, et al., 2019; Belloy, Naeyaert, et al., 2018; Majeed et al., 2009; Thompson, Pan, Magnuson, Jaeger, & Keilholz, 2014). These recurrent spatiotemporal patterns of whole brain BOLD activity were termed Quasi-periodic patterns (QPPs) and demonstrate transient, anticorrelated flow of BOLD activity in the TPN and DMN. The principles of the pattern finding algorithm are shown in figure 1-8. First, all preprocessed rsfMRI scans from all subjects within one group are concatenated to create one image series. In step 1, at a random image frame in the image series the consecutive BOLD images are used to create an initial seed-template. The length of this template is based on a predefined window size. In step 2, the template is incrementally shifted along the image series and a mean Pearson correlation is calculated between the BOLD activity in

each voxel of the template and “windowed” image series. Instances when the average

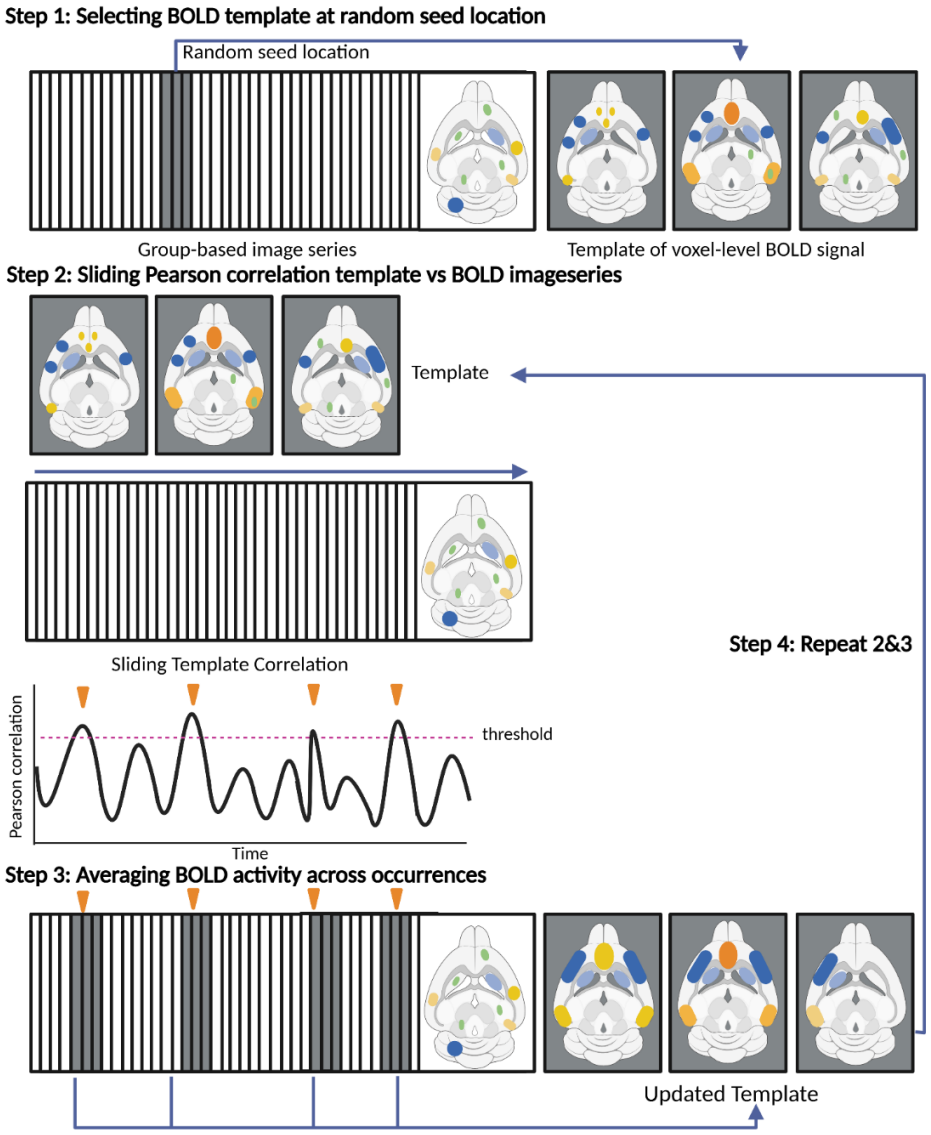

Figure 1-8: Algorithm for the extraction of Quasi-periodic patterns of BOLD activity.

Pearson correlation exceeds the detection threshold (0.2) are saved and for each voxel their BOLD activity for these instances are averaged to update the template (step 3). This updated template is then used to repeat step 2 and 3 until the template does not change between two consecutive runs, resulting in a QPP. The complete process is

repeated with different seed templates starting at a random image frame, to obtain 200 QPPs which are further clustered to get the representative QPPs. These QPP patterns have been demonstrated to be highly similar across species, since these recurrent patterns of BOLD activity involving the DMN and TPN have een observed in humans, rats, mice and monkeys (Figure 1-9).

QPPs have spatial and temporal properties, which might be altered in neurological diseases. Spatial properties involve the extent of spatial activation, whereas examples of the temporal properties of QPPs are the occurrence rate of QPPs and the timing of the peak activity within certain regions during a QPP. Interestingly, spatial and temporal alterations in QPPs have been observed in people with attention deficit hyperactivity disorder (ADHD), specifically in regions known to be disrupted in ADHD, suggesting that QPPs are sensitive to detect network disturbances in neurological disorders.

At present, a large number of studies have been investigating dynamic properties of FC in AD. The first study used SWA to investigate dynamic FC in AD patients. They observed that AD patients spent less time in a brain state where posterior DMN is strongly activated and more time in states with higher anterior DMN function (D. T. Jones et al., 2012). Longitudinal studies investigating dynamic FC across the AD spectrum further demonstrated altered dFC in patients with SCD and MCI in the temporal and frontal networks together with alterations in the DMN. These findings supported the hypothesis that the BOLD oscillatory patterns are progressively altered across the AD spectrum eventually leading to a smaller repertoire of functional states in the brain of AD patients (Cordova-Palomera et al., 2017; Demirtas et al., 2017). In addition, a recent study in patients with SCD, also observed decreased occurrence of a brain state where DMN was activated, while other networks were deactivated (Liang et al., 2021), suggesting that dynamic FC can be used to disentangle network alterations at early stages of AD. Moreover, several studies aiming to use dynamic FC properties as a biomarker for AD were able to discriminate early MCI patients from healthy subjects (X. Chen, Zhang, & Shen, 2016; X. Chen et al., 2017). In addition, our lab has demonstrated that QPP

properties improve classification of a mouse model of amyloidosis (Belloy, Naeyaert, et al., 2018). However, the biological underpinnings of dynamic FC are still poorly understood and disease mechanisms underlying the dynamic FC alterations in AD remain elusive. **One of the aims of this thesis is to use QPP analysis to unravel network dysfunction in AD at presymptomatic stages of AD and to elucidate underlying neuropathological mechanisms to gain a better insight into synaptic dysfunction at early stages of AD.**

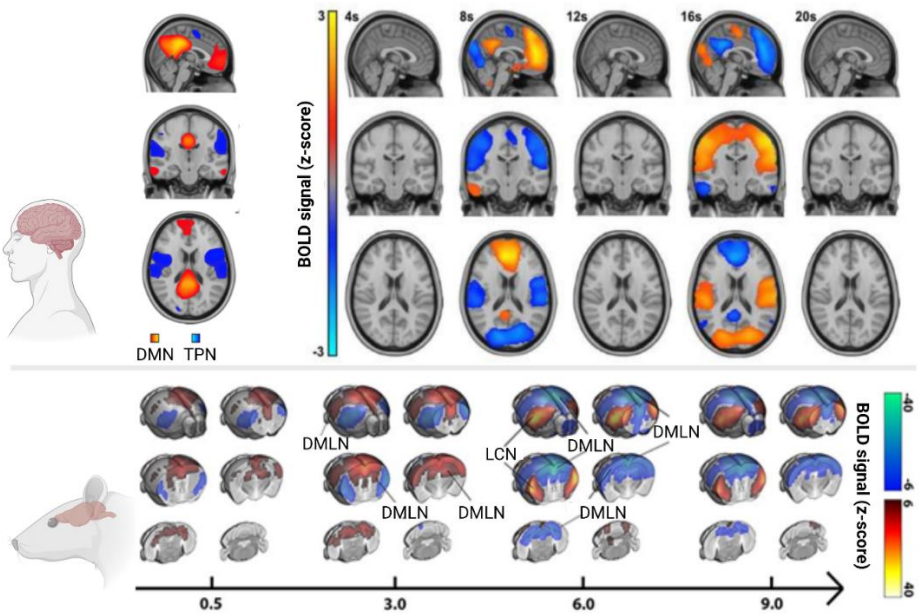

Figure 1-9: Quasi-periodic patterns in humans and rodents. QPPs presented involve regions belonging to the default mode network (DMN) and task positive network (TPN) in humans (top) and their analogues in rodents, default mode-like network (DMLN) and lateral cortical network (LCN) (bottom). Figure adapted from Belloy visual + ADHD abbas

1.2.3 Investigating effects of network specific modulation using rsfMRI

We have described two major networks in the brain that have complex and poorly understood interactions, and which have been shown to be altered in several neurological disorders. The regulation of these networks is still elusive, but researchers

have demonstrated that neuromodulatory systems have important roles in the regulation of whole-brain networks. Neuromodulation is the alteration of neuronal and synaptic properties by neurons and/or by substances released by neurons. One of the main neuromodulatory systems in the brain is the cholinergic system, which uses Acetylcholine (ACh) to modulate neuronal activity. The cholinergic system has been shown to be important in various cognitive functions, such as attention, learning and memory, sleep and consciousness (Alger, Nagode, & Tang, 2014; Bloem, Poorthuis, & Mansvelder, 2014; Hasselmo, 2006; Solari & Hangya, 2018; Vazquez & Baghdoyan, 2001; Zaborszky et al., 2018). The most important source of cholinergic neurons is the basal forebrain (BFB), a heterogenous subcortical region consisting of four nuclei, namely the medial septum (MS), nucleus basalis of Meynert (NBM), the substantia innominate (SI) and the horizontal limbs of the diagonal band of Broca (HDB). Cholinergic neurons originating from these structures project to the complete cortex and hippocampus (Bloem, Schoppink, et al., 2014). Recent studies suggest that the basal forebrain cholinergic system (BFCS) plays an important role in the regulation of whole brain network activity, in particular the DMN (Alves et al., 2019; Chaves-Coira, Martin-Cortecero, Nunez, & Rodrigo-Angulo, 2018; Espinosa, Alonso, Lara-Vasquez, & Fuentealba, 2019; Fritz et al., 2019; Klaassen, Heiniger, Vaca Sanchez, Harvey, & Rainer, 2021; Nair et al., 2018; Turchi et al., 2018).

In AD, imbalance in synaptic function is hypothesized to alter network activity, which in turn drives disease progression. Interestingly, the basal forebrain cholinergic system (BFCS) is one of the first brain systems affected by AD (Cantero et al., 2020; Fernandez-Cabello et al., 2020; Schmitz et al., 2018; Teipel et al., 2022; Teipel, Fritz, Grothe, & Alzheimer's Disease Neuroimaging, 2020). The currently available symptomatic treatments available are aiming to restore this synaptic transmission by increasing cholinergic transmission and/or decreasing glutamatergic transmission. However, these therapeutics only delay the onset of symptoms, possibly due to the fact that the treatment is only started once symptoms are present. Moreover, the current treatments induce side effects due to the fact that the concentration of the targeted

neurotransmitters is increased across the whole brain, while only certain circuits are affected. **Circuit specific restoration of network activity at early stages of AD could be valuable treatments to restore neurotransmission in the brain.**

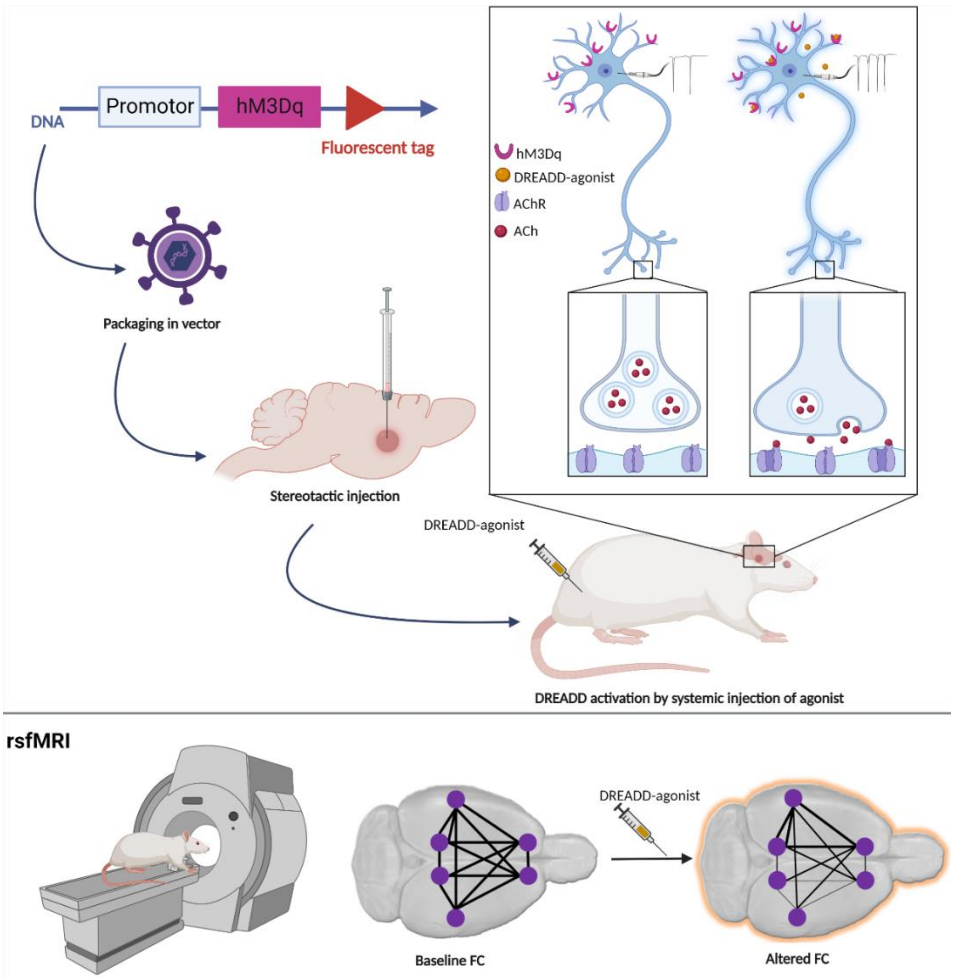

Figure 1-10: Schematic overview of the DREADDs technology for neural modulation. DNA coding for a specific promotor, DREADD receptor (hM3Dq) and fluorescent tag is first packaged into a viral vector, which will be injected into the target brain area during stereotactic surgery. The DREADD receptor can be stimulated by using a selective DREADD-agonist, resulting in an increase in action potentials and release of neurotransmitters such as acetylcholine (ACh) and activation of postsynaptic receptors such as the cholinergic receptors (AChR). This selective modulation of neurotransmission alters activity and functional connectivity (FC) of functional networks, which can be detected using resting state functional MRI (rsfMRI).

To understand the functional organization of the brain, it is essential to discover how neuromodulatory signaling alters whole brain network activity in health and in disease. Several studies have used a combination of pharmacological stimulation with rsfMRI to investigate the effects of activation or inhibition of specific neurotransmitter systems on different resting state networks. However systemic administration of pharmacological compounds induces changes in neurotransmission across the whole brain. Over the past years, several methods have been developed to perform cell-type specific modulation, such as chemogenetics, that allow investigation of the *in vivo* effects of circuit specific activation or inactivation on behavior and/or network activity (Roth, 2016). Chemogenetic tools, such as designer receptors exclusively activated by designer drugs (DREADDs) rely on the viral expression of receptors which respond exclusively to a synthetic ligand (Figure 1-10). DREADDs are used to increase or decrease neuronal activity upon systemic administration of an inert agonist. Combining chemogenetic tools with rsfMRI allows investigation of the effects of circuit specific stimulation on whole-brain network activity, offering important insights into brain function (Kosten, Emmi, Missault, & Keliris, 2022; Peeters, Missault, Keliris, & Keliris, 2020).

1.3 Direct measurements of neuronal activity to evaluate network function

Cognitive processes require the coordination of activity of different neuronal populations, which are widely distributed across the brain. Neuronal activation is marked with an increase of the membrane potential of a neuron. As a result, neuronal activity can be measured invasively at the cellular level (intra- or extracellular neuronal spike recordings), at a local level (local field potentials (LFP)), or even global, at cortical levels (electroencephalograms (EEG)). These techniques offer the advantage, compared to rsfMRI, of acquiring the data at a higher temporal resolution (in ms) and relatively easy interpretation, as these techniques are a direct measurement of potential oscillations. EEG signals can be measured simultaneously across the whole brain.

However, localization of the EEG signal is challenging, limiting the spatial resolution. On the other hand, the spatial information of LFPs is limited, as only a small region can be targeted with the electrodes. However, analysis of LFPs does allow interrogation of specific neuronal circuits. A major confound of rsfMRI in rodents is the need for anesthesia, which limits the direct translation of the results to humans, since rsfMRI in humans is not performed under anesthesia. Moreover, research has demonstrated that different types of anesthesia affect the neurovascular coupling and therefore, the BOLD response, which further hampers the biological interpretation of BOLD alterations. **EEG and LFP recordings can be performed while animals are freely moving, offering the opportunity to interrogate network function during different behavioral states. This can provide valuable insights into network dysfunction during different types of behavior, and provide further knowledge about how this impairment of neuronal activity is linked with symptoms of AD.**

1.3.1 Electroencephalography (EEG)

Electroencephalography or EEG is a technique which uses electrodes placed on the scalp of a patient, to measure electrical activity in the brain. When an action potential (strong depolarizing membrane potential) arrives at the presynaptic terminal, neurotransmitters are released in the synaptic cleft. These neurotransmitters will bind to their receptor which is located on the membrane of the postsynaptic neuron, where it will open an ion channel. Based on the type of synapse (excitatory or inhibitory), a net inflow of positively charged or negatively charged ions will enter the neuron, either creating a depolarization (EPSP) or hyperpolarization (IPSP) of the membrane potential of the postsynaptic neuron (Figure 1-11A). The summation of these postsynaptic potentials is the basis for the EEG signal. The local intraneuronal depolarization caused by an EPSP creates a relative negatively charged extracellular environment around the soma of the neuron. Which in turn creates a relatively positively charged extracellular environment around the apical dendrite of the neuron, hence creates a change in potential at the brain surface (Figure 1-11B). The constant excitation and inhibition of

cortical neurons leads to constantly varying local oscillations in potential on the surface of the brain, that are measured with EEG.

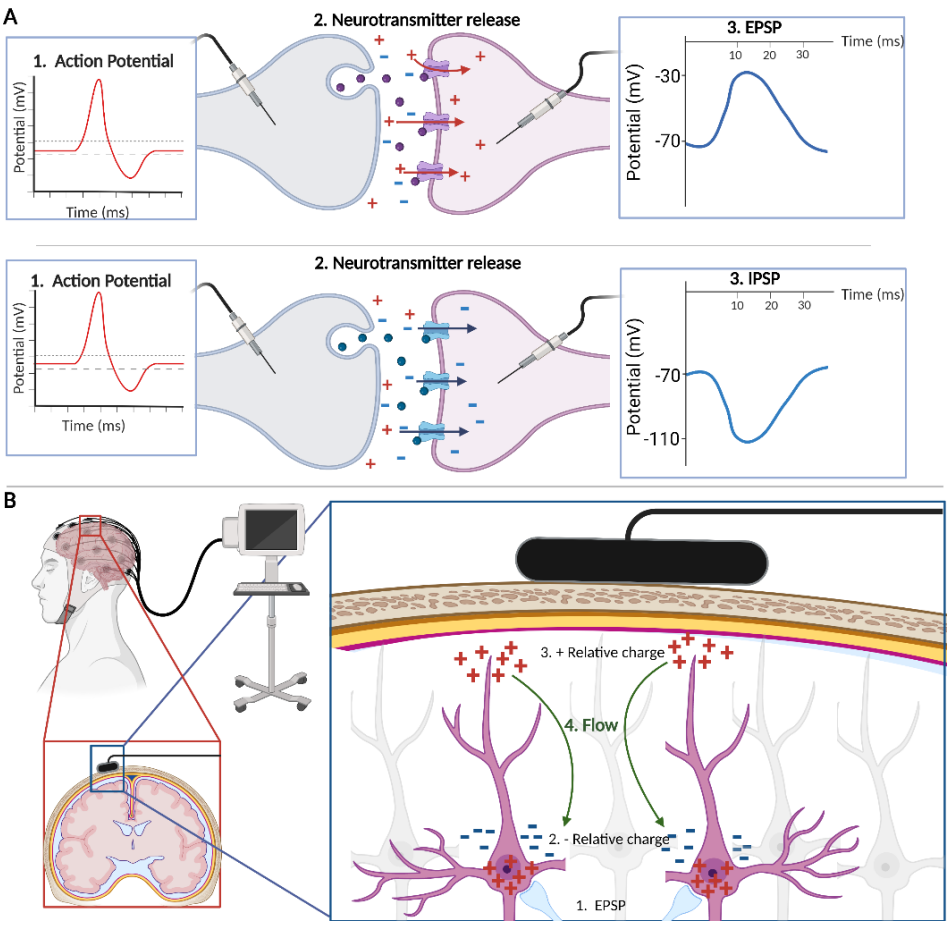

Figure 1-11: Basis of neurotransmission and EEG signal. A) Action potentials induce neurotransmitter release at the presynaptic terminal of the synapse. These released neurotransmitters bind to their respective ionotropic receptors, which facilitate flow of ions to the inside of the postsynaptic neuron. The inflow of charge creates either a slow depolarization (excitatory postsynaptic potential EPSP) or hyperpolarization (inhibitory postsynaptic potential IPSP) of the membrane potential. This local intracellular change in charge induces a change in the relative charge of the extracellular matrix surrounding the soma of the neuron. Therefore, the apical dendrite of the neuron is positively charged. This constantly changing charge at the surface of the brain is the signal measured with EEG.

The brain oscillations measured with EEG have different frequencies and the power of these different frequencies are heavily dependent on the location where the EEG is measured, and behavioral state. The main frequency bands of human EEG are delta (0.5-4 Hz), theta (5-8 Hz), alpha (8-13 Hz), beta (14-30 Hz) and gamma waves (30-120 Hz). Healthy aging causes changes in the activity of the brain that are reflected in EEG recordings and include a reduction in the amplitude of alpha activity (8–13 Hz), and an increase in delta (1–4 Hz) and theta (4–8 Hz) power (Ishii et al., 2017). Research has demonstrated that physiological EEG variations are pathologically exacerbated in AD patients. EEG anomalies in AD patients can be grouped into three categories: change in frequency pattern, reduction in the complexity, also known as the non-linearity, of EEG signals, and perturbation in EEG synchrony across regions (Monllor et al., 2021). In MCI and AD patients, a "slowing of the EEG signal" is observed, where the power of alpha and beta rhythms are decreased, while the power of delta and theta oscillations are increased (Monllor et al., 2021). This deceleration has been shown to be correlated with cognitive performance, disease severity and severity of AD pathology such as amyloidosis and tauopathy (Monllor et al., 2021).

EEG signals are caused by the interaction of different sources of oscillations. Therefore, non-linear analysis methods have been introduced to study the EEG signals and to quantify the complexity of the EEG signals (Dringenberg, 2000). The complexity of the EEG signals are thought to reflect the amount of information that is integrated within a neural system (Tononi, Edelman, & Sporns, 1998). Research has demonstrated that the complexity of the EEG signals in patients with MCI and AD decreases, suggesting altered information processing. This decreased complexity is thought to be related to the EEG slowing, since this deceleration lowers the complexity of the EEG signals (Dauwels et al., 2011). Synchronization between spatially distinct neuronal populations reflects the interaction between neural networks, which can be quantified with spectral coherence. This coherence is quantified by the spectral covariance of oscillatory activity between two spatially separated electrode locations. Research has demonstrated that resting-state EEG coherence is reduced for faster rhythms, but increased for slower EEG rhythms

in AD patients compared to healthy controls (Locatelli, Cursi, Liberati, Franceschi, & Comi, 1998). In addition, several studies observed altered direction of information flow, suggesting that the AD pathology affects both coherence and directionality of information flow across the brain (Babiloni et al., 2009).

EEG is measured on the scalp, which acts as a lowpass filter, reducing the detectability of high frequency oscillations. Moreover, even though it's common practice in human research, results obtained from EEG are not specific to certain diseases, especially since the lack of spatial information. However, in preclinical models, we have the opportunity to measure neuronal signals on a more sensitive scale which allows us to detect fast oscillatory events at specific regions in the brain by using an invasive technique called electrophysiology. Here, an electrode will be placed in the brain tissue, to directly measure the relative changes in extracellular potentials, so-called local field potentials (LFPs), which allows the detection of higher frequency oscillations (<300Hz). Moreover, activity of individual neurons, which is measured as fast spikes (>1000 Hz) in the raw signals, can be observed, if the electrode is placed in close proximity to a neuron. This allows direct investigation of neuronal spiking activity. An advantage of electrophysiology is that this technique allows targeting of specific circuits, depending on where the electrode is placed. This could offer novel insights into neuronal activity during specific tasks in, for example, memory related circuitry.

1.3.2 *In vivo* electrophysiology of the hippocampal circuit

One of the main brain regions involved in memory is the hippocampus, which is located in the medial temporal lobe. Previous research evaluating local field potentials and neuronal activity during different hippocampal dependent behaviors, has elucidated several aspects of how the brain is coding (spatial) memories. Investigating hippocampal electrophysiology offers opportunities to investigate alterations in the memory related circuitry in neurological disorders, such as AD. The hippocampus is imperative for healthy memory function, and damage to the hippocampus is known to severely impair short-term and long-term episodic memory, and spatial memory formation. This

organized brain structure is highly similar across species and consists of several subfields, the CA1, CA2, CA3 and CA4 and the dentate gyrus (DG) (Figure 1-12A). Each of these subfields have a very distinct structure, consisting of several layers which each contain different neurons or neuronal structures belonging to specific pathways. The main neuronal pathway in the hippocampus is the tri-synaptic pathway, which conveys input from the entire brain to the hippocampus in a cortico-hippocampal loop. The signals from the cortical regions enter the hippocampus through the entorhinal cortex (Ent). Projections originating from the Ent to the DG form the perforant pathway (Figure 1-12B). These fibers form synaptic connections onto the dendrites of the granular neurons of the DG. This information is further transported through the so-called mossy fibers projecting to pyramidal neurons in the CA3 layer. The pyramidal neurons relay this information to the pyramidal neurons in the CA1 layer though the Schaffer collaterals. CA1 pyramidal cells provide the final output to the entire cortex through projections back to the Ent (Buzsaki et al., 2003; Colgin et al., 2009; Deng, Aimone, & Gage, 2010; Kitabatake, Sailor, Ming, & Song, 2007; Strange, Witter, Lein, & Moser, 2014).

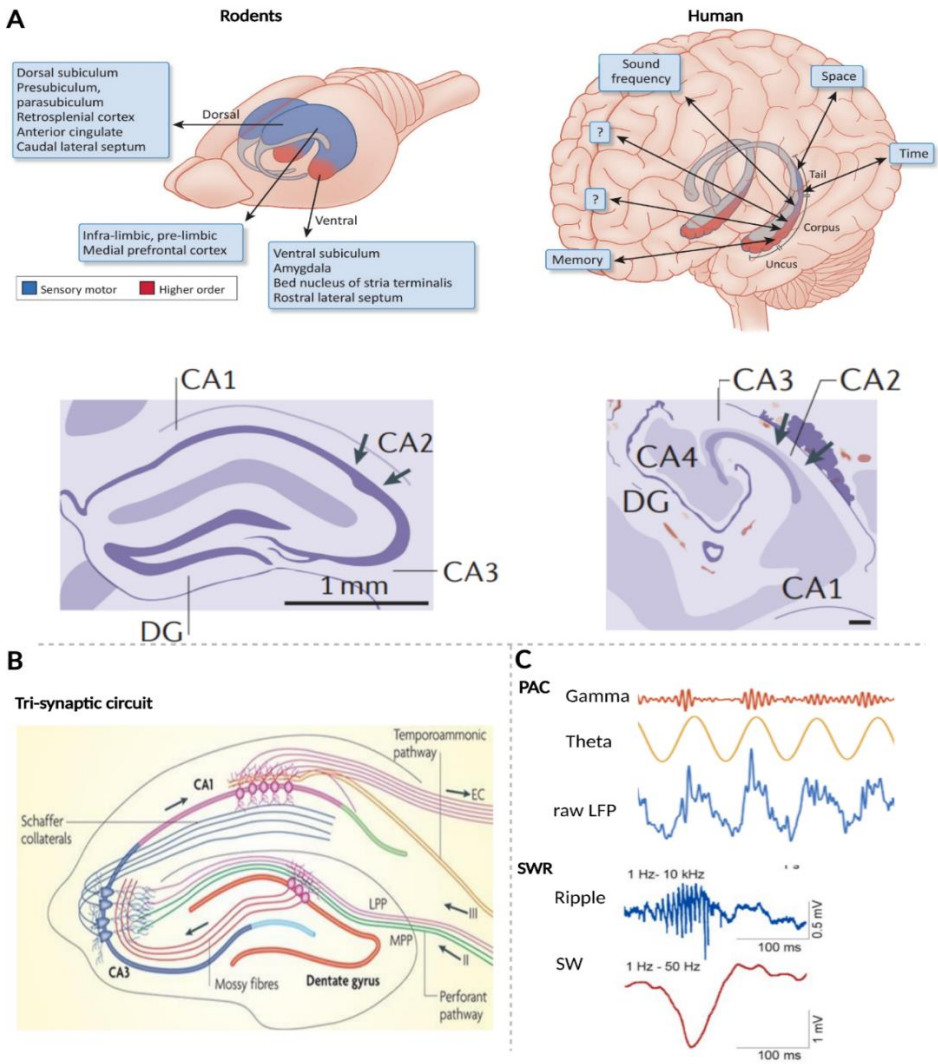

Figure 1-12: Anatomy of the hippocampus in rodents and humans. A) The hippocampus of rodents (left) versus the hippocampus in humans (right). The bottom panels show the different subfields of the hippocampi. B) The rodent tri-synaptic pathway as depicted by solid arrows. C) Hippocampal oscillatory characteristics. Gamma amplitude (red) is modulated by theta phase (yellow). The raw trace is shown in blue. Example of a SWR event in the rat hippocampus. Figure adapted from (Buzsaki & Tingley, 2018; Colgin et al., 2009; Deng et al., 2010; Strange et al., 2014).

The well-defined circuitry and its lamellar organisation makes the hippocampus an ideal region to study the mechanisms of network oscillations and therefore, oscillatory

activity within the hippocampus has been extensively studied (Figure 1-12C). The oscillatory activity in the hippocampus is characterized by different types of oscillations, which are in part also occurring in the cortex. The most prominent hippocampal brain activity is rhythmic theta activity in the frequency range between 5-12 Hz, which is dominant during rapid eye movement sleep (REM), grooming and movement. Theta oscillations within the hippocampus are highly synchronized with theta oscillations across cortical regions such as the somatosensory cortex and frontal cortices (Bland & Oddie, 2001; Solomon et al., 2017). These hippocampal theta oscillations have been linked to attentional processes, information processing, cognition, and higher brain functions (Bland & Oddie, 2001; Buzsaki et al., 2003; Z. Gu & Yakel, 2022; Hasselmo, 2006; Solomon et al., 2017). GABAergic neurons in the medial septum (MS), one of the BFB nuclei, target inhibitory interneurons in the hippocampus and induce rhythmic disinhibition of the pyramidal neurons in the hippocampus, therefore generating the theta rhythm. In addition, the theta rhythm is regulated by cholinergic projections originating from the MS (Buzsaki et al., 2003; Colgin, 2016; Z. Gu & Yakel, 2022; Somogyi, Katona, Klausberger, Lasztoczi, & Viney, 2014; Stoiljkovic, Kelley, Nagy, & Hajos, 2015). Studies in patients suffering from AD have demonstrated that alterations in power oscillations are heavily dependent on the disease stage. Studies in animal models of AD observed decreases in theta power at different stages of AD, which have been correlated to memory deficits and are thought to be caused by functional impairment of GABAergic septal hippocampal neurons by soluble Aβ (Caravaglios et al., 2010; Nimmrich, Draguhn, & Axmacher, 2015; Scott et al., 2012; Stoiljkovic et al., 2016; Stoiljkovic, Kelley, Horvath, & Hajos, 2018; Stoiljkovic et al., 2019; Villette et al., 2010; J. Wang et al., 2017).

A second prominent hippocampal rhythm are gamma oscillations (25-150Hz) which have been demonstrated to be involved in memory encoding and memory retrieval (Buzsaki et al., 2003; Colgin, 2016; Trimper, Galloway, Jones, Mandi, & Manns, 2017). Gamma frequencies can be divided in two brain rhythms, based on its origin and the frequency. Activity in the lower frequency ranges (25-55 Hz) have been termed slow gamma oscillations and are driven by the CA3 region. These oscillations synchronize CA1 and

CA3 activity, thereby supporting memory retrieval. Fast gamma oscillations (60-160 Hz) are driven by the Ent and synchronize CA1 activity with Ent activity, supporting memory encoding (Colgin et al., 2009). Gamma oscillations are generated by inhibitory interneurons in the hippocampus. In healthy subjects and animals, an increase in the power of slow and fast gamma oscillations is observed during memory encoding, sensory processing and wake immobility (Bragin et al., 1995). This increase in gamma power appears to predict if memory formation will be successful in humans but also in mice (Matsumoto et al., 2013; Palop & Mucke, 2016; Sederberg et al., 2007). A number of studies have reported conflicting observations regarding gamma oscillations in patients (Basar, 2013). These divergent findings are thought to be caused by methodological differences, and the difficulty to measure these high frequency oscillatory events through the skull using EEG (Basar, 2013; Byron, Semenova, & Sakata, 2021; Nimmrich et al., 2015). Electrophysiological measurements in different mouse models of AD observed decreased gamma power in animal models for AD, suggestive of cognitive deficits (Carr, Karlsson, & Frank, 2012; Gillespie et al., 2016; Nakazono, Jun, Blurton-Jones, Green, & Igarashi, 2018).

The amplitude of the hippocampal gamma rhythm is modulated by the phase of theta, a phenomenon named phase-amplitude coupling (PAC) (Figure 1-12C). Theta driven modulation of gamma oscillations has been thought to play an important role in the execution of cognitive functions. The strength of the PAC has been shown to increase during learning. Moreover, the PAC strength is also directly correlated with an increased chance of correctly performing a cognitive task, suggesting that PAC facilitates the transfer of information in the brain (Fell & Axmacher, 2011; Kitchigina, 2018; Tort, Komorowski, Eichenbaum, & Kopell, 2010; Tort, Komorowski, Manns, Kopell, & Eichenbaum, 2009). In patients with AD-related dementia and MCI, a decreased theta-gamma PAC was observed when compared with healthy subjects, which worsened as the disease progressed (M. S. Goodman et al., 2018). Similar decreases of theta-gamma PAC have been observed in rodent models for AD. Interestingly, impairment of theta-gamma PAC can already be observed before the onset of Aβ plaque formation in the

APP23 mice and in (Aβ overexpressing) TgCRND8 mice (Goutagny et al., 2013; Kitchigina, 2018), suggesting early synaptic dysfunction within the hippocampal circuitry.

Another hippocampal oscillatory event is the sharp-wave ripple (SWR), which consists of a high frequency ripple oscillation (150-250 Hz) in the pyramidal layer of the CA1 region, together with a sharp wave (15Hz) in the stratum radiatum of CA1 (Figure 1-12C). These LFP patterns are mainly observed during wake immobility, slow wave sleep and consummatory behavior. SWRs are thought to be the hallmark of memory replay, as during a SWR, large populations of pyramidal neurons are activated, often in sequences that recapitulate past or potential future experiences (Buzsaki, 2015; Colgin, 2016). The sharp waves and ripples are thought to be separate events with distinct origins. The sharp waves are excitatory events originating from the CA3, which induce locally generated ripple oscillations in the CA1 pyramidal layer. The ripple events are generated by a delicate interaction between excitatory pyramidal neurons and local GABAergic interneurons that, if disrupted, can lead to pathological forms of activity which impair memory processes (Buzsaki, 2015; Buzsaki et al., 2003; Caccavano et al., 2020; Colgin, 2016; Sanchez-Aguilera & Quintanilla, 2021; Zhen et al., 2021). Research has shown that several features of SWR are altered in advanced stages of AD. SWR abundance, peak spectral frequency (PSF) and amplitude was decreased in several animal models of AD (Benthem et al., 2020; Caccavano et al., 2020; Fernandez-Ruiz et al., 2019; Gillespie et al., 2016; Oliva, Fernandez-Ruiz, Fermino de Oliveira, & Buzsaki, 2018; Sanchez-Aguilera & Quintanilla, 2021; Stoiljkovic et al., 2019; Witton et al., 2016; Zhen et al., 2021). However, these studies focussed on advanced stages of AD. Early synaptic dysfunction is known to induce hyperexcitability in cortical and subcortical circuits, which could interfere with SWR activity.

1.4 Brainstates and behavioral states

The activity of the brain is constantly wandering between states, and this affects not only our responses to sensory inputs, but also our ability to process the constant flow of information, make decisions, and take appropriate actions. We are always checking our

surroundings, constantly interpreting all sensory input, to predict and be able to react if the situation is dangerous or not. To adequately meet these demands, humans and animals must continuously integrate sensory input, memories, expectations, and motor commands. As mentioned earlier, researchers observed that even during rest, the brain is highly active and several networks are continuously activating and deactivating (Vidaurre, Smith, & Woolrich, 2017). These fluctuations of brain activity are not random noise, but they represent the various needs of the central nervous system, and they are tightly linked to the behavioral state the subject is in. You can think of the state of the brain as a dot in a high dimensional space, where each position corresponds to activity of relevant neurons or brain regions (Figure 1-13A). This dot will move through this space over time, but not all locations will be visited as often as others, creating a number of discrete brain states which are tightly linked with behavioral variations in arousal, attention, and movement (McCormick, Nestvogel, & He, 2020). Each brain state is characterized by distinct patterns of neuronal activation and EEG signatures, and different neuronal systems are active during different behavioral states (Figure 1-13). These alterations in neuronal activity are also reflected in local field potentials. The next chapters will discuss different behavioral states, their LFP characteristics and EEG/LFP alterations observed in AD. The first section will describe the awake state, which is divided into active wake and wake immobility (1.4.1), after which two behavioral states occurring during sleep, non-rapid eye movement sleep (NREM) and rapid eye movement sleep will be described (REM) (1.4.2).

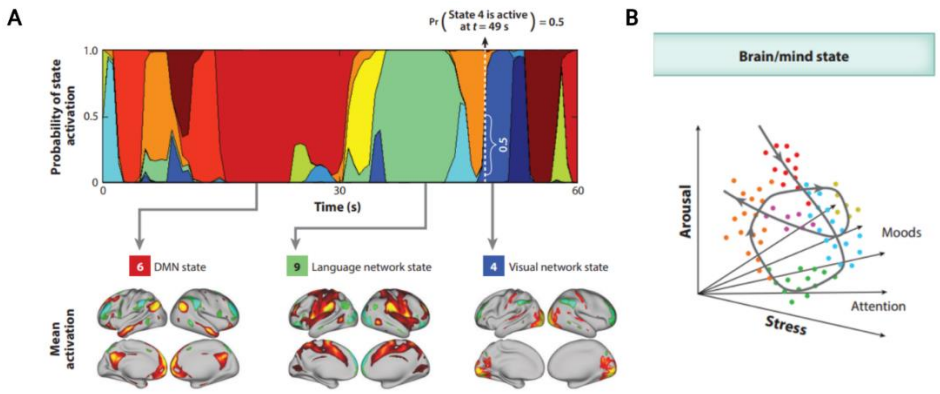

Figure 1-13: Behavior and brain activity move through preferred states. A) Continuously varying brain states in human fMRI activity. This is an example of the different fMRI states in one human subject for 60 seconds (top). Each state is characterized by the mean activation (bottom). B) The principle of brain states representing a dot moving through a high dimensional space, would result in clouds of preferred brain states. DMN = default mode network. Figure adapted from (McCormick et al., 2020; Vidaurre et al., 2017)

1.4.1 Awake behavioral states

As mentioned before, cyclic alterations in brain states occur while subjects are awake and represent the integration of sensory and emotional information to continuously interpret the surroundings. Brain activity is highly dependent on vigilance state and arousal, for example, brain oscillatory activity during exploration of a novel environment is different than oscillatory activity when a subject is at rest. Awake behavioral states can be divided into active wake and wake immobility and both states are characterized by fast, desynchronized cortical activity and a high muscle tone (Figure 1-14). EEG activity during active wake, for example while a subject is involved in a spatial memory task, is characterized by high cortical activation, where faster frequencies like beta and gamma dominate the cortical EEG. In the hippocampus, theta waves and gamma waves are the most dominant frequencies. This allows the subject to integrate all sensory inputs and for example, store spatial information. Wake immobility is when a subject is at rest and is characterized by a reduction in sensory processing. Wake immobility facilitates memory through activity consolidation mechanisms, similar to when a subject

is asleep. EEG activity is dominated by slower waves, such as alpha waves, delta waves and theta waves (Brokaw et al., 2016). Within the hippocampus, electrophysiological correlates of memory consolidation, such as Sharp-wave ripples, have been observed in rodents and humans during wake immobility (Axmacher, Elger, & Fell, 2008; Carr, Jadhav, & Frank, 2011). These characteristics in oscillatory activity during these two behavioral states are caused by differences in the delicate interplay of several wake- and arousal promoting neurotransmitter systems. Peripheral stimuli activate glutamatergic neurons in the reticular formation and ascending reticular activating system in the brainstem, which project to either the nucleus intralaminari of the thalamus (dorsal pathway) or to the BFB, hypothalamus, and cortex (ventral pathway) to mediate cortical activation and arousal (Figure 1-15). Several neurotransmitter systems are involved in the regulation of wake, which will be discussed in the next paragraph as separate entities (table 1-1). However, we should keep in mind that these systems are likely to interact with each other given their anatomical connections and similar targets.

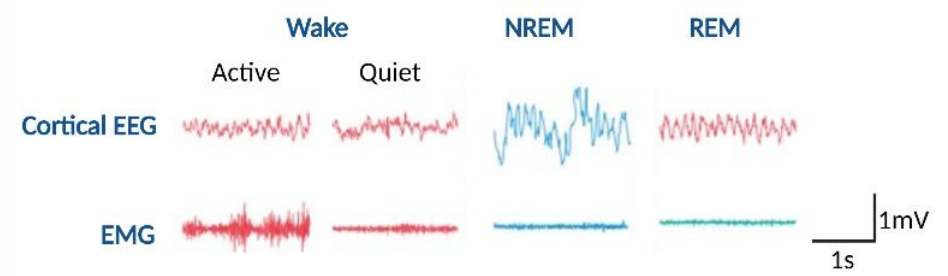

Figure 1-14: EEG and electromyography (EMG) characteristics different behavioral states. Wakefulness is separated in active wake and wake immobility. Active wake is characterized by desynchronized cortical activity and high muscle tone, in contrast, during wake immobility muscle tone is decreased. During NREM sleep, synchronized, high amplitude, slow EEG activity can be observed, together with a low EMG signal. During REM Sleep, cortical desynchronization can be observed in the absence of EMG activity. Figure adapted from (B. E. Jones, 2020)

Wake-promoting monoaminergic neuron types produce noradrenaline (NA), serotonin (5-HT), dopamine (DA) and histamine and they directly innervate the cortex, BFB and lateral hypothalamus. The highest firing rates of these monoaminergic neurons are

observed during active wake, while the firing rate lower NREM sleep, and almost completely silent during REM sleep. (B. E. Jones, 2005, 2020; Scammell, Arrigoni, & Lipton, 2017). The locus coeruleus (LC) is the source of NA in the brain. The LC has been implicated to play an important role in the large-scale reorganization of networks in response to surprise, which is crucial for behavioral adaptation and the switching between exploration and exploitation behaviors (Avery & Krichmar, 2017). Serotonin is produced in the raphe nuclei and has been demonstrated to promote wakefulness. However, these neurons are also important regulators of mood and reward, and further work is needed to define the specific conditions during which they contribute the most to arousal (Scammell et al., 2017). Dopamine (DA), another monoaminergic neurotransmitter is released from the ventral tegmental area, substantia nigra and periaqueductal gray. DA agonists have been demonstrated to increase wakefulness, while lesioning of DA circuits reduces it. However, DA neurons do not show the traditional firing rate pattern observed in the other monoaminergic wake-promoting regions as the firing rate of dopaminergic neurons is not the highest during the awake state. Research has demonstrated that DA signaling induces wakefulness especially under conditions of high motivation (Eban-Rothschild, Rothschild, Giardino, Jones, & de Lecea, 2016; Scammell et al., 2017). The tuberomammillary nucleus (TMN) is the sole source of histamine in the brain. Antihistaminic drugs have been shown to induce drowsiness and histaminergic neurons in the TMN have high firing rates during awake states (Scammell et al., 2017).

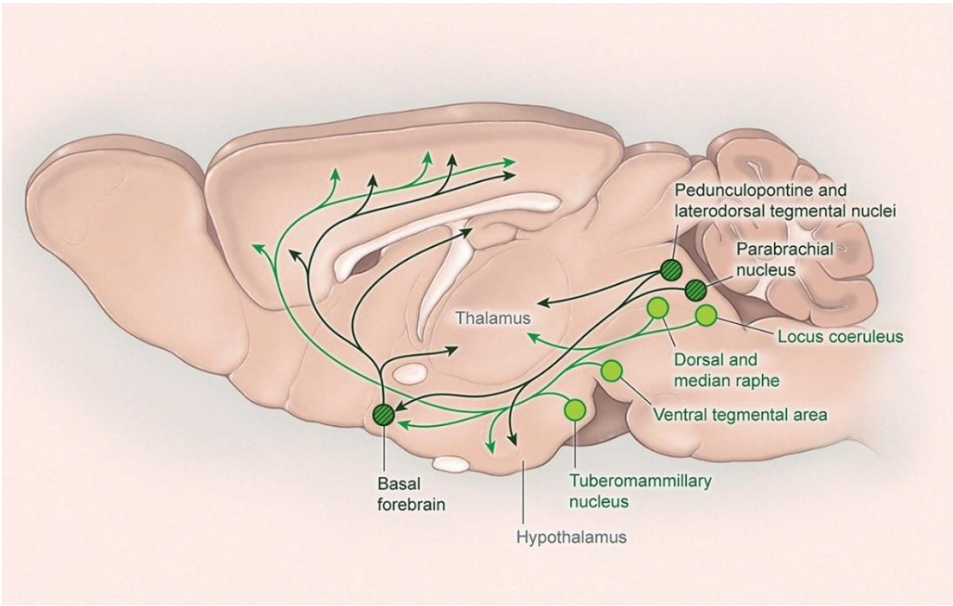

Figure 1-15: Wake promoting pathways. Several neurochemical circuits promote arousal and desynchronized cortical activity which is observed during wakefulness. Monoaminergic neurons (light green) directly innervate the cortex as well as several subcortical regions including the thalamus and hypothalamus. Wake promoting signals also arise from the parabrachial nucleus and cholinergic nuclei in the brainstem and the basal forebrain (Dark green). Figure adapted from (Scammell et al., 2017).

The BFB is a subcortical brain region which contains GABAergic, glutamatergic, and cholinergic neurons (see 1.2.3). The cholinergic neurons in the MS and NBM innervate the hippocampus and the entire cortex respectively and have been demonstrated to be strongly involved in various cognitive processes, such as attention, memory, sensory processing, and cortical plasticity (Gielow & Zaborszky, 2017; Lin, Brown, Hussain Shuler, Petersen, & Kepecs, 2015). Moreover, research consistently demonstrates that BFB cholinergic neurons promote fast cortical activity, however, it is less clear if these neurons are necessary for wakefulness itself. In contrast, GABAergic neurons in the BFB are strongly wake promoting, since stimulation of these neurons dramatically increases wakefulness for several hours by reducing activity of cortical inhibitory neurons (Anaclet et al., 2015). The role of glutamatergic BFB neurons is less understood, but they do seem

to promote cortical activation through projections to cortical and subcortical arousal-promoting regions.

Orexins are neuropeptides produced by the lateral hypothalamus (LH) which are essential for the regulation of wakefulness and REM sleep. Orexinergic neurons innervate all wake-promoting brain regions and the cortex, where they excite target neurons (Figure 1-16). Firing rates of these neurons are highest during wakefulness, especially during periods of high locomotor activity. Suppression of orexinergic neurons increases wakefulness and decreases REM sleep for several hours (Adamantidis, Zhang, Aravanis, Deisseroth, & de Lecea, 2007; Sasaki et al., 2011). Orexin signaling mainly induces arousal in response to homeostatic challenges. Food deprivation for example, increases wake and encourages locomotor activity to promote foraging (Yamanaka et al., 2003).

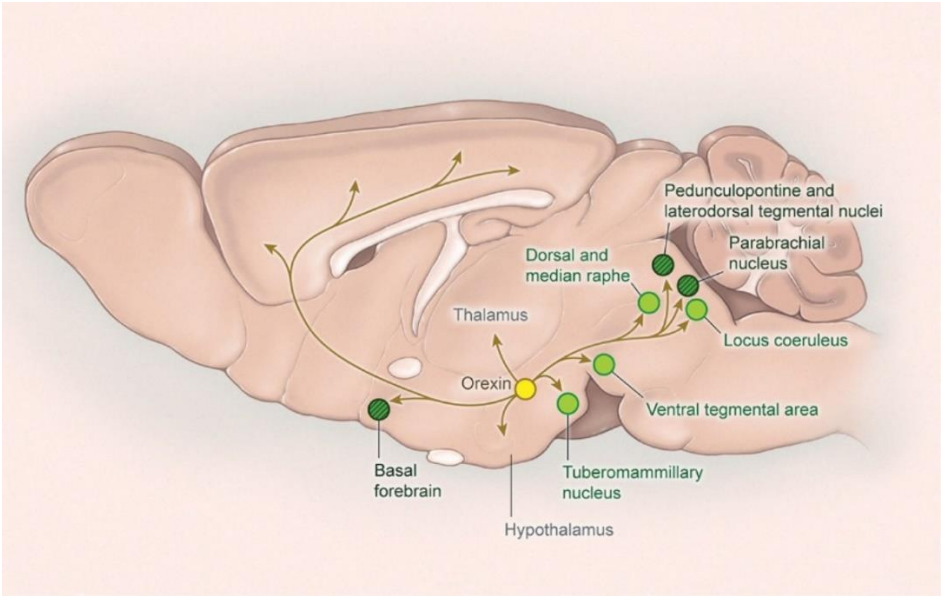

Figure 1-16: Projections of the Orexin Neurons. Orexin is produced in the lateral hypothalamus which projects to neurons in the cortex, thalamus, and all wake-promoting areas. Figure adapted from (Scammell et al., 2017)

In AD, several of the aforementioned neurotransmitter systems are affected at different stages of the disease. Research has demonstrated that the BFB is one of the first brain

regions affected by AD and mainly the cholinergic neurons residing in the BFB are very vulnerable for AD related pathology (Cantero et al., 2020; Fernandez-Cabello et al., 2020; Kilimann et al., 2014; Scheef et al., 2019; Schmitz et al., 2018). Moreover, accumulation of tau starts in the LC, where it is known to interfere with noradrenergic signaling (A. M. Goodman et al., 2021; Kelly et al., 2019; Rorabaugh et al., 2017). Altered noradrenergic signaling is associated with impaired cognition, and pharmacological modulation of NA concentrations in the brain have been demonstrated to improve cognition in animal models of AD (Rorabaugh et al., 2017). The relationship between orexin and AD has been mostly discussed in the context of AD related sleep disturbances. Dysregulation of orexin concentrations in the cerebrospinal fluid (CSF) have been observed in AD patients, where increased orexin was observed at late stages of AD, which was associated with decreased sleep efficiency and REM sleep disturbances (F. Gao, Liu, Tuo, & Chi, 2021). In addition, orexin receptor antagonists have been demonstrated to improve sleep quality and reduce AD pathology (Duncan et al., 2019; Zhou et al., 2020). The aforementioned results demonstrate that several neurotransmitter systems are impaired in AD. However, the relative contribution of the different systems to network dysfunction and behavioral alterations remains poorly understood, especially at presymptomatic stages of AD. **Detection of these disturbances in neurotransmission could aid in the early detection of AD and could provide important novel insights into therapeutic strategies to restore neurotransmitter imbalance at preclinical stages of AD.**

Table 1-1: Brain regions and neurotransmitters involved in sleep/wake regulation

BRAIN REGION	NT	BEHAVIORAL STATE				FUNCTION
		Active Wake	Wake immobility	NREM	REM	
BASAL FOREBRAIN	ACh	+++	+	---	+++	Cortical activity /desynchronization
BASAL FOREBRAIN	GABA	+++	+	---	+++	Cortical activity /desynchronization, wake promoting
BASAL FOREBRAIN	GLUT	+	+	---	+	Cortical activity /desynchronization
BRAINSTEM (PONS)	ACh	+++	+	---	+++	Cortical activity /desynchronization, wake promoting
LOCUS COERULEUS	NE	+++	+	---	Silent	Increased vigilance and attention to stimuli
RAPHE NUCLEI	5-HT	+++	+	---	---	Cortical activation, locomotion
TUBERO MAMILLARY NUCLEUS	Hist	+++	+	---	Silent	Cortical activation (direct and indirect through cholinergic system)
LATERAL HYPOTHALAMUS	Orexin	+++	+	---	Silent	Cortical activation (direct and indirect through regions involved in arousal)
VLPO	GABA	---	-	+++	+++	Inhibition arousal-promoting areas
SLD	Glut	---	---	---	+++	REM promoting region

NT = neurotransmitter, VLPO = ventrolateral preoptic area, ACh = acetylcholine, NE = noradrenaline, 5-HT = serotonin, GABA = y-aminobutyric acid, Hist = Histamine, Glut = glutamatergic, VLPO ventrolateral preoptic area, SLD = sublaterodorsal nucleus, RF = reticular formation, , NREM = Non rapid eye movement, REM = rapid eye movement. Table adapted from (Franco-Perez, Ballesteros-Zebadua, Custodio, & Paz, 2012)

1.4.2 Sleep

Sleep is a complex behavioural state defined by the complete loss of behavioural control and consciousness. It is essential for many vital functions including development, energy conservation, brain waste clearance, modulation of immune responses and cognition (Zielinski, McKenna, & McCarley, 2016). Sleep is characterized by the cyclic occurrence of non-REM (NREM) sleep, which induces slow wave sleep (SWS) and REM sleep (Figure 1-17). Daily cycles of wakefulness and sleep are tightly regulated by interactions between wake promoting and sleep promoting neural circuitry. During wakefulness,

cholinergic neurons in the brainstem and BFB, noradrenergic neurons in the LC, serotonergic neurons in the raphe nuclei and orexinergic neurons in the lateral hypothalamus stimulate cortical activation and behavioural arousal (Table 1-1, Figure 1-17B). Each of these neuronal populations modulates different aspects of wakefulness-related functions in the brain.

Transitions from wakefulness to sleep occur due to inhibition of these arousal systems by GABAergic projections originating from the ventrolateral preoptic area (VLPO). Reciprocal inhibitory connections between the VLPO and arousal systems create a flip-flop mechanism which allows fast transitions between sleep and wake. During prolonged periods of wakefulness, metabolic products, mainly adenosine originating from astrocytes, build up in the interstitial fluid of the brain, which activated the VLPO. This activation of the VLPO inhibits the arousal related regions, inducing sleep. Orexinergic neurons in the LH, which receive homeostatic input regarding hunger, satiety, and circadian rhythm, are able to re-activate the arousal related regions in response to homeostatic needs, such as hunger. This activation of arousal system inhibits the VLPO, causing awakening of the subject (Brown, Basheer, McKenna, Strecker, & McCarley, 2012; Franco-Perez et al., 2012; W. Boron, 2016; Zielinski et al., 2016).

In addition to the sleep/wake flip-flop system, a REM-on/REM-off system is present in the brain. This system regulates the switch between NREM and REM through reciprocal inhibitory connections between the ventrolateral periaqueductal grey matter (vlPAG), the REM-off centre and the sublaterodorsal nucleus (SLD), REM-on centre (Figure 1-17C). The SLD sends projections to the cholinergic neurons in the BFB and pontine nuclei, inducing cortical arousal and genital activity associated with REM sleep. Moreover, neurons in the SLD innervate inhibitory interneurons, which inhibit spinal motor neurons, causing REM associated muscle atonia. Signals from the LH in response to homeostatic inputs inhibit the vlPAG, therefore promoting wakefulness (Brown et al., 2012; Herice, Patel, & Sakata, 2019; W. Boron, 2016; Weber & Dan, 2016).

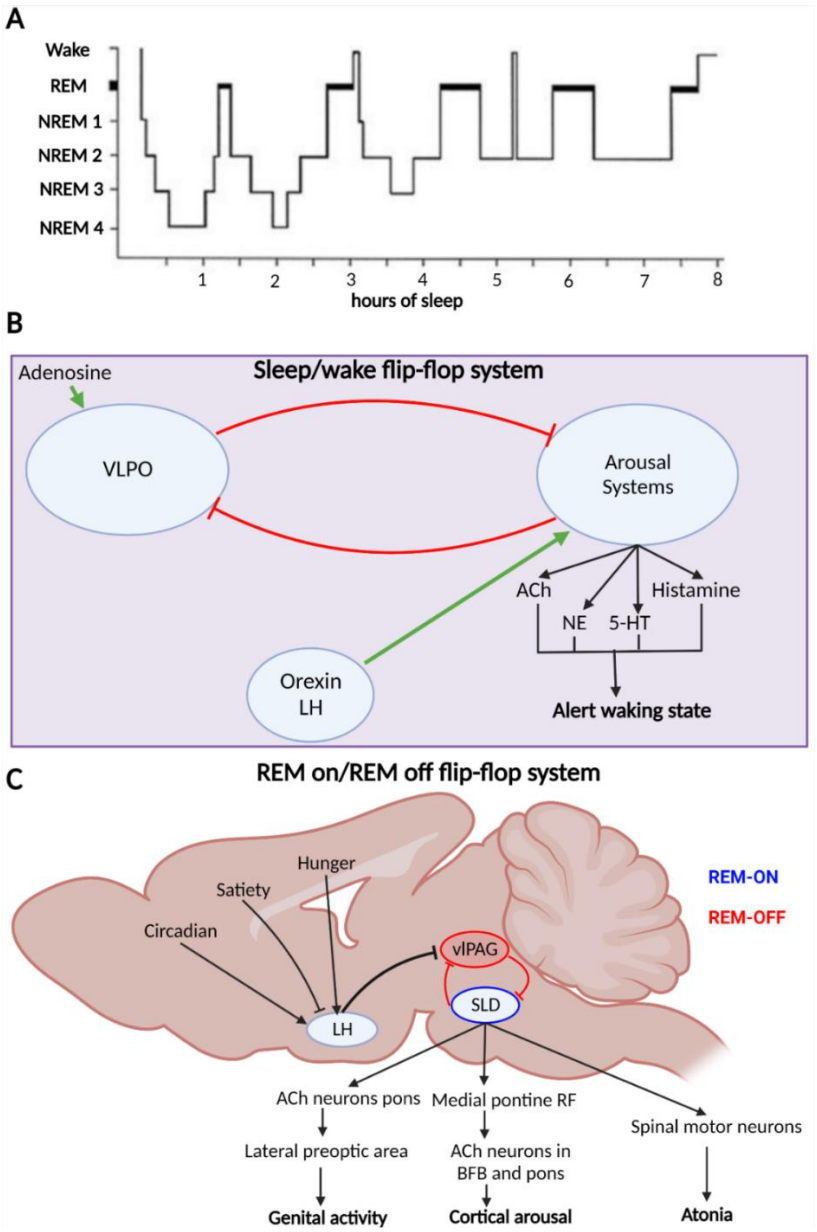

Figure 1-17: Sleep architecture and regulation. A) Human sleep architecture showing the cyclic patterns of REM and different NREM stages during sleep. B) The sleep/wake flip-flop system which uses reciprocal inhibitory connections between the sleep promoting VLPO and wake promoting arousal systems. Orexinergic signaling from the LH stimulates arousal systems, while adenosine, a product produced in astrocytes during prolonged wakefulness, simulates the VLPO. C) The REM on/REM off flip-flop system uses reciprocal inhibitory connections between the REM-off center

(vlPAG) and REM-on center (SLD). Excitatory projections from the SLD target cholinergic neurons in the pons and basal forebrain to induce genital activity and arousal. Moreover, projections from the SLD target inhibitory neurons projecting to the spinal motor neurons, which induce muscle atonia during REM sleep. The REM-off center is modulated by the orexinergic neurons in the LC, which inhibit the REM-off center, causing the subject to wake up if these neurons in the LH are activated. VLPO = ventrolateral preoptic area, ACh = acetylcholine, NE = noradrenaline, 5-HT = serotonin, LH = lateral hypothalamus, vlPAG = ventrolateral periaqueductal grey, SLD = sublaterodorsal nucleus, RF = reticular formation. Figure adapted from (Herice et al., 2019; W. Boron, 2016).

The different sleep states can be distinguished using EEG/LFP recordings, as NREM and REM sleep both display distinct oscillatory patterns (Figure 1-14). Delta waves (1-4Hz) are the dominant frequency of brain oscillations during NREM sleep. In addition, Sharp-wave ripples occur in the hippocampal circuit during NREM sleep. These fast oscillatory events described in section 1.3.2 are a hallmark of memory replay and consolidation occurring most frequently during NREM sleep.

The regulation of sleep requires a delicate interplay between several neurotransmitter systems, of which some are affected already at early stages of AD. Approximately 60% of the people suffering from AD develop sleep disturbances (Casagrande, Forte, Favieri, & Corbo, 2022; Kang, Lee, & Lim, 2017; Vitiello & Borson, 2001) (Figure 1-18). These disturbances in sleep architecture and sleep quality are thought to be the result of neurodegenerative processes affecting the neuronal circuits regulating sleep. The majority of the studies on sleep alterations in AD focused on later, symptomatic stages of AD and observed disturbed circadian rhythm, sleep fragmentation and decreased REM and NREM sleep time in AD patients (Kang et al., 2017; Kent, Strittmatter, & Nygaard, 2018; Winer & Mander, 2018). However, recent studies suggest that sleep disturbances occur very early in the course of AD (Hita-Yanez, Atienza, Gil-Neciga, & Cantero, 2012; Kang et al., 2017; Liguori et al., 2020; Winer & Mander, 2018). Researchers hypothesize that this is due to early alterations in synaptic function in regions responsible for the regulation of sleep. Evaluation of sleep and oscillatory brain activity during sleep at very early stages of AD might lead to novel biomarkers to detect AD at these preclinical stages and it would offer novel insights into early neuropathological mechanisms of AD. Moreover, treating early alterations in sleep could be a valuable therapeutic target, since disturbances have been known to exacerbate AD pathology (Casagrande et al., 2022; Y. E. Ju, Lucey, & Holtzman, 2014; Kang et al., 2017; L. Xie et al., 2013).

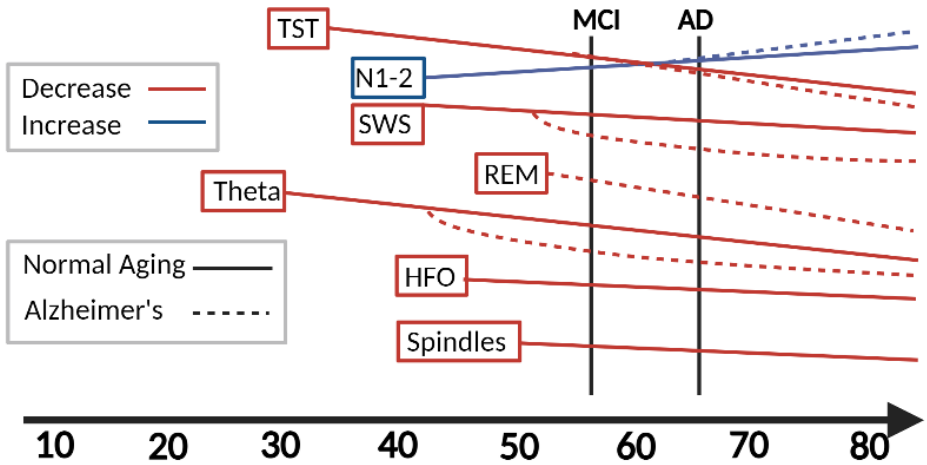

Figure 1-18: Changes in sleep architecture during aging and in AD. Alterations in sleep macroarchitecture during healthy aging (solid lines) and in AD (dotted lines) of several sleep parameters. It becomes apparent that sleep disturbances seem to arise before cognitive symptoms are present. TST = total sleep time, N1-2 = light NREM sleep, SWS = deep stages NREM, REM = rapid eye movement, MCI = mild cognitive impairment, AD = Alzheimer's disease, HFO = high frequency oscillations. Figure adapted from (Romanella et al., 2021)

Rodents are an ideal model for sleep studies since behavioral states can be easily measured with EEG or LFPs and the high homology between the neurocircuitry and neurochemistry of sleep with that of humans. Moreover, studies in rodents allow pharmacological and/or genetic manipulations of sleep circuitry. However, there are some differences in sleep architecture, since rodents are so-called polyphasic sleepers, meaning that they cycle through many sleep bouts and wake bouts during light and during dark. Moreover, rodents are nocturnal animals, meaning that they sleep during the light phase, and are active during the dark phase (Figure 1-19). Despite the differences in sleep architecture and circadian rhythmicity, rodent models for AD are still often used to evaluate sleep disturbances in AD. Interestingly, similar changes in sleep architecture, such as sleep fragmentation, altered circadian rhythmicity and less time spent in NREM and REM and decreased power of slow oscillations have been observed in different rodent models of AD (Benthem et al., 2020; Duncan et al., 2022; Kent et al., 2018; Kreuzer et al., 2020; Roh et al., 2012; Wisor et al., 2005; B. Zhang et

al., 2005). These results demonstrate the high translational value of sleep research in AD models. **Using animal models of AD to investigate sleep alterations has several advantages, such as the possibility to investigate very early stages of the disease, follow up sleep alterations over the progression of the disease and evaluate the effects of manipulation of sleep circuits.**

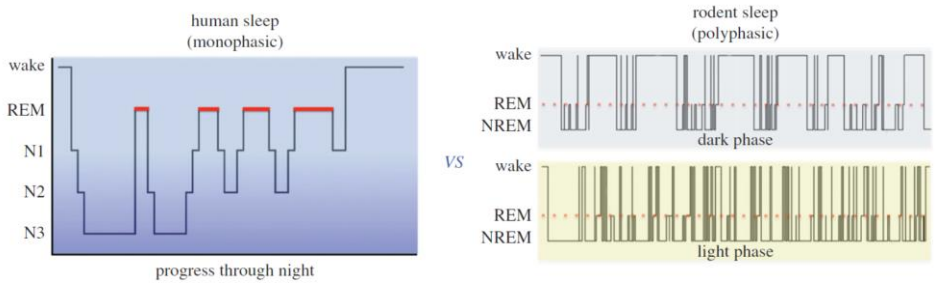

Figure 1-19: Sleep architecture in humans versus rodents. Humans have a monophasic sleep, meaning that they sleep for several hours and cycle through different sleep stages during this period. However, rodents are polyphasic sleepers, meaning that they have more sleep cycles during both day and night. Moreover, rodents are nocturnal animals, and therefore display more REM and NREM sleep during the light phase, compared to the dark phase. Figure adapted from (Mong & Cusmano, 2016)

2. Objectives & Outline

Due to the aging world population, the number of people suffering from Alzheimer Disease (AD), a severe neurodegenerative disorder leading to dementia, is expected to dramatically increase (Brayne & Miller, 2017). AD is a progressive disorder, in which the accumulation of toxic amyloid-beta aggregates and neurofibrillary tangles disrupts neuronal function. The protein deposits induce neuronal loss and severe cognitive deficits and behavioral alterations, which affect the activities of daily living, eventually resulting in the need for 24-hour care. AD is characterized by a long preclinical phase, where there is a progressive accumulation of Aβ and tau, in the absence of cognitive symptoms (Braak, Thal, Ghebremedhin, & Del Tredici, 2011; Sperling et al., 2011). The advantage of this long preclinical phase is that there is time to interfere with the disease before irreversible damage is inflicted to the brain. But to do this, we need to be able to detect AD at this preclinical phase, which is currently still not feasible, since AD is mainly diagnosed based on cognitive symptoms observed with neuropsychological examinations (Aisen et al., 2017).

A vast amount of AD research is focusing on finding early biomarkers of AD, to offer the opportunity to detect AD and to start therapeutic treatment at presymptomatic stages before extensive damage is afflicted to the brain (De Roeck, Engelborghs, & Dierckx, 2016; Dubois et al., 2014). Several cerebrospinal fluid (CSF) biomarkers have been discovered which allow detection of $A\beta_{1\text{-}40}$, $A\beta_{1\text{-}42}$, total tau and pTau concentrations. The combination of several CSF biomarkers have been shown to be sensitive for AD and are to some extend capable of differentiation between different causes of dementia. However, obtaining CSF requires a lumbar puncture and therefore limits the use of this technique (Bouwman et al., 2022; Somers, Goossens, Engelborghs, & Bjerke, 2017). Several imaging biomarkers are currently used to evaluate loss of brain volume (structural magnetic resonance imaging) and amyloidosis (e.g., Positron emission tomography (PET)) (Ishii et al., 2017; Ruan et al., 2016; Sharma & Singh, 2016). The non-

invasive nature of MRI and PET is a major advantage, however, the changes observed with these techniques in AD occur at a relatively late stage.

Synaptic dysfunction has been demonstrated to induce alterations in activity and connectivity of functional brain networks (Shah et al., 2015). Interestingly, these network disturbances can be detected using noninvasive resting state functional MRI (rsfMRI) (Badhwar et al., 2017; Ben-Nejma et al., 2019; Y. Gu et al., 2020; H. Li et al., 2017). Moreover, several studies have demonstrated that synaptic dysfunction occurs very early in AD, even before amyloid accumulations are observed (Ben-Nejma et al., 2019; Latif-Hernandez et al., 2019; Shah et al., 2018; Shah et al., 2016). Therefore, rsfMRI is a promising tool to develop non-invasive biomarkers for AD**.** However, standard FC measures have been demonstrated to suffer from several caveats, such as a lack of specificity for AD, therefore limiting its potential as a biomarker. Interestingly, several advanced analyses methods of rsfMRI data have been demonstrated to be sensitive to altered network activity in people suffering from AD from healthy controls. Moreover, by taking into account the dynamic properties of FC, researchers were able to classify people suffering from subjective cognitive decline and AD compared to healthy controls, suggesting that these novel measures could have the potential to be used as presymptomatic biomarker (Hohenfeld, Werner, & Reetz, 2018; Liang et al., 2021; Moguilner et al., 2021; Yamada et al., 2017). Quasi-periodic pattern (QPP) analysis is a recent technique which investigates recurrent patterns of network activity, which are highly similar across species. Recent studies observed that these QPPs are able to detect alterations in network disturbances in neurological disorders such as ADHD and AD (Abbas, Bassil, & Keilholz, 2019; Belloy, Shah, et al., 2018).

One of the first networks affected in AD is the hippocampal network, which is imperative for proper memory function. The hippocampus is a small structure in the medial temporal lobe, which is involved in the encoding and consolidation of spatial and episodic memory, cognitive functions which are impaired at the early symptomatic stages of AD (Axmacher et al., 2008; Basar, 2013). The mechanisms by which the

hippocampus encodes, and stores memories has been an important topic in research for several decades (Belluscio, Mizuseki, Schmidt, Kempter, & Buzsaki, 2012; Buzsaki, 2006, 2015; Buzsaki et al., 2003; Buzsaki & Tingley, 2018; Colgin, 2016). Several characteristics of hippocampal neuronal activity have been linked to memory processes, which have been demonstrated to be altered during different stages of AD (Bazzigaluppi et al., 2018; Benthem et al., 2020; Caccavano et al., 2020; A. M. Goodman et al., 2021; Goutagny et al., 2013). However, it is still unknown how hippocampal function is altered at very early stages of AD, and what mechanisms are contributing to this network dysfunction.

The synaptic dysfunction occurring at early stages of AD has been demonstrated to impair connectivity of brain networks, leading to alterations in behavior such as memory problems (Latif-Hernandez et al., 2019; Shah et al., 2018). Very subtle behavioral alterations due to altered network function, could be driving disease progression, since several important (homeostatic) brain processes would be disrupted. Sleep is a complex behavioural state defined by the complete loss of behavioural control and consciousness and is essential for energy conservation, synaptic plasticity and homeostasis, brain waste clearance, modulation of immune responses and cognition (Zielinski et al., 2016). Daily cycles of wakefulness and sleep are tightly regulated by interactions between wake-promoting and sleep promoting neural circuitry, of which several are thought to be affected by AD already at presymptomatic stages. Several studies have demonstrated that sleep disturbances occur very early in the course of AD (Hita-Yanez et al., 2012; Kang et al., 2017; Liguori et al., 2020; Winer & Mander, 2018). Evaluation of sleep and brain activity during sleep at very early stages of AD might lead to novel biomarkers to detect AD at these preclinical stages and it would offer novel insights into early neuropathological mechanisms of AD. Moreover, treating early alterations in sleep could be a valuable therapeutic target, since sleep disturbances have been demonstrated to exacerbate AD pathology (Casagrande et al., 2022; Y. E. Ju et al., 2014; Kang et al., 2017; L. Xie et al., 2013).

Despite decades of research and numerous clinical trials aiming to stop the progression of AD by breaking down protein aggregates and inhibiting the production of these proteins, there is still no disease modifying therapy available for AD (Mehta, Jackson, Paul, Shi, & Sabbagh, 2017; Yiannopoulou, Anastasiou, Zachariou, & Pelidou, 2019). The continuously failing clinical trials highlight the importance of finding novel therapeutic targets which can alter disease progression. However, disease mechanisms at early stages of AD, especially during the preclinical phase, are still elusive. Recent studies have demonstrated that early network imbalance, caused by synaptic dysfunction due to the accumulation of soluble amyloid species, drives disease progression in AD (Bi et al., 2020; Busche & Konnerth, 2015; Maestu, de Haan, Busche, & DeFelipe, 2021; Styr & Slutsky, 2018). Therefore, researchers hypothesize that restoring the network imbalance at early stages of the disease could slow down or stop the disease progression of AD (Busche et al., 2015; Styr & Slutsky, 2018). However, insights into the disease mechanisms underlying presymptomatic network dysfunction are still lacking. Investigation of network dysfunction during different behavioral states could provide valuable insights into which neuronal systems are affected at the presymptomatic stages of disease. And maybe in the future, by targeting these affected systems, an effective disease modifying treatment could be developed.

The overall aims of this PhD project were to investigate aberrations in whole brain network activity and hippocampal oscillatory activity at pre- and early-plaques stages of AD and to evaluate how these are linked to histopathological AD-related alterations and behavioral disturbances. For this purpose, we used a multimodal approach where we combined rsfMRI, hippocampal measurements of neuronal activity in freely behaving animals and histological analysis. We investigated pre-plaque and early plaque stages of AD, using the TgF344-AD rat model, which displays all phenotypical hallmarks of AD. First, we investigated whole brain alterations in network activity using rsfMRI combined with histology to gain insights into disease mechanisms contributing to the changes in network activity (**chapter 3)**. Next, we used hippocampal electrophysiology to evaluate neuronal activity and hippocampal function during different sleep stages and

during exploration of a novel environment**.** In addition, analysis of the abundance of cholinergic, glutamatergic, and GABAergic synapses was performed to gain insight into synaptic alterations which might contribute to the altered hippocampal activity (**chapter 4 & 5**). Cholinergic neurons in the basal forebrain (BFB) have been demonstrated to be vulnerable for AD pathology, leading to cholinergic deficits already at early stages of the disease. **In the next step, we aimed to investigate the effects of modulating cholinergic signaling on the functional connectivity in whole-brain networks**. Therefore, we used designer receptors exclusively activated by designer drugs (DREADDs) to modulate the neuronal activity of BFB cholinergic neurons in healthy rats and evaluated the effects of the DREADD stimulation on whole brain functional connectivity using rsfMRI in **chapter 6**.

2.1 Objective 1: Disentangle disruption of whole-brain network activity at pre- and early-plaque stages of AD in TgF344-AD rats

Before evaluating alterations in recurrent patterns of network activity, it was important to validate that the timepoints we selected for the analyses would correspond to pre- and early-plaque stages of AD. Therefore, histological analysis was performed to evaluate AD related pathology. These results confirmed that at 4-months of age, soluble amyloid pathology was present in the brain, in the absence of amyloid plaques or tau tangles and that the first amyloid plaques could be observed at 6 months of age. Next, we performed whole-brain resting state functional MRI in TgF344-AD rats and wildtype littermates. We used quasi-periodic pattern analysis to investigate how BOLD activity is altered during recurrent patterns of brain activity. We compared spatial and temporal properties of whole brain network activity between groups. In addition, we've performed histological analysis of neuro-inflammation and quantified the amount of glutamatergic, GABAergic, and cholinergic synapses to gain insight into possible disease mechanisms contributing to the changes observed in the rsfMRI. The results are reported in **chapter 3**.

2.2 Objective 2: Unravel synaptic dysfunction during different behavioral states during pre-plaque and early-plaque stages of AD

The hippocampus is a subcortical structure which is highly involved in the encoding and consolidation of episodic and spatial memory (Buzsaki et al., 2003; Buzsaki & Tingley, 2018). Moreover, it is one of the first structures affected in AD, resulting in cognitive deficits such as memory impairments (Braak et al., 2011). Early accumulation of amyloid induces alterations in neuronal excitability within the hippocampal circuit, resulting in alterations in oscillatory activity and cognitive deficits (Caccavano et al., 2020; A. M. Goodman et al., 2021; Goutagny et al., 2013). To evaluate if oscillatory activity within the hippocampus is altered at pre-plaque and early-plaque stages of AD, electrophysiological recordings in the CA1 layer of the hippocampus were performed. The recordings were acquired from freely moving animals, allowing the evaluation of hippocampal activity during different behavioral states, which are regulated by different neuromodulatory systems (Fontanini & Katz, 2008; McCormick et al., 2020). This could provide new insights into the neuromodulatory underpinnings of (hippocampal) network dysfunction during pre- and early-plaque stages of AD.

We first wanted to evaluate how hippocampal function and network activity was altered during different sleep stages, namely rapid eye movement sleep (REM) and non-rapid eye movement sleep (NREM), since hippocampal-dependent memory consolidation is a process which occurs mainly during sleep. Moreover, given the observation that sleep architecture and circadian rhythmicity have been shown to be altered in AD, we aimed to evaluate if behavioral alterations in sleep were observed during these early stages of AD. Hippocampal oscillatory activity in the CA1 region and sleep architecture were compared between TgF344-AD rats and wild-type littermates during the pre- and early-plaque stage of AD. In addition, histological analysis was performed focusing on the amount of glutamatergic, GABAergic, and cholinergic synapses in the dentate gyrus and CA1 layer of the hippocampus. The results of this study are represented in **chapter 4.**

Next, we wanted to investigate hippocampal function while the TgF344-AD rats were exploring a novel environment, since the hippocampus is known to play an important role in spatial navigation and online encoding of spatial memories (Buzsaki, 2006; Buzsaki & Tingley, 2018). Electrophysiological signals from the CA1 layer of the hippocampus were recorded while the animals were exploring an open field (consisting of a square box of 1x1 meter, guided by cues on the wall). We evaluated explorative behavior, spatial navigation, and hippocampal oscillatory activity to gain insights into early hippocampal dysfunction during pre-plaque stages of AD. The results are described in **chapter 5.**

2.3 Objective 3: Effects of circuit specific basal forebrain cholinergic activation on whole-brain functional connectivity

The cholinergic system is an important neuromodulatory system involved in various cognitive functions, such as attention and memory (Anaclet et al., 2015; Gritton et al., 2016; W. Li et al., 2015; Solari & Hangya, 2018). Research has demonstrated that the cholinergic neurons, originating from the BFB, are important for healthy cognitive function (Nair et al., 2018; Turchi et al., 2018). Cholinergic neurons residing in the BFB project to the entire cortex and hippocampus and have been demonstrated to be extremely vulnerable for AD pathology, leading to a loss of cholinergic neurons already at early stages of the disease (Dringenberg, 2000; X. Du, Wang, & Geng, 2018). Several studies observed that BFB degeneration precedes the cortical spread of amyloid in patients suffering from AD, further suggesting the early involvement of this structure in AD. Moreover, these studies have demonstrated that the reduced BFB volume is correlated with decreased cognition in AD and that it can predict the conversion from mild cognitive impairment to AD related dementia (Brueggen et al., 2015; Fernandez-Cabello et al., 2020; Teipel et al., 2022; Xia et al., 2022). Current symptomatic treatments aimed at increasing the amount of acetylcholine in the brain have been shown to alleviate cognitive symptoms and slightly delay disease progression in AD.

Since the cholinergic system is an important modulator of whole brain network activity, we wanted to investigate how unilateral activation of BFB cholinergic neurons in the nucleus basalis of Meynert, affects functional connectivity within the default-mode like network. Therefore, we used chemogenetic tools combined with rsfMRI to elucidate the role of the cholinergic BFB in the regulation of network activity. This proof-of concept study provides novel insights into the effects of circuit specific, cholinergic activation. The results are presented in **chapter 6.**

Finally, **chapter 7** concludes with a general discussion in which we elaborate on potential disease mechanisms during pre- and early-plaque stages of AD, based on the outcomes of this PhD dissertation.

3. Unraveling whole-brain alterations in network interaction at pre-plaque and early-plaque stages of AD

This chapter is based on:

M. van den Berg, M. H. Adhikari, M. Verschuuren, I. Pintelon, T. Vasilkovska, J. Van Audekerke, S. Missault, L. Heymans, P. Ponsaerts, W. H. De Vos, A. Van der Linden, G. A. Keliris and M. Verhoye (2022). "Altered basal forebrain function during whole-brain network activity at pre- and early-plaque stages of Alzheimer's disease in TgF344-AD rats." Alzheimers Res Ther **14**(1): 148

3.1 Abstract

Background: Imbalanced synaptic transmission appears to be an early driver in Alzheimer's Disease (AD) leading to brain network alterations. Early detection of altered synaptic transmission and insight into mechanisms causing early synaptic alterations would be valuable treatment strategies. This study aimed to investigate how whole-brain networks are influenced at pre- and early-plague stages of AD and if these manifestations are associated with concomitant cellular and synaptic deficits.

Methods: To this end, we used an established AD rat model (TgF344-AD) and employed resting state functional MRI and quasi-periodic pattern (QPP) analysis, a method to detect recurrent spatiotemporal motifs of brain activity, in parallel with state-of-the-art immunohistochemistry in selected brain regions.

Results: At the pre-plaque stage, QPPs in TgF344-AD rats showed decreased activity of the basal forebrain (BFB) and the default-mode like network. Histological analyses revealed increased astrocyte abundance restricted to the BFB, in the absence of amyloid plaques, tauopathy and alterations in number of cholinergic, GABAergic, and glutamatergic synapses. During the early-plaque stage, when mild amyloid-beta (Aβ) accumulation was observed in the cortex and hippocampus, QPPs in the TgF344-AD rats normalized suggesting the activation of compensatory mechanisms during this early disease progression period. Interestingly, astrogliosis observed in the BFB at the pre-plaque stage was absent at the early-plaque stage. Moreover, altered excitatory/inhibitory balance was observed in cortical regions belonging to the default mode-like network. In wild-type rats, at both time-points, peak activity in the BFB preceded peak activity in other brain regions – indicating its modulatory role within QPPs of brain activity. However, this pattern was eliminated in TgF344-AD suggesting that alterations in BFB-directed neuromodulation have a pronounced impact in network function in AD.

Conclusions: This study demonstrates the value of rsfMRI and advanced network analysis methods to detect early alterations in BFB function in AD, which could aid early diagnosis and intervention in AD. Restoring the global synaptic transmission, possibly by modulating astrogliosis in the BFB might be a promising therapeutic strategy to restore brain network function and delay the onset of symptoms in AD.

3.2 Introduction

Alzheimer's disease (AD) is a severe neurodegenerative disorder with an insidious onset of disease. Due to an aging society, an increasing number of people are expected to suffer from this incurable disorder, bringing enormous economic and societal burden. Despite decades of research and numerous clinical trials, disease-modifying therapies are still lacking, mainly due to the incomplete insight into the pathological mechanisms of AD (Anderson et al., 2017). AD is characterized by a progressive accumulation of two toxic proteins, the amyloid-beta (Aβ) and hyperphosphorylated tau (pTau), inducing neuronal loss, cognitive impairment, and dementia. Since the accumulation of Aβ is one of the earliest events in AD pathology, it has long been hypothesized that it triggers the formation of pTau and neurodegeneration. However, Aβ plaque accumulation is not linearly correlated with dementia symptoms. Interestingly, neuronal hyperexcitability (resulting from increased glutamatergic and decreased GABAergic signalling) has been observed prior to plaque formation [3-6]. This hyperexcitability exacerbates the formation of soluble Aβ species, therefore, driving disease progression [6]. Soluble monomeric and oligomeric Aß have been demonstrated to be neurotoxic to cholinergic neurons originating from the basal forebrain (BFB), causing the BFB to become affected during early stages of AD (X. Q. Chen & Mobley, 2019). Studies have demonstrated that decreased BFB volume precedes the cortical spread of Aß (Fernandez-Cabello et al., 2020; A. M. Hall, Moore, Lopez, Kuller, & Becker, 2008). The BFB has been implicated in the modulation of cognition, specifically the projections from the diagonal band of Broca, substantia innominata and the nucleus basalis of Meynert (NBM) to the cortex (Lozano-Montes et al., 2020; Nair et al., 2018). Moreover, the BFB is known to be an important modulator of network activity and is involved in cortical network switching

between brain states by exerting direct and/or indirect control on the prefrontal cortex (Espinosa, Alonso, Morales, et al., 2019; W. Li et al., 2015; Turchi et al., 2018). Therefore, alterations in BFB signalling due to AD pathology might lead to early disruption of network activity in the brain.

Resting state functional MRI (rsfMRI) is a non-invasive MRI technique, which uses the blood oxygen level dependent (BOLD) contrast to indirectly assess spontaneous neuronal activity while the subject is at rest. Low frequency, temporally correlated fluctuations of BOLD activity between brain regions, have been shown to consistently exist across certain distally located areas that are defined as resting state networks (Allen et al., 2011; J. Grandjean et al., 2020; N. Xu et al., 2022). Moreover, the strength of temporal correlation is thought to be representing functional connectivity (FC) between the nodes of these networks. We recently demonstrated that activation of cholinergic neurons in the NBM induces a decrease of FC in the default-mode like network (DMLN) (Peeters, van den Berg, et al., 2020), a major resting state network active during self-referential tasks such as mind wandering and introspection (Raichle, 2015). Numerous clinical rsfMRI studies have detected FC alterations in patients with Mild Cognitive Impairment and AD-related dementia, as well as in animal models of AD. Aberrations in FC were mainly observed in the default mode network and have been linked to cognitive and behavioral performance setting it as an important target for therapies (Anckaerts et al., 2019; Herdick et al., 2020; Pan et al., 2017; Shah et al., 2013; Shah et al., 2016; van Harten et al., 2018; Y. Xie et al., 2019).

Recent advances in dynamic rsfMRI analysis approaches revealed fundamental new insights regarding regional involvement, and regulation of so-called brain states, by considering the dynamic, temporal properties of FC (Filippi, Spinelli, Cividini, & Agosta, 2019; Jalilianhasanpour et al., 2021; Sendi et al., 2021). In addition, other dynamic analysis methods - related but not identical to FC - have also been proposed and offer some important advantages such as increased time resolution and a better estimation of the instantaneous or short-term relationship of activity across areas (Abbas, Belloy,

et al., 2019; Gutierrez-Barragan et al., 2019; X. Liu et al., 2018; Thompson et al., 2014). One such method is the Quasi-periodic pattern (QPP) analysis, which detects recurrent, relatively short-lived spatiotemporal motifs of whole-brain activity using the BOLD signal. One of the strengths of QPPs is that they are a sensitive method to directly demonstrate the anti-correlated activity between the default mode-like network, and the lateral cortical network (LCN) in rodents (Belloy, Naeyaert, et al., 2018) - the rodent analog of the so called task positive network in humans, a network that has been shown to be activated in cognitive and attention demanding tasks (N. Xu et al., 2022). Thus, we speculated that QPP analysis would be very powerful and could offer novel insights into spatial and temporal alterations in neuronal activity during specific recurrent brain states at pre-plaque stages of AD. Moreover, QPP analysis could potentially uncover regions involved in the modulation and regulation of these states and networks.

Imbalance in synaptic function appears to be an early driver of AD progression (Bi et al., 2020; Brier, Thomas, & Ances, 2014; Busche et al., 2015; Maestu et al., 2021; Small, 2008). Thus, sensitive measures of early network disturbances could assist in the development of promising biomarkers for early diagnosis of AD. Moreover, targeting the impaired network function during this presymptomatic phase might prove imperative for disease modifying treatments. However, the mechanisms underlying the early network dysfunction, are still unknown. In this study we hypothesized that during the pre-plaque stage, alterations in BFB activity induce changes in whole brain, recurrent patterns of brain activity involving the DMLN and LCN, which can be detected with rsfMRI and QPP analysis. We test this hypothesis using rsfMRI in a well characterized, highly translational TgF344-AD rat model of AD, which bears human APP_{swe} and $PS1_{\Delta E9}$ mutations, resulting in an age-dependent accumulation of Aβ depositions (R. M. Cohen et al., 2013), endogenous pTau accumulation, (Joo et al., 2017; Rorabaugh et al., 2017), and cognitive deficits, akin to human AD (Braak et al., 2011). Further, to unravel the concomitant cellular and synaptic deficits underlying network alterations, QPP analysis was complemented with state-of-the-art histological investigation of relevant brain areas such as BFB and nodes of the DMLN and LCN

3.3 Material and Methods

3.3.1 Animals and ethical statement

TgF344-AD and F344 rats for this study were bred in-house. Heterozygous TgF344-AD rats were purchased from the RRRC (RRID:RGD_10401208) and were coupled with F344 rats (Charles River, Italy). The male offspring was used in this study. Fifteen male TgF344-AD rats and 11 wildtype (WT) littermates underwent rsfMRI scans at both 4 and 6 months of age. The four-month timepoint represents the pre-plaque stage of AD, with accumulation of soluble amyloid species in the absence of amyloid plaque depositions, while the six-month timepoint has been shown to represent an early-plaque stage in TgF344-AD rats (R. M. Cohen et al., 2013). An additional 42 male rats were used for histological (6 WT and 6 TgF344-AD rats for both time points), and biochemical analysis (3 WT and 6 TgF344-AD rats for both time points). Animals were group housed with a 12h light/dark cycle (lights on at 7 am) and with controlled temperature (20 – 24°C) and humidity (40-60%) conditions. Standard food and water were provided ad libitum. All procedures were in accordance with the guidelines approved by the European Ethics Committee (decree 2010/63/EU) and were approved by the Committee on Animal Care and Use at the University of Antwerp, Belgium (approval number: 2019-06).

3.3.2 *In vivo* MRI procedures

Rats were anesthetized using isoflurane (5% for induction and 2% during handling procedures). The animals were endotracheally intubated and mechanically ventilated (70 breaths per minute) using a ventilator (Microventilator, Carfil, Belgium) under 2% isoflurane. Ear bars were used to fix the head of the animal and a cannula was placed in the tail vein, after which an intravenous bolus injection of medetomidine (0.05 mg/kg, Domitor®, Pfizer, Germany) and Pancuroniumbromide (0.5 mg/kg, VWR, Belgium) was administered. The constant intravenous infusion of medetomidine (0.1 mg/kg/h) and Pancuroniumbromide (0.5 mg/kg/h) was started 15 minutes after the administration of the bolus and the isoflurane concentration was gradually lowered to 0.4%. Animal

physiology was closely monitored during the handling and the scanning. Body temperature was maintained at (37 ± 0.5) °C using a feedback controlled warm air circuitry (MR-compatible Small Animal Heating System, SA Instruments, Inc., USA). A pressure-sensitive pad (sampling rate 225 Hz; MR-compatible Small Animal Monitoring and Gating system, SA Instruments, Inc., USA) was used to record the breathing rate. Additionally, a pulse oximeter was placed on the hind paw of the animal to monitor the heart rate and blood oxygenation (MR-compatible Small Animal Monitoring and Gating System, SA Instruments, Inc., USA).

3.3.2.1 MRI acquisition

Data were acquired using a 9.4T Biospec MRI system (Bruker BioSpin, Germany) with Paravision 6 software, using a 2x2 array receiver head radiofrequency coil. To allow uniform slice positioning, T2-weighted TurboRARE images were acquired along three directions (TR 2500ms, TE 33ms, FOV (30x30) mm^2, matrix [128x128]). Magnetic field inhomogeneity was corrected by local shimming in an ellipsoid volume of interest covering the brain. Resting state functional MRI (rsfMRI) was acquired using a single shot gradient echo EPI-sequence (TR 600ms, TE 18ms, FOV (30 x 30) mm^2, matrix [96 x 96], 12 coronal slices of 1.0 mm, slice gap 0.1mm, 1000 repetitions). RsfMRI scans started 35 minutes after the initial bolus administration and the total scan time was 10 min. Intravenous infusion of medetomidine and Pancuroniumbromide anaesthesia was terminated after completion of the rsfMRI scan and isoflurane was increased to 2%. Next, T2-weighted 3D images were acquired using a 3D RARE sequence (TR 2500 ms, effective TE 44 ms, FOV (30x30x22) mm^3, matrix [256x256x128], RARE-factor 16). At the end of the scan session, a subcutaneous injection of 0.1 mg/kg atipamezole (Antisedan®, Pfizer, Germany) was administered to counteract the effects of the medetomidine anaesthesia and the animals were put on a second ventilator and heating pad to recover. All animals recovered within 1 hour after the end of the scan session, except for two 4-month-old TgF344-AD rats that did not recover after the scan session due to premature extubation.

3.3.2.2 Data preprocessing

Pre-processing of the data including debiasing, normalisation, realignment, smoothing, and co-registration was performed using SPM12 software (Statistical Parametric Mapping). First, we performed debiasing on the 3D RARE scans in order to remove the smooth, spatially varying intensity gradient induced by the receiving RF coil. Next, we created a study-specific 3D template from a subset (4M 11 WT/15 TG - 6M 11 WT/ 13Tg) of animals debiased 3D RARE scans in Advanced Normalization Tools (ANTS). Then, all rsfMRI images were realigned to the first image using a 6-parameter rigid body spatial transformation estimated using a least-square approach. Next, rsfMRI images were coregistered to the anatomical 3D scan of the same imaging session using a global 12-parameter affine transformation with mutual information as the similarity metric. The anatomical 3D scan was finally spatially normalized to the study-specific 3D template using a global 12-parameter affine transformation followed by a non-linear deformation protocol. The combined transformation (realignment and spatial normalization to the template) is applied to realign all EPI and co-register them to the 3D RARE template. Finally, ventricles were masked out of the data and in-plane smoothing was performed using a Gaussian kernel with full width at half maximum of twice the voxel size.

3.3.2.3 Quasi-periodic pattern (QPP) analysis

Global signal regression, quadratic detrending, demeaning and Fischer z-score transformation was performed on pre-processed rsfMRI scans, after which the scans were filtered between 0.01-0.17 Hz using a Butterworth band pass filter. Next, rsfMRI scans of all subjects were concatenated per genotype and per age to create four image series. QPPs were extracted from each image series using a modified algorithm first described by (Majeed et al., 2009), which detects recurrent, spatiotemporal patterns of BOLD activity. The first step in this algorithm extracts a template, which is a set of a pre-specified number (i.e., window size) of consecutive BOLD images, is selected at a random seed time frame within the image series. This template is then incrementally shifted along the image series, and the average, voxel wise spatial correlation of the BOLD signals, restricted to a brain mask, of the template and the successive image-series

segments of the same is calculated. The resulting correlation time-series is termed the sliding template correlation (STC). Local peaks in the STC with peak correlation exceeding a threshold of 0.2 are identified and the corresponding image series segments are averaged, voxel-wise, to form an updated template. This correlation threshold is based on previous studies which detected QPPs in humans and mice (Belloy, Naeyaert, et al., 2018; Majeed et al., 2009). This process is repeated until the spatial correlation between the updated and previous template is at least 0.99 resulting in a QPP. Thereafter the whole process is repeated with a new random seed location. The length of the template and hence the resulting QPP defined by the user prior to the extraction. The number of QPPs extracted for each image series is based on the number of chosen random seeds points. In this study, 200 QPPs were identified for each genotype and age, with a length of 6 TR (3.6s) and 15 TR (9s), consistent with a template of 6 and 15 consecutive BOLD images. These lengths were selected based on previous literature describing QPPs in rats (Majeed et al., 2009).

For both short and long window size, 200 QPPs were hierarchically clustered based on their temporal and spatial similarity, using correlation distance as a metric, to identify clusters of similar QPPs. The advantage of hierarchical clustering is that this method does not require prior knowledge about the number of clusters present in the data. Temporal similarity between a pair of QPPs was measured in terms of Pearson's correlation between their sliding template correlation time-courses. To obtain spatial similarity, one of the two QPPs is circularly shifted one image frame at a time and for each shift, a Pearson's correlation between its voxel-wise BOLD signal with that of the other unshifted QPP is obtained. Spatial similarity between the two QPPs is the maximum value of correlation across ws shifts, where ws is the window size. The spatio-temporal distance between every pair of QPPs is obtained by taking the Euclidian distance of the spatial and temporal domain distances. Using this NxN (N = number of QPPs) distance matrix, we performed hierarchical clustering to identify similar QPPs. This will result in a clustered distance matrix in which all the QPPs are hierarchically sorted according to distance. Plotting this distance matrix using a colour map makes it

easier to interpret the results (Fig 3-4). Next, we identified optimal # of clusters and their representative QPPs. First different clustering solutions, with different number of clusters were obtained. For each clustering solution, the silhouette coefficient for each QPP was calculated using its average within-cluster distance and between-cluster distances. These individual coefficients were averaged across QPPs and the clustering solution with the highest value was identified as the optimal solution. Next, out of the K clusters, robust clusters were objectively identified using several criteria including a minimum cluster size of 20 QPPs. In addition, QPPs should occur in at least 90% of the subjects for at least 50% of the QPPs within that cluster. The QPPs with the highest occurrence within their cluster, as measured by the instances the STC exceeds the threshold of 0.2, were selected as representative QPPs (rQPPs) for that cluster.

To visualize and identify the sequential regional activation and deactivation pattern that characterize a specific rQPP, one sample t-tests (two-tailed, FDR $p<0.05$, minimum cluster size 10 voxels, Matlab) were performed using the BOLD signals of the instances at which the local peaks in STC exceed the threshold of 0.2. Clusters of QPPs were matched between groups using a spatial cross correlation coefficient after which the activation patterns of spatially matched rQPPs (Pearson correlation coefficient >0.70) were compared using a two-sample t-test (two-tailed, FDR $p<0.05$, minimum cluster size 10 voxels, Matlab). The effect size was estimated by calculating the Cohens d on the ROI based time courses for each BOLD image of the rQPP separately. Each QPP has its own STC from the image series they are derived from, which can be used to extract occurrence rates at the subject level. Cluster-wise occurrence rate, defined as the average across occurrence rates of the QPPs that constitute the cluster, of matched clusters were compared between groups using an unpaired two-sample t-test (two-tailed, FDR $p<0.05$, Matlab).

To evaluate propagation of activity within QPPs, 9s QPPs were extracted and representative QPPs were selected based on hierarchical clustering as described above. Representative QPPs of the TgF344-AD rats were phase-aligned to the QPP of the WT

animals based on maximal spatial correlation between the rQPPs across groups, ensuring that the phase of DMLN activation of the rQPPs is the same across groups. To evaluate BOLD activity within QPPs in specific regions of interest (ROI), group averaged BOLD-time courses from each ROI were extracted from the image series and plotted. Next, the peak timings of the (non-z-scored) BOLD signal within each voxel in a ROI was averaged across all QPP-occurrences over the group, to create voxel-wise distribution of mean peak timings within each ROI. Unpaired two-sample t-tests (FDR $p<0.05$, Matlab) were performed to compare mean, across ROI voxels, peak timings between regions within each group in order to identify significant differences in the timing of peak activity of regions.

3.3.3 Immunohistochemistry

3.3.3.1 Immunofluorescent stainings

To evaluate AD pathology and alterations in synaptic markers, histological analyses were performed on cryosections of 12 TgF344-AD rats (4 months N=6, 6 months N=6) and 12 WT littermates (4 months N=6, 6 months N=6). The rats were deeply anesthetized using an intravenous injection of pentobarbital (Dolethal®, Vetoquinol, Belgium). Cardiac perfusion was performed with an ice-cold PBS solution, followed by a 4% paraformaldehyde solution (Merck Millipore, Merck KGaA, Darmstadt, Germany) for fixation of the tissues. Brains were surgically removed and post-fixed in 4% paraformaldehyde solution after which a sucrose gradient (5%, 10% and 20%) was applied. Brains were snap frozen in liquid nitrogen and stored at -80 °C until further processing. For immunohistochemistry, hemispheres were separated, and left hemispheres were embedded in OCT-embedding medium for sectioning. At Bregma levels 0.4, 1.40 and 3.90, sagittal sections of 12 µm were made using a Leica CM1950 cryomicrotome (Leica BioSystems, Belgium), thaw mounted on VWR Superfrost Plus micro slides (VWR, Leuven, Belgium) and dried for 2 hours at 37°C.

All immunohistochemical incubations were carried out at RT, using non-consecutive sections per Bregma level and staining. Primary and secondary antibodies were diluted

in blocking buffer containing 0.01M PBS, 10% normal horse serum, 0.01% bovine serum albumin, 0.05% thimerosal, and 0.01% sodium azide. In short, sections were preincubated for 30 min in blocking buffer containing 1% Triton X-100 before an overnight incubation with the primary antibodies. Glial cells were visualized with a combination of GFAP (1:200, Goat, Abcam, Ab53554, RRID:AB_880202) and Iba1 (1:500, Rabbit, Fujifilm Wako Chemicals, 019-19741, RRID:AB_839504). To investigate the synaptic excitatory/inhibitory balance a triple staining was performed using VGAT (1:200, Rabbit, Synaptic Systems, 131003, RRID:AB_887869); VGLUT (Guinea Pig, Synaptic Systems, 135304, RRID:AB_887878); VAChT (1:100, Goat, Merck, ABN100, RRID:AB_2630394). For the detection of the immunoreactivity, the sections were incubated for 4 hours with the appropriate combination of fluorescent-conjugated secondary antibodies (Jackson Immunoresearch, West Grove, USA). Followed by a nuclear counterstain using 4',6-diamidino-2-phenylindole (DAPI, Sigma-Aldrich, Hoeilaart, Belgium) for 10 min at room temperature. Samples were mounted in Citifluor AF1 (EMS, Hathfield, USA) or the permanent Citifluor PVP-1+ Antifadent (EMS) for whole slide imaging. Respective single-labeling studies which resulted in comparable staining, were performed to rule out nonspecific findings resulting from the multiple-staining process. Negative staining controls were performed by substitution of non-immune sera for the primary or secondary antisera.

To follow the progression of the AD Aβ-plaques and pTau were visualized. X-34 was used as pan-Aβ marker and pTau was specifically detected using a mouse AT8 antibody (1:500, pSer202/Thr205/PSer208, Invitrogen, MN1020, RRID:AB)223647). This antibody was labelled with a near-infrared fluorescent tag (PerkinElmer VivoTag 680XL) following the manufacturer's protocol. Sections were permeabilized for 15 min with 0.02% Triton in 0.01M PBS prior to a 20 min incubation with x-34 (10 µM) in 40% ethanol. In a next step, sections were further incubated for 30 min with blocking buffer containing 1% Triton X-100 followed by an overnight incubation with AT8 antibody diluted in blocking buffer. Propidium Iodide (5 µg/ml; 5 min; Sigma Aldrich) was used as a nuclear stain.

Sections were mounted using a permanent mounting medium Citifluor PVP-1+ Antifadent.

3.3.3.2 Image acquisition

To acquire images of fluorescently stained sections, a Zeiss Axioscan Z1 (Zeiss, Leuven, Belgium) was used with a Zeiss Colibri 7 solid-state light source of which the 385 nm, 475 nm, 555 nm, and 630 nm were used, a filter set 90 HE LED suitable for the applied fluorescent dyes (DAPI, FITC, Cy3 and Cy5) and a Hamamatsu Orca Flash 4.0 V3 digital camera. Zeiss Zen software was used to control the image acquisition and stitching. Whole slide scanning was done with a10x Plan-apo objective (NA 0.45).

Confocal images of immunolabeled tissue sections were acquired with a Perkin Elmer Ultraview Vox dual spinning disk confocal microscope, mounted on a Nikon Ti body using a 40x Plan Apo objective (NA 0.95). Lasers with wavelength 405 nm, 488 nm, 561nm and 640nm were used in combination with a quadruple dichroic and 445/60 - 525/50 - 615/70 - 705/90nm emission filters. Detection was done on a Hamamatsu C9100-50 CMOS camera. Image acquisition was done using Volocity software. Regions of interest were localized based on the DAPI staining. Per animal, 3 images were acquired on 3 non-consecutive sections in 3 axial positions separated by a 2µm spacing.

3.3.3.3 Image analysis

Image analysis for neuroinflammation and Aß and pTau pathology was done using the free, open-access image analysis software QuPath (v0.3.0) (Bankhead et al., 2017). On whole section images the regions of interest were annotated manually based on the nuclear counterstain. For each marker, an intensity threshold was manually defined to measure the positive area percentage with respect to the annotated region. For each marker the threshold settings were kept constant for all regions and ages studied.

Image analysis of the synaptic excitatory/inhibitory ratio was done in FIJI image analysis software (Schindelin et al., 2012). A macro script was written for FIJI image analysis

software [1] to detect synaptic markers and measure their intensity and is available on GitHub (https://github.com/DeVosLab/SynapseDetection). This script is built on modules that were already integrated in similar image analysis pipelines previously developed (Verschuuren et al., 2019; Verstraelen et al., 2020). After maximum projection of the Z-stacks, synaptic marker spots were enhanced using a single or multi-scale Laplace filter with user-defined kernel sizes. For each marker the threshold settings were kept constant for both groups and ages studied. A manually defined threshold per region was applied to segment the spots after which an additional max finding (and region growing) step was included to untangle clustered spots. Only spots that had a projected area within a specific range (0.20 – 3.00 µm) were retained. Images with more than 10000 spots were discarded to exclude over segmented images. During manual verification of images, it was noticed that cholinergic markers labeled cell bodies in MS, HDB/SI & NBM regions. The cell bodies were excluded from the search region to avoid the detection of spots within these cell bodies. Detection of cell bodies was done after applying a median filter with a large user-defined kernel size. followed by a user-defined threshold and detection of objects larger than 20 µm. Moreover, the manual verification of the images showed differences between glass slides in the GABA-ergic and glutamatergic stainings. The variability between glass slides was reduced by taking the ratio of the number of glutamatergic and GABA-ergic synapses. Therefore, the ratio of excitatory and inhibitory synapses is used as a measure instead of the absolute number of synapses.

3.3.4 ELISA

TgF344-AD rats (4 months N=6, 6 months N=6) and WT littermates (4 months N=3, 6 months N=3) were deeply anesthetized with an intravenous injection of pentobarbital (Dolethal®, Vetoquinol, Belgium) after which cardiac perfusion with an ice-cold PBS solution was performed. The brains were surgically removed, separated by hemisphere and snapshot frozen in liquid nitrogen. Both hemispheres were stored at -80 °C until further processing.

Next, Aβ was extracted using an adapted protocol first described by Izco et al. (2013) (Izco, Pesini, Perez-Grijalba, Fandos, & Sarasa, 2013). Briefly, right hemispheres were homogenized (100 mg tissue/mL) on ice using Tris buffered saline (TBS, Sigma) supplemented with protease inhibitors (HALT, Invitrogen, ThermoFisher Scientific, Belgium). After two short blasts of sonication (30 seconds), homogenates were centrifuged for 90 minutes at 20800 g. Supernatans, which contained the TBS soluble fraction of amyloid monomers and oligomers, was collected, aliquoted and stored at -80 °C for further analysis.

Sandwich-ELISA assays were performed according to the manufacturer's guidelines, to detect monomeric Aβ 1-40 (Invitrogen, KHB3481, ThermoFisher Scientific, Belgium) and Aβ 1-42 (Invitrogen, KHB3441, ThermoFisher Scientific, Belgium) and oligomeric Aβ species (Invitrogen, KHB3491, ThermoFisher Scientific, Belgium). All kits were sensitive to human recombinant AB species. The ELISA signal was quantified using a microplate reader (Versamax, GE Healtcare, Belgium).

3.3.5 Statistics

Regarding the pathological stainings (Aβ-plaques and pTau) and neuro-inflammatory stainings (astrogliosis and microgliosis), outliers were detected per genotype, age, and region, based on principal component analysis. Measurements with a T^2 statistics indices higher than the 95% confidence interval were excluded. Two-way ANOVA (genotype, age, genotype*age) per region were performed to evaluate differences in %Area in p-tau, astrogliosis and microgliosis. In case of a significant interaction, post-hoc tests were performed using Student's t-test with FDR correction ($p<0.05$). For the analysis of the synaptic markers, outlier detection was performed using the interquartile range (1.5x IQR) per genotype, age, and region on all individual images (3 per animal). Animals with less than 2 images were excluded and the remaining images were averaged for each animal. A second outlier detection was performed on the subject averages, using PCA. Two-way ANOVAs (genotype, age, genotype*age) per region were used to evaluate differences in vGLUT/vGAT ratio and the number of cholinergic synapses, followed by a

post-hoc FDR-corrected Student's t-test (FDR $p<0.05$). All statistical analyses were performed in JMP Pro 16. For statistical analysis of the ELISA data, both wild-type groups were combined, since no significant differences between ages were observed in this group. Protein concentrations of all animals were normalized to the mean concentration of the WT. Next, Mann-Whitney U tests (Bonferroni corrected) were performed between groups, using GraphPad Prism 9.0.

3.4 Results

3.4.1 Histological evaluation of AD-pathology in 4-month-old TgF344-AD rats

Previous histological analysis in the TgF344-AD rat model demonstrated an age-dependent development of Aß pathology and tauopathy. From 6 moths onwards, Aβ-plaques and pTau accumulations were observed in the TgF344-AD rats (R. M. Cohen et al., 2013; Joo et al., 2017). The goal of this study was to investigate how network activity was altered before Aß plaques were present in the brain, during the so-called pre-plaque stages of AD. Therefore, immunohistochemical and biochemical analyses were performed in 4-month-old, our assumed pre-plaque stage, and 6-month-old TgF344-AD rats. Soluble Aß species were investigated by performing ELISA immune assays on brain homogenates of complete hemispheres. Four-month-old TgF344-AD rats demonstrate significantly increased concentrations of TBS soluble Aβ monomers, Aβ1-40 ($p=0.0021$), Aβ1-42 ($p=0.0021$) and oligomers (Aβ-o) ($p=0.0129$) compared to WT (Figure 3-1A). While the concentrations of Aβ-o and Aβ1-40 remained at the same concentrations in 6-month-old TgF344-AD rats **(**Aβ-o; $p=0.5368$, Aβ1-40; $p= 0.0931$), the concentrations of Aβ1-42 significantly increased in TgF344-AD rats from 4 to 6 months of age ($p=0.0022$).

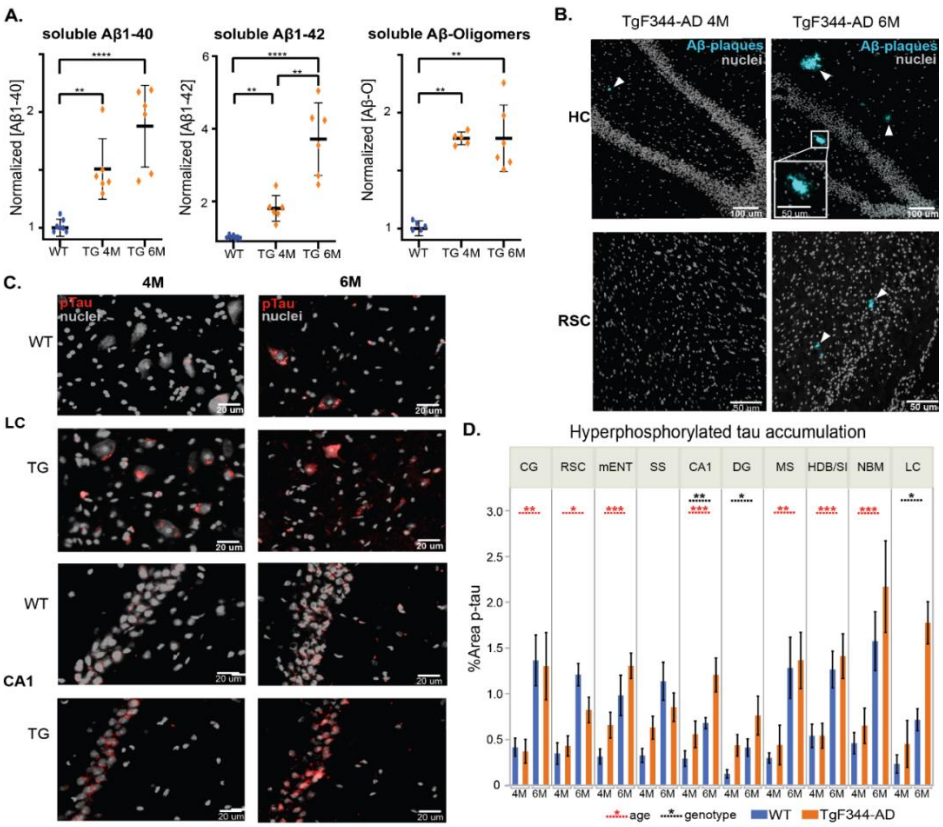

Figure 3-1: Aβ pathology and pTau-pathology in TgF344-AD rats. A) Biochemical analysis of soluble Aβ monomers and oligomers. Graphs show the mean +/- SEM. The marks show the concentrations of each individual animal, individual values were normalized to the mean values of the WT across both ages. Mann-Whitney U-tests with Bonferroni correction for multiple comparisons were performed to evaluate statistical differences in concentrations. B) Representative histological images of Aβ-plaques(light blue - arrowheads) in TgF344-AD rats. Nuclei are counterstained in grey. C) Representative images of pTau accumulation (red) in the locus coeruleus (LC) and CA1 region of the hippocampus (CA1). Nuclei are counterstained in grey. D) Graphs represent the percentage area positive for pTau (mean +/- SEM). Blue color represents the wild-type (WT) animals, while orange represents the TgF344-rats. Dashed lines indicate significant genotype effects (black) or age effects (red). *p<0.05, ** p<0.01, *** p<0.001, **** p<0.0001. CG = cingulate cortex, RSC = retrosplenial cortex, mENT = medial entorhinal cortex, SS = somatosensory cortex, MS = medial septum, DG = Dentate gyrus, LC = locus coeruleus, HDB/SI = horizontal limb of the diagonal band of Broca/Substantia Innominata, NBM = nucleus basalis of Meynert

Immunohistochemistry (IHC) with a pan- Aβ marker X-34 demonstrated the absence of amyloid plaques in the cortex, hippocampus and BFB in 4-month-old TgF344-AD rats, except one animal with a small plaque present in the hippocampus. At 6 months of age, accumulation of Aβ-plaques were observed in the hippocampus and cortex in all TgF344-AD rats (Figure 3-1B). Immuno-histochemical analysis of AT8-stained pTau accumulations revealed a significant effect of age in the cingulate cortex (CG), horizontal limb of the diagonal band of Broca and substantia innominata (HDB/SI), medial septum (MS), medial entorhinal cortex (mENT), nucleus basalis of Meynert (NBM) and retrosplenial cortex (RSC) with increased pTau in both WT and TgF344-Ad rats at 6-months of age compared with 4 months (Figure 3-1C, D). A significant genotype effect was observed in the locus coeruleus (LC), demonstrating increased pTau accumulation in the TgF344-AD rats. In addition, a significant genotype effect was observed in the dentate gyrus (DG), showing an increased pTau accumulation in the TgF3440AD rats, whereas a significant effect of age and genotype was observed in the CA1 region of the hippocampus, both showing an increased pTau accumulation over time and increased pTau in the TgF344-AD rats compared to WT (Supplementary table 3-1). Aforementioned results indicate that the 4-month-old timepoint is a pre-plaque stage in TgF344-AD rats, while the 6-month-old timepoint resembles the early-plaque stage.

3.4.2 Quasi-periodic pattern analysis in 4-month-old TgF344-AD rats and WT littermates

The great majority of studies investigating network aberrations in AD employed classical FC analysis. Thus, as a first and reference estimate of network aberrations in our model we performed region of interest (ROI) based analysis starting at 4-month-old TgF344-AD rats and littermate WT controls. Selected ROIs were important functional nodes of the default mode-like network (DMLN), hippocampal network (Hipp), lateral cortical network (LCN), sensory cortical network (Sens) and subcortical network excluding the hippocampal network and were based on the F344 atlas (Goerzen et al., 2020).

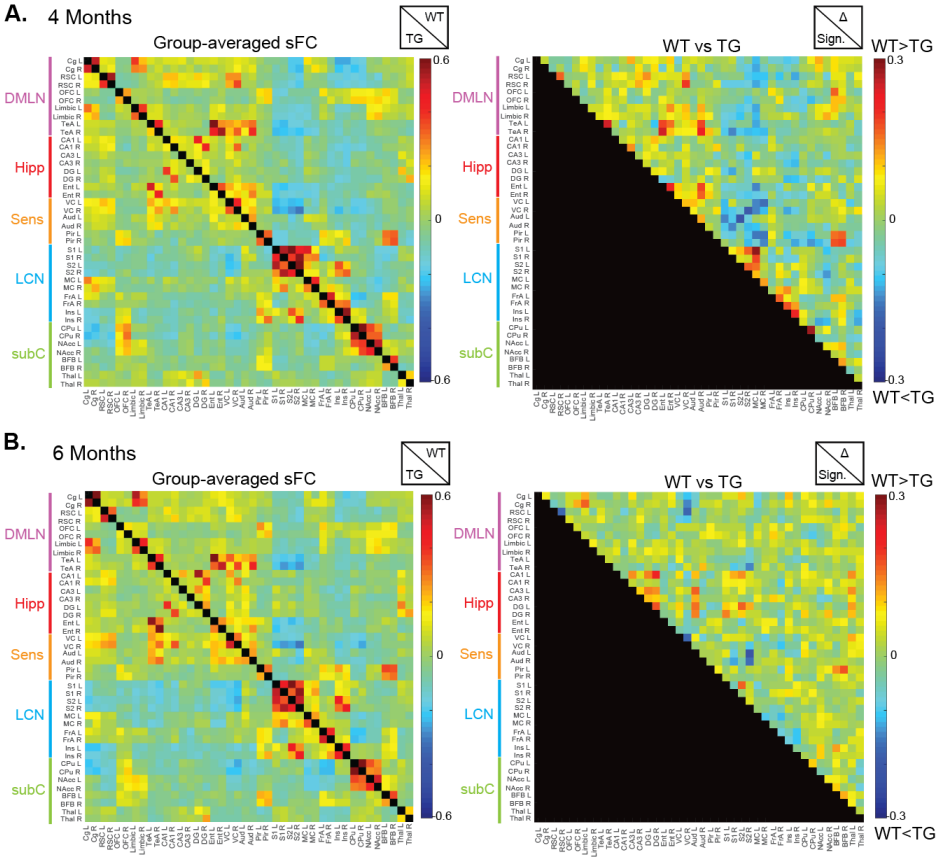

Figure 3-2: ROI based analysis demonstrates no significant differences in static FC between TgF344-AD (TG) rats and Wild-type (WT) littermates. ROI based matrices which displays the z-scored FC between ROI-pairs for the WT (top half of matrix) and TG (bottom half of matrix) at 4 months of age (A) and 6 months of age (B). Two-sample t-test (FDR $p<0.05$) demonstrates no significant differences in FC between groups, as is shown on the right matrix. DMLN = default mode-like network, Hipp = hippocampal network, Sens = sensory network, LCN = lateral cortical network, subC = subcortical network, L = left, R = right, Cg = cingulate cortex, RSC = retrosplenial cortex, OFC = orbitofrontal cortex, TeA = temporal association cortex, DG = dentate gyrus, VC = visual cortex, Aud = auditory cortex, Pir = Piriform cortex, S1 = primary somatosensory cortex, S2 = secondary somatosensory cortex, MC = motor cortex, FrA = frontal association cortex, Ins = insular cortex, CPu = caudate putamen, NAcc = nucleus Accumbens, BFB = basal forebrain, Thal = thalamus

In figure 3-2, the FC matrix including the group-averaged z-scored FC between each ROI pair is presented. In both groups and at both ages, FC can be observed within the LCN and between regions belonging to the DMLN, Hip and Sens networks. In the WT animals, anti-correlation can be observed between these networks and the LCN as is demonstrated by the blue color of the connections between these regions. This anti-correlation has a lower correlation value in the TgF344-AD rats at 4 months of age. However, two-sample statistical tests revealed no significant differences between genotypes after FDR correction, suggesting that static FC was not altered at the pre-and early plaque stage of AD in the TgF344-AD rats (Figure 3-3, Supplementary table 3-2).

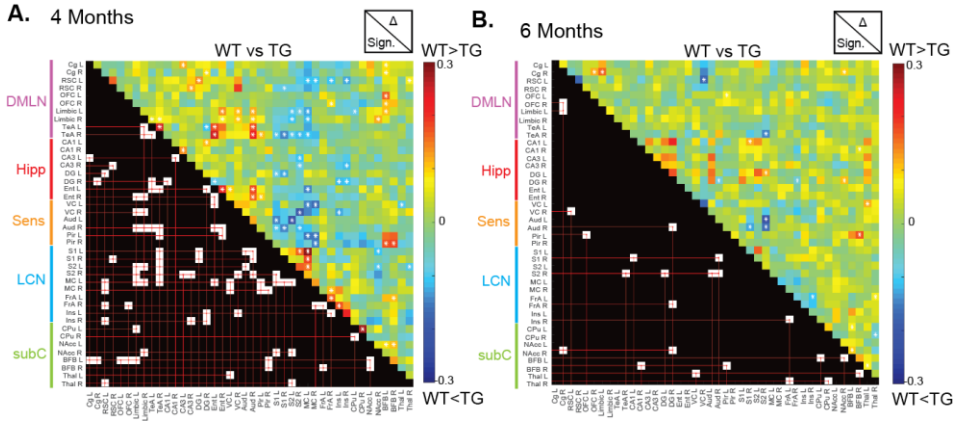

Figure 3-3: ROI based analysis without FDR correction. FC difference matrices which displaying the results of an uncorrected two-sample t-test demonstrating significant differences in FC (white boxes lower half of the matrix) which do not survive FDR correction. DMLN = default mode-like network, Hipp = hippocampal network, Sens = sensory network, LCN = lateral cortical network, subC = subcortical network, L = left, R = right, Cg = cingulate cortex, RSC = retrosplenial cortex, OFC = orbitofrontal cortex, TeA = temporal association cortex, DG = dentate gyrus, VC = visual cortex, Aud = auditory cortex, Pir = Piriform cortex, S1 = primary somatosensory cortex, S2 = secondary somatosensory cortex, MC = motor cortex, FrA = frontal association cortex, Ins = insular cortex, CPu = caudate putamen, NAcc = nucleus Accumbens, BFB = basal forebrain, Thal = thalamus

Subsequently, to potentially unravel subtle differences in network function that the static FC analysis was not sensitive enough to show, quasi-periodic pattern (QPP)

analysis was performed. Based on previous findings in mice, 200 short 3.6s QPPs were extracted at the group level for each genotype at 4-months of age. These short group-level QPPs were expected to reveal the brain dynamics of single brain states (Belloy, Naeyaert, et al., 2018; Belloy, Shah, et al., 2018). Next, hierarchical clustering was performed on the 200 extracted QPPs to identify clusters of patterns representing a unitary or very similar brain states based on the similarity between their spatial and temporal properties (see M&M 3.3.2.3). The clustering revealed two large clusters in the wildtype (WT) rats, whereas multiple smaller clusters could be observed in the TgF344-AD rats (Figure 3-4).

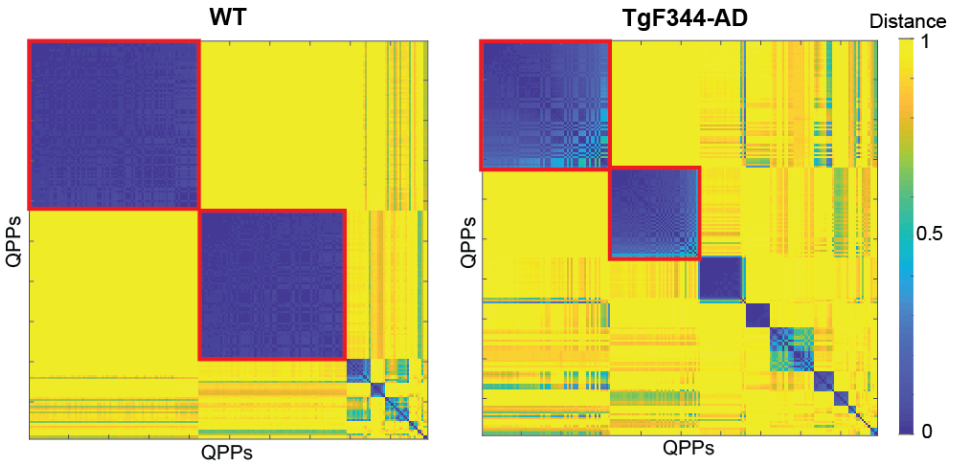

Figure 3-4: Hierarchical clustering based on Spatiotemporal properties of QPPs of 4-month-old WT and TgF344-AD rats. Distance matrices of the clustering solution in the wild-type (WT) animals (left) and TgF344-AD rats (right). Colors indicate the distance between a pair of QPPs. Red squares mark the clusters of QPPs which were robust according to the criteria, and which were used in further analysis.

The QPPs with the highest occurrence rate were named as representative QPPs (rQPPs) for each cluster. Two anti-correlated group-level rQPPs were observed in the WT and TgF344-AD rats (Figure 3-5). The first rQPP, referred to as QPP-DMLN^{+}, showed co-activation of regions belonging to the DMLN (i.e. CG, RSC, orbitofrontal cortex (OFC), prelimbic cortex (PrL), infralimic cortex, visual cortex (VC), and auditory cortex) and co-deactivation of regions belonging to the lateral cortical network (LCN) (i.e., primary, and

secondary somatosensory cortices, primary and secondary motor cortices, frontal association cortex and the caudate putamen) (Figure 3-5 A&B). The second rQPP, referred to as QPP-LCN^{+}, showed the opposite pattern with a deactivated DMLN and activated LCN (Figure 3-5C). Both rQPPs showed a high spatial similarity between groups.

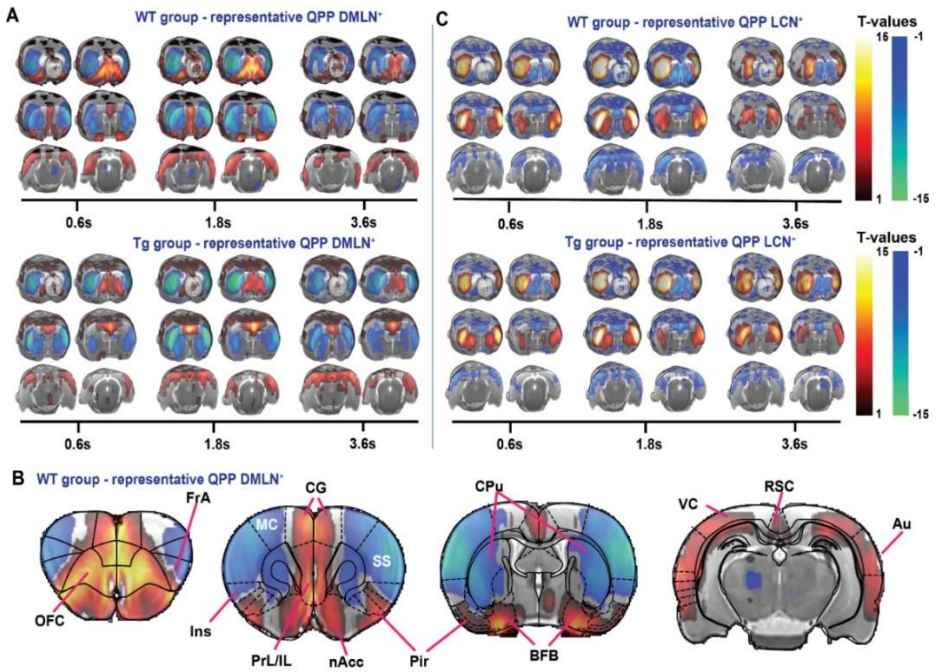

Figure 3-5: Visualization of group-level rQPPs of 4-month-old TgF344-AD rats (Tg) and wildtype littermates (WT). Results of one-sample t-test (FDR p<0.05, minimum cluster size 10 voxels) of QPP-DMLN (A) and QPP-LCN (C) visualized on the study-specific 3D template, demonstrating rQPPs for each experimental group. The T-maps represent voxels with a statistically significant higher (red, yellow) / lower (blue green) BOLD activity at the occurrences of the QPP relative to the mean BOLD signal across all time points of the image series.(p<0.05, FDR corrected). B) Regional outlines of coronal slices of the Paxinos atlas overlaid on the T-map of QPP-DMLN+ of the WT. OFC = Orbitofrontal cortex, FrA = Frontal Association cortex, MC = motor cortices, SS = somatosensory cortices, Cg = cingulate cortex, PrL = Prelimbic cortex, IL = Infralimbic cortex, Ins = insular cortex, nAcc = nucleus Accumbens, CPu = Caudate Putamen, BFB = basal forebrain, Pir = Piriform cortex, VC = visual cortices, RSC = retrosplenial cortex, Au = auditory cortex.

Alterations in neuronal activity can lead to differences in regional activation during certain brain states, which could induce spatial differences in activation within rQPPs. Therefore, voxel-level co-activations and co-deactivations in both matched rQPPs were compared between groups (Figure 3-6A, B). Significant differences in BOLD activity within QPP-LCN^{+} were observed and included higher involvement of the somatosensory and motor cortices in the TgF344-AD rats (Figure 3-6A-B, Supplementary table 3-3). Moreover, differences in spatial BOLD activation were also observed within QPP-DMLN^{+} (Figure 3-6, Supplementary table 3-3). In 4-month-old TgF344-AD rats, BOLD activity was significantly reduced in regions belonging to the DMLN, mainly the entorhinal cortex, OFC and PrL (Cohen's d = 0.75). Interestingly, an increased BOLD activity was observed in the CG of TgF344-AD rats (Cohen's d = 0.40), a hub region within the DMLN, indicating a potential disinhibition of this area in AD. In addition, the basal forebrain region (BFB), was found to be significantly co-activated with regions belonging to the DMLN in the WT animals, but not in TgF344-AD rats (Cohen's d = 0.80). The observed loss of co-activation between the BFB and the DMLN in TgF344-AD rats within QPPs at the pre-plaque stage, as well as the disinhibition of CG that has strong connections to BFB, strongly corroborate the important role of BFB in the regulation of network activity and are consistent with the spatial alterations observed in QPP-DMLN^{+} .

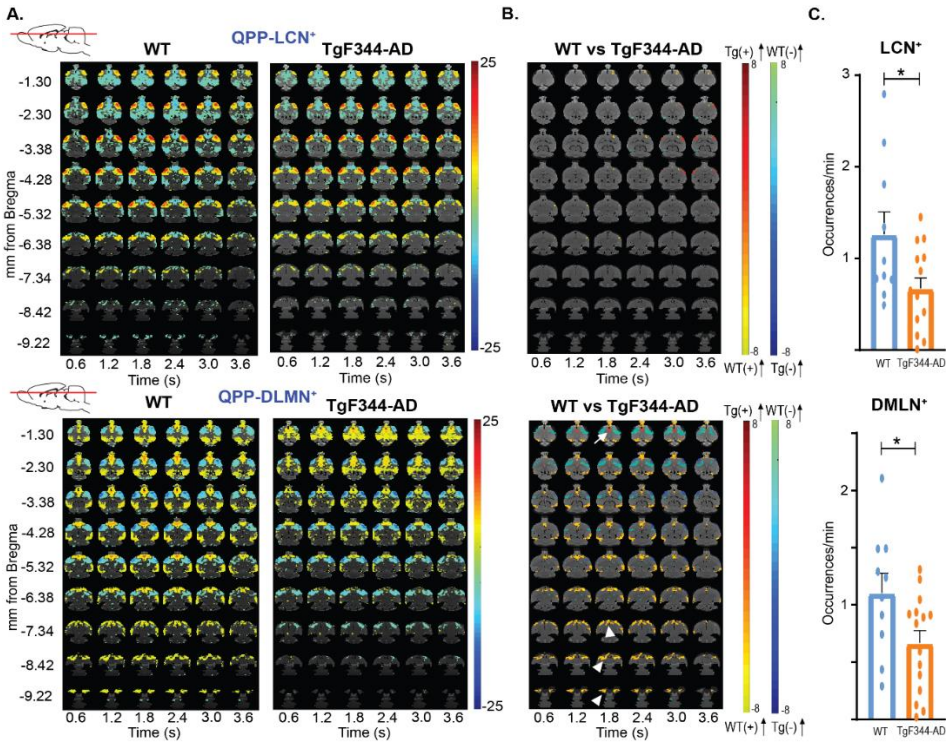

Figure 3-6: Spatiotemporal alterations in network activity in 4-month-old TgF344-AD rats (Tg) as compared to control littermates (WT). A) T-maps (two-tailed one sample t-tests, FDR p<0.05, minimal cluster size 10) show the two rQPPs in each group. B) T-maps of the two-sample t-test (two-tailed two sample t-tests, FDR p<0.05, minimal cluster size 10) between the rQPPs of TgF344-AD and WT rats. The warm colors (red/yellow) indicate a significant difference in BOLD activity between groups for voxels which are positive (activated) in the original QPP of the WT group. The right color bar (light blue/dark blue) indicate significant genotype differences for voxels which were deactivated in the original QPP of the WT group. For the QPP-DMLN+, TgF344-AD rats demonstrate a significantly lower involvement of the OFC, PrL, Ent and BFB is observed (arrowheads), together with a significantly increased activity of the CG (arrow). C) Comparison of cluster wise-occurrence rates between groups (mean +/- SEM, two-sample t-test, two-tailed, FDR, p<0.05) demonstrate significantly lower occurrences in the TgF344-AD rats for both QPPs. *p<0.05.

Having established alterations in the spatial structure of the QPP-DMLN$^+$ in the TgF344-AD rats, we then proceeded to analyse if the frequency of occurrence of QPPs would

also change across the groups. Therefore, average occurrence rates were calculated for each group (for methods check section 3.4.3.3). Significantly decreased occurrence rates of QPPs were observed for both the QPP-DMLN$^+$ and the QPP-LCN$^+$ clusters in the 4-month-old TgF344-AD rats when compared to WT (Figure 3-6C, $p_{QPP\text{-}DMLN} = 0.0427$, $p_{QPP\text{-}LCN} = 0.0449$), demonstrating that the instances of coordinated network activity were less common in the TgF344-AD animals during the pre-plaque stage.

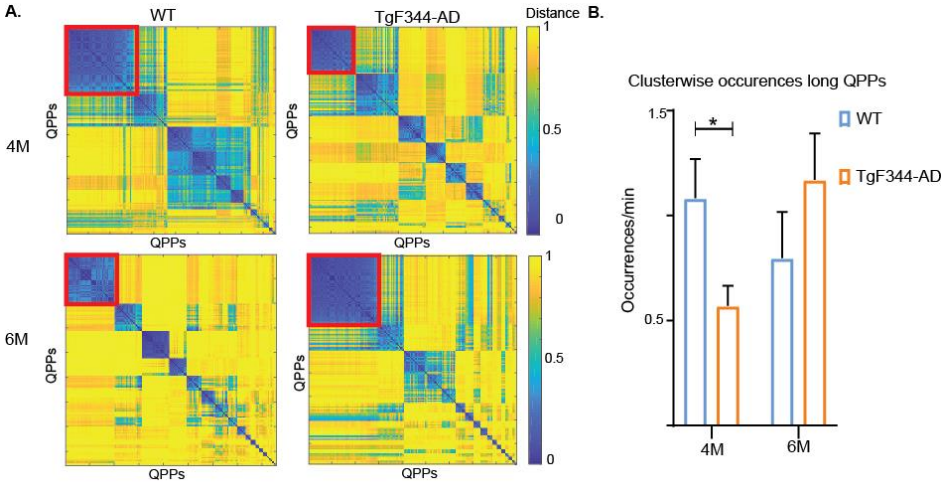

Figure 3-7: Analysis of 9 second long QPPs at 4 and 6 months-old TgF344-AD and WT rats. A) Distance matrices based on the results of the hierarchical clustering of all 200 extracted QPPs. Yellow colors indicate a high distance, while blue colors mean a small distance (high similarity). After applying all criteria to select robust clusters, only 1 cluster remained for each group at each time point. B) Statistically lower cluster wise occurrence rates for long QPPs at 4 months, but not at 6 months (two sample t-tests, FDR $p<0.05$)

As indicated above, short duration QPPs resemble unitary brain states depicting co-modulation of brain regions around their peak activity. To investigate if other longer duration QPPs exist and/or to uncover the temporal evolution of brain activity around the short duration QPPs we proceeded with the detection of longer patterns (9 seconds = 15 TRs) in the two groups. In this case, spatiotemporal clustering resulted in one cluster of rQPPs in each group (Figure 3-7). rQPPs were again visualized using a one-sample t-test, and were phase-aligned (Figure 3-8A). Visual inspection of the resulting pattern

revealed that this 9s long rQPP showed the network activity prior to, and during the complete QPP-DMLN^{+} brain state.

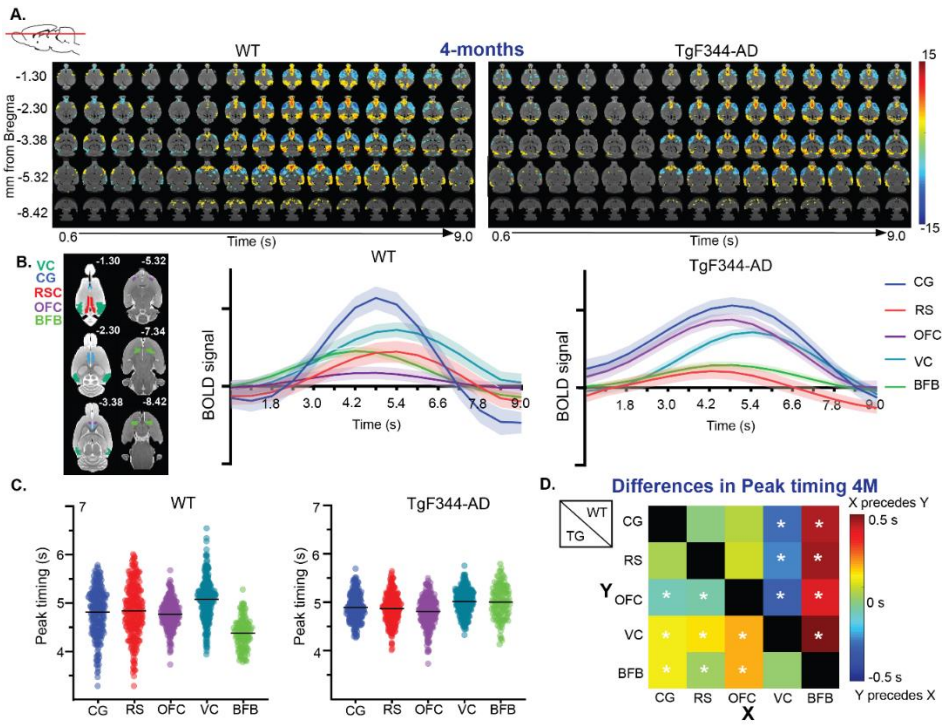

Figure 3-8 Long QPPs to investigate propagation of network activity A) T-maps (two-tailed one sample t-tests, FDR p<0.05, minimal cluster size 10) show the long rQPP in each group. Colors indicate T-values. B) average BOLD time courses within regions of interest during 9-second QPPs. C) Peak timings averaged across occurrences for each voxel within a certain region. Dots represent the distribution of average peak timing of individual region of interest (ROI)-specific voxels; the black lines represent the mean peak timing across all ROI-specific voxels. D) Differences (peaky-peakx) in mean peak timing across voxels for each connection. The top half represents the wildtype (WT) animals, while the lower half represents the TgF344-AD rats (Tg). Unpaired two-sample t-tests (FDR p<0.05) between regions were performed to evaluate if peak timing was significantly different between ROIs. CG = Cingulate cortex, OFC = orbitofrontal cortex, RSC/RS = retrosplenial cortex, HC = hippocampus, BFB = basal forebrain. * p<0.05.

Thus, to better visualize the activity evolution around this brain state, we extracted the BOLD time courses of ROIs that demonstrated large, regional differences in spatial activity in the short QPP-DMLN^{+} and altered rQPP occurrences (Figure 3-8B). This revealed that peak activity in co-modulating ROIs showed differences in time. To statistically evaluate if activity in certain brain regions precedes the activity in other regions, differences in voxel-wise peak timing were investigated separately for the rQPP of each group. Propagation of BOLD activity across regions was evaluated by comparing the peak times of each voxel in a certain region of interest, averaged across different rQPP occurrences. Statistical comparison of the distributions of voxel wise peak times demonstrated that peak activity in the BFB, on average, preceded the peak activity in regions belonging to the DMLN in the WT animals, as is demonstrated by the significant difference in peak timings between the BFB and other regions within the WT animals (Figure 3-8 C-D, Supplementary table 3-4). This indicates that the BFB was leading the DMLN activity within rQPPs in the WT animals. In addition, peak activity within the visual cortex lagged behind peak activity in other regions of the DMLN. In the TgF344-AD rats on the other hand, BFB activity did not significantly precede the activity in other regions of the DMLN within rQPPs. Instead, peak timing in the OFC preceded the peak timings in other regions, demonstrating an altered sequence of regional activation within rQPPs in the TgF344-AD rats at pre-plaque stage.

3.4.3 Quasi-periodic pattern analysis in 6-month-old TgF344-AD rats and WT littermates

Since we observed large spatial and temporal differences in whole brain network activity during the pre-plaque stage, we wondered how these patterns of brain activity would develop at the early-plague stage given that scientists have previously shown that plagues at this AD stage have a neuroprotective role (Bishop & Robinson, 2004; Brody, Jiang, Wildburger, & Esparza, 2017). To answer this question, rsfMRI and QPP-analysis was performed on the same animals at 6 months of age when plaques start to appear in this animal model. Similar to the analysis at 4 months, two-hundred short duration QPPs were extracted in each group, and clustered using hierarchical clustering. In both

groups, two clusters were identified, resulting in a QPP-DMLN^{+} and QPP-LCN^{+} (Figure 3-9).

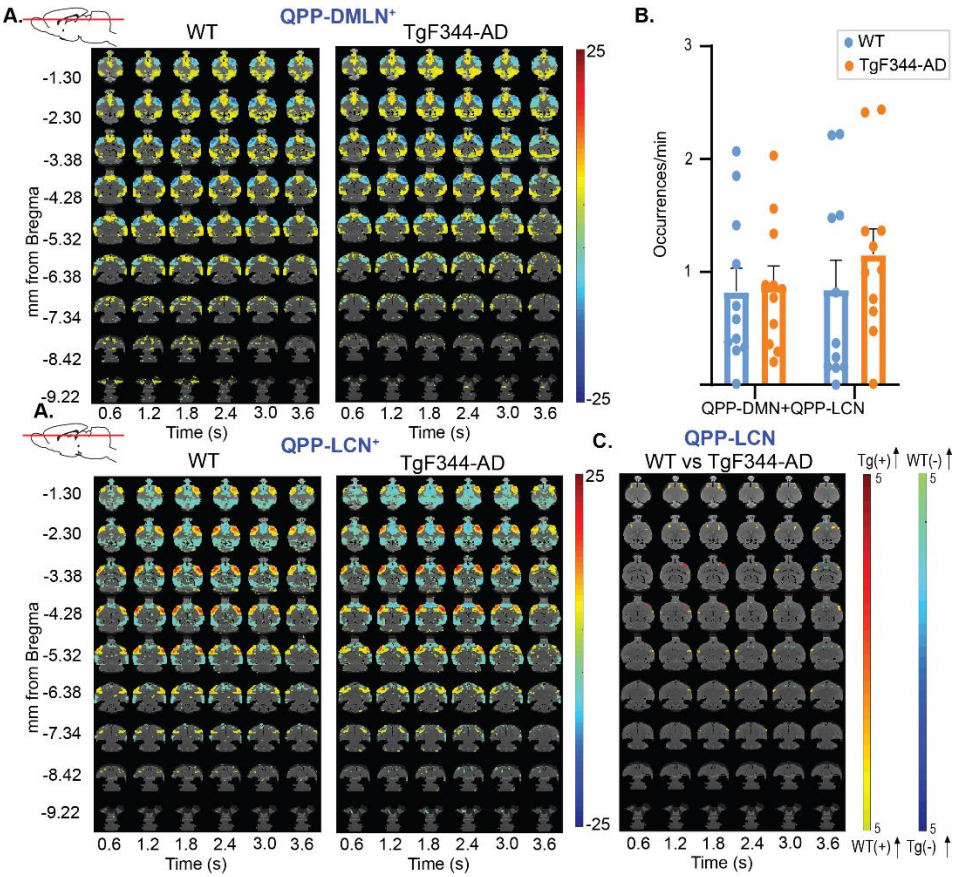

Figure 3-9: Spatiotemporal alterations in network activity in 6-month-old TgF344-AD rats (Tg) as compared to control littermates (WT). A) T-maps (two-tailed one sample T-tests, FDR p<0.05, minimal cluster size 10) show the two rQPPs in each group. Comparison of cluster wise-occurrence rates between groups (two-sample t-test, two-tailed, FDR p<0.05) demonstrate no significant differences in occurrence of both QPPs between groups. C) T-maps (two-tailed two sample T-tests, FDR p<0.05, minimal cluster size 10) between rQPP-LCN. The warm colors (red/yellow) indicate a significant difference in BOLD activity between groups for voxels which are positive (activated) in the original QPP of the WT group. The right color bar (light blue/dark blue) indicate significant genotype differences for voxels which were deactivated in the original QPP of the WT group.

Compared to the 4-month time-point, 2-sample t-tests revealed less prominent inter-group differences in voxel-level co-activations in six-month old rats (Figure 3-9, Effect size – Supplementary table 3-3). Spatial alterations in QPP-LCN^{+} included a decreased BOLD activity in the somatosensory cortex, while the BOLD activity in the CPu was significantly higher in the TgF344-AD rats. When comparing cluster-averaged occurrence rates between groups, we observed no significant difference in occurrence rates for QPP-DMLN^{+} ($p=0.294847$), and QPP-LCN^{+} ($p=0.126209$). These results suggest that network activity within rQPPs in TgF344-AD rats at pre-plaque stages, normalized and closer resembled the activity of age-matched WT littermates.

The aforementioned results demonstrated increased spatiotemporal similarity of short rQPPs between groups during the early-plaque stage. Given that the spatiotemporal changes coincided with altered sequential BOLD activity observed in TgF344-AD during the pre-plaque stage, we asked if at the early-plaque stage, the sequence of activation was also closer to the WTs. Therefore, 9-second-long QPPs were extracted in each group. Spatiotemporal clustering again resulted in one cluster of robust QPPs in each group.

Representative QPPs were visualized using a one-sample t-test, were phase-aligned and differences in voxel-wise peak timing were evaluated separately for the rQPP of each group (Figure 3-10). In WT rats, BFB activity preceded the activity in other regions of the DMLN, similar to what was observed at the pre-plaque stage in WT rats, which suggested BFB activity was leading the activity in the DMLN (Figure 3-10). In contrast, In TgF344-AD rats, peak activity in the OFC preceded the activity in other regions during the rQPP in the TgF344-AD rats, similar to the pre-plaque stage, which demonstrated that the altered sequence of activation was persistent at the early-plaque stage. To investigate if BFB peak timings differed between groups and across ages, an ANOVA analysis was performed on the voxel-wise peak timings in the BFB. A significant interaction effect ($p = 0.0008$), genotype effect ($p = < 0.0001$) and age effect ($p = 0.0007$) were observed. Post hoc students t-tests (FDR $p<0.05$) demonstrated a significant difference in the BFB

peak timings between WT and TgF344-AD rats at both ages (p_{4M} = <0.0001, p_{6M} = <0.0001). In addition, a significant age effect was observed in the TgF344-AD rats ($p_{TgF344-AD}$ = < 0.0001), but not in WT rats (p_{WT} = 0.9848), suggesting that, in contrast to the peak timing in the TgF344-AD rats, BFB peak timing in the WT remained stable over time.

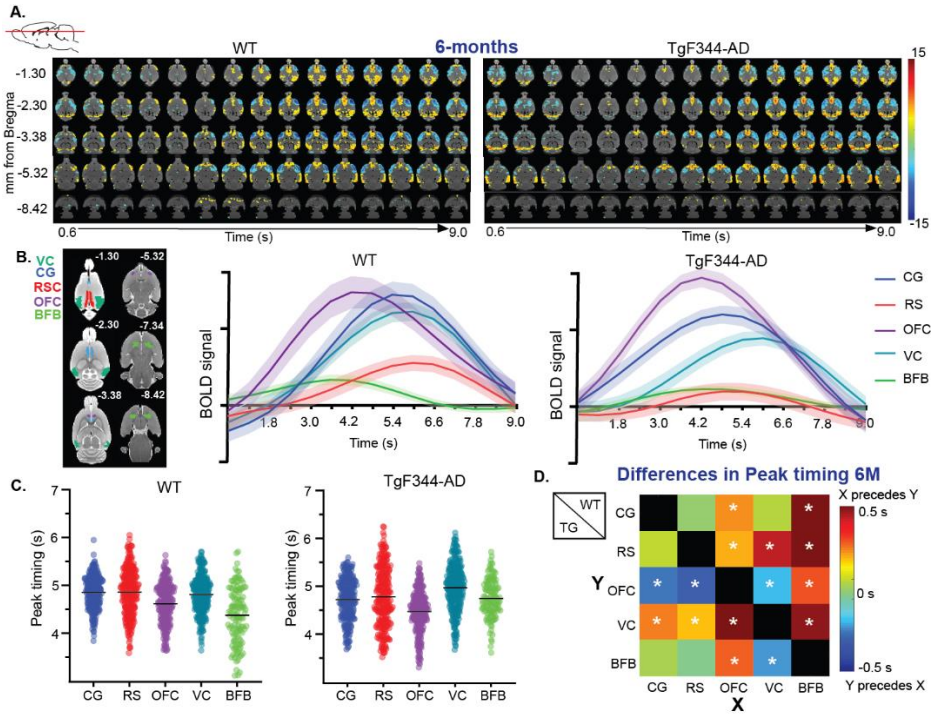

Figure 3-10: Long QPPs to investigate propagation of network activity at the early-plaque stage

A) T-maps (two-tailed one sample t-tests, FDR p<0.05, minimal cluster size 10) show the long rQPPs in each group. Colors indicate T-values. B) average BOLD timecourses within regions of interest during 9-second QPPs. C) Peak timings averaged across occurrences for each voxel within a certain region. Dots represent the distribution of average peak timing of individual region of interest (ROI)-specific voxels; the black lines represent the mean peak timing across all ROI-specific voxels. D) Differences (peaky-peakx) in mean peak timing across voxels for each connection (X=row, Y=column). The top half represents the wildtype (WT) animals, while the lower half represents the TgF344-AD rats (Tg). Unpaired two-sample t-tests (FDR p<0.05) between regions were performed to evaluate if peak timing was significantly different between ROIs. CG = Cingulate cortex, OFC = orbitofrontal cortex, RSC = retrosplenial cortex, HC = hippocampus, BFB = basal forebrain. * p<0.05

3.4.4 Immunohistochemical evaluation of neuro-inflammation and synaptic alterations

Accumulation of (soluble) Aβ and pTau are associated with increased abundance of (reactive) astrocytes and microglial cells. To investigate if neuroinflammation was present in the TgF344-AD rats during the pre-and early-plaque stages, immunohistochemistry was performed using glial fibrillary acidic protein (GFAP) and Iba-1 staining for astrocytes and microglial cells respectively (Figure 3-11 A-B) in 7 different brain regions, which either showed differences in the QPPs (CG, RSC, Ent, SS) or regions which are part of the BFB nuclei (MS, HDB/SI, NBM). Statistical analysis (two-way ANOVA, age, genotype, age*genotype) revealed a significant interaction between age and genotype in the nucleus basalis of Meynert (NBM) ($p=0.0262$) (Supplementary table 3-5). Post-hoc analysis demonstrated a significantly higher GFAP signal in the NBM in 4-month-old TgF344-AD rats compared with age-matched WT ($p=0.0366$), which was not present at 6 months ($p=0.5880$). Moreover, a significant decrease in GFAP levels over time was observed in tissue slices from TgF344-AD rats ($p=0.0072$), an effect which was not present in the WT ($p=0.9064$). Interestingly, a significant genotype effect ($p=0.0269$) was observed in another nucleus of the BFB, the horizontal limb of the diagonal band of Broca and substantia innominata (HDB/SI), demonstrating increased abundance of astrocytes in the TgF344-AD rats, which was mainly present at 4-months of age (Figure 3-11 A-B). These results suggest that the astrogliosis in the NBM and HDB/SI is present during the pre-plaque stage but disappears at the early-plaque stage in TgF344-AD rats. Moreover, significantly higher levels of GFAP were observed in the RSC of TgF344-AD rats (genotype $p = 0.0372$), mainly at 6-monhts of age. In the RSC, increased astrogliosis is observed at both ages. When comparing the microglial abundance, no significant genotype differences were observed. However, a significant age effect was observed in the MS, Ent, NBM and SS (Supplementary table 3-6), indicating a decrease of microglial abundance over time.

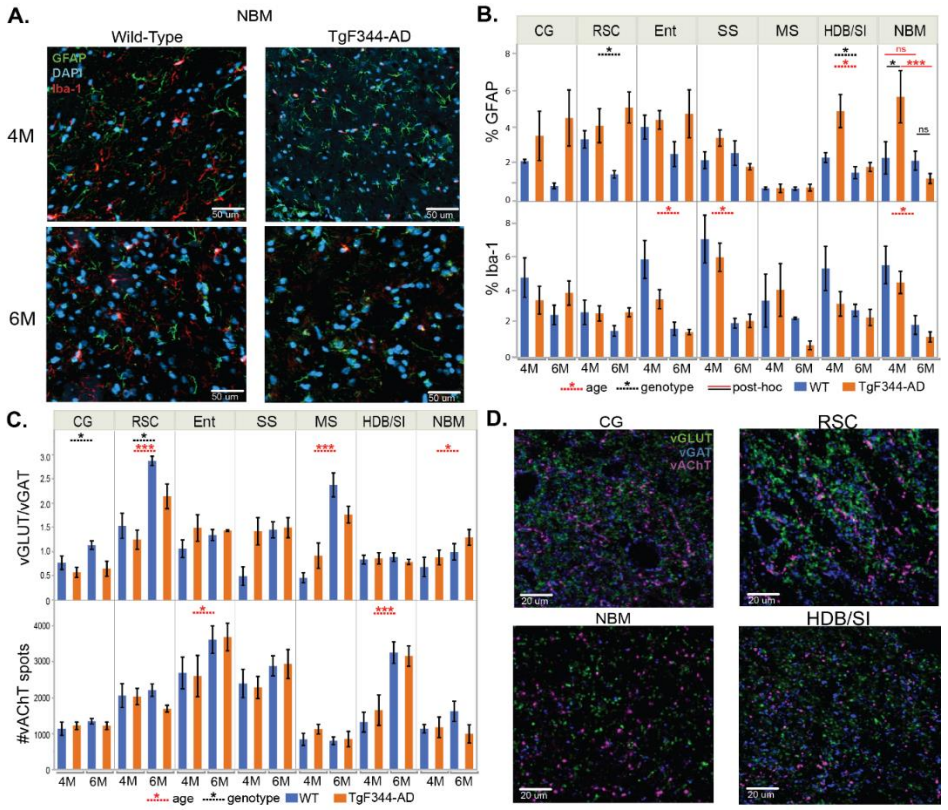

Figure 3-11: Histological evaluation of neuroinflammation and synaptic alterations. A) Representative images showing astrocytes (green, GFAP) and microglia cells (red, Iba-1) in nucleus basalis of Meynert (NBM). Nuclei were counterstained with DAPI (blue). B) Graphs represent the %area positive for GFAP (top) or %area positive for Iba-1 (mean +/- SEM) (bottom) for each brain region. Dashed lines indicate significant genotype effects (black) or age effects (red). Solid lines indicate significant differences between genotypes (black) or ages (red) after Student t-test (FDR $p<0.05$) when genotype*age interaction was significant. C) Graphs represent the mean vGLUT/vGAT ration (top) and spot count of vAChT (bottom) (mean +/- SEM). Blue represents the WT animals, while orange represents the TgF344-rats. D) Representative images of the triple staining (vGLUT in green, vGAT in blue, vAChT in magenta) of three different regions in a representative 4-month-old WT rat. *$p<0.05$, **$p<0.01$ ***$p<0.001$. CG = cingulate cortex, RSC = retrosplenial cortex, Ent = entorhinal cortex, SS = somatosensory cortex, MS = medial septum, HDB/SI = horizontal limb of the diagonal band of Broca/Substantia Innominata, NBM = nucleus basalis of Meynert. vAChT = vesicular acetylcholine transporter, vGAT = vesicular GABA transporter, vGlut = vesicular glutamate transporter, WT = wild-type

Increased concentrations of (soluble) Aβ and pTau might induce alterations in neurotransmission of GABAergic and glutamatergic neurons, which could result in an imbalance between excitatory and inhibitory synapses. Studies have demonstrated that alterations in the excitatory/inhibitory balance could induce alterations in BOLD activity. To investigate if alterations in cortical and subcortical excitatory/inhibitory (E/I) balance were present in the TgF344-AD rats in regions which demonstrated altered regional activation within QPPs, histological analysis of glutamatergic and GABAergic synapses was performed. The ratio of the number of glutamatergic and GABAergic synapses (vGLUT/vGAT) was compared between groups using a two-way ANOVA (Figure 3-11 C-D). The analysis demonstrated a significant genotype effect in the RSC and CG, indicating a shift in E/I balance towards decreased excitation or increased inhibition in the TgF344-AD rats. No significant genotype effects were observed in other brain regions. Significant age effects were observed in the RSC, MS and NBM of the WT and TgF344-AD rats indicating an increased vGLUT/vGAT ratio (Figure 3-11 C-D, Supplementary table 3-7).

Cholinergic neurons which reside in the BFB and project to the entire cortex, have been implicated in the modulation of cortical networks and are known to be vulnerable for (soluble) Aβ-induced toxicity. We hypothesized that alterations in cholinergic signalling could be responsible for the spatiotemporal alterations observed in the QPPs during the pre-plaque stage. Therefore, immunohistochemical evaluation of cholinergic synapses was performed to evaluate if the abundance of cholinergic synapses was decreased in the cortex and BFB. Synaptic counts for cholinergic synapses (vAChT) demonstrated significant age effects in the Ent and HDB/SI, where the cholinergic synaptic density at 6-months was increased compared to 4-months in both groups. However, no significant genotype effects were observed in the abundance of cholinergic synapses (Figure 3-11D, Supplementary table 3-8).

3.5 Discussion

This study investigated whole-brain, recurrent patterns of brain activity, at early stages of AD in a highly translational rat model of AD. At 4 months of age, during the pre-plaque

stage, significant inter-genotype differences in voxel-level activation were observed in QPP-DMLN^{+}, which mainly involved decreased BOLD activity in the BFB and regions belonging to the DMLN, together with an increased BOLD activity in the CG. Moreover, peak BOLD activity in the BFB preceded peak activity in other regions in wild-types, but not in TgF344-AD rats. These results suggest differences in neuronal mechanisms modulate the spatial involvement of brain regions in TgF344-AD rats. The differences in network activity coincided with, astrogliosis, limited to the NBM, HDB/SI, and RSC in the absence of Aβ depositions and pTau in cortical and subcortical regions. In addition, a decreased E/I ratio was observed at the pre-plaque stage, suggestive of increased inhibition or decreased excitation in the CG and RSC, two hub regions of the DMLN. However, at 6 months of age, during the early-plaque stage, spatiotemporal properties of QPPs in the TgF344-AD rats were more similar to the WT littermates, while altered sequence of BOLD activation persisted in the TgF344-AD rats. Interestingly, astrogliosis in the BFB was absent at the early-plaque stage, while decreased excitation and/or increased inhibition in the CG and RSC persisted at the early-plaque stage, suggesting an important role of early astrogliosis in the NBM in global network alterations.

3.5.1 Static functional connectivity vs QPP analysis of rsfMRI data in TgF344-AD rats

Previous research involving QPP analysis investigated the relationship between QPPs and static FC, by evaluating FC before and after regression of QPPs in humans. They observed a decrease in sFC between the default-mode network and task-positive network after the regression of the main QPP, demonstrating that QPPs contribute to static FC (Abbas, Belloy, et al., 2019). Thus, the synchronous co-activation events that QPPs reflect, do contribute to static FC. However, sFC is calculated based on the whole BOLD-time course, on which the short window QPPs - demonstrating temporary high FC, only have a small contribution. The current study performed a region-of interest-based analysis of static FC which did not result in significant differences between genotypes after multiple comparison correction. On the other hand, we did observe significant spatial alterations in QPPs in several regions, mainly belonging to the DMLN.

When looking at the observed differences in sFC, without FDR correction (Figure 3-3, Supplementary table 3-2), differences between regions belonging to the LCN and DMLN were observed at 4 months of age, consistent with our QPP analysis. In addition, sFC differences between the BFB and DMLN regions were observed at the pre-plaque stage. These differences did not survive the FDR correction, but it does indicate that the changes observed in the QPPs are to a lesser extent present in the sFC differences at 4 months of age. In addition, at 6 months, differences in sFC become less abundant, similar to what we observe in the QPPs at that timepoint. These results suggest that QPP analysis is more sensitive to early alterations in network function than static FC analysis.

3.5.2 AD pathology and behavioural alterations in TgF344-AD rats

Amyloid pathology is one of the major histopathological hallmarks of AD. Cortical and hippocampal Aβ-plaques have been observed from 6-months onwards in TgF344-AD rats (R. M. Cohen et al., 2013; Sare et al., 2020), as is observed in the current study. At 4-months of age, Aβ-plaques were absent, as has been observed before in 4-month old TgF344-AD rats (Sare et al., 2020). The current study observed increased concentrations of soluble Aβ species in 4-month-old TgF344-AD rats, which is in line with the results of a recent study which observed increased concentrations of soluble Aβ1-40 and Aβ1-42 in blood samples of 3-month-old TgF344-AD rats(Ratner et al., 2021). A previous study has observed pTau accumulation in the locus coeruleus observed at 6 months of age in TgF344-AD rats (Rorabaugh et al., 2017), similar to our observation in the current study. However, no other studies have investigated pTau accumulation in other brain regions at 4 and/or 6 months of age. Only a few studies have investigated cognitive and behavioral alterations in 4-month-old TgF344-AD rats. The two studies from two different facilities have observed altered spatial navigation and spatial memory in 4-month-old TgF344-AD rats using frequently used behavioral tests (e.g., Barnes Maze and Active Allothetic Place Avoidance test) (Fowler et al., 2022; Proskauer Pena et al., 2021). Another research group observed impairments in working memory in 5-month-old TgF344-AD rats, but not at later time points (Tudela et al., 2019). In contrast, a different research group did not observe significant differences in spatial memory in 4-month-old

TgF344-AD rats in the Morris water Maze but did find differences at later time points (Berkowitz et al., 2018). These results clearly illustrate the variability of the behavioral test results, which are possibly induced by the use of different behavioral assays and different research groups. Nevertheless, the current study observed altered activity in the BFB, of which the cholinergic projections to the hippocampus, RSC and parietal cortex are important in spatial navigation and spatial memory (Solari & Hangya, 2018). The altered activity in the BFB and DMLN observed in the QPPs could be indicative of cognitive impairments. Moreover, the current study observed astrogliosis in the NBM and RSC, together with a decreased E/I ratio in the RSC, which might be important cellular pathological processes contributing to the behavioral alterations observed in aforementioned studies.

3.5.3 Spatial and temporal alterations in DMLN activity in AD

The observed QPPs in this study demonstrated two unitary brain states, namely an activated state of DMLN with LCN deactivated (i.e., QPP-DMLN$^+$) and an activated state of LCN with DMLN deactivated (i.e., QPP-LCN$^+$). Similar QPPs have been observed in mice and humans (DMN and TPN) (Belloy et al., 2021; Belloy, Naeyaert, et al., 2018; Yousefi & Keilholz, 2021). In TgF344-AD rats we found a decreased frequency of occurrence of both short duration QPPs, and the presence of prominent spatial alterations in QPP-DMLN$^+$ during the pre-plaque stage. Key differences consisted mainly of a decreased co-activation of the BFB with the DMLN, decreased BOLD activity within the DMLN and an increased BOLD activity in the CG in TgF344-AD rats. These results are consistent with similar observations describing changes in the QPP-DMN$^+$ in a recent study in patients with subjective cognitive decline, a self-perceived cognitive deterioration which is thought to be associated with an increased risk for developing AD related MCI. Using dynamic FC analyses in healthy controls and patients with subjective cognitive decline, Liang et al. observed decreased occurrence of a brain state where DMN was activated, while other networks were deactivated (Liang et al., 2021). This brain state resembles the QPP-DMLN observed in this study. The analogy between the findings of Liang et al.

and the current study suggest similar alterations in DMLN activity are observed in patients with subjective cognitive decline and at pre-plaque stages in the TgF344-AD rat.

3.5.4 BFB dysfunction in AD

Changes in BFB volume measured by MRI have been observed at early stages of AD in patients and have been proven to be related to early BFB degeneration (Grothe et al., 2014; Herdick et al., 2020; Scheef et al., 2019). Moreover, decreases in BFB volume are predictive of an increased risk of conversion from mild cognitive impairment (MCI) to dementia (Brueggen et al., 2015). During the presymptomatic, prodromal stages, BFB degeneration, detected with volumetric MRI analysis, precedes the spread of cortical Aβ pathology (Schmitz et al., 2018; Schmitz, Nathan Spreng, & Alzheimer's Disease Neuroimaging, 2016). Since functional changes precede volumetric changes, BFB FC could be a potential earlier biomarker for AD. A recent study in patients with subjective cognitive decline demonstrated a significantly decreased FC between the BFB and the hippocampus (Chiesa et al., 2019). In addition, a recent study observed significant correlations between BFB connectivity, cerebrospinal fluid biomarkers and blood serum biomarkers of AD in patients at different stages of the AD (Teipel et al., 2022), strengthening the hypothesis that alterations in BFB FC could be used to detect AD at early stages. Future experiments using QPP analysis on data of (presymptomatic) AD patients would be valuable to investigate if our finding can be translated to human-AD, i.e., study if the disconnection between the BFB and the DMN within QPPs could be used as an early biomarker of AD.

3.5.5 Altered BFB modulatory function during whole-brain network activity in AD

The mechanisms leading and modulating the whole-brain network activity are still poorly understood. A recent study in humans investigated propagation of activity within QPPs across different brain regions, in order to elucidate brain regions driving the QPP activity. In all QPPs observed in humans, peak activity within the thalamus, brainstem

and deep nuclei preceded cortical activity (Yousefi & Keilholz, 2021). Partially in agreement with the findings in humans, the current study shows that in WT rats at both ages, the peak of BOLD activity within the BFB precedes the activity within the DMLN, suggesting an important role of the BFB in coordinating the network activity in rats and humans. Further evidence of the modulating role of the BFB in human network activity was presented in a recent study by Harrison et al. (2021), where they observed that the deactivation of the BFB precedes the deactivation of the DMN during tasks in human subjects. Moreover, dynamic causal modelling, an analysis technique used to assess the direction of FC, confirmed that the BFB was driving the changes in DMN upon task initiation (Harrison et al., 2021). In addition, other studies state that projections from the BFB are thought to drive waves of propagating activity from anterior to posterior brain areas, as is observed in the QPPs (Massimini, Huber, Ferrarelli, Hill, & Tononi, 2004; Pais-Roldan et al., 2021). Together, these observations support our hypothesis that the BFB could act as an important leader and modulator of whole-brain network activity within QPPs in healthy humans and rats. In the TgF344-AD rats, differences in propagation of activity within the DMLN were observed at both ages, where activity in the BFB does not precede the activity in the DMLN. Instead, the activity in the OFC precedes the activity in other regions. These findings imply that different neuronal mechanisms could be leading the QPPs in the TgF344-AD rats, in the absence of the modulating input from the BFB. Further research focusing on causal connections between the BFB and DMLN regions could provide valuable insights into the direction of information flow in TgF344-AD rats at different disease stages, which might be translated to early stages of human AD.

3.5.6 Alteration in excitatory/inhibitory balance in AD

The rsfMRI results of the current study demonstrate an increased similarity of spatiotemporal properties of QPPs between WT and TgF344-AD rats at the early-plaque stage, while at the pre-plaque stage, large spatiotemporal differences are observed (Supplementary table 3-3). This could imply that compensatory mechanisms are at play in the early-plaque stage that counteract the alterations in network activity observed

during the pre-plaque stage. In line with the observations of the current study, compensatory mechanisms occurring at early stages of AD have been observed in different mouse models of AD (Ammassari-Teule, 2020; Neuman et al., 2015). Previous work from our lab demonstrated an imbalance in excitatory and inhibitory transmission coincided with alterations in FC in the DMLN in an amyloidosis mouse model of AD. Moreover, paradoxical upregulation of presynaptic glutamatergic synapses has been observed in the frontal cortex of MCI patients (Bell, Bennett, & Cuello, 2007), in the absence of alterations in GABAergic synapses (Bell et al., 2007; Mitew, Kirkcaldie, Dickson, & Vickers, 2013)(for a review (Merlo, Spampinato, & Sortino, 2019)). In addition, a recent study demonstrated increased activity of interneurons at the pre-plaque stage in APP/PS1 mice (Hijazi et al., 2020). In the current study, the excitation-inhibition balance was evaluated within each region in terms of ratio of synaptic density of glutamatergic and GABAergic markers. We demonstrate that this ratio was decreased in the RSC and CG both at the pre-plaque and early-plaque stage in the TgF344-AD rats, indicating a shift towards decreased excitation or increased inhibition in these cortical regions. This is in concordance with the aforementioned hyperexcitability of interneurons in APP/PS1 mice (Hijazi et al., 2020). The first histological study in the TgF344-AD rats did not show any significant neuronal loss in the cortex and/or hippocampus at 6 months of age (R. M. Cohen et al., 2013). However, they did observe decreased number of neurons from 16 months onward. These findings were replicated by Morrone et al. in 2022 using MRS. They observe decreased NAA from 15 months onward. Interestingly, they also observe decreased glutamate in the transgenic animals at 9 months of age (Morrone, Lai, Bishay, Hill, & McLaurin, 2022). Another study has demonstrated significant neuronal loss in the hippocampus and cortex of 9-month-old TgF344-AD rats. Investigation of GABA-ergic interneurons shows that at 9 months, significantly lower numbers of somatostatin interneurons were present in the TgF344-AD rats. Moreover, signs of dystrophic somatostatin neurons were observed at this age. Interesting, at 12 months of age, a compensatory increase in parvalbumin-positive GABA-ergic interneurons was observed in the TgF344-AD rats (Munoz-Moreno, Simoes, Tudela, Lopez-Gil, & Soria, 2022). However, no studies evaluating GABA-ergic and

glutamatergic neuronal loss have been performed in 4- and 6-month-old TgF344-AD rats. Therefore, we cannot explain the decreased excitation/increased inhibition observed in the current study as a result of loss of glutamatergic and/or GABA-ergic neurons.

However, the current results are not in concordance with the aforementioned observations of increased glutamatergic synaptic density at early stages of AD in MCI patients. This might be explained by the fact that the pre-plaque and early-plaque stages in the TgF344-AD rat resemble early preclinical stages, not MCI stages in patients (R. M. Cohen et al., 2013; A. L. R. Hernandez, Ding, Simley, McMahon, & Carter, 2021). Histological evaluation of synaptic markers in aged TgF344-AD rats, resembling the MCI stage, might reveal similar changes in synaptic density as is observed in MCI patients. Moreover, the apparent restoration of WT-like QPP patterns in the TgF344-AD rats at the early-plaque stage could not be accounted for by the histological quantification of synapses. Although this suggests that the compensation is not caused by a difference in the number of synapses, it doesn't mean that neuronal signalling is not altered. Future research on the molecular level regarding synaptic activity and transmission could offer insights into the mechanisms underlying the observed compensation of network activity during the early-plaque stage.

3.5.7 Cholinergic synaptic dysfunction in AD

The cholinergic neurons in the BFB are highly susceptible to early AD pathology, hence the observation that the BFB is one of the first regions affected in AD. Ex vivo studies in patients with limited Aβ pathology, observed increased metabolic activity and increased expression of genes involved with synaptic activity in cholinergic neurons in the NBM (Braak & Braak, 1991; Dubelaar et al., 2006; Lau et al., 2013). Moreover, density of cholinergic synapses in the cortex was increased, during the pre-plaque stage in a mouse model of AD, followed by decreased cholinergic density at advanced stages of AD (L. Hu, Wong, Cote, Bell, & Cuello, 2003). The current study did not observe significant differences in the number of cholinergic synapses in the cortex or the BFB regions in the

TgF344-AD rats at the pre-plaque, nor at the early-plaque stage. This is in agreement with a post-mortem study in AD patients that only observed loss of cholinergic synapses during the late symptomatic stage (Tiraboschi et al., 2000), but not with aforementioned studies which observed increased cholinergic synaptic density and increased cholinergic activity. This might be explained by the differences between animal models and differences in sensitivity of the detection method. Moreover, the absence of alterations in cholinergic synaptic density does not exclude alterations in cholinergic synaptic transmission at the molecular level, since soluble Aß monomers and oligomers have been shown to interfere with cholinergic synaptic signalling (for a review, (Kar, Slowikowski, Westaway, & Mount, 2004)). However, future research regarding cholinergic neurotransmission in early TgF344-AD rats is needed to validate this hypothesis. A recent study demonstrated an age-dependent increase in nicotinic acetylcholine receptors in WT F344 rats starting from 6 months onwards, which was absent in age-matched TgF344-AD rats, leading to a significant difference in receptor density between genotypes at 9 months of age (Chaney et al., 2021). Similarly, the current study observed age effects in the HDB/SI and Ent demonstrating an increased cholinergic synaptic density in both groups at 6 months of age, without significant differences between groups.

3.5.8 Astrogliosis might contribute to spatiotemporal alterations in activity patterns during pre-plaque stage

Histological analysis in 4-month-old TgF344-AD rats demonstrates astrogliosis in the NBM and HDB/SI, which diminishes at 6 months of age. Similar trends have been observed in a mouse model of AD, where astrogliosis was observed during the pre-plaque stage in APP/PS1 mice, which decreased at the early plaque stage (D. Wang et al., 2018). Interestingly, the astrogliosis during the pre-plaque stage which diminishes at the early-plaque stage is comparable to the observations in the rsfMRI data, where the spatiotemporal properties of the QPPs in the TgF344-AD rats are also more similar to the WT littermates at 6 months of age. Astrocytes are important in synaptic homeostasis and regulation of glutamatergic neurotransmission by the reuptake of glutamate from

the synaptic cleft (Fullana et al., 2020; Huang et al., 2018; E. Lee & Chung, 2019; J. H. Lee et al., 2021; Scimemi et al., 2013). Moreover, reactive astrocytes in AD induce local changes in GABAergic and cholinergic signalling (Osborn, Kamphuis, Wadman, & Hol, 2016). Animal studies have demonstrated that modulation of specific neuronal populations within the BFB, including GABAergic and cholinergic neurons, induce alterations in BOLD fluctuations and electrical activity within the DMLN in macaques and rats (Espinosa, Alonso, Lara-Vasquez, et al., 2019; Lozano-Montes et al., 2020; Peeters, van den Berg, et al., 2020; Turchi et al., 2018). Given the fact that projections from the BFB to the cortex are important modulators of BOLD activity, alterations in local neurotransmission in the NBM and HDB/SI, due to astrogliosis, might contribute to the spatial alterations in whole-brain patterns of activity observed in the current study at the pre-plaque stage. Interestingly, a recent study published in bioRxiv observed that early FC disruptions in the CG, which was observed in APP^{NL-F} mice before plaques were present in the brain, was accompanied by decreased astrocytic signalling. Moreover, Shah et al. demonstrated that astrocytes have important regulatory function of network activity, which was affected in early AD (Disha Shah, 2022). This is in agreement with the findings of the current study where astrogliosis in the BFB is coinciding with large spatiotemporal differences in BOLD activity in BFB. Further research focusing on the role of astrogliosis in network alterations at the pre-plaque stage of AD is necessary to investigate the interaction between neuron and reactive astrocytes, which could offer valuable insights into novel therapeutic strategies to counteract network imbalance at preclinical stages of AD.

3.5.9 Limitations of the study

There are several limitations to the study. First, the rsfMRI scans in this study were performed in isoflurane and medetomidine anesthetized rats. This combination is known to reduce FC in the subcortical structures such as the hippocampus, a structure affected early in AD. Alterations in network activity in the hippocampus could not be evaluated in the current study. However, a rsfMRI study has demonstrated that FC under this anaesthesia protocol is very close to the FC patterns observed in awake rats

(Paasonen, Stenroos, Salo, Kiviniemi, & Grohn, 2018). In addition, it would be valuable to investigate early network dysfunction not at rest, but during a task. Functional MRI studies at pre-plaque and early-plaque stages of AD could offer novel insights into network dysfunction of task-related networks. Secondly, this study only used male rats to limit the variability and the number of animals used in this study, since previous FC studies observed differences in static FC between genders. However, studies have demonstrated that disease progression is faster in women compared to men and sex differences have also been observed in animal models for AD (Mielke, 2018). A recent study in TgF344-AD rats showed that amyloid-pathology and neuroinflammation is more severe in females. But, cognitive and behavioral deficits were found to be less severe in female rats compared to male rats (Osama Chaudry, 2022). Moreover, an electrophysiology study demonstrated that the onset of synaptic dysfunction in the hippocampal circuit occurs later in females (9M) compared to males (6M), possibly due to the neuroprotective effects of estrogen (Smith & McMahon, 2018), demonstrating that gender differences are also present in TgF344-AD rats. Future studies including females would be valuable to validate the current findings in female TgF344-AD rats and to improve translation to humans. Third, the current study did not investigate the pathological mechanisms underlying the astrogliosis in the BFB in the absence of amyloid plaques. Future experiments focusing on the mechanisms underlying the increased astrocyte abundance and the role of the inflammation in the progression of AD would be valuable to evaluate if this astrogliosis is a valuable therapeutic target. In addition, the histological analysis was not performed on the same animal cohort as the rsfMRI, limiting the possibility to correlate the histological findings to the MRI results. Future studies correlating MRI results to histological alterations should be performed to validate our findings. The biochemical analysis was performed on brain homogenate of intact hemispheres. It would be valuable to perform amyloid ELISA's on specific brain regions, to gain a better understanding of which regions are affected first by soluble Aβ species. The immunohistochemical stainings of the GFAP and Iba-1 of the 4-month-old animals and the 6-month-old animals were performed in two separate batches, which could influence the quality of the stainings, inducing false positive age effects. In

addition, Iba-1 and GFAP are general markers for astrocytes and microglial cells and therefore not only stained activated astrocytes and microglial cells. Future stainings to evaluate neuroinflammation would benefit from using markers which exclusively target activated microglia and astrocytes. In addition, due to large variability in the quality of the stainings of GABA-ergic and glutamatergic synapses, we were not able to differentiate between an increased number of inhibitory-, or a decreased number of excitatory synapses. Future studies to quantify the number of glutamatergic and GABA-ergic synapses using different techniques would be valuable to provide insights into the neuronal imbalance during the pre-plaque and early-plaque stage of AD. Moreover, the study did not include any behavioral evaluation of memory function. It would be interesting to include a memory task to investigate how the altered network activity correlates to alterations in behavior at pre-plaque and early-plaque stages of AD. To conclude, the current study only focused on early stages of AD, which are thought to correspond to preclinical stages in humans. Including a later timepoint corresponding to MCI patients would be valuable to evaluate how network activity changes during healthy aging and AD progression.

3.6 Conclusions

In conclusion, our data demonstrates that QPP analysis on rsfMRI data is a promising tool to evaluate spatiotemporal alterations in brain activity during early stages of AD. The results provide insights into macroscale changes in network function in AD at pre-plaque and early-plaque stages, which are thought to be caused by altered BFB function. This observed altered BFB activity during the QPPs, might prove to be an important biomarker of presymptomatic AD, possibly aiding early detection and early intervention in AD. Future research using QPP analysis in (presymptomatic) AD patients would be valuable to examine the translational potential of the current findings. Moreover, further research of the particular role of astrogliosis in the BFB nuclei remains necessary to gain a better understanding in order to elucidate potential therapeutic targets to restore the aberrant network function at preclinical stages of AD.

3.7 Supplementary Information

3.7.1 Supplementary tables

Supplementary table 3-1: p-values two-way ANOVA pTau

pTau	*Age*Genotype*	*Genotype*	*Age*
CG	0,9699	0,8299	0,0016
RS	0,3607	0,8738	0,0109
Ent	0,9525	0,0559	0,0007
SS	0,2271	0,8903	0,0685
CA1	0,3425	0,0066	0,0008
DG	0,9027	0,049	0,0537
MS	0,9137	0,6721	0,0019
HDB/SI	0,7068	0,6779	0,0004
NBM	0,5721	0,2408	0,001
LC	0,1473	0,0169	0,0596

Statistical analysis of the %area pTau between groups and ages, accompanying figure 3-1. CG = cingulate cortex, RS = retrosplenial cortex, Ent = entorhinal cortex, SS = somatosensory cortex, DG = dentate gyrus, MS = medial septum, HDB/SI = horizontal limb of the diagonal band of Broca/substantia innominata, NBM = nucleus basalis of Meynert, LC = locus Coeruleus.

Supplementary table 3-2

	4 Months			**6 Months**	
Connection	**NO FDR**	**FDR p<0.05**	**Connection**	**NO FDR**	**FDR p<0.05**
Cg L-CA3 L	0.004572	0.310912516	CG R - OFC R	0.037731	0.996217
Cg L-BFB L	0.0428	0.452362018	CG R - Limbic L	0.007888	0.996217
Cg R-DG R	0.029925	0.441358644	CG R - NAcc R	0.023084	0.996217
Cg R-BFB L	0.021608	0.441358644	RSC L - VC R	0.019694	0.996217
RSC L - DG L	0.005966	0.310912516	OFC L - Pir L	0.029186	0.996217
RSC L - MC L	0.048716	0.482118744	TeA R - S2 R	0.039435	0.996217
RSC L - MC R	0.035527	0.441358644	CA1 L - S1 R	0.019032	0.996217
RSC L - FrA R	0.032318	0.441358644	CA1 R - BFB R	0.048509	0.996217
RSC L - Ins R	0.023681	0.441358644	DG L - S2 R	0.005793	0.996217
RSC L - Thal R	0.030434	0.441358644	DG R - Aud R	0.019306	0.996217
RSC R - CA3 R	0.037874	0.441358644	DG R - FrA R	0.038933	0.996217
RSC R - S1 R	0.039962	0.441358644	DG R - NAcc R	0.01786	0.996217
OFC L - BFB L	0.00664	0.310912516	VC L - Thal L	0.019745	0.996217
OFC R - FrA R	0.041174	0.443133724	Aud L - S2 R	0.006001	0.996217

OFC R - BFB L	0.00801	0.313462792
Limbic L - Ent R	0.002935	0.310912516
Limbic L - VC R	0.011572	0.357813665
Limbic L - Aud R	0.006022	0.310912516
Limbic L - S2 L	0.035254	0.441358644
Limbic L - S2 R	0.03868	0.441358644
Limbic L - MC L	**0.000897**	**0.257341465**
Limbic L - CPu L	0.030139	0.441358644
Limbic L - BFB L	0.011194	0.357813665
Limbic R - TeA L	0.040339	0.441358644
Limbic R - TeA R	0.027054	0.441358644
Limbic R - Ent R	0.040496	0.441358644
Limbic R - VC R	0.007583	0.310912516
Limbic R - Aud R	0.037326	0.441358644
Limbic R - S2 L	0.006159	0.310912516
Limbic R - MC L	0.003935	0.310912516
Limbic R - Nacc R	0.038079	0.441358644
TeA L - TeA R	0.014949	0.396984614
TeA L - DG R	0.03066	0.441358644
TeA L - Ent L	0.027908	0.441358644
TeA L - Aud R	0.045215	0.469032389
TeA R - Ent L	0.003832	0.310912516
TeA R - Aud R	0.012823	0.368014375
TeA R - Pir L	0.020042	0.441358644
TeA R - S1 L	0.013564	0.376722946
TeA R - S1 R	**0.000596**	**0.256527495**
TeA R - S2 L	0.037873	0.441358644
TeA R - S2 R	0.015215	0.396984614
TeA R - MC L	0.038483	0.441358644
CA1 L - DG R	0.026123	0.441358644
CA1 R - CA3 L	0.004031	0.310912516
CA3 L - S2 R	0.006799	0.310912516
CA3 R - S2 R	0.038274	0.441358644
CA3 R - Ins R	0.030496	0.441358644
DG L - S1 L	0.029963	0.441358644
DG L - S1 R	0.003009	0.310912516
DG R - Ent L	0.031331	0.441358644
DG R - Ins L	0.006884	0.310912516
DG R - Ins R	0.005896	0.310912516
Ent L - Ent R	0.004227	0.310912516
Ent L - VC L	0.022572	0.441358644
Ent L - Aud R	0.011636	0.357813665
Ent L - MC L	0.024182	0.441358644
Ent R - Aud R	0.019545	0.441358644
Ent R - Pir L	0.049298	0.482337892
VC L - MC L	0.040352	0.441358644
VC L - MC - R	0.027543	0.441358644
VC L - Thal L	0.028635	0.441358644
VC R - S2 R	0.017624	0.433546875
Aud R - S1 R	0.039051	0.996217
Aud R - S2 R	0.005965	0.996217
Pir L - BFB R	0.023854	0.996217
FrA L - Ins R	0.033751	0.996217
FrA L - Thal R	0.0319	0.996217
CPu L - BFB L	0.023623	0.996217
CPu R - Thal R	0.035732	0.996217
NAcc R - BFB L	0.041065	0.996217
BFB R - Thal L	0.025308	0.996217

VC R - Ins L	0.043082	0.452362018
Aud L - S1 L	0.03781	0.441358644
Aud L - S2 L	0.040204	0.441358644
Aud R - S1 L	0.035917	0.441358644
Aud R - S1 R	0.010543	0.357813665
Aud R - S2 R	0.027555	0.441358644
Pir L - MC L	0.019059	0.441358644
Pir L - MC R	0.002261	0.310912516
Pir R - MC R	0.008717	0.326314849
Pir R - BFB L	0.015962	0.404210954
Pir R - BFB R	0.037396	0.441358644
S1L - S2 R	0.012436	0.368014375
S1 L - MC L	**0.000136**	**0.11678127**
S1L - NAcc R	0.027633	0.441358644
S1R - MC L	0.011617	0.357813665
S2 L - MC L	0.037242	0.441358644
S2 L - NAcc R	0.026678	0.441358644
S2 L - Thal R	0.007319	0.310912516
MC R - FrA R	0.048438	0.482118744
FrA L - FrA R	0.046875	0.480467409
FrA L - BFB R	0.02425	0.441358644
FrA R - Ins L	0.033938	0.441358644
CPu L - CPu R	0.006175	0.310912516
NAcc L - BFB L	0.027758	0.441358644
NAcc L - BFB R	0.048705	0.482118744

Statistical results accompanying figure 3-2 and figure 3-3. P values of the statistically different connections in static FC between WT and TgF344-AD rats after uncorrected two-sample t-test before and after FDR correction.

Supplementary table 3-3: Effect sizes short QPPs

		CG	RSC	BFB	VC	OFC-PRL
		Cohens d	Cohens d	Cohens d	Cohens d	Cohens d
4M QPP DMLN+	**0.6s**	0.5307	0.3315	0.6159	0.0592	0.7650
	1.2s	0.4961	0.3364	0.7635	0.2374	0.8311
	1.8s	0.3975	0.2815	0.8289	0.3232	0.8347
	2.4s	0.3192	0.2054	0.9898	0.3261	0.7843
	3.0s	0.3095	0.1332	0.8546	0.2542	0.6928
	3.6s	0.3657	0.0769	0.7435	0.0995	0.5605
	Average	**0.4031**	**0.2274**	**0.7993**	**0.2166**	**0.7447**
4M QPP LCN+	**0.6s**	0.2561	0.0473	0.0773	0.1131	0.5217
	1.2s	0.0236	0.1445	0.1889	0.3957	0.7992
	1.8s	0.2102	0.3026	0.2424	0.5697	0.8506
	2.4s	0.2985	0.3764	0.2213	0.5730	0.6479
	3.0s	0.2472	0.3743	0.1467	0.4647	0.8381
	3.6s	0.0779	0.3161	0.0537	0.2970	0.9669
	Average	**0.1856**	**0.2601**	**0.1550**	**0.4022**	**0.7707**
6M QPP LCN+	**0.6s**	0.2038	0.0685	0.3812	0.2894	0.3290
	1.2s	0.2005	0.0193	0.3881	0.2062	0.3799
	1.8s	0.1545	0.0477	0.3588	0.0174	0.3907
	2.4s	0.1051	0.1068	0.2835	0.2268	0.3561
	3.0s	0.0811	0.1381	0.1731	0.4070	0.2796
	3.6s	0.0978	0.1347	0.0552	0.3143	0.1956
	Average	**0.1405**	**0.0859**	**0.2733**	**0.2435**	**0.3218**
6M QPP DMLN+	**0.6s**	0.1766	0.2181	0.0087	0.4699	0.2099
	1.2s	0.1807	0.2908	0.0384	0.3341	0.1243
	1.8s	0.1573	0.0926	0.0871	0.07677	0.0251
	2.4s	0.1433	0.1282	0.1171	0.2086	0.0371
	3.0s	0.1492	0.3155	0.1167	0.4509	0.0388
	3.6s	0.1649	0.4150	0.0845	0.5973	0.0216
	Average	**0.1620**	**0.2434**	**0.0755**	**0.3563**	**0.0761**

Statistical results accompanying figure 3-6 and figure 3-9. Effect sizes based on the voxel-averaged timecourses within each ROI. d= 0.1-0.2 very small effect size, d = 0.2-0.5 small effect size, d = 0.5-0.8 – medium effect size, d>0.8 = Large effect size

Supplementary table 3-4: p-values statistical comparison voxel-wise mean peak timings within groups

	4M				6M			
	WT		TG		WT		TG	
	Diff (s)	FDR p<0,05	Diff (s)	FDR p<0,05	Diff (s)	FDR p<0,05	Diff (s)	FDR p<0,05
CG-BFB	0,4380	<0,0001	-0,1103	0,0036	0,5149	<0,0001	-0,0232	0,6230
CG-OFC	0,0384	0,3330	0,0877	0,0017	0,2237	<0,0001	0,2518	<0,0001
CG-RS	-0,0288	0,5346	0,2286	0,4210	-0,0056	0,8806	-0,0587	0,3640
CG-VC	-0,2658	<0,0001	-0,1205	0,0014	0,0442	0,1275	-0,2455	<0,0001
RS-VC	-0,2370	<0,0001	0,1438	<0,0001	0,4235	0,123	-0,1867	0,0014
RS-OFC	0,0672	0,1020	0,0684	0,02110	0,1901	<0,0001	0,3102	<0,0001
RS-BFB	0,4668	<0,0001	-0,0129	0,0004	0,5205	<0,0001	0,0354	0,5590
OFC-VC	-0,3042	<0,0001	0,1991	<0,0001	-0,1901	<0,0001	-0,4968	<0,0001
OFC-BFB	0,3996	<0,0001	-0,1980	<0,0001	0,2912	<0,0001	-0,2748	<0,0001
VC-BFB	0,7038	<0,0001	0,01344	0,8440	0,4707	<0,0001	0,222	<0,0001

Statistical results accompanying figure 3-8 and figure 3-10. Differences (Diff) in mean voxel-wise peak timings between different regions in seconds in wildtype (WT) and TgF344-AD rats (TG). Significant difference in peak timings between regions was evaluated using a two-sample t-test with FDR correction ($p < 0.05$).

Supplementary table 3-5: p-values two-way ANOVA Astrogliosis

GFAP	*Age*Genotype*	*Genotype*	*Age*
CG	0,3614	0,0724	0,9826
RSC	0,0936	0,0372	0,8474
mENT	0,3602	0,182	0,5808
SS	0,0657	0,6707	0,3552
MS	0,8643	0,8081	0,958
NBM	0,0581	0,0269	0,0027
HDB/SI	0,0262	0,0183	0,9064

Statistical results accompanying figure 3-11. Statistical analysis of the %area GFAP between groups and ages. CG = cingulate cortex, RS = retrosplenial cortex, Ent = entorhinal cortex, SS = somatosensory cortex, MS = medial septum, HDB/SI = horizontal limb of the diagonal band of Broca/substantia innominata, NBM = nucleus basalis of Meynert

Supplementary table 3-6: p-values two-way ANOVA Microgliosis

Iba-1	*Age*Genotype*	*Genotype*	*Age*
CG	0,1571	0,8388	0,3466
RSC	0,2556	0,37	0,3707
Ent	0,1241	0,0937	0,0003
SS	0,5429	0,6633	0,0001
MS	0,3092	0,6105	0,0529
HDB/SI	0,3118	0,1338	0,55
NBM	0,8146	0,2123	0,0001

Statistical results accompanying figure 3-11. Statistical analysis of the %area Iba-1 between groups and ages. CG = cingulate cortex, RS = retrosplenial cortex, Ent = entorhinal cortex, SS = somatosensory cortex, MS = medial septum, HDB/SI = horizontal limb of the diagonal band of Broca/substantia innominata, NBM = nucleus basalis of Meynert

Supplementary table 3-7: p-values two-way ANOVA vGLUT/vGAT

vGLUT/vGAT	*Age*Genotype*	*Genotype*	*Age*
CG	0,2649	0,0199	0,0879
RSC	0,3099	0,0283	0,0001
Ent	0,3686	0,1561	0,5679
SS	0,0548	0,0792	0,0469
MS	0,0232	0,7135	0,0001
HDB/SI	0,505	0,6998	0,95
NBM	0,7753	0,1531	0,0427

Statistical results accompanying figure 3-11. Statistical analysis of the ratio of glutamatergic and GABAergic synapses between groups and ages. CG = cingulate cortex, RS = retrosplenial cortex, Ent = entorhinal cortex, SS = somatosensory cortex, MS = medial septum, HDB/SI = horizontal limb of the diagonal band of Broca/substantia innominata, NBM = nucleus basalis of Meynert

Supplementary table 3-8: p-values ANOVA cholinergic synaptic count

#Cholinergic	*Age*Genotype*	*Genotype*	*Age*
CG	0,4059	0,8895	0,4253
RSC	0,2947	0,2502	0,6918
Ent	0,8684	0,9815	0,0402
SS	0,8174	0,9282	0,1037
MS	0,472	0,3097	0,336
HDB/SI	0,5189	0,7353	0,0001
NBM	0,1872	0,2538	0,5551

Statistical results accompanying figure 3-11. Statistical analysis of the number of cholinergic synapses between groups and ages. CG = cingulate cortex, RS = retrosplenial cortex, Ent = entorhinal cortex, SS = somatosensory cortex, MS = medial septum, HDB/SI = horizontal limb of the diagonal band of Broca/substantia innominata, NBM = nucleus basalis of Meynert

4. REM fragmentation, hippocampal network dysfunction and cholinergic compensation at the pre-plaque and early-plaque stages of AD

This chapter is based on:

M. van den Berg, L. Heymans, D. Toen, M.A. Adhikari, M. Verschuuren, I. Pintelon, W. De Vos, A. van der Linden, M. Verhoye, G.A. Keliris. “REM fragmentation, hippocampal network dysfunction and cholinergic compensation at the pre-plaque and early-plaque stages in TgF344-AD rats “

manuscript in preparation

4.1 Abstract

The hippocampus plays an imperative role in cognitive processes and its function is altered already at very early stages of AD. Memory consolidation occurs mainly during sleep and research has demonstrated that sleep characteristics and hippocampal function during sleep are altered in AD. However, how sleep architecture and hippocampal function is affected at very early stages of the disease is still unknown. Moreover, mechanisms underlying the observed changes in AD are still elusive. We hypothesized that Aβ-induced alterations in neurotransmitter signalling (cholinergic, glutamatergic and/or GABAergic) at pre-plaque and early-plaque stages of AD, disrupt sleep architecture and hippocampal oscillatory activity during sleep. To this end, we performed 24-hour hippocampal electrophysiological measurements in TgF344-AD rats and wild-type littermates at pre- and early-plaque stages of AD, to evaluate circadian rhythmicity, sleep architecture and hippocampal oscillatory activity during sleep. Moreover, immunohistochemical analysis of the number of glutamatergic, GABAergic and cholinergic synapses in the hippocampus was performed to elucidate possible disease mechanisms.

We observed a significantly increased probability for shorter REM bouts, suggestive of REM sleep fragmentation, in TgF344-AD rats at the pre-plaque stage, which recovered at the early-plaque stage. In addition, we observed during REM sleep a significantly decreased fast gamma power in TgF344-AD rats, irrespective of age and decreased theta-gamma coupling was observed in the high gamma range at the pre-plaque stage, which was partially compensated in the early-plaque stage. Moreover, theta-gamma coupling in the low gamma range was significantly increased during the pre-plaque stage in TgF344-AD rats but returned to WT levels at the early-plaque stage. These results suggest a partial functional compensation of network activity during early-plaque stage of AD during REM sleep. During NREM sleep, we did not observe altered power across different frequency bands, but we did observe a significantly increased duration of sharp wave-ripples (SWR), electrophysiological phenomena closely linked to memory consolidation. Interestingly, we observed an increased number of cholinergic synapses

in the hippocampus during the early-plaque stage in TgF344-AD rats, suggestive of basal forebrain cholinergic compensation mechanisms. The results from this study offer novel insights into early alterations in sleep architecture and hippocampal function. Moreover, they demonstrate the presence of cholinergic compensation mechanisms during the early-plaque stage of AD which ensures a partial functional recovery of hippocampal function and sleep architecture.

4.2 Introduction

Alzheimer's Disease (AD) is a progressive neurodegenerative disorder characterized by the accumulation of extracellular amyloid-beta (Aβ) plaques, intracellular tau-aggregation, synaptic dysfunction, and neuronal loss, resulting in cognitive dysfunction and eventually, dementia. Neuropathological changes underlying AD start 10-20 years before the onset of cognitive symptoms, with accumulation of Aβ being the first identifiable hallmark (Braak & Braak, 1991; Braak et al., 2011; Sperling et al., 2011). Studies have demonstrated that soluble Aβ species (sAβ), which are the precursors of Aβ plaques, interfere with synaptic function before cognitive symptoms become apparent (Ben-Nejma et al., 2019; Busche et al., 2012; Hector & Brouillette, 2020; S. Li & Selkoe, 2020; T. Ma & Klann, 2012; Shah et al., 2018; Shah et al., 2016).

Brain regions and pathways important for sleep and wake regulation (Brown et al., 2012), such as the cholinergic system (Vazquez & Baghdoyan, 2001) and locus coeruleus (Van Egroo, Koshmanova, Vandewalle, & Jacobs, 2022), are affected early by Aβ and tau accumulation (Braak & Braak, 1991; Braak et al., 2011; Van Erum, Van Dam, & De Deyn, 2019). Recent studies have demonstrated that soluble Aβ interferes with sleep regulation inducing increased or decreased wakefulness depending on the oligomer species present in the brain (Kincheski et al., 2017; Ozcan, Lim, Leighton, Allison, & Rihel, 2020). In addition, several studies have observed changes in sleep architecture and efficiency during asymptomatic stages of AD in humans (Y. E. Ju et al., 2014) and animal models of AD (Roh et al., 2012; J. Wang, Ikonen, Gurevicius, van Groen, & Tanila, 2002). Under physiological circumstances, Aβ levels in the interstitial fluid and cerebrospinal

fluid are modulated by the sleep-wake cycle (Lucey & Bateman, 2014). Neuronal activity increases the generation and release of Aβ (Cirrito et al., 2005), leading to increased extracellular Aβ levels during wakefulness. Aβ is cleared from the interstitial fluid during sleep by the enhanced activity of the glymphatic system, therefore decreasing Aβ levels (L. Xie et al., 2013). These observations suggest a vicious cycle between sleep and Aβ dynamics, wherein altered sleep architecture result in increased extracellular Aβ and aggregation, which in turn further disrupts sleep, therefore, driving AD progression (Roh et al., 2012). However, the neuropathological mechanisms underlying Aβ induced sleep disruptions remain elusive.

Sleep is imperative for hippocampus-dependent memory processes and sleep disruption leads to decreased cognitive performance (Killgore, 2010). Hippocampal neuronal activity underlies memory consolidation through specific, coordinated electrophysiological events such as Sharp-wave ripples (SWR), slow oscillations and theta-gamma coupling. Several studies have observed alterations in hippocampal neuronal oscillations, which coincided with cognitive alterations, in different animal models of AD (Bazzigaluppi et al., 2018; Benthem et al., 2020; Caccavano et al., 2020; Mably, Gereke, Jones, & Colgin, 2017; Stoiljkovic et al., 2019). These phenomena rely heavily on the delicate interplay of GABAergic, glutamatergic, and cholinergic neurotransmission. Perturbations of these neurotransmitter systems due to the early accumulation of soluble Aβ could disrupt these oscillatory events at pre-plaque stages of AD, and might prove to be an interesting biomarker, and therapeutic target for AD.

We hypothesized that Aβ-induced alterations in neurotransmitter signalling (cholinergic, glutamatergic and/or GABAergic) at pre-plaque and early-plaque stages of AD, disrupt sleep architecture and hippocampal oscillatory activity during sleep. Therefore, we have performed 24-hour hippocampal electrophysiological measurements in 4-month-old TgF344-AD rats, displaying soluble Aβ pathology in the absence of Aβ plaques, and 6-month-old TgF344-AD rats demonstrating pTau accumulation in the LC and hippocampal and cortical Aβ plaques. We aimed to evaluate

sleep disturbances and hippocampal function during sleep during early, presymptomatic stages of AD, since the selected ages highly resemble these early stages of AD. In addition, histological analyses of GABAergic, glutamatergic, and cholinergic synapses in the hippocampus was performed to further investigate possible disease mechanisms underlying the electrophysiological and behavioral alterations. Investigation of the synaptic mechanisms underlying sleep disturbances and hippocampal dysfunction during sleep, might offer novel insights which could prove to be an interesting therapeutic target.

4.3 Material and Methods

4.3.1 Animals and ethical statement

All procedures were in accordance with the guidelines approved by the European Ethics Committee (decree 2010/63/EU) and were approved by the Committee on Animal Care and Use at the University of Antwerp, Belgium (approval number: 2019-06). Electrophysiological experiments were performed in 4-, and 6-month-old TgF344-AD rats (N=7/N=5) and wildtype littermates (N=5/N=5). Rats were group housed prior to the electrode implantation but housed separately afterwards. An additional 24 male rats were used for histological analysis of pathology and synaptic markers (6 WT and 6 TgF344-AD rats for each time point). All animals were kept on a reversed, 12h light/dark cycle, with controlled temperature (20 – 24°C) and humidity (40-60%) conditions. Standard food and water were provided ad libitum.

4.3.2 Chronic hippocampal electrophysiological measurements

4.3.2.1 Surgical procedure

Anesthesia was induced using 5% isoflurane (Isoflo ®, Abbott Laboratories) (medical air 1L/min) and maintained using 2-3% isoflurane (at 1L/min) during the surgery. Animals were placed in a stereotaxic frame and a craniotomy was made above the right dorsal hippocampus (AP -3.00, ML 2.50). A 16-channel laminar electrode (E16+R-100-S1-L6 NT,

Atlas Neuro-engineering, Belgium) with internal reference was carefully lowered (DV 2.5-3.5 mm) into the dorsal hippocampus. The pointy tip feature of the electrode allows penetration of the dura without the need to open or remove the dura. The exact depth of the recording sites was identified online by the layer-specific local field potentials (LFP) of the hippocampus. The craniotomy was sealed with a sterile silicone gel (Kwik-Cast, WPI). Stainless steel screws were drilled into the skull overlaying the olfactory bulb, frontal cortex, left hippocampus, and cerebellum, of which the latter served as ground electrode. The implant was covered in several layers of dental cement (Stoelting) and the wound was closed. Rats were treated with antibiotics until three days after the surgery (5 mg/kg, Enrofloxacin (Baytril ®, Bayer) in drinking water) and analgesics were administered (0.05mg/kg Buprenorphin (Temgesic ®, Indivior Europe Limited) subcutaneous during surgery, followed by 2 daily injections of 5 mg/kg Carprofen (Rimadil®, Pfizer) for two days after surgery. Rats were allowed to recover for at least 7 days prior to the LFP recordings.

4.3.2.2 Neurophysiological data acquisition

Prior to the recordings, animals were habituated for at least 24 hours to the ventilated, light-regulated recording chamber and recording setup. Using a wireless electrophysiology system (W2100 system, Multichannel systems, Germany), electrophysiological signals (LFPs, neuronal spiking activity, and EMG activity) were acquired for 24 hours while the animal was freely behaving or sleeping in its home cage at a sampling frequency of 10 kHz. During these measurements, animals were maintained on the 12/12h reversed light/dark cycle and had ad libitum access to food and water.

4.3.3 Validation of electrode position

Anesthesia was induced with 5% isoflurane and was maintained at 2-2.5%. An electrical current (30 µA, 3 s) was applied via the electrode at the top, middle, and bottom channels to allow validation of the electrode position. Thereafter, the animals were euthanized via intravenous injection of 50 mg/kg pentobarbital (Dolethal ®, Vetoquinol,

Belgium), followed by cardiac perfusion with ice-cold phosphate-buffered saline (PBS) and 4% Paraformaldehyde (Merck Millipore, Merck KGaA, Darmstadt, Germany). The brains were surgically removed and postfixed for 4-6 hours using 4% PFA. A sucrose gradient was applied (5%, 10%, and 20% Sucrose in 0.1M PBS), after which the brains were snap frozen using liquid nitrogen and stored at -80°C until further processing. The frozen brains of the animals were sliced into 12 µm thick coronal sections using a cryostat (Cryostar NX 70, Thermo Fisher Scientific). The sections were stained with Nissl staining (Cresyl Violet 0.1%, Sigma-Aldrich) and studied under the light microscope to validate the position of the electrodes for each animal.

Each layer of the hippocampus has distinct functions and therefore, distinct oscillatory activity. The main focus of this study is on the different layers of the CA1 region. Therefore, histological electrode validation was performed. Based on the location of the tip of the electrode (Fig 4-1), we could infer which channels were placed in the different layers of CA1. These channel locations were further validated by the distinct oscillatory patterns of the different hippocampal layers, such as occurrence of sharp wave-ripples and theta power across different hippocampal layers. This channel information was used in further analyses. For 2 WT animals, validation was not possible because the lesions weren't visible under the microscope and are not shown in the figure. However, a comparison of the distinct oscillatory patterns with other WT animals showed no differences. Therefore, they were still included in the data analysis.

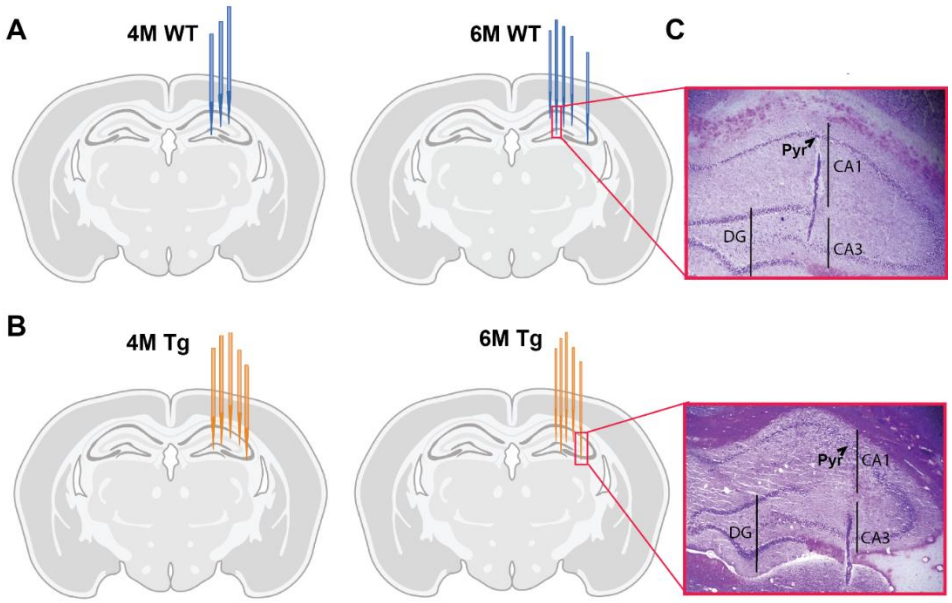

Figure 4-1: histological validation of electrode position. A) Schematic overview of electrode position in 4-month-old Wild type (WT) animals. Each blue electrode represents track of the electrode of a different WT subject. B) Schematic overview of the electrode position in 4-month-old TgF344-AD (Tg) animals. Each orange electrode represents track of the electrode of a different Tg subject. The red insert shows exemplary light microscopy images of Nissl-stained brain slices showing the electrode trace in the hippocampus of a WT animal (A) and TgF344-AD rat (B). Exemplary images of the electrode validation (C) where the arrow points towards the pyramidal layer (Pyr) of the CA1 region of the hippocampus. DG = Dentate Gyrus

4.3.4 Analysis

4.3.4.1 Sleep architecture and fragmentation

An automated sleep scoring algorithm was used to determine vigilance states for each 10 second epoch based on the theta-delta ratio and EMG activity. Each 10 second epoch was labeled as wake, rapid eye movement sleep (REM) or non-rapid eye movement sleep (NREM). Next, the automatic sleep scoring was checked and adjusted through visual inspection by two independent investigators. The scores of the two investigators were combined to a single score per animal that was used in our further analysis of sleep

architecture. Epochs which were scored differently were re-evaluated to reach a consensus. The percentage time spent in each vigilance state was calculated in 3h time periods across the 24h recording and statistically compared using a two-way ANOVA (genotype, age, genotype*age), followed by post-hoc FDR-corrected student T-tests. Sleep bout lengths during the light and dark phase were derived, and a cumulative probability plot and Kolmogorov-Smirnov tests (FDR corrected $p<0.05$) were used to evaluate differences in sleep fragmentation between genotypes.

4.3.4.2 Power analysis of hippocampal LFP's

For each channel on the electrode, power spectra were calculated for each vigilance state using a Fast Fourier Transform in Brainstorm (Tadel, Baillet, Mosher, Pantazis, & Leahy, 2011) using the Welch's method (window size 20s, 50% overlap). Power spectra were normalized to the sum of the power across all LFP frequencies (0.5-250 Hz) to minimize variation in amplitude due to differences in exact placement of the electrode. Normalized power spectra were averaged across genotypes separately for each state. Next, power for each vigilance state was calculated for specific frequency bands of interest, i.e., delta (0.4-4 Hz), low theta (5-8 Hz), high theta (8-12 Hz), low gamma (30-45 Hz), high gamma (60-120 Hz) and sharp-wave ripple (120-250) (table 4-1). The power across the three channels with the highest power at each frequency were averaged for each subject and compared between groups and ages.

Table 4-1 Frequency bands of interest

Frequency band	*Frequency range (Hz)*
Delta	0.5-4
Low theta	5-8
High theta	8-12
Slow gamma	30-45
Fast gamma	60-120
High frequency oscillations	120-250

4.3.4.3 Phase-Amplitude coupling (PAC)

The amplitude of the hippocampal gamma rhythm is modulated by the phase of theta, a phenomenon named phase-amplitude coupling (PAC). To evaluate the strength of the theta-gamma coupling, the modulation index (MI) was used, that after bandpass filtering uses the phase of the slow oscillation and the amplitude envelope of the fast oscillation to create a complex vector of which the length represents the amplitude of each fast oscillation whereas the phase of the slow oscillation is represented by the angle. In the case of an absence of PAC, these vectors form a roughly uniform circular shape centered around zero, however if there is modulation, then the amplitude at a certain phase is higher, which will create a bump in the polar plot. The MI represents the length of this mean vector length (Fig 4-2, for a detailed description of calculations we refer to (Canolty et al., 2006; Tort et al., 2010)).

The analysis of the PAC was performed on one channel, which was located in the pyramidal layer of the CA1, based on histological electrode validation (described in section 4.3.3). First, for each subject, a comodulogram was calculated which demonstrates the MI for each pair of frequencies. The theta band (5-12 Hz) and gamma band (30-120 Hz) were divided into 1Hz bins and for each combination of theta and gamma frequencies the mean modulation index across each REM epoch was calculated and averaged across all REM epochs to create a subject based comodulogram. Next, a group-averaged comodulogram was computed in Matlab which demonstrated for each group the main frequencies of modulation. The main frequency modes of modulation were examined and were used to perform a time-resolved PAC (tPAC) analysis. tPAC computes the MI between specific frequency bands estimated from the group-averaged comodulogram for each 1 second epoch. The advantage of this method is that it allows more reliable quantification of the strength of the PAC. The obtained MI were averaged across epochs for each subject and the mean was statistically compared between groups and ages.

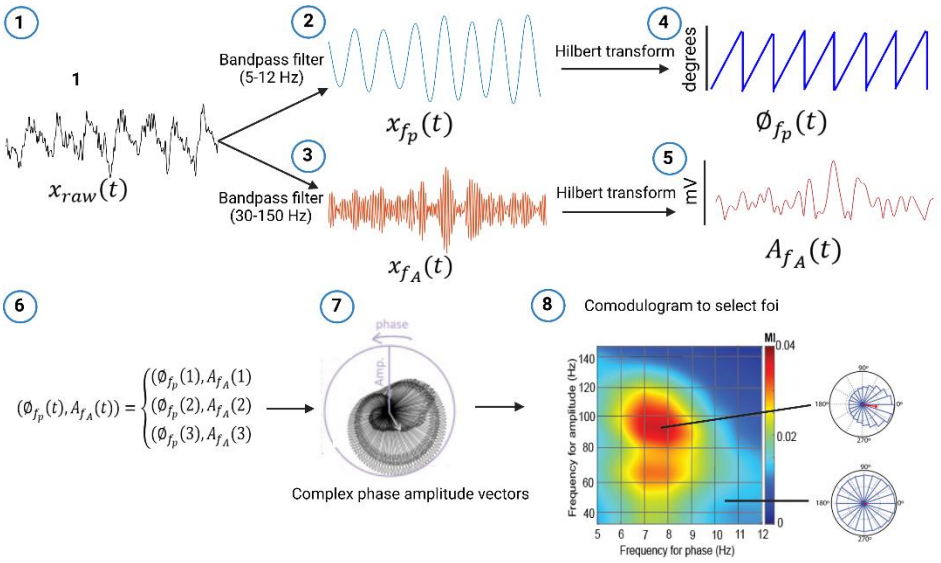

Fig 4-2: Calculating the theta-gamma coupling strength using the modulation index. 1) Raw hippocampal LFP trace during REM sleep. Bandpass filtering was applied on the raw data trace to filter the data within the frequency ranges of interest, i.e., theta frequencies (5-12 Hz) (2) and gamma frequencies (30-150 Hz) (3). A Hilbert transformation is applied on the filtered data to extract the phase of the slow oscillation (4) and the amplitude (envelope) of the fast oscillation (5). A complex time series (6) is then constructed and used to obtain the mean amplitude values at each 20 degree phase bin and plotted for each gamma oscillation in a complex plain (7). The MI is finally obtained by applying a normalized entropy measure to the mean amplitude vector. The comodulogram plot is constructed by representing in color scale the MI values of multiple phase-amplitude frequency pairs, where a warm color indicates high PAC and cold colors indicate low coupling. Foi = frequency of interest. Figure is adapted from (Samiee & Baillet, 2017; Tort et al., 2008).

4.3.4.4 Offline detection and analysis of sharp-wave ripples

Analysis of sharp wave-ripple activity was performed on one channel which was placed in the CA1 layer of the hippocampus, based on the electrode validation as described in section 4.3.3. All pre-processing steps were conducted using the Fieldtrip toolbox (Oostenveld, Fries, Maris, & Schoffelen, 2011). First, to detect ripples in the pyramidal layer of CA1, the wide-band signal was band-pass filtered between 120 and 250 Hz using a 400th order Butterworth infinite response filter and was afterwards down-sampled

from 10 kHz to 1200 Hz (Fig 4-3 1). Filtered data was segmented based on the NREM epochs obtained in Neuroscore. The segmented data was z-scored (Fig 4-3 2), rectified (Fig 4-3 3) and smoothed (Fig 4-3 4) using a rectangular filter window with a length of 8 ms, generating the ripple power signal (Molle, Yeshenko, Marshall, Sara, & Born, 2006). SWRs were identified in the channels which were placed in the pyramidal layer of the CA1, based on the electrode validation described in 4.3.3. If the power within the ripple band exceeded a threshold of 4 standard deviations from the mean. Events were expanded until the power fell below 2 standard deviations (Fig 4-3 4). Events with a duration shorter than 30ms (Fig 4-3 5) and/or a peak spectral frequency lower than 140 Hz were discarded (Fig 4-3 6). Subsequently, a thresholding algorithm was applied to detect sharp waves in the stratum radiatum. Signals in the channel which demonstrated strong sharp waves were band pass filtered between 0.5 and 20Hz using a 400^{th} order Butterworth filter. Sharp wave events which lasted between 20ms and 400ms were detected when the power exceeded the threshold of 2.5 standard deviations from the mean (Oliva et al., 2018). Ripples that co-occurred with SW were kept for further analysis. The power in the SWR band, the peak spectral frequency and the duration of events were extracted and were compared between groups and ages.

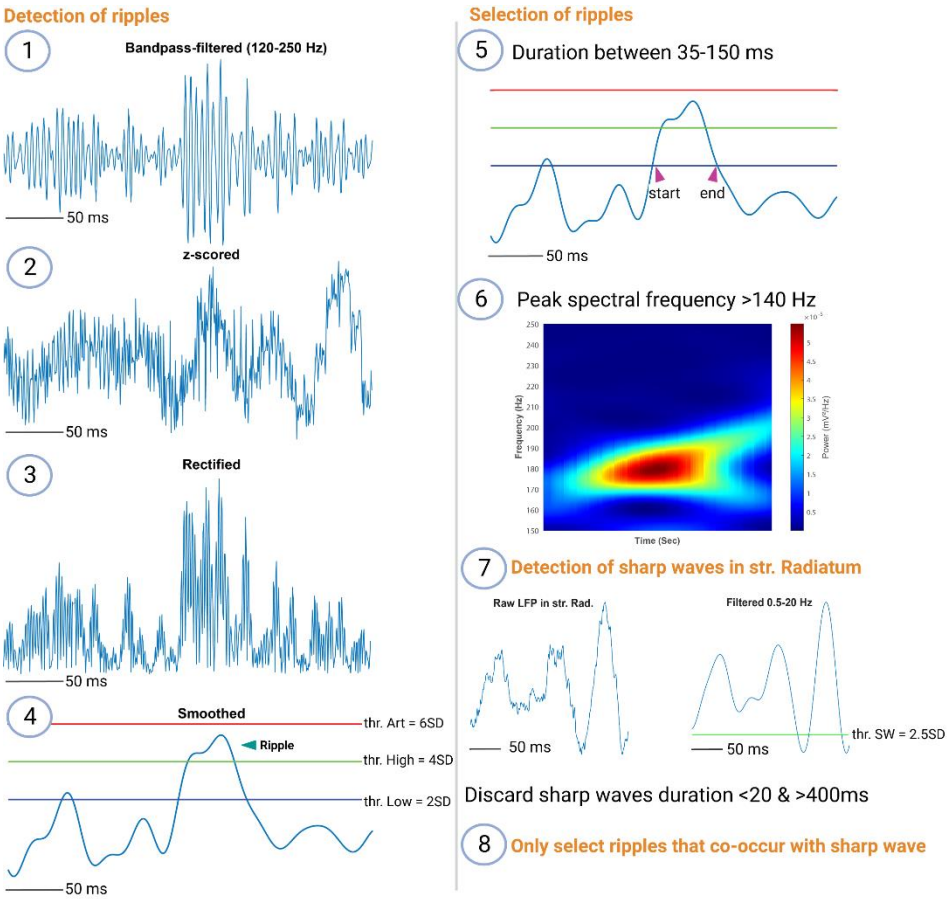

Fig 4-3: Sharp-wave ripple detection algorithm. 1-4) Exemplary traces of raw data after the different preprocessing steps. Raw LFP signals were down sampled (not shown), bandpass-filtered (1), z-scored (2), rectified (3) and smoothed (4). Instances when the signal exceeded the threshold of 4 SD (green line) were selected as tentative SWR events. 5) the beginning and end of the SWR were marked when the smoothed signal dropped below 2 SD (blue horizontal line) and these start and end time were used to discard ripples which were shorter then 30ms and longer then 150ms. 6) Frequency of the ripple is calculated and events with a maximum frequency below 140Hz are discarded. 7) sharp waves are detected in a separate channel placed in the stratum radiatum based on a threshold mechanisms (green line). 8) Only ripples which co-occur with the sharp wave will be selected for further analyses.

4.3.5 Histology

4.3.5.1 Immunofluorescent stainings

To evaluate AD alterations in synaptic markers, histological analyses were performed on cryosections (N = 6 per genotype and age) as described in chapter 3. Briefly, brains were extracted as described in 4.3.3, and hemispheres were separated. Next, left hemispheres were embedded in OCT-embedding medium for sectioning. At 0.4-, 1.40- and 3.90-mm lateral from the midline, sagittal sections of 12 µm were made using a Leica CM1950 cryomicrotome (Leica BioSystems, Belgium), thaw-mounted on VWR Superfrost Plus micro slides (VWR, Leuven, Belgium) and dried for 2 hours at 37°C. All immunohistochemical incubations were carried out at RT. Sections were pre-incubated for 30 min in blocking buffer containing 1% Triton X-100 before an overnight incubation with the primary antibodies (Table 4-2). For the detection of the immunoreactivity, the sections were incubated for 4 hours with the appropriate combination of fluorescent-conjugated secondary, followed by a nuclear counterstain using 4',6-diamidino-2-phenylindole (DAPI, Sigma-Aldrich, Hoeilaart, Belgium) for 10 min at room temperature. Samples were mounted in Citifluor AF1 (EMS, Hathfield, USA). Respective single-labeling studies which resulted in comparable staining, were performed to rule out nonspecific findings resulting from the multiple-staining process. Negative staining controls were performed by substitution of non-immune sera for the primary or secondary antisera.

Table 4-2: Primary antibodies used in the current study

TARGET	SUPPLIER	CATALOGUE NUMBER	RRID	DILUTION
VGAT	Synaptic Systems	131003	AB_887869	1:200
VGLUT	Synaptic Systems	135304	AB_887878	1:200
VACHT	Merck	ABN100	AB_2630394	1:1000

4.3.5.2 Image acquisition

Confocal images of immunolabeled tissue sections were acquired with a Perkin Elmer Ultraview Vox dual spinning disk confocal microscope, mounted on a Nikon Ti body using a 40x Plan Apo objective (NA 0.95). Lasers with wavelength 405 nm, 488 nm, 561nm and 640nm were used in combination with a quadruple dichroic and 445/60 - 525/50 - 615/70 - 705/90nm emission filters. Detection was done on a Hamamatsu C9100-50 CMOS camera. Image acquisition was done using Volocity software. Regions of interest were localized based on the DAPI staining. Per animal, 3 images were acquired on 3 non-consecutive sections in 3 axial positions separated by a 2 µm spacing.

4.3.5.3 Image analysis

Image analysis of the synaptic excitatory/inhibitory ratio was done in FIJI image analysis software (Schindelin et al., 2012) as described in chapter 3. A macro script was written for FIJI image analysis software to detect synaptic markers and measure their intensity and is available on github (https://github.com/DeVosLab/SynapseDetection) (Verschuuren et al., 2019; Verstraelen et al., 2020). After maximum projection of the Z-stacks, synaptic marker spots were enhanced using a single or multi-scale Laplace filter with user-defined kernel sizes. For each marker the threshold settings were kept constant for both groups and ages studied. A manually defined threshold per region was applied to segment the spots after which an additional max finding (and region growing) step was included to untangle clustered spots. Only spots that had a projected area within a specific range (0.20 – 3.00 µm) were retained. Images with more than 10000 spots were discarded to exclude over segmented images.

4.3.6 Statistics

The statistical analysis of the data was performed using the JMP Pro software (Version 16, SAS Institute Inc., Cary, NC, 1989 – 2021). For the statistical analysis of the sleep architecture, power across different frequency bands, SWR characteristics, and PAC, outlier detection was performed on group level for each age using principal component analysis (PCA). Measurements with a T^2 statistic index higher than the 95% confidence

interval were excluded. A two-way ANOVA (genotype, age, genotype*age) per region was performed. In case of a significant genotype*age interaction, post-hoc Student's t-tests were performed. A false discovery rate correction using the Benjamini-Hochberg procedure was applied to correct for multiple comparisons (FDR $p<0.05$). The interaction term was removed no significant interaction was observed and a two-way ANOVA (genotype, age) was used to evaluate genotype or age effects.

Regarding the analysis of the synaptic markers, outlier detection was performed using the interquartile range (1.5x IQR) per genotype, age, and region on all individual images (3 per animal). Animals with less than 2 images were excluded and the remaining images were averaged for each animal. A second outlier detection was performed on the subject averages, using principal component analysis (PCA). Measurements with a T^2 statistics indices higher than the 95% confidence interval were excluded. A two-way ANOVA (genotype, age, genotype*age) per region was used to evaluate differences in vGLUT/vGAT ratio and the number of cholinergic synapses. In case of a significant genotype*age interaction, post-hoc FDR-corrected Student's t-test (FDR $p<0.05$) were performed. The interaction term was removed no significant interaction was observed and a two-way ANOVA (genotype, age) was used to evaluate genotype or age effects. Graphical representation of the data was obtained using GraphPad Prism (version 9.2.0 for Windows, GraphPad Software, San Diego, California USA, www.graphpad.com).

4.4 Results

4.4.1 Macro architectural changes during sleep

Research has demonstrated that alterations in sleep rhythm precede cognitive alterations in AD (Casagrande et al., 2022; F. Zhang et al., 2019). We investigated if alterations in circadian rhythms were present at pre-plaque and early-plaque stages of AD represented by the two age groups of rats, 4- and 6-month-old respectively. No significant differences between genotype were observed in total time spent in NREM or REM (Figure 4-4, Supplementary table 4-1). However, significant age effects were

observed with both REM and NREM during the inactive phase, where the amount of NREM sleep was increased, while the amount of REM was decreased at 6 months of age (Fig 4-4, Supplementary table 4-1). Analysis of the time spent in each vigilance state for each 3-hour epoch demonstrated that circadian rhythmicity was observed in both groups at both ages, where the amount of NREM and REM was higher during the lights on period when compared to the lights off period (Fig 4-5).

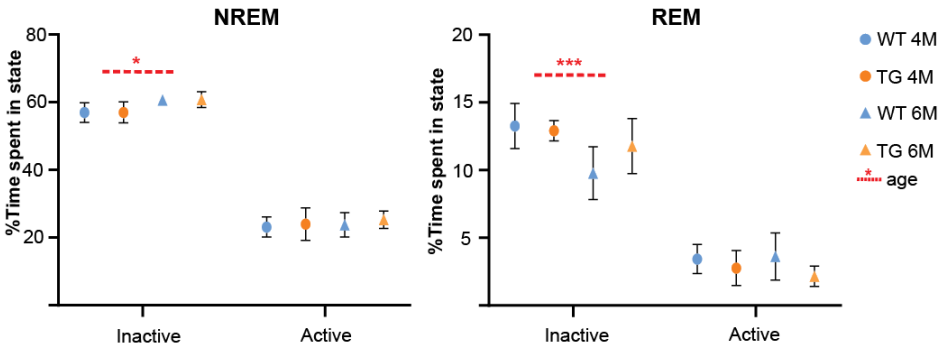

Figure 4-4: Total sleep time during active and inactive phase. Plots demonstrate the mean percentage time spent (+/- SEM) in NREM (left) or REM (light) during the inactive and active phase. ANOVA analysis reveals significant age effects from 4 to 6 months of age in the amount of NREM and REM during the inactive phase. * p<<0.05, *** p<<0.001

When comparing the time spent in REM across 3-hour epochs, significant genotype effects (p=0.0256, p=0.0146) were observed during the active period, demonstrating decreased time spent in REM between Z18- Z21, and an increased time spent in REM between Z21- Z24 in TgF344-AD rats (Fig 4-5A, Supplementary table 2). Significant age effects (Z9-Z12 p=0.0042, Z12-Z15 p=0.0156) were observed during the light phase, demonstrating decreased REM time in 6-month-old animals compared to 4-month-old animals during the inactive phase (Fig 4-5A). We observed significant interaction effects (Z6-Z9 p=0.0306, Z9-Z12 p=0.0029) at rest phase in NREM sleep. Posthoc analysis revealed an increased time spent in NREM between Z6-Z9 in 4-month-old TgF344-AD rats compared to age-matched WT rats (p=0.0486), while the time spent in NREM between Z9-Z12 was significantly lower in these 4-month-old TgF344-AD rats compared

to WT littermates (p=0.018). These results suggest minor alterations in circadian rhythm were present at early stages of AD in TgF344-AD rats.

Sleep fragmentation, characterized by shorter duration of sleep bouts and increased frequency of wakening, has been frequently observed in patients suffering from AD (Kent, Feldman, & Nygaard, 2021). Sleep fragmentation was evaluated by investigation of the cumulative distribution of all NREM and REM sleep bout lengths and performing Kolmogorov-Smirnov tests (FDR $p<0.05$) to investigate if the distribution is different between groups (Fig 4-5B). Significantly increased probability of shorter REM bouts was observed in 4-month-old TgF344-AD rats ($p = 0.0428$), as demonstrated by the steeper slope or the cumulative distribution plot at shorter bouts, but not in 6-month-old TgF344-AD rats ($p = 0.0786$). NREM sleep bout length was not significantly different between groups ($p_{4M} = 0.1109$, $p_{6M} = 0.4706$).

4.4.2 Micro architectural changes in sleep

Aβ and pTau have been known to interfere with synaptic function, hence induce altered oscillatory activity, which in turn is linked to cognitive symptoms of AD (A. M. Goodman et al., 2021; T. Ma & Klann, 2012). This altered synaptic transmission has been linked to altered power at different frequencies of interest (Gaubert et al., 2019; Kent et al., 2018; Musaeus et al., 2018). During NREM sleep, a significant age effect was observed in the delta band, demonstrating a decreased power at 6-months of age in both groups. In addition, significant age effects were detected in the fast gamma band, showing an increase in the power of these frequencies over time. However, no significant genotype effects were observed in the power across different frequency bands during NREM sleep (Fig 4-6A&B, Supplementary table 4-4). In contrast, during REM sleep, a significant genotype effect ($p = 0.0455$) was present in the fast gamma power, demonstrating a reduction in fast gamma oscillations in the TgF344-AD rats irrespective of age (Fig 4-6C&D, Supplementary table 4-5).

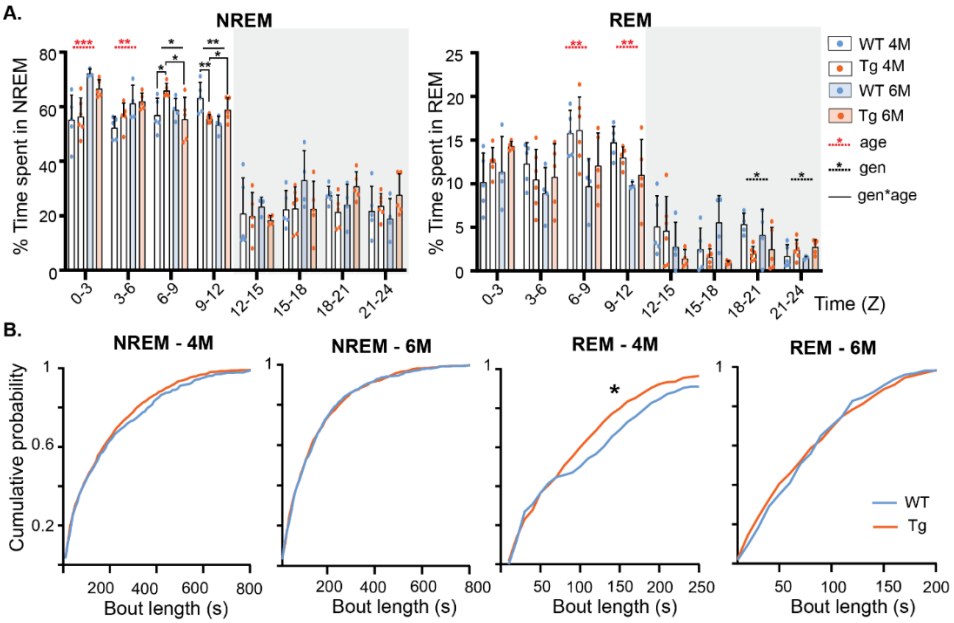

Figure 4-5: Circadian rhythm in TgF344-AD rats. A). Percentage time spent in NREM (left) or REM (lift) during 3-hour epochs. On the x-axis Zeitgeber time (Z) is represented. Bars demonstrate the mean +/- SEM across animals within each group, whereas dots represent subject values. Between Z0 and Z12, lights are on, between Z12 and Z24, lights are off (Grey zone). Two-way ANOVA's (genotype (gen), age, genotype*age) per epoch were used to test for statistical differences B). Cumulative probability plots of sleep bout lengths for each group. The left panels show the cumulative distribution of NREM bouts, while the right plots show the cumulative distribution of REM bouts. Kolmogorov-Smirnov tests (FDR p<0.05) were performed to evaluate if distributions were significantly different. * p< <0.05, ** p<<0.01, *** p<<0.001

Phase-amplitude coupling (PAC) is an electrophysiological phenomenon where the amplitude of fast oscillations is modulated by the phase of slower oscillations. Theta driven modulation of gamma oscillations during REM sleep has been implicated in memory processing and has been demonstrated to be an important mechanism of synaptic plasticity and synaptic homeostasis (Bergmann & Born, 2018). Alterations in synaptic function could impair theta-gamma coupling, therefore we evaluated PAC during REM sleep. First, the main frequencies modulated by theta frequencies were analysed using a comodulogram as described previously (Tort et al. 2010), where the

level of PAC in each frequency pair was assessed by calculating the Modulation Index across an entire REM segment (Tort et al., 2010). These comodulograms demonstrate coupling between theta frequencies (6.5-9 Hz) and high gamma (80-100 Hz) in all groups (Fig 4-7A). Interestingly, strong coupling was observed between theta (6.5-9 Hz) and low gamma oscillations (30-45 Hz) mainly in 4-month-old TgF344-AD rats.

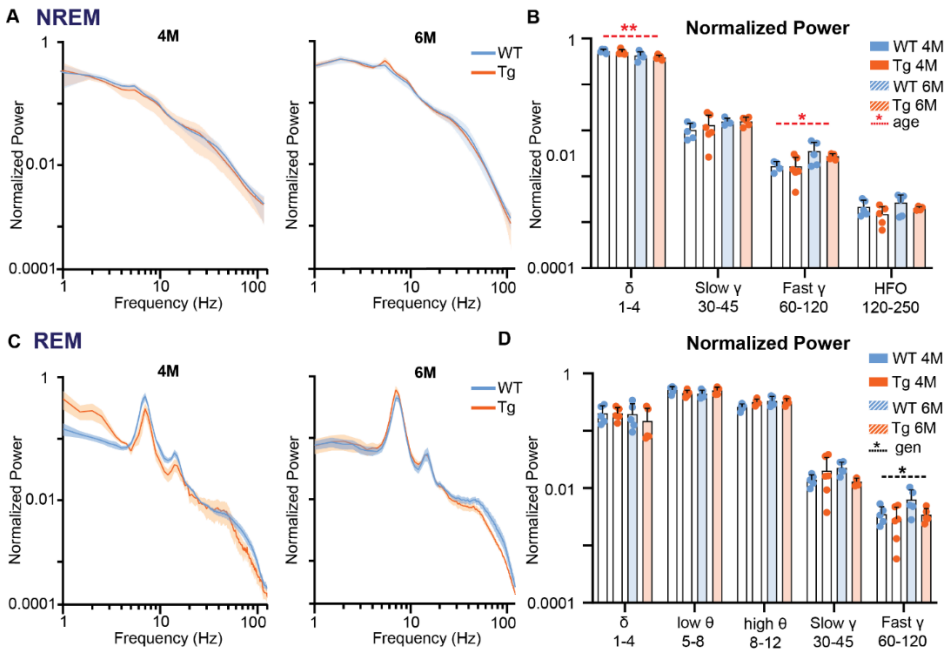

Figure 4-6: Power during NREM and REM sleep in TgF344-AD rats and wildtype littermates. A&C) Mean normalized power spectra during NREM (A) and REM (C). Shading indicates SEM across the group. B&D) Averaged normalized power across distinct frequency bands of interest (+/- SEM). Dots represent individual subject values. * p< <0.05, ** p<<0.01. WT = wild-type, Tg = TgF344-AD, M = months

Next, to evaluate the strength of the PAC, a time-resolved PAC analysis was performed. For each of the frequency bands of interest, based on the comodulograms, a separate tPAC analysis was performed. All REM bouts were segmented into 1-second epochs and for each 1-second epoch, the MI between target theta and gamma oscillations was calculated and averaged across epochs, to create a subject-based MI averaged across epochs. These subject-averages were statistically compared between groups and trials.

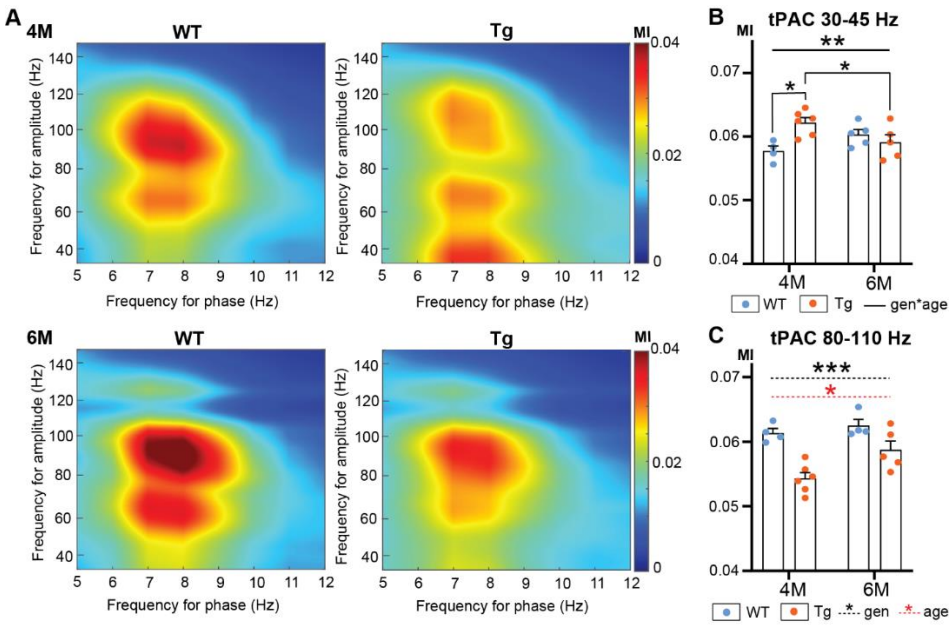

Figure 4-7: Hippocampal theta-gamma coupling in TgF344-AD rats during REM sleep. A) Comodulogram averaged across subjects demonstrating main frequencies of coupling. Color bar indicates the strength of the modulation index at different frequencies of theta (x-axis) and gamma (y-axis). B) Mean (+/- SEM) MI across subjects between theta-frequencies (6.5-9 Hz) and low gamma frequencies (30-45 Hz). Dots represent subject MI values. C) Mean (+/- SEM) MI across subjects between theta frequencies (6.5-9 HZ) and high gamma frequencies 80-110 Hz. Dots represent subject MI values. * p<<0.05, *** p<<0.001, gen = genotype, Tg = TgF344-AD, WT = wild-type, MI = modulation index

Next, time-resolved PAC analysis was performed to evaluate for each 1s segment of REM sleep, the strength of the theta-gamma coupling between theta and both gamma oscillations. Statistical analysis of the PAC between theta and low-gamma oscillations demonstrates a significant genotype*age interaction (p = 0.0074) (Supplementary table 4-6). Post-hoc analysis revealed a significantly higher PAC in 4-month-old TgF344-AD rats compared to age-matched WT littermates (p = 0.0152), which was absent at 6 months of age (p = 0.3723) (Fig 4-7B). In addition, a significant decrease in PAC was observed across ages in TgF344-AD rats (p = 0.049), returning the coupling strength to the same levels as in the WT littermates. Moreover, a decreased MI was observed in the coupling between theta and high frequency gamma oscillations in the TgF344-AD rats (p = 0.0002)

(Fig 4-7C, Supplementary table 4-6). Moreover, a significant age effect was observed, demonstrating an increase in the strength of PAC in the 6-month-old rats, which is mainly driven by an increasing MI in the TgF344-AD rats over time.

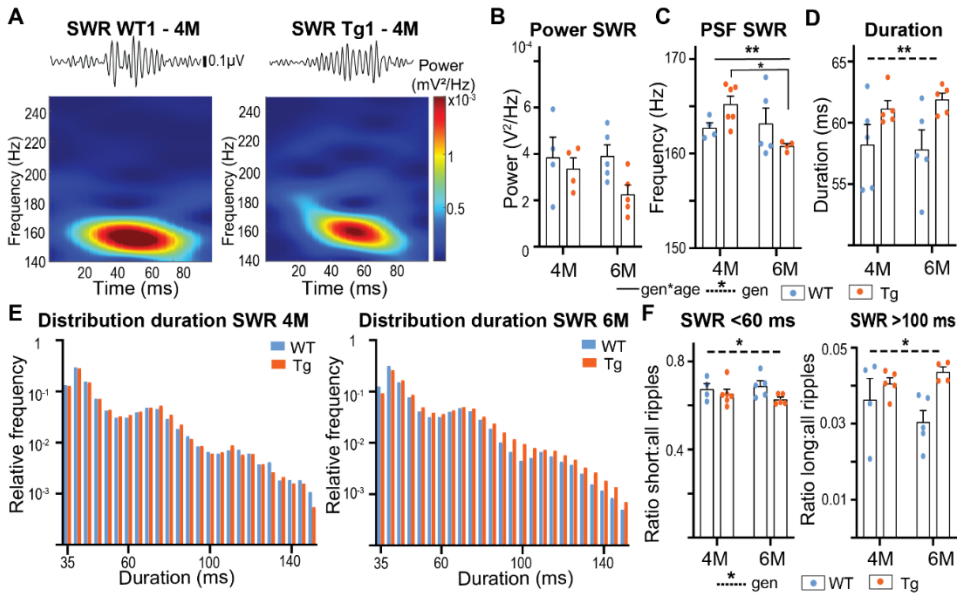

Figure 4-8: Sharp-wave ripples in TgF344-AD rats during NREM sleep. A) Illustrative Sharp-wave ripple (SWR) of a wildtype (WT) and TgF344-AD (Tg) rat. Trace shows filtered data (120-250Hz) of the ripple, while the bottom time-frequency plot demonstrates the frequency and power of the ripple. B) Mean power (+/- SEM) of SWR across subjects did not show significant genotype or age effects. C) Mean (+/- SEM) peak spectral frequency (PSF) of the SWR demonstrates a decreased PSF in the TgF344-AD rats across ages. D) Mean (+/- SEM) duration of SWR events showing a significantly increased duration of SWR in TgF344-AD rats. E) Histograms showing the group average relative frequency of each duration of SWR at 4 months (left) and 6 months (right). Based on the distribution, the ripples were divided into short ripples <60ms, medium ripples 60-100ms and long ripples >100 ms. F) The number of short ripples (left) and long ripples (right) vs all ripples. Bar plots show mean +/- SEM, whereas dots represent subject values. * p<<0.05, ** p<<0.01

Alterations in NREM sleep microarchitecture, such as decreased power of slow oscillations, have been associated with impaired cognitive performance. During NREM sleep, sharp-wave ripples which are fast oscillatory events in the CA1 regions of the hippocampus, have been thought to be a hallmark of memory replay and therefore,

have been implicated to play an important role in memory consolidation (Buzsaki, 2015). To investigate if SWR activity was already altered at pre-plaque and early-plaque stages of AD in the TgF344-AD rats, SWR were extracted as described in section 4.3.4.4 and several characteristics were examined (Fig 4-8).

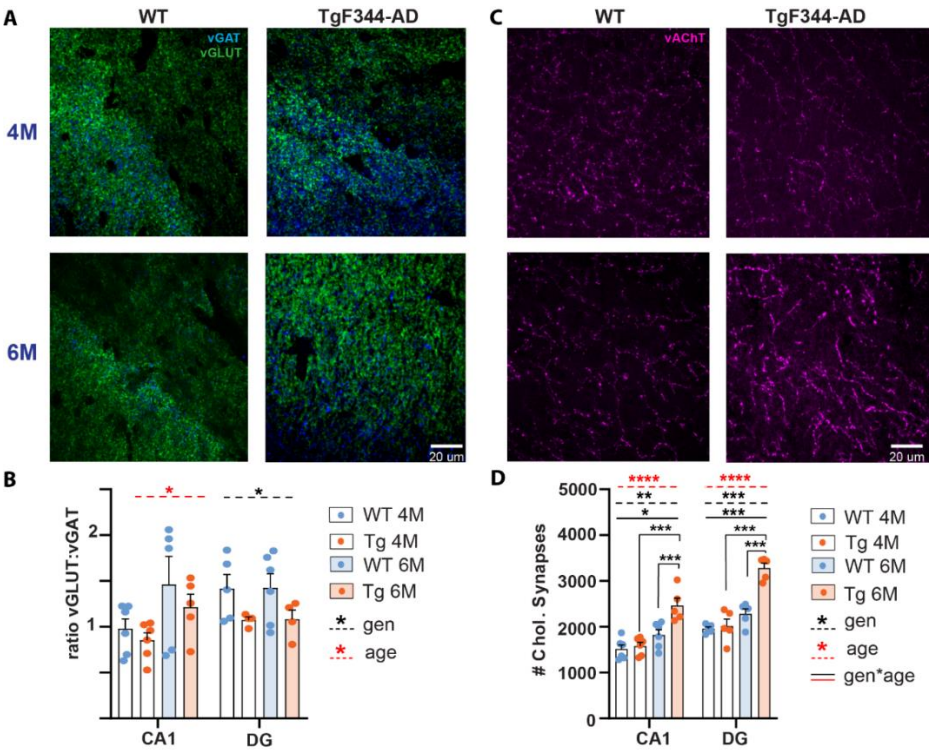

Figure 4-9: Alterations in excitatory/inhibitory synaptic balance and cholinergic synaptic density. A&C) Exemplary images of the glutamatergic (green), GABAergic synapses (blue) (A) and cholinergic synapses (magenta) (C) in the CA1 layer of the hippocampus in wild-type littermates (WT) (left) and TgF344-AD rats (right) at 4 and 6 months of age. B&D) Group-averaged vGLUT/vGAT ratio (B) and number of cholinergic synapses (D) per region of interest. Bars represent the mean +/- SEM. ANOVA analysis was performed to test for statistical differences. DG = dentate gyrus. TG = TgF344-AD. * p<<0.05, ** p<<0.01, *** p<<0.001

No significant genotype or age effects were observed for the power of the SWR (Fig 4-8B, Supplementary table 4-7). A significant interaction effect (p = 0.0379) was observed in the peak spectral frequency (PSF) of the SWR oscillations (Fig 4-8C, Supplementary

table 4-7, 4-8). Post-hoc t-tests demonstrated a significant age effect in the TgF344-AD rats where the PSF decreased with age (p= 0.0380), an effect that was absent in the WT littermates (p = 0.7676). No genotype differences were observed at 4 (p = 0.2236) and 6 months (p = 0.1944) of age. We did observe a significant genotype effect in the duration of the SWR (p = 0.0088), demonstrating an increased duration of SWR in the TgF344-AD rats (Fig 4-8D, Supplementary table 4-7). Histograms of the relative frequency for each duration demonstrates a skewed distribution (Fig 4-5E). Next, all SWR events were divided into short ripples (<60 ms), medium ripples (60-100 ms) and long ripples (>100 ms). Statistical analysis demonstrates a decreased fraction of short ripples ($p_{genotype}$ = 0.0473, Supplementary table 9) and an increased fraction of long SWR ($p_{genotype}$ = 0.0160, Supplementary table 4-9) in the TgF344-AD rats, demonstrating that the relative number of long duration ripples is increased at early stages of AD in the TgF344-AD rats. The ratio of medium duration ripples was not significantly different between groups ($p_{genotype}$ = 0.4066, Supplementary table 4-9).

4.4.3 Cholinergic sprouting and excitatory/inhibitory synapse imbalance

To determine if the altered oscillatory activity observed in the TgF344-AD rats coincided with altered synaptic density, immunohistochemistry was performed which quantified the amount of cholinergic, glutamatergic, and GABAergic synapses in the CA1 and dentate gyrus (DG) (Fig 4-9, Supplementary table 4-10). Analysis of the excitatory/inhibitory balance (ratio between glutamatergic and GABAergic synapses) revealed significant age effects in the CA1 layer of the hippocampus (p_{age} = 0.0248) demonstrating an increased excitation and/or decreased inhibition at 6 months of age. Interestingly, a significantly decreased excitation and/or increased inhibition was observed in the DG ($p_{genotype}$ = 0.0215) in the TgF344-AD rats already at 4-months of age.

The septo-hippocampal pathway is the main source of cholinergic input to the hippocampus and has been implicated in the modulation of hippocampal oscillatory activity, especially during REM sleep (Z. Gu & Yakel, 2022; Solari & Hangya, 2018). When

statistically comparing the abundance of cholinergic synapses, significant interaction effects were observed in the DG ($p = 0.0003$) and in the CA1 ($p = 0.0180$) (Fig 4-9C-D, Supplementary table 4-11). Cholinergic synaptic density in both regions was increased at 6-month of age in TgF344-AD rats compared to WT littermates (Supplementary table 4-12). Moreover, a significant increase in cholinergic synapses was observed over time in the TgF344-AD rats in both hippocampal regions.

4.5 Discussion

The aim of the current study was to evaluate how circadian rhythm, sleep macro-architecture and sleep micro-architecture are altered at pre-plaque and early-plaque stages of AD in TgF344-AD rats. We observed no significant differences in percentage of time spent in NREM and REM, suggesting circadian rhythmicity is unaltered at early phases of AD in TgF344-AD rats. However, we did observe REM fragmentation demonstrated by a significantly decreased REM bout length in the TgF344-AD rats at the pre-plaque stage, but not the early-plaque stage. In addition, we observed micro-architectural changes in oscillatory activity during REM and NREM sleep. In TgF344-AD rats, a significantly decreased fast gamma power was observed during REM sleep. Moreover, a decreased phase amplitude coupling between theta and fast gamma oscillations was observed in the TgF344-AD rats at both ages. Interestingly, at 4 months of age in TgF344-AD rats, a significant increase in PAC was present between theta and slow gamma oscillations, which was absent at 6 months of age. During NREM sleep we did not observe alterations in power of different oscillations. However, when investigating properties of SWR, we observed an increased duration of in TgF344-AD rats, mainly at 6 months of age, while the power of the oscillations and peak spectral frequency was not significantly different between genotypes. These alterations in oscillatory activity during sleep coincided with changes in synaptic density of GABAergic, Glutamatergic, and cholinergic synapses, where a decreased excitation and/or increased inhibition was observed in the dentate gyrus TgF344-AD rats at both ages. Interestingly, a paradoxical increase of cholinergic synapses was observed only at 6 months of age in the hippocampus of TgF344-AD rats.

4.5.1 SWR disturbances

Sharp-wave ripples during NREM are considered a key mechanism for memory consolidation during which the excitatory input from the CA3, as reflected by the sharp wave, induces fast local oscillations (ripples) in the pyramidal layer of CA1 region (Buzsaki, 2015). These ripple events are induced by a delicate interaction between excitatory neurons and GABAergic interneurons that, if disrupted, can lead to pathological forms of activity which leads to memory impairments (Benthem et al., 2020; Ego-Stengel & Wilson, 2010; Sanchez-Aguilera & Quintanilla, 2021; Zhen et al., 2021). Several studies observed altered properties of SWR in various mouse models of AD, which displayed decreased SWR power, decreased SWR frequency and reduced occurrence of ripples (for a review (Sanchez-Aguilera & Quintanilla, 2021)). These alterations were mainly attributed to reduced inhibitory control of the hippocampal network (Caccavano et al., 2020; Witton et al., 2016; Y. Xu, Zhao, Han, & Zhang, 2020). The current study didn't observe genotypic alterations in power, nor spectral frequency of SWR in TgF344-AD rats, which can be the result of the different disease stage in the current study, since the aforementioned studies focussed on late-stage AD (e.g. late post-plaque stages). However, we did observe an increased duration of SWR in TgF344-AD rats, which could be indicative of an increased memory demand in AD (Fernandez-Ruiz et al., 2019). Several studies have also observed the abnormal fast SWR (>250Hz) in animal models of AD, which are not observed in wild-type littermates. These fast ripples are thought to be caused by altered firing patterns of pyramidal neurons (Aivar, Valero, Bellistri, & Menendez de la Prida, 2014; Foffani, Uzcategui, Gal, & Menendez de la Prida, 2007; Sanchez-Aguilera & Quintanilla, 2021). It would be interesting if this aberrant SWR activity is present at pre-plaque and early-plaque stages of AD in the TgF344-AD rats.

4.5.2 REM fragmentation in AD

Research over the past decades demonstrated physiological changes in circadian rhythm and sleep architecture, such as earlier chronotype, reduced total sleep time and increased sleep fragmentation, emerge during the normal aging process (Mander,

Winer, & Walker, 2017; Romanella et al., 2021). Approximately 60% of the people suffering from AD develop sleep disturbances similar to those reported in normal aging, but with a greater magnitude (Casagrande et al., 2022; Kang et al., 2017; Vitiello & Borson, 2001). Alterations in sleep already occur at early stages of AD, and research has demonstrated that sleep disturbances exacerbate AD pathology by increased production of AB and decreased clearance of pTau and AB (Duncan et al., 2022; Y. S. Ju et al., 2017; Liguori et al., 2020; Roh et al., 2012). The majority of the studies on sleep alterations in AD focused on later, symptomatic stages of AD and observed disturbed circadian rhythm, sleep fragmentation and decreased REM and NREM sleep time in patients and in animal models of AD (Kang et al., 2017; Kent et al., 2018; Winer & Mander, 2018). In addition, several patient studies have studied alterations in circadian rhythm and sleep characteristics in patients suffering from MCI, which mainly observed alterations in NREM sleep (Hita-Yanez et al., 2012). However, the current study did not observe alterations in time spent in NREM and/or NREM fragmentation at the pre-plaque and early-plaque stage in TgF344-AD rats, possibly due to the early disease stage investigated in this study.

Instead, the current study revealed increased probability of shorter REM bouts at pre-plaque stage, which disappeared during the early-plaque stage, in the TgF344-AD rats, in the absence of decreased time spent in REM. Previous studies in 16-month old TgF344-AD rats observed increased fragmentation of both REM and NREM, without differences in time spent in these vigilance states (Kreuzer et al., 2020), suggesting that the alterations in sleep architecture worsen as the disease progresses in TgF344-AD rats, similar to what is observed in human AD (Casagrande et al., 2022; M. Hu et al., 2017; Kang et al., 2017). In addition, several studies in other animal models of AD observed alterations in REM sleep macro-architecture (Filon et al., 2020; Wisor et al., 2005; B. Zhang et al., 2005). Animal studies in J20 mice and Tg2576 mice displayed decreased time spent in REM and shorter REM bout length, without alterations in NREM, implying that REM changes precede NREM changes also in other mouse model of AD, similar to what is observed in the TgF344-AD rats (Filon et al., 2020; B. Zhang et al., 2005). Interestingly a study which involved patients with subjective cognitive decline, a self-

perceived cognitive deterioration which is associated with an increased risk for developing AD, also observed decreased time spent in REM sleep (Liguori et al., 2020). In addition, a longitudinal follow up study in people with patients who converted from MCI so AD-related dementia reported reduced REM sleep (Carnicelli et al., 2019), demonstrating that reduced time spent in REM is associated with a higher risk of developing dementia (Pase et al., 2017). Aforementioned results imply that alterations in REM sleep also occur early in human AD, often in the absence of NREM disturbances.

The disease mechanisms underlying early changes in REM sleep in AD remain elusive and research is trying to unravel the role of different neurotransmitter systems in REM sleep disruptions in AD. One of the proposed pathological mechanisms is that (soluble) AB and tau pathology disrupt the neuronal function in brain regions important in the regulation of sleep (Kent et al., 2021; Weber & Dan, 2016). One obvious link is the early accumulation of pTau in the locus coeruleus (LC), a region involved in the regulation of sleep-wake transitions. LC neurons are silent during REM sleep, which is critical for brain excitability and emotional regulation during sleep (Van Egroo et al., 2022). Early accumulation of pTau in the LC, which is observed in the TgF344-AD rat model, might lead to insufficient LC silencing, inducing restless REM sleep. Restless REM sleep has been associated with impaired emotional adaptation during REM sleep, which could lead to increased anxiety (Wassing et al., 2019), as is observed in TgF344-AD rats already at 5-months of age (Pentkowski et al., 2018). Moreover, the LC receives dense orexin innervation important in the regulation of REM sleep (Bourgin et al., 2000), where orexin has an excitatory effect on LC neurons. Studies have demonstrated that orexin levels are increased in MCI patients with REM sleep disturbances, suggesting that insufficient LC silencing might be the result of increased orexin signalling in the brain of MCI patients (Gabelle et al., 2017; Liguori et al., 2020). Moreover, animal experiments have demonstrated that AB and pTau are important regulators of expression levels of orexin receptors (Z. Liu, Wang, Tang, Zhao, & Wang, 2019). Until now, no research investigated orexin and/or noradrenaline signalling during different vigilance states in TgF344-AD rats.

Acetylcholine originating from brainstem nuclei, known as the REM-ON centre, are key regulators of REM sleep (Kent et al., 2021; Wisor et al., 2005). Studies in the Tg2576 mouse model of AD observed degeneration of pontine cholinergic nuclei, which coincided with impaired REM sleep (B. Zhang et al., 2005). During REM sleep, cortical and hippocampal ACh concentrations are very high, causing cortical activation mainly induced by the release of ACh from basal forebrain cholinergic neurons (Vazquez & Baghdoyan, 2001). Degeneration of the basal forebrain cholinergic nuclei occurs early in AD and has been shown to be predictive of amyloid burden (Teipel et al., 2022; Teipel et al., 2020). Increasing ACh with cholinesterase inhibitors, a type of drug commonly used to delay disease progression in AD, is associated with increased amounts of REM sleep, which is in turn correlated with improvement of cognitive function in MCI patients (Kanbayashi et al., 2002; Mizuno, Kameda, Inagaki, & Horiguchi, 2004; Moraes Wdos et al., 2006; Wisor et al., 2005) . Aforementioned results might indicate that at the pre-plaque stage in TgF344-AD rats, alterations in cholinergic signalling, caused by the accumulation of soluble AB, are contributing to the REM sleep fragmentation.

4.5.3 Altered theta-gamma coupling in TgF344-AD rats

Phase amplitude coupling between theta and gamma sub-bands where the phase of theta oscillations modulates the amplitude of the gamma oscillations, is an important hallmark of hippocampal oscillatory activity during cognitive tasks and REM sleep. Research has demonstrated that PAC is important for memory consolidation and synaptic plasticity (Bergmann & Born, 2018; Colgin, 2015). The modulation of different gamma bands, namely slow gamma (30-60 Hz) and fast gamma (60-130 Hz) is postulated to reflect different memory processes. Studies have demonstrated that the coupling between theta phase and slow gamma oscillations is enhanced after successful retrieval of memories in humans (Mormann et al., 2005) and rodents (Igarashi, Lu, Colgin, Moser, & Moser, 2014; Tamura, Spellman, Rosen, Gogos, & Gordon, 2017; Tort et al., 2009). Moreover, slow gamma synchronizes CA1 with the inputs from CA3, a region critical in memory retrieval (Colgin et al., 2009), suggesting that coupling between theta and slow gamma is mainly involved in memory retrieval, rather than memory encoding. Instead,

PAC between theta and high gamma (60-130 Hz) is thought to be important for sensory processing and memory encoding (Belluscio et al., 2012; Bieri, Bobbitt, & Colgin, 2014; E. L. Newman, Gillet, Climer, & Hasselmo, 2013). Several studies observed spatial memory impairments in TgF344-AD rats, already at 4 months of age (Fowler et al., 2022; Proskauer Pena et al., 2021). The observed decreased PAC might be an electrophysiological correlate of these memory impairments, however, electrophysiological measurements during cognitive tasks would be necessary to correlate behavior with alterations in PAC.

Numerous studies have observed alterations in theta gamma coupling in people suffering from MCI or advanced AD. MCI patients demonstrated with decreased theta gamma coupling, which was correlated with decreased memory performance, and which further declined in patients with AD related dementia (M. S. Goodman et al., 2018). Similar decreases in theta gamma coupling were also observed in a variety of mouse models of AD, even before AB plaques were present in the brain (Etter et al., 2019; Mably et al., 2017; Park et al., 2020; Stoiljkovic et al., 2016; Stoiljkovic et al., 2015) and in 9 to 10 month old TgF344-AD rats (Bazzigaluppi et al., 2018; Stoiljkovic et al., 2018; Stoiljkovic et al., 2019), similar to the observations in the current study. Moreover, Bazzigaluppi et al. 2018 observed that PAC between theta and low gamma was preserved in 6-month-old TgF344-AD rats, similar to the observations in the current study where the coupling between gamma and slow theta is unaltered (Bazzigaluppi et al., 2018). However, at the pre-plaque stage we observe an increased PAC between theta and slow gamma in TgF344-AD rats. The disease mechanisms underlying alterations in PAC are still elusive, however, studies have observed that the changes in PAC coincided with interneuron dysfunction (Park et al., 2020; Stoiljkovic et al., 2015; Stoiljkovic et al., 2019) alterations in cholinergic signalling in the hippocampus (Stoiljkovic et al., 2015) and accumulation of pTau and (soluble) AB (Bazzigaluppi et al., 2018; Etter et al., 2019; Stoiljkovic et al., 2018).

4.5.4 Compensatory mechanisms at early-plaque stage

In the current study we observed mainly alterations in REM sleep architecture and oscillatory activity during REM sleep. The genotypic differences observed at 4 months were larger than the differences at 6 months, mainly due to age effects in TgF344-AD rats which allowed the recovery of oscillatory activity in the TgF344-AD rats to become more similar to the WT rats. Interestingly, we observe a paradoxical increase in cholinergic synapses in the hippocampal regions, a mechanism postulated to be a sign of compensation for loss of cholinergic tone at earlier stages (Dubelaar et al., 2006; L. Hu et al., 2003; Lau et al., 2013). Similar paradoxical increases in cholinergic synapses have been observed at pre-plaque stages in APP/PS1 mice and MCI patients (DeKosky et al., 2002; L. Hu et al., 2003). This increase in cholinergic synapses is a phenomenon which is commonly observed after glutamatergic lesioning of the mEnt, resulting in a loss of glutamatergic input to the hippocampus (Bott et al., 2016; Naumann, Deller, Bender, & Frotscher, 1997). This glutamatergic denervation of the hippocampus is known to induce hyperexcitability in several hippocampal regions, including the DG and CA1 layer (Naumann et al., 1997). Recent studies have demonstrated that the increase in cholinergic innervation compensates for network hyperactivity, which has been associated with recovery of spatial memory (Bott et al., 2016; Traissard et al., 2007). This suggests that the cholinergic sprouting might be an important early compensation mechanism in AD which slows down disease progression, by restoring the network imbalance (Bott et al., 2016; L. Hu et al., 2003).

The REM associated alterations observed in this study are strongly modulated by the cholinergic system (Brown et al., 2012; Z. Gu & Yakel, 2022; Watson, Baghdoyan, & Lydic, 2012), strengthening the assumption that compensatory mechanisms are present at 6 months of age in TgF344-AD rats. We observed a similar pattern in the functional MRI study in the TgF344-AD rats described in chapter 3. In this study we observed large alterations in whole brain network activity at four months of age in TgF344-AD rats, while the network activity at 6 months of age was very similar to the patterns observed in the WT rats. In addition, we observed altered involvement of the basal forebrain

region mainly at 4-months of age coinciding with astrogliosis in the nucleus Basalis of Meynert, which provides cholinergic modulation to the entire cortex (van den Berg et al., 2022). In contrast, alterations in oscillatory activity during NREM sleep, during which ACh modulation is virtually absent, became worse over time in the TgF344-AD rats. Aforementioned results provide strong evidence for cholinergic compensatory mechanisms at the early-plaque stage of AD in TgF344-AD rats which improve hippocampal network function.

4.5.5 Future perspectives

Recent studies have observed abnormal high frequency oscillations (250-500 Hz) in the hippocampus of different mouse models of AD. These oscillations were most abundant during SWS and were highly similar to high frequency oscillations observed in animal models of epilepsy. These oscillations are thought to be the result of increased excitability due to AD. Tg2576 mice even showed these abnormal high frequency oscillations prior to amyloid deposition (Lisgaras & Scharfman, 2023). It would be interesting to evaluate the presence of these oscillations at the pre- and early-plaque stage in the TgF344-AD rats as it could point towards increased excitability during early stages of AD. Moreover, detection of this aberrant activity might serve to be a diagnostic biomarker (Lisgaras & Scharfman, 2023).

4.6 Supplementary Material

4.6.1 Supplementary tables

Supplementary table 4-1: ANOVA of total time spent in REM and NREM during active and inactive phase

	REM			NREM		
	*Age*Genotype*	*Age*	*Genotype*	*Age*Genotype*	*Age*	*Genotype*
ACTIVE	0.1574	0.0162	0.4233	0.9875	0.0068	0.9546
INACTIVE	0.5336	0.6705	0.1096	0.8565	0.5680	0.5306

Statistical results accompanying figure 4-4

Supplementary table 4-2: ANOVA of time spent in certain vigilance state across 3-hour epochs

	WAKE			REM			NREM		
	*Age*Gen*	*Age*	*Gen*	*Age*Gen*	*Age*	*Gen*	*Age*Gen*	*Age*	*Gen*
Z0-Z3	0.3242	0.0335	0.3635	0.7903	0.2547	0.0570	0.2782	0.0005	0.6065
Z3-Z6	0.9378	0.1393	0.0082	0.2238	0.3733	0.9142	0.4225	0.0044	0.2446
Z6-Z9	0.0990	0.0175	0.1786	0.5178	0.0042	0.4131	0.0306	0.1213	0.3107
Z9-Z12	0.0051	0.0136	0.7189	0.2426	0.0156	0.7034	0.0029	0.0943	0.5875
Z12-Z15	0.5079	0.3773	0.6084	0.7801	0.0707	0.5596	0.6259	0.9263	0.5405
Z15-Z18	0.1148	0.3196	0.3741	0.0694	0.2561	0.0256	0.1922	0.2595	0.2781
Z18-Z21	0.1596	0.6296	0.8794	0.3610	0.7949	0.0146	0.0255	0.2735	0.8959
Z21-Z24	0.3240	0.7388	0.1322	0.5963	0.8334	0.0565	0.3014	0.7687	0.1419

Statistical results accompanying figure 4-5. Gen = genotype

Supplementary table 4-3: post-hoc analysis time spent in certain vigilance state

	WAKE Z9-Z12	NREM Z6-Z9	NREM Z9-Z12	NREM Z18-Z21
	P-values (FDR p<0.05)	*P-values (FDR p<0.05)*	*P-values (FDR p<0.05)*	*P-values (FDR p<0.05)*
WT4M – TG4M	0.0318	0.0486	0.018	0.1437
WT4M – WT6M	0.0036	0.6163	0.0092	0.3705
TG4M – TG6M	0.7283	0.0408	0.2165	0.0748
WT6M – TG6M	0.09359	0.3724	0.0759	0.1854

Statistical results accompanying figure 4-5

Supplementary table 4-4: results of ANOVA of power across different frequency bands during NREM

	DELTA	GAMMA SLOW	GAMMA FAST	HFO
GENOTYPE	0.2762	0.5123	0.4396	0.1030
AGE	0.0011	0.1263	0.0121	0.2176
GENOTYPE*AGE	0.8726	0.6217	0.4742	0.9901

Statistical results accompanying figure 4-6

Supplementary table 4-5: results of ANOVA of power across different frequency bands during REM

	DELTA	THETA LOW	THETA HIGH	GAMMA SLOW	GAMMA FAST
GENOTYPE	0.5371	0.9540	0.2591	0.8145	0.0455
AGE	0.4344	0.6698	0.0778	0.8184	0.0555
GENOTYPE*AGE	0.5420	0.0444	0.1267	0.0594	0.2259

Statistical results accompanying figure 4-6

Supplementary table 4-6: results of ANOVA of PAC between theta and low and high gamma frequencies

	LOW GAMMA (30-45 HZ)	HIGH GAMMA (80-110 HZ)
GENOTYPE	0.0945	0.0002
AGE	0.7953	0.0146
GENOTYPE*AGE	0.0074	0.1506

Statistical results accompanying figure 4-7

Supplementary table 4-7: results of ANOVA of power, peak spectral frequency, and duration of SWR

	POWER	PSF	DURATION
GENOTYPE	0.0604	0.9842	0.0088
AGE	0.3701	0.0851	0.6787
GENOTYPE*AGE	0.3151	0.0379	0.6392

Statistical results accompanying figure 4-8

Supplementary table 4-8: post-hoc analysis of the peak spectral frequency of SWR

	P-VALUES (FDR P<0.05)
WT4M – TG4M	0.2236
WT4M – WT6M	0.7676
TG4M – TG6M	0.0380
WT6M – TG6M	0.1944

Statistical results accompanying figure 4-8

Supplementary table 4-9: results of ANOVA the ratio between short, medium, and long ripples vs all ripples

	SHORT	MEDIUM	LONG
GENOTYPE	0.0473	0.4066	0.0160
AGE	0.8175	0.1253	0.6600
GENOTYPE*AGE	0.3697	0.6751	0.1833

Statistical results accompanying figure 4-8

Supplementary table 4-10: results of ANOVA of vGLUT/vGAT ratio in hippocampal regions

	CA1	DG
GENOTYPE	0.1960	0.0215
AGE	0.0248	0.9538
GENOTYPE*AGE	0.5347	0.9999

Statistical results accompanying figure 4-9

Supplementary table 4-11: results of ANOVA of number of cholinergic synapses in hippocampal regions

	CA1	DG
GENOTYPE	0.0048	0.0001
AGE	<0.0001	<0.0001
GENOTYPE*AGE	0.0180	0.0003

Statistical results accompanying figure 4-9

Supplementary table 4-12: post-hoc analysis of number of cholinergic synapses in the CA1 and DG

	CA1	DG
WT 4M – TG 4M	0.6660	0.7170
WT 4M – WT 6M	0.0792	0.0570
TG 4M – TG 6 M	0.0004	0.0002
WT 6M – TG 6M	0.0016	0.0004

Statistical results accompanying figure 4-9

5. Hippocampal network impairment during explorative behavior and wake immobility at the pre-plaque stage of AD

This chapter is based on:

M. van den Berg, D. Toen ,M. Verhoye and G.A. Keliris (2023) Alterations in theta-gamma coupling and sharp wave-ripple, signs of prodromal hippocampal network impairment in the TgF344-AD rat model. Front. Aging Neurosci. 15:1081058. doi: 10.3389/fnagi.2023.1081058

5.1 Abstract

Alzheimer's disease (AD) is a severe neurodegenerative disorder caused by the accumulation of toxic proteins, amyloid-beta (Aβ) and tau, which eventually leads to dementia. Disease-modifying therapies are still lacking, due to incomplete insights into the neuropathological mechanisms of AD. Synaptic dysfunction is known to occur before cognitive symptoms become apparent and recent studies have demonstrated that imbalanced synaptic signalling drives the progression of AD, suggesting that early synaptic dysfunction could be an interesting therapeutic target. Synaptic dysfunction results in altered oscillatory activity, which can be detected with electroencephalography and electrophysiological recordings. However, the majority of these studies have been performed at advanced stages of AD, when extensive damage and cognitive symptoms are already present. The current study aimed to investigate if the hippocampal oscillatory activity is altered at pre-plaque stages of AD.

The rats received stereotactic surgery to implant a laminar electrode in the CA1 layer of the right hippocampus. Electrophysiological recordings during two consecutive days in an open field were performed in 4–5-month-old TgF344-AD rats when increased concentrations of soluble Aβ species were observed in the brain, in the absence of Aβ-plaques.

We observed a decreased power of high theta oscillations in TgF344-AD rats compared to wild-type littermates. Sharp wave-ripple (SWR) analysis revealed an increased SWR power and a decreased duration of SWR during wake immobility in TgF344-AD rats. The alterations in properties of SWR and the increased power of fast oscillations are suggestive of neuronal hyperexcitability, as has been demonstrated to occur during presymptomatic stages of AD. In addition, decreased strength of theta-gamma coupling, an important neuronal correlate of memory encoding, was observed in the TgF344-AD rats. Theta-gamma phase amplitude coupling is associated with the execution of cognitive functions and might be a specific measure of working memory functioning in humans. Studies have demonstrated that mild cognitive impairment patients display

decreased coupling strength, similar to what is described here. The current study demonstrates altered hippocampal network activity occurring at pre-plaque stages of AD and provides insights into prodromal network dysfunction in AD. The alterations observed could aid in the detection of AD during presymptomatic stages.

5.2 Introduction

Alzheimer's Disease (AD) is a severe neurodegenerative disorder characterized by the progressive accumulation of extracellular amyloid-beta (Aβ) plaques, intracellular tau-aggregation, synaptic dysfunction, and neuronal loss, resulting in cognitive dysfunction and eventually, dementia. Despite decades of research, disease-modifying therapies are still lacking, mainly due to incomplete insights into the neuropathological mechanisms of AD. Studies have demonstrated that the neuropathological changes underlying AD start 10-20 years before the onset of cognitive symptoms, with the accumulation of Aβ being the first identifiable hallmark (Braak & Braak, 1991; Braak et al., 2011; Sperling et al., 2011). The soluble Aβ species, which are the precursors of the Aβ plaques, are known to interfere with synaptic dysfunction and therefore network function, long before cognitive symptoms are apparent (Ben-Nejma et al., 2019; Busche et al., 2012; Hector & Brouillette, 2020; S. Li & Selkoe, 2020; T. Ma & Klann, 2012). Research has demonstrated that imbalanced synaptic function drives disease progression during presymptomatic stages of AD, making this an interesting target for future therapies (Bi et al., 2020; Styr & Slutsky, 2018; Witton et al., 2016).

The hippocampus is a brain structure in the medial temporal lobe, which is strongly involved in memory processes. Moreover, the hippocampus is one of the first regions affected in AD (Braak & Braak, 1991; Braak et al., 2011). The main function of the hippocampus is consolidation and retrieval of memories, by integrating of sensory information with previously encoded information. This process can be observed mainly in the tri-synaptic hippocampal circuit, where the activity of the pyramidal excitatory neurons in the CA1 and CA3 layers is balanced by inhibitory interneurons (Buzsaki, 2015;

Ego-Stengel & Wilson, 2010). This results in various hippocampus specific oscillatory characteristics, such as sharp-wave ripples (SWR) and phase amplitude coupling (PAC).

SWR are fast oscillatory events which occur mainly during wake immobility and during sleep (Buzsaki, 2006, 2015). SWR are the hallmark of memory replay, as during SWR, large population of pyramidal neurons are activated, often in sequences that recapitulate past or potential future experiences (Buzsaki, 2015; Colgin, 2016). The sharp waves and ripples are thought to be separate events with distinct origins. The sharp waves are excitatory events originating from the CA3, which induce locally generated ripple oscillations in the CA1 pyramidal layer. The ripple events are generated by a delicate interaction between excitatory pyramidal neurons and local GABAergic interneurons that, if disrupted, can lead to pathological forms of activity which impair memory processes (Buzsaki, 2015; Buzsaki et al., 2003; Caccavano et al., 2020; Colgin, 2016; Sanchez-Aguilera & Quintanilla, 2021; Zhen et al., 2021). During SWR, slow gamma oscillations have been observed throughout the entire hippocampus. These slow gamma oscillations are thought to synchronize oscillatory activity across the hippocampus, which enables memory activation (Carr et al., 2012; Gillespie et al., 2016; Sanchez-Aguilera & Quintanilla, 2021). Numerous studies have demonstrated that hyperactivity in the hippocampal circuits is associated with memory deficits at later stages of AD in different mouse models of AD (Bakker, Albert, Krauss, Speck, & Gallagher, 2015; Donegan, Boley, Yamaguchi, Toney, & Lodge, 2019; Ratner et al., 2021; Setti, Hunsberger, & Reed, 2017; Wilson, Ikonen, Gallagher, Eichenbaum, & Tanila, 2005; Yassa et al., 2010).

The amplitude of the hippocampal gamma rhythm is modulated by the phase of theta, a phenomenon named phase-amplitude coupling (PAC). The strength of this coupling has been shown to be increased during learning. Moreover, the PAC strength is also directly correlated with an increased chance of correctly performing a cognitive task, suggesting that PAC improves the transfer of information in the brain (Fell & Axmacher, 2011; Kitchigina, 2018; Tort et al., 2010; Tort et al., 2009). In patients with AD-related

dementia and mild cognitive impairment (MCI), a decreased theta-gamma PAC was observed when compared with healthy subjects, which worsened as the disease progressed (M. S. Goodman et al., 2018). Similar decreases of theta-gamma PAC have been observed in rodent models for AD (Gauthier-Umana, Munoz-Cabrera, Valderrama, Munera, & Nava-Mesa, 2020; Goutagny et al., 2013). However, alterations in PAC during pre-plaque stages of AD have not been evaluated thoroughly.

Hippocampal function and neuronal activity are heavily dependent on brain states, which are strongly linked to different types of behavior (Fontanini & Katz, 2008; McCormick et al., 2020). Besides the brain states during sleep, several brain states can be defined based on the level of arousal, attention and movement, such as locomotor/exploration and wake immobile (Kay & Frank, 2019). Different neuronal circuits and hippocampal subcircuits are involved in these dynamic states which are tightly regulated by neuromodulatory systems (Buzsaki, 2006; Trimper et al., 2017). Changes in the activity of these neuromodulatory systems have been shown to affect oscillatory patterns during specific types of behaviors (Gordon, Lacefield, Kentros, & Hen, 2005; Gurevicius, Lipponen, & Tanila, 2013; Trimper et al., 2017). Investigating changes in oscillatory activity during behavioral states could therefore offer novel insights into underlying neuromodulatory disease mechanisms (Nimmrich et al., 2015). Neuromodulatory systems such as the noradrenergic system and cholinergic system have been demonstrated to be affected at early stages of AD, which could influence oscillatory hippocampal activity during different behavioral states (Braak & Braak, 1991; Braak et al., 2011; Byron et al., 2021; Dubelaar et al., 2006; Gurevicius et al., 2013; van den Berg et al., 2022).

Early synaptic dysfunction has been demonstrated to disrupt network activity. The majority of the hippocampal local field potential (LFP) animal studies were performed at relatively advanced stages, when Aβ were already present in the brain. However, sAβ species have been demonstrated to alter network activity before Aβ-plaques are present in the brain, therefore, we hypothesized that early AD related pathological changes

would interfere with hippocampal network function in the pre-plaque stage of AD (Ben-Nejma et al., 2019; Shah et al., 2016; van den Berg et al., 2022). Moreover, we hypothesized that this hippocampal dysfunction would be different between behavioral states, which might offer new insights into early neuropathological mechanisms underlying AD-related hippocampal network disruption. Therefore, hippocampal local field potential recordings were performed in the highly translational TgF344-AD rat model, while animals were exploring an open field.

5.3 Materials and Methods

5.3.1 Animals and ethical statement

All procedures were in accordance with the guidelines approved by the European Ethics Committee (decree 2010/63/EU) and were approved by the Committee on Animal Care and Use at the University of Antwerp, Belgium (approval number: 2019-06). Electrophysiological experiments were performed in 4-month-old TgF344-AD rats (N=5) and wild-type littermates (N=5). Rats were group-housed prior to implantation but housed separately afterward. All animals were kept on a reversed, 12h light/dark cycle, with controlled temperature (20 – 24°C) and humidity (40-60%) conditions. Standard food and water were provided ad libitum.

5.3.2 Chronic hippocampal electrophysiological measurements

5.3.2.1 Surgical procedure

A laminar electrode was implanted in the CA1 layer of the right dorsal hippocampus, as is described in chapter 4.3.2.1.

5.3.2.2 Neurophysiological data acquisition

The electrophysiological recordings were acquired during the open field test (OFT) when the animals were 4.5 months old. The open field setup consisted of a square box (1m x 1m), a camera mounted to the ceiling that captured the complete open field (sampling

rate camera: 30 frames per second), and visual cues on the walls to assist spatial orientation. The animals were placed in the open field, without prior habituation, for two consecutive days for the duration of 1 hour on the first day (trial 1) and 20 minutes on the second day (trial 2). Sugar cubes were used to promote explorative behavior when the animals were in the box. Hippocampal LFP's were recorded using a wireless, 16-channel headstage (sampling rate 25kHz, W2100 system, Multichannel Systems, Germany) and animal movement was tracked using Anymaze soft- and hardware (Anymaze, Stoelting, Dublin). TTL pulses were used to synchronize the video recording and LFP acquisitions.

5.3.2.3 Validation of the electrode position

Validation of the electrode position was performed as described in chapter 4.3.3.

5.3.2.4 Behavioral states and segmentation

Based on pre-defined speed thresholds originating from the animal tracking, we classified the behavior during each video frame into exploration (> 0.05 m/s), grooming (0-0.05 m/s), and wake immobility (0 m/s) (Hoydal, Wisloff, Kemi, & Ellingsen, 2007; Sharif, Tayebi, Buzsaki, Royer, & Fernandez-Ruiz, 2021). The main focus was to investigate how hippocampal activity is altered during exploration and wake immobility behavior, therefore, we excluded epochs which were scored as grooming for all further analyses (Buzsaki, 2015; Colgin, 2016). Moreover, epochs with a duration shorter than 1 second were removed from further behavioral and electrophysiological analysis. Video recordings were used to validate the classified behavior of the animals. The TTL pulses stored in the LFP data were used to synchronize the brain activity with the video frames, to facilitate segmentation of the LFP signals into the two behavioral states using Fieldtrip (Oostenveld et al., 2011).

5.3.2.5 Analysis of the power and phase-amplitude coupling

The analyses performed were the same as in chapter 4, and include comparison of the power within certain frequency bands (table 5-1)(for the methods, check 4.3.4.2), evaluation of the phase amplitude coupling (for the methods, check 4.3.4.3)

Table 5-1 Frequency bands of interest

Frequency band	*Frequency range (Hz)*
Delta	0.5-4
Low theta	5-8
High theta	8-12
Slow gamma	30-45
Fast gamma	60-120
High frequency oscillations	120-250

5.3.2.6 Analysis of sharp wave-ripple analysis

All pre-processing steps and were conducted as described in chapter 4 (4.3.4.4). SWR were identified in the top channel which was placed in the pyramidal layer of the CA1 when the ripple power exceeded the threshold of 3SD from the channel mean. Events were expanded until the power fell below 2SD, events with a duration shorter than 30ms and/or a peak spectral frequency lower than 140 Hz were discarded. Afterward, a thresholding algorithm was applied to detect sharp waves in the stratum radiatum (Oliva et al., 2018). Signals in the channel which demonstrated strong sharp waves were bandpass filtered between 0.5 and 40 Hz using a 400^{th} order Butterworth filter. Sharp wave events which lasted between 20ms and 400ms were detected when the power of the filtered signal exceeded the threshold of 2.5SD from the mean. Only ripples that co-occurred with SW were kept for further analysis. Power in the SWR band, peak spectral frequency, duration, and spectral frequency in the slow gamma range during the SWR were extracted and were statistically compared between groups, state, and trial.

SWR occurrence is dependent on electrode placement and electrode properties. To limit this bias, a ratio between the occurrence of SWR during exploration and wake immobility was calculated and was statistically compared between groups and trial.

5.3.3 Behavioral analysis

During the experiments in the OFT, the animals were tracked based on the center point of the body for the complete length of the trial via Anymaze. Based on this tracking, the total distance that each animal travelled in the open field was extracted for each trial. Secondly, during the open field test, the open field was divided into an outer and an inner area (Figure 5-5). This separation was used to extract the following parameters: the time each animal spent in the inner area, the total distance travelled in the area and the number of entrances to the inner area per animal were extracted. The different behavioral parameters were statistically compared to evaluate the effects of genotype and trial. Next, all trials were segmented into epochs of 5 minutes to evaluate if behavioral genotypical differences were observed during specific moments in the trial and the parameters were compared between groups, trial, and epoch.

5.3.4 Statistics

The statistical analysis of the data was performed using the JMP Pro software (Version 16, SAS Institute Inc., Cary, NC, 1989 – 2021). Regarding the analysis of the power of the hippocampal oscillations and SWR characteristics a linear mixed model analysis (LMM) was performed, to evaluate the main effects of genotypes, state and trial and the interactions (genotypes*state, genotypes*trial, state*trial, genotypes*state*trial) of these effects. First, outliers were detected per genotype, state, and trial, based on principal component analysis. Data points with a T2 statistics indices higher than the 95% confidence interval were excluded from the analysis. Next, random intercept models were constructed for each frequency band and/or SWR parameter, with genotype, state and trial and the interactions between these variables as fixed effects and the variable subject as a random effect. A Posthoc test was performed if significant main effects and/or interaction effects were observed, using the Students T-test followed by a false discovery rate (FDR) correction using the Benjamini-Hochberg method with $p < 0.05$. The Benjamini-Hochberg procedures was used to calculate the q-value, which represents the FDR corrected p-value.

Regarding the analysis of the PAC, the occurrence rate ratio of SWRs and the analysis of the behavior of the rats across the entire trial, a LMM was used to evaluate the main effects of genotypes, trial and the interaction between genotypes and trial for each behavioral state. Outlier detection was again performed using a principal component analysis based on the T2 statistics as described earlier. Next, a random intercept model was generated for each behavioral state and frequency band of interest. Genotype, trial, and genotype*trial were used as fixed effects, and subjects was used as random effects. In the case when no significant genotype*trial interaction was present, the interaction was removed from the LMM, and the model was recalculated using genotype and trial and those p values are reported. In case of significant main effects and/or interaction effects were observed, Students T-test were performed, followed by a FDR correction using the Benjamini-Hochberg method with $p < 0.05$. The Benjamini-Hochberg procedures was used to calculate the q-value, which represents the FDR corrected p-value.

To evaluate if behavioral performance was altered during different stages of the trial, an additional statistical analysis was performed on the epoched data. A LMM with epoch, genotype and epoch*genotype as fixed effects and subject as random effect were used. The interaction term was removed from the model in case it was not significant, and the model was recalculated using genotype and trial as fixed effects, and those p values are reported. In case of significant main effects and/or interaction effects were observed, post hoc tests were performed as described above.

Graphical representation of the data was obtained using GraphPad Prism (version 9.2.0 for Windows, GraphPad Software, San Diego, California USA, www.graphpad.com).

5.4 Results

5.4.1 Altered power of hippocampal oscillations in TgF344-AD rats while exploring a novel environment

Aβ and pTau are known to interfere with synaptic function and thus are expected to induce altered oscillatory activity which is linked to the cognitive symptoms of AD (Ben-Nejma et al., 2019; Busche et al., 2012; Hector & Brouillette, 2020; S. Li & Selkoe, 2020; T. Ma & Klann, 2012). These alterations have been linked to altered spectral power at different frequencies of interest. To visually evaluate potential differences in the power of different neuronal oscillations between genotypes and different behavioral states, the mean power across all frequencies was calculated and statistically compared between genotypes, state, and trial. Figure 5-1 demonstrates the power spectra during wake immobility and exploration for both genotypes during trial one (Fig 5-1A). The power within certain frequency bands of interest was quantified and the results are shown in figure 5-1B-G. We observed no significant trial effects in any of the classical frequency bands (δ, θ, and γ). However, for the high frequency oscillations (120-250 Hz) we did observe a significant trial effect in TgF344-AD rats (Fig 5-1F).

A significant behavioral state effect ($p = 0.0281$) was observed for the mean power of delta oscillations demonstrating an increased power during explorative behavior when compared with wake immobility behavior for both the TgF344-AD rats and their WT littermates (Fig 5-1B, supplementary table XXX). A significant state effect was also observed for the mean power of low theta oscillations ($p = 0.0035$) demonstrating an increased power during wake immobility behavior when compared with explorative behavior for both genotypes (Fig 5-1C). A significant state ($p = 0.0277$) and genotype effect ($p = 0.0474$) were observed for the mean power of the high theta oscillations. The overall power in the high theta range was decreased in TgF344-AD rats compared to WT littermates. Moreover, high theta power during explorative behavior was found to be increased, which was mainly driven by the WT rats (Fig 5-1D).

Similarly, a significant genotype*state interaction ($p = 0.009$) was also observed for the mean power of the slow gamma oscillations. Post-hoc analysis demonstrated an increased power during wake immobility behavior when compared with explorative behavior for the TgF344-AD rats ($q = 0.000025$, Fig 5-1E) but not in WT rats ($q = 0.4235$). Moreover, no significant differences in slow gamma power were observed between genotype during both stages (Supplementary table 5-2).

Similarly, a significant genotype*state effect was also observed ($p = 0.0046$) for the mean power of the fast gamma oscillations. Post-hoc analysis demonstrated an increased power during explorative behavior when compared with wake immobility behavior for the TgF344-AD rats ($q = 0.0021$, Fig 5-1F, Supplementary table 5-2).

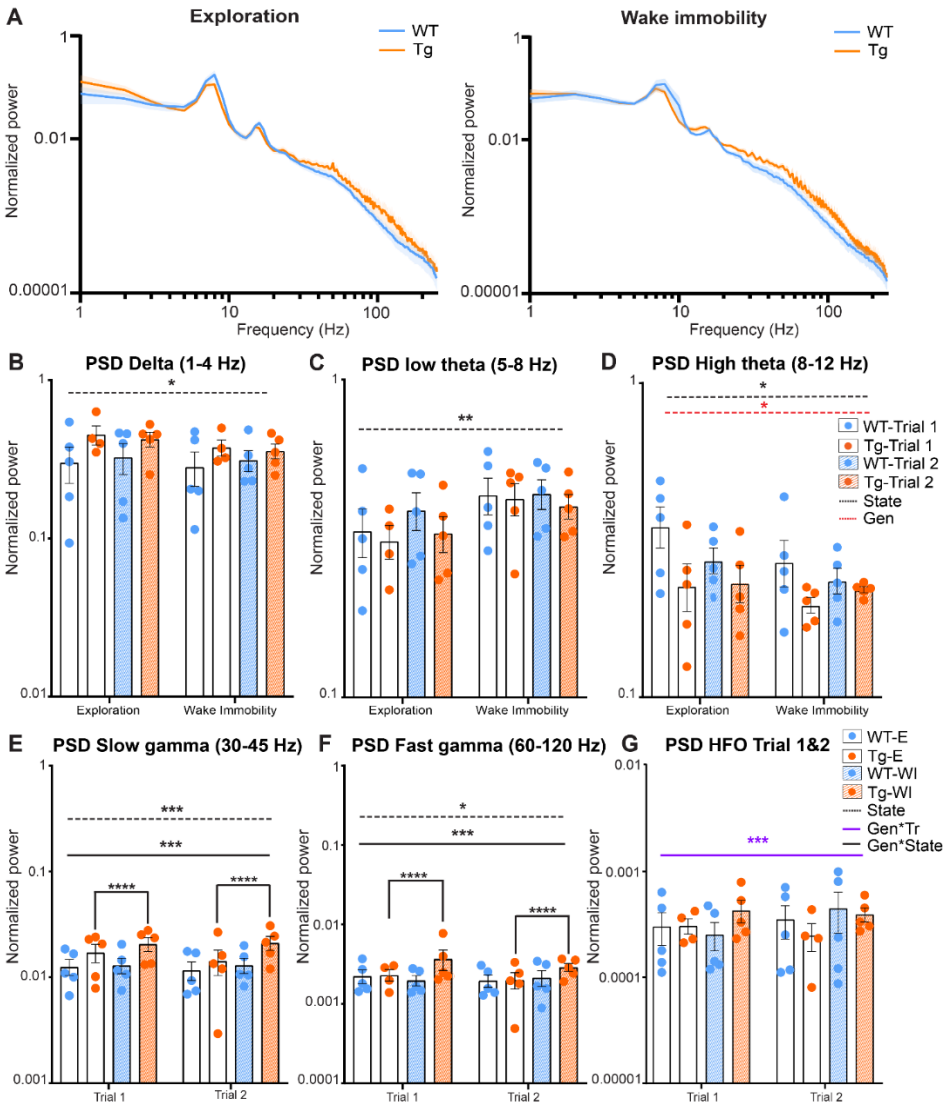

Figure 5-1: Power during explorative and wake immobility behavior in TgF344-AD rats and wildtype littermates. A) Mean normalized power spectra during exploration (left) and wake immobility (right) at trial 1. Shading indicates the SEM across the groups. B-D) Averaged normalized power (mean +/- SEM) of the delta oscillations (B), low theta oscillations (C) and high theta oscillations (D) at trial 1 and trial 2 during exploration (E) and wake immobility (WI). E-G) Averaged normalized power (mean +/- SEM) of slow gamma oscillations (E), fast gamma oscillations (F) and high frequency oscillations (HFO) (G) during E and WI across trials. PSD = power spectral density *p = < 0.05, ** p = < 0.01, *** p = < 0.001, **** q = < 0.0001

Lastly, a significant genotype*trial interaction (p = 0.0191) was observed for the mean power of the high frequency oscillations, range [120-250 Hz]. However, post-hoc analysis demonstrated no significant difference between genotypes or trials (Fig 5-1G, Supplementary table 5-3).

5.4.2 Decreased modulation of gamma amplitude in TgF344-AD rats

Phase-amplitude coupling (PAC) is an electrophysiological phenomenon where the amplitude of the fast oscillations (gamma oscillations) is modulated by the phase of the slower oscillations (theta oscillations). The theta-gamma PAC has an important function in both memory encoding and memory retrieval, functions which are known to be affected in AD (Bergmann & Born, 2018; Witton et al., 2016).

In order to calculate PAC, the main frequencies by which theta frequencies modulate the amplitude of gamma oscillations were analysed by calculating a group-average comodulogram as described previously (Tort et al.). The theta band (5-12 Hz) and gamma band (30-120 Hz) were divided into 1Hz bins and for each combination of theta and gamma frequencies the mean modulation index across all epochs from each subject was calculated to create a subject based comodulogram for each trial, which was averaged to create group-averaged comodulograms. In WT, comodulograms demonstrated coupling between theta frequency 6.5-10 Hz and fast gamma 55-90 Hz during exploration (Fig 5-2B) and between theta frequency 6.5-9 Hz and fast gamma 60-90 Hz during wake immobility (Fig 5-2C). The comodulogram of the Tg animals demonstrated similar peaks as well as a second coupling between theta frequency 6.5-9 Hz and slow gamma 35-45 Hz during exploration (Fig 5-2B).

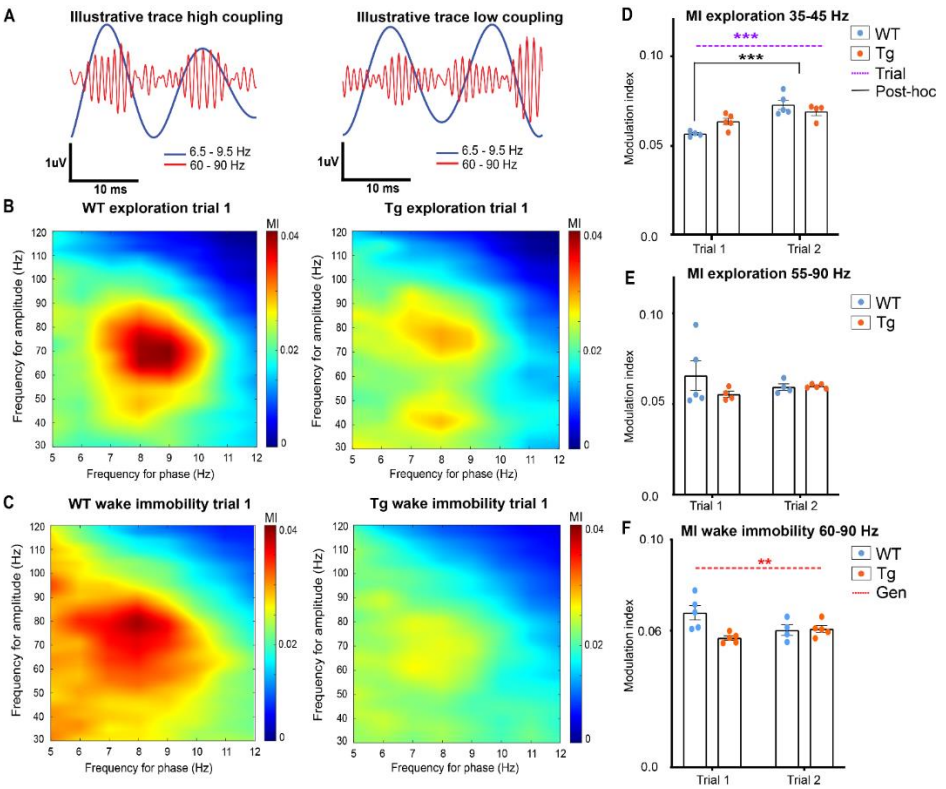

Figure 5-2: Hippocampal theta-gamma coupling in TgF344-AD rats during exploration and wake immobility. A) Illustrative filtered traces (theta range in blue, gamma range in orange) of a respective wildtype (WT) and TgF344-AD (Tg) subject during exploration. The amplitude of the gamma oscillations in the left trace demonstrated high coupling to the phase of theta, whereas in the right trace the amplitude of the gamma oscillations is less coupled to the theta phase. Average comodulograms demonstrate main frequencies of modulation during exploration (B) and wake immobility (C) in WT rats (left) and Tg rats (right). Colors indicate the strength of the PAC as calculated by the modulation index (MI) for different frequencies of theta (x-axis, phase-determining frequency) and gamma (y-axis, frequency for amplitude) (paragraph 2.2.5.3). Comodulograms demonstrate coupling between 6.5-9 Hz and 35-45 Hz, and 6.5-9 Hz and 55-90 Hz during exploration. During wake immobility, coupling between 6.5-9Hz and 60-90Hz were observed. D-E-F) time resolved PAC analysis results. Time-resolved averaged MI between theta (6.5-9Hz) and gamma frequencies (35-45Hz) during exploration (D, E) and during wake immobility (F). Bars indicate mean MI (+/- SEM), dots represent subject values. * p = < 0.05, ** p= < 0.01, ***p = < 0.001/q = < 0.001

Next, to evaluate the strength of the PAC, a time-resolved PAC analysis was performed. For each of the frequency bands of interest according to the comodulograms a separate tPAC analysis was performed. For each 1-second-long segment of data, the MI between target theta and gamma oscillations was calculated and averaged across epochs, to create a subject-based MI over time. These subject-averages were statistically compared between groups and trials.

During exploration, no significant interaction, nor genotype or trial effects were observed in the coupling between fast gamma (55-90 Hz) and theta (6.5-10Hz), demonstrating that the PAC during exploration is not different between 4-month-old TgF344-AD rats and WT littermates (Fig 5-2E, Supplementary table 5-4). Statistical analysis of the theta-gamma coupling strength between slow gamma (35-45 Hz) and theta (6.5-9Hz) demonstrated a significant trial effect ($p = 0.0003$) demonstrating an increased coupling during trial 2, and a significant interaction effect ($p = 0.0181$). Post-hoc analysis reveals a significant increase in coupling strength between trials in WT ($q = 0.0009$), but not in TgF344-AD rats (Fig 5-2D, Supplementary table 5-5). No interaction effect or trial effect were observed in the strength of the PAC during wake immobility (Fig 5-2F, Supplementary table 5-4). However, statistical analysis of the PAC during wake immobility demonstrated a significant genotype effect ($p = 0.0284$). This showed that the MI in TgF344-AD rats were significantly lower during wake immobility compared to WT littermates irrespective of trial, however, when looking at the Fig 5-2F, this decrease seems more prominent in trial 1.

5.4.3 Altered SWR activity in TgF344-AD rats while exploring novel environment

SWR are an important feature of memory function and are thought to represent a major factor in online memory consolidation and offline memory replay. SWRs are present both during exploration and wake immobility and are the result of the delicate interplay between inhibitory and excitatory neurons in the CA1 layer. The slow gamma oscillations observed during SWR are a phenomenon characteristic for SWR during waking and these

oscillations have been associated with synchrony between the CA3 and CA1 layer. This synchronization is hypothesized to enable coordinated memory reactivation in the hippocampus, a process that might be disrupted in AD (Carr et al., 2012; Gillespie et al., 2016; Sanchez-Aguilera & Quintanilla, 2021).

After SWR extraction, SWR occurrence rates, peak spectral frequency (PSF) of SWR and slow gamma oscillations, the power of SWRs and slow gamma oscillations and the duration of the ripples was statistically compared using LMM (Supplementary table 5-6, Fig 5-3). Analysis of the SWR occurrence rates showed a significant trial effect ($p = 0.0342$), demonstrating an increased occurrence rate of SWR during trial 2 compared with trial 1 (Supplementary table 5-7, Fig 5-3C).

A significant genotype effect was observed in the power at SWR frequencies ($p = 0.0013$), showing a significantly higher power in TgF344-AD rats compared to WT littermates (Fig 5-3D). The PSF of the SWR frequencies showed a significant state effect ($p = 0.002$) demonstrating a higher PSF_{SWR} during exploration compared to wake immobility (Fig 5-3E). Studies have demonstrated that the duration of SWRs is altered in animal models of AD (Sanchez-Aguilera & Quintanilla, 2021). Analysis of the duration of the SWR in TgF344-AD rats demonstrated a significant interaction effect (genotype*state*trial $p = 0.0286$). Post-hoc analysis shows a significant decreased duration of SWR during wake immobility in TgF344-AD rats during trial 2 ($q = 0.0252$), but not during trial 1 (Supplementary table 5-8, Fig 5-3F).

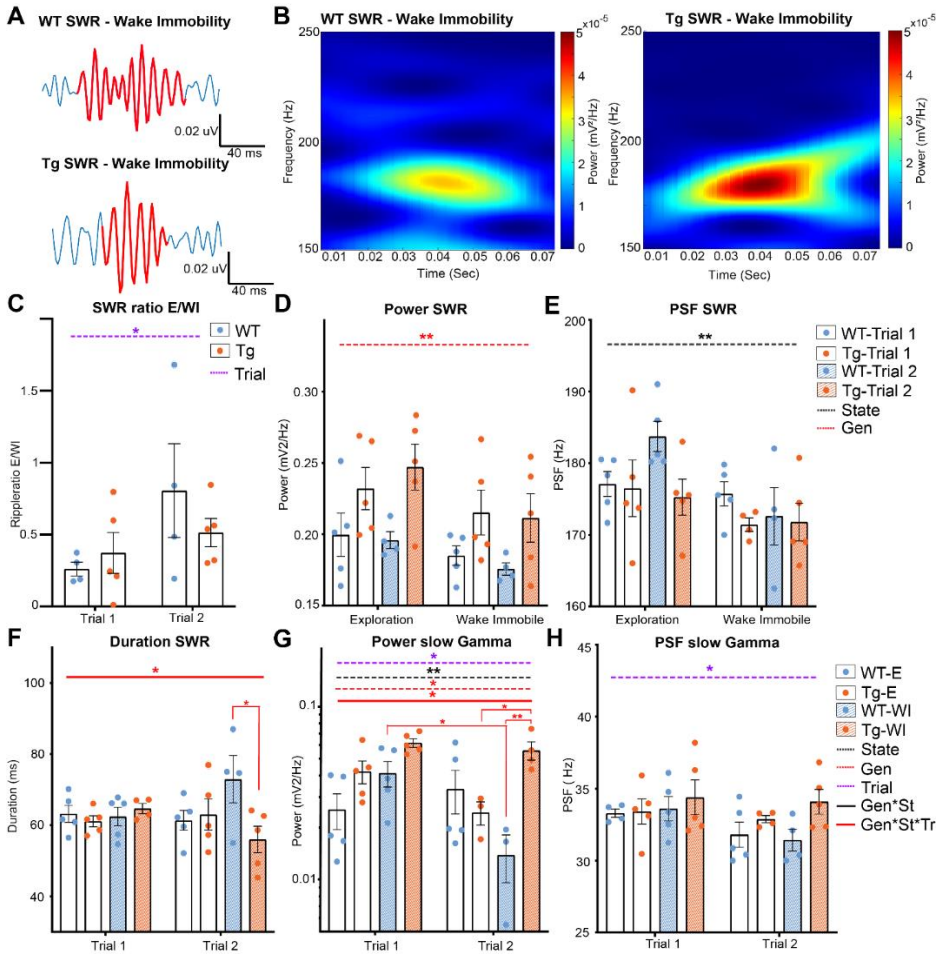

Figure 5-3: Analysis of different parameters for SWR in TgF344-AD rats during exploration and wake immobility. A) Illustrative traces of bandpass filtered SWR (120-250 Hz) during wake immobility and corresponding time-frequency plot (B) demonstrating the power of the ripple oscillation at different frequencies over time for the wildtype (WT) and TgF344-AD (Tg) rat. C) SWR occurrences ratio between exploratory/wake immobility for each animal. D) The mean power within the SWR frequency band for each behavioral state. E) Peak spectral frequency of the SWR for each behavioral state. F) Duration of SWR in milliseconds (ms) separated for each trial. G) The power of slow gamma oscillations during SWR was separated for each trial. H) The peak spectral frequency of slow gamma during exploration and wake immobility separated for each trial. Bars represent mean +/- SEM; individual values are represented by the dots. * p = < 0.05/q = < 0.01, ** p = < 0.01/ q = < 0.01.

Analysis of the slow gamma frequencies showed a significant genotype ($p = 0.0177$), trial ($p = 0.0082$) and state effect ($p = 0.0229$) in the power of the slow gamma oscillations, together with a significant interaction between those parameters ($p = 0.046$). Post-hoc analysis revealed a significant decrease in power in WT rats during wake immobility between trial 1 and trial 2 ($q = 0.0488$) (Fig 5-3G, Supplementary Table 5-8). In addition, a significant difference in power was observed between WT and TgF344-AD rats during wake immobility in trial 2, but not during trial 1 ($q = 0.0096$). Moreover, a significantly higher power during wake immobility with respect to exploration was observed in the TgF344-AD rats in trial 2 ($q = 0.0496$). A significant trial effect ($p = 0.0346$) was observed in the PSF at the slow gamma frequencies demonstrating a significantly higher PSF during trial 1 compared to trial 2 (Fig 5-3H).

5.4.4 Alterations in oscillatory activity concur with measures of increased anxiety

Previous studies in TgF344-AD rats observed increased anxiety in the open field test from 4 months onward. Behavioral analysis was performed to validate these findings in our TgF344-AD rats. Increased anxiety in rats in the open field is characterized by spending more time in the outer area and less motor activity during exploration (Fig 5-4A). Total distance travelled, total distance travelled in the inner area, time spent in the inner area, and the number of entries to the inner area of the open field were extracted and statistically compared between trials and genotype. A significant genotype effect was observed in the time spent in the inner area, showing a significantly decreased time spent in the inner area in TgF344-AD rats during both trials ($p = 0.018$) (Figure 5-4, supplementary table 5-10). For all parameters, a significant trial effect was observed (Figure 5-4, Supplementary Table 5-10), demonstrating decreases in total distance travelled, distance travelled in the inner area, time spent in the inner area, and number of entries in the inner area during the second trial.

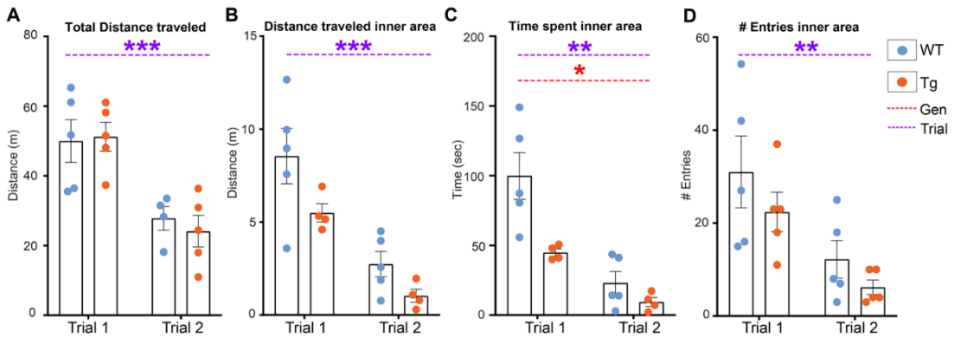

Figure 5-4: Behavioral analysis OFT across trials. A) Total distance traveled in meters across trials. B) Distance traveled in the inner area in meters across trials. C) Time spent in seconds in the inner area of the open field across trials. D) Number of entries of the inner area across trials. Bars represent mean +/- SEM; individual values are represented by dots. *p < 0.05 **p = < 0.01, ***p = < 0.001.

Therefore, a second analysis was performed separately for each trial, to evaluate if genotypical differences were present during specific epochs within each trial. Trials were segmented into epochs of 5 minute and statistically compared. Statistical analysis showed significant main epoch effects for all parameters during trial 1 demonstrating decreased explorative behavior over the duration of each trial (Figure 5-5 B-C, Figure 5-6A-B, Supplementary table 5-11). No significant genotype or interaction effects were observed in the total distance travelled, suggesting that explorative behavior was not altered in TgF344-AD rats (Figure 5-5B, Supplementary table 5-11). However, a significant genotype ($p = 0.0001$) and interaction effect ($p = 0.0001$) was observed in the time spent in the inner area. TgF344-AD rats spent less time in the inner area during several epochs, mainly during the first half of the trial (Figure 5-5C, Supplementary table 5-12). Moreover, a significant interaction effect was observed in the distance travelled in the inner area (Supplementary table 5-13). During the second epoch, the TgF344-AD demonstrated a decreased distance travelled in the inner area (Figure 5-6A, supplementary table 5-13). No significant genotype or interaction effects were observed in the number of entries into the inner area (Supplementary table 11).

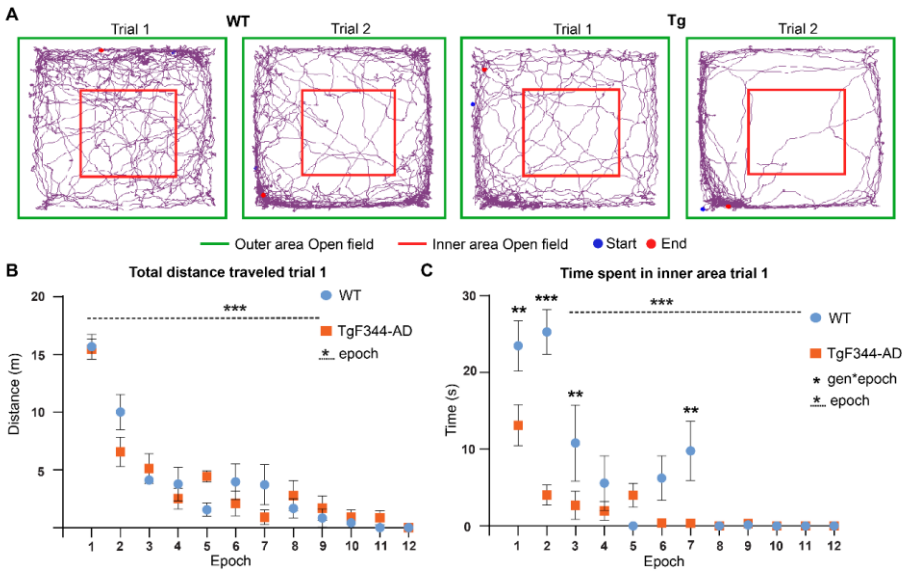

Figure 5-5: Behavioral analysis OFT during trial 1. A) Movement traces of representative wild-type (WT) (left) and TgF344-AD (Tg) (right) rat during trial 1 and trial 2. The start position is indicated with the blue dot and the end position is indicated with the red dot. The 1x1m open field is divided into an inner area (red) and outer area (green). B) Total distance traveled in meters across different 5-min epochs during trial 1. C) Time spent in seconds in the inner area of the open field across different 5-minute epochs during trial. Plots represent mean +/- SEM. ** q = <0.01, *** p/q = <0.001.

During trial 2, significant epoch effects were again observed in all aforementioned parameters, showing decreased locomotion and exploration over the duration of the trial in both groups (Figure 5-6C-F, Supplementary table 5-14). Moreover, a significant genotype effect was observed in the number of entries of the inner area (Figure 5=6F, Supplementary table 14). However, no significant genotype effects or interaction effects were observed in the other behavioral parameters during trial 2. Aforementioned result suggest increased anxiety was present in TgF344-AD rats, mainly during trial 1.

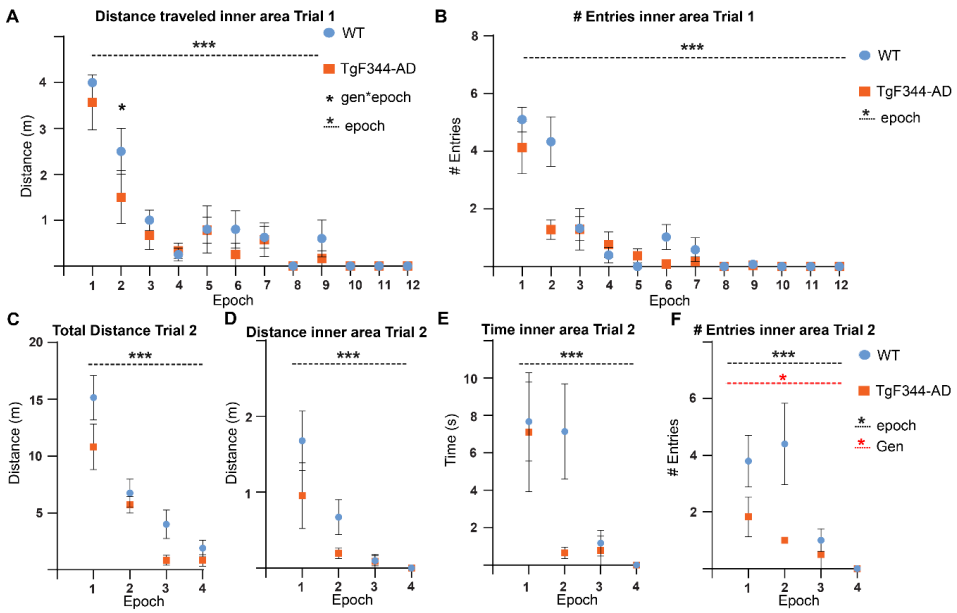

Figure 5-6: Behavioral analysis OFT across 5-minute epochs. A) Total distance traveled in the inner area during trial one across different epochs. B) Number of entries into the inner area during trial one across the different epochs. Total distance traveled (C), distance traveled in inner area (D), time spent in the inner area (E) and number of entries in the inner area (F) during trial 2 across epochs. Figures show mean +/- SEM. * p = < 0.05, *** p= <0.001

5.5 Discussion

This study aimed to investigate if hippocampal network activity is altered during explorative behavior at the pre-plaque stage of AD, using hippocampal electrophysiology in freely moving TgF344-AD rats and WT littermates. We observed a significantly decreased power in high theta oscillations in TgF344-AD rats. In addition, a decreased strength of PAC, an important electrophysiological mechanism underlying hippocampal dependent memory processes, was observed in TgF344-AD rats during wake immobility. SWR analysis revealed no significant differences in ripple ratios between genotypes, however, significantly increased power of SWR was observed in TgF344-AD rats, together with a significant decrease in the duration of the ripples. Moreover, significant genotype, trial and state effects were observed in the power of

slow gamma oscillations during SWR, which is thought to represent the interaction between the CA3 and CA1 regions of the hippocampus. The aforementioned results demonstrate that hippocampal activity in TgF344-AD rats is already altered before amyloid plaques are present in the brain, mainly while the animals were in the wake immobility state. These differences in oscillatory activity concurred with increased anxiety behavior in TgF344-AD rats, in the absence of differences in locomotion.

5.5.1 AD pathology in TgF344-AD rats

TgF344-AD rats display progressive Aβ plaque accumulation in the cortex and hippocampus starting from 6 months of age (R. M. Cohen et al., 2013). Studies recently demonstrated that at four months of age, increased concentrations of soluble Ab monomers and oligomers were present in the brains of TgF344-AD rats, in the absence of cortical and hippocampal Ab plaques (Ratner et al., 2021; Sare et al., 2020; van den Berg et al., 2022). In addition, TgF344-AD rats display p-tau accumulation in the locus coeruleus from 6 months onwards (Rorabaugh et al., 2017). However, no studies yet have examined if pTau accumulations are present at 4 months of age. Impaired spatial memory in the Barnes maze has been observed in TgF344-AD rats starting from 4 months of age (Fowler et al., 2022) , suggesting hippocampal impairments are already present during the pre-plaque stage of AD as is observed in the current study. In addition, working memory impairments and delayed memory retention have been observed in 6-month-old female TgF344-AD rats (Bernaud et al., 2022). Moreover, cholinergic dysfunction and neuroinflammatory responses have been observed from 6 months onward in TgF344-AD rats (Chaney et al., 2021). These results highlight the diverse phenotype of the TgF344-AD rats which highly resembles human AD.

The majority of the electrophysiological studies in animal models for AD pathology have been done in the late phases of AD. Electrophysiological studies observed alterations in oscillatory activity in the hippocampus of TgF344-AD rats from 9 months onward (Bazzigaluppi et al., 2018; Stoiljkovic et al., 2019). To our knowledge, this study is one of the few electrophysiological studies performed at the pre-plaque stage in TgF344-AD

rats. Several studies have investigated alterations in hippocampal synaptic function and/or network function in TgF344-AD rats using electrophysiological measurements. *In vitro* investigation of the tri-synaptic circuit in the hippocampus demonstrated increased long-term potentiation and hyperexcitability in dentate granule cells in 6-month-old male TgF344-AD rats, which was shown to be driven by increased noradrenergic postsynaptic signalling (A. M. Goodman et al., 2021; Smith et al., 2022; Smith & McMahon, 2018). Interestingly, a recent MRI study we performed did demonstrate alterations in whole brain network activity in 4-month-old TgF344-AD rats, suggesting that the presence of soluble Aβ species interferes with network function already before Aβ plaques are present in the brain of TgF344-AD rats (chapter 4) (van den Berg et al., 2022).

Many efforts were made from different research groups to characterize the behavioral and cognitive alterations in TgF344-AD rats. Studies have demonstrated significantly increased anxiety in TgF344-AD rats from 4-5 months of age (Pentkowski et al., 2018), which persisted while the animals were aging (Kelberman et al., 2022; Tournier et al., 2021). A recent study demonstrated hyperexcitability in the basolateral amygdala, a central part of the fear circuitry, in 6-month-old and 12-month-old TgF344-AD rats which display increased anxiety compared to age-matched WT littermates (C. M. Hernandez, Jackson, Hernandez, & McMahon, 2022). The aforementioned results demonstrate increased anxiety-like behavior in TgF344-AD rats starting from four months of age. This is in accordance with the results from the current study, where a significant decrease in time spent in the inner area of the open field was observed in TgF344-AD rats in comparison with their WT littermates. Significant trial effects were observed in all behavioral parameters, which demonstrated decreased distance travelled and decreased time spent in inner area during the second trial. These results suggest that the TgF344-AD rats do recognize the OFT as a familiar environment during the second trial, hinting that spatial memory is still intact at the pre-plaque stage of AD (Giovannini et al., 2001; Sare et al., 2020).

5.5.2 Alterations in power of hippocampal oscillations in TgF344-AD rats

The frequency and amplitude of oscillations are heavily dependent on vigilance and behavior. In the current study we compared the power of brain oscillations during exploration and during wake immobility. Theta oscillations are present in the whole HC during active exploration and rapid-eye-movement (REM) sleep but also during memory encoding and retrieval (Bauer, Buckley, & Bast, 2021; Colgin, 2016). In animals, theta oscillations can be divided into two types, type I, or atropine insensitive theta (6-12 Hz) which is dominant during exploration and type II, or atropine sensitive theta (4-9 Hz), which is dominant during wake immobility (Buzsaki, 2002; Z. Gu & Yakel, 2022; Kramis, Vanderwolf, & Bland, 1975). In the current study we observed for both groups these expected state effects for low theta (type II) and high theta (type I). In addition, a decreased power of type I theta oscillations was observed in 4-month-old TgF344-AD rats. These results are in concordance with previous studies which observed a decreased theta power in 9-month old TgF344-AD rats (Stoiljkovic et al., 2019). The power of theta oscillations in people suffering from AD is heavily dependent on the disease stage, with increases in theta power observed in MCI patients and patients suffering from AD related dementia (Byron et al., 2021; Jafari, Kolb, & Mohajerani, 2020; Musaeus et al., 2018). However, only a limited number of animal studies have investigated alterations in theta power during presymptomatic stages of AD. Injection of amyloid 1-40 monomers has been shown to induce decreases in hippocampal theta power (Colom et al., 2010), whereas amyloid plaques have been associated with increases in cortical theta power (Spinelli et al., 2022, Jafari et al., 2020). Decreased theta power has been observed in several animal models of AD, even in the absence of Aβ plaques. These decreases in theta power have been correlated to memory deficits and are thought to be caused by functional impairment of GABAergic septal hippocampal neurons by soluble Aβ (Caravaglios et al., 2010; Nimmrich et al., 2015; Scott et al., 2012; Villette et al., 2010; J. Wang et al., 2017). Both type I and type II theta oscillations are also directly influenced by cholinergic neurons of medial septum (Bauer et al., 2021; Z. Gu & Yakel, 2022). This could in part be responsible for the observed decreased theta since the cholinergic neurons in nuclei of the basal forebrain have been shown to be susceptible

to AD pathology (Brueggen et al., 2015; Fernandez-Cabello et al., 2020; Grothe et al., 2014; Herdick et al., 2020; Jeong et al., 2016).

The current study observed a significant increase in power of both slow and fast gamma oscillations in TgF344-AD rats during wake immobility compared to exploration, an effect which was not observed in WT littermates. In healthy subjects and animals, an increase in the power of slow and fast gamma oscillations is observed during memory encoding, sensory processing and wake immobility, similar to what is observed in the current study (Bragin et al., 1995). This increase in gamma power appears to predict if memory formation will be successful in humans but also in mice (Matsumoto et al., 2013; Palop & Mucke, 2016; Sederberg et al., 2007). However, several studies have demonstrated that neuronal hyperactivity can be observed at the prodromal stages of AD, which can lead to an increased power of slow and fast gamma oscillations (Hector & Brouillette, 2020). This increased gamma power was associated with cognitive performance or memory processing since neuronal hyperactivity perturbs hippocampal network function. Some studies have suggested that the increased gamma power during early stages of AD could be the result of compensatory mechanisms (Gaubert et al., 2019; Mondadori et al., 2006; Morrone et al., 2022). Moreover, a number of studies have reported conflicting observations regarding gamma oscillations. These divergent findings are thought to be caused by methodological differences (Byron et al., 2021; Nimmrich et al., 2015). In the current study we did not observe genotype effects in gamma oscillations at the pre-plaque stage in TgF344-AD rats.

5.5.3 Phase-amplitude coupling

Theta-gamma PAC can be found in different species including mice, rats, and humans. Research has shown that the theta-gamma PAC plays an important role in the execution of cognitive functions and might be a specific measure of working memory functioning in humans (Canolty & Knight, 2010; M. S. Goodman et al., 2018). The modulation of different gamma bands, namely slow gamma (30-60 Hz) and fast gamma (60-130 Hz) appears to be linked to different memory processes. Research has demonstrated that

the coupling between theta phase and slow gamma oscillations is increased after successful retrieval of memories in humans (Mormann et al., 2005) and rodents (Igarashi et al., 2014; Tamura et al., 2017; Tort et al., 2009). Synchronization of CA1 with the inputs from CA3 by the slow gamma suggest that the coupling between theta and slow gamma is dominantly involved by memory retrieval rather than memory encoding. The PAC between theta and high gamma (60-130 Hz) is thought to be important for sensory processing and memory encoding (Belluscio et al., 2012; Bieri et al., 2014; E. L. Newman et al., 2013). Electrophysiological experiments in the hippocampus of healthy rats, and in the non-epileptogenic hippocampus of patients have shown that the strength of the theta-gamma PAC will increase during learning (Kitchigina, 2018; Tort et al., 2009; Tort et al., 2008). It seems that the theta-gamma PAC strength is correlated directly with the increase in correctly performing a cognitive task and that the temporal coordination of neural spikes by theta-gamma PAC improves the transfer of information in the brain (Fell & Axmacher, 2011; Kitchigina, 2018; Tort et al., 2009). Moreover, increased PAC between low theta oscillations and both low and fast gamma oscillations in the HC during memory retrieval is also correlated with (memory) task performance (Vivekananda et al., 2021). Research also showed that in humans, fast and slow gamma oscillations are linked to different phases of the low theta oscillations which correspond with findings in animal studies (Colgin et al., 2009; Vivekananda et al., 2021). Thus, theta-gamma PAC might have an important role in memory processes in the HC.

Different preclinical and clinical studies in animal models for AD and in patients with AD have demonstrated decreased that a theta-gamma PAC can be observed (Bazzigaluppi et al., 2018; M. S. Goodman et al., 2018; Goutagny et al., 2013; Kitchigina, 2018), similar to the observations in the current study. Interestingly, impairment of theta-gamma PAC was observed before the onset of Aβ plaque formation in the APP23 mice and in (Aβ overexpressing) TgCRND8 mice (Goutagny et al., 2013; Kitchigina, 2018). Moreover, a study in TgF344-AD rats observed decreased cortical PAC in 9-month-old TgF344-AD rats, which coincided with cerebrovascular dysfunction and vascular remodelling, suggestive of a role for neurovascular dysfunction in PAC (Joo et al., 2017). The current study observed decreased PAC in fast gamma frequencies during wake immobility

(Figure 5-2), suggesting that sensory processing and memory retrieval might be impaired in TgF344-AD rats at the pre-plaque stage. In WT rats, an increased MI in slow gamma coupling was observed between trial 1 and trial 2, which was absent in TgF344-AD rats. Since slow gamma oscillations have been linked to memory retrieval, these results might suggest that the memory retrieval is impaired in TgF344-AD rats. However, future analyses which record hippocampal activity during cognitive tasks could give novel insights into alterations in memory retrieval and memory encoding during pre-plaque stages of AD. The disease mechanisms underlying alterations in PAC are still elusive, however, studies have observed that the changes in PAC coincided with interneuron dysfunction (Park et al., 2020; Stoiljkovic et al., 2015; Stoiljkovic et al., 2019) alterations in cholinergic signalling in the hippocampus (Stoiljkovic et al., 2015) and accumulation of pTau and (soluble) Aβ (Bazzigaluppi et al., 2018; Etter et al., 2019; Stoiljkovic et al., 2018).

5.5.4 Sharp wave-ripples

Memory consolidation is primarily associated with sleep while memory retrieval (or replay) is associated with waking behavior. Awake memory replay is mainly seen during brief periods of wake immobility, which will be enhanced during both novel and rewarding behaviours (Carr et al., 2011). SWR are irregularly occurring LFP patterns that are observed during immobility, slow wave sleep and consummatory behavior. SWR are the hallmark of memory replay and consolidation, as during SWR a large population of HC neurons is activated, often in sequences that recapitulate past or potential future experiences (Buzsaki, 2015; E. A. Jones, Gillespie, Yoon, Frank, & Huang, 2019). During exploration, the HC shows a high presence of theta oscillations (7-14 Hz) and during wake immobility theta oscillations will be replaced by SWR to process information obtained during exploration (Girardeau & Zugaro, 2011). This is also reflected in the results of the current study since the ripple ratio shows higher ripple occurrence during wake immobility compared to exploration.

We observed increased slow gamma power, SWR power and decreased duration of SWR in TgF344-AD rats at pre-plaque stage of AD. Similar decreases in the duration of SWR have been observed in several animal models for AD (Sanchez-Aguilera & Quintanilla, 2021; Zhen et al., 2021). Interestingly, an *in vitro* study on hippocampal slices of a mouse model of AD observed a similarly increased slow gamma power, SWR power and decreased duration, which was caused by dysfunction of parvalbumin positive interneurons (Caccavano et al., 2020). Research has shown that altered spike-timing and phase-locking of spiking during SWRs will interfere with the induction of synaptic plasticity (Cuestas Torres & Cardenas, 2020; Sadowski, Jones, & Mellor, 2016). Neuronal hyperactivity associated with early stages of AD, such as interneuron dysfunction as is observed in other animal models of AD, could interfere with the spike-locking during SWRs and therefore shorten the duration of the SWR (Caccavano et al., 2020; English et al., 2014; Fernandez-Ruiz et al., 2019). Input from the CA3 region is also an important modulator of SWR activity and gamma activity. *In vitro* studies have observed that SWRs and gamma oscillations can be directly modulated by modulating the activity of excitatory pyramidal neurons of the CA3 layer (Geschwill et al., 2020). In addition, the medial entorhinal cortex (mEnt) is the major input of somatosensory information to the hippocampus (Axmacher et al., 2008; Igarashi et al., 2014). Disruption of entorhinal signalling has been demonstrated to decrease SWR duration during wake immobility (Oliva et al., 2018; Yamamoto & Tonegawa, 2017). The mEnt is a region affected early by (soluble) Aβ pathology and *in vitro* electrophysiological studies in TgF344-AD rats at 6 months of age has demonstrated hyperexcitability in the synapses between the mEnt and dentate gyrus (Smith et al., 2022; Smith & McMahon, 2018). The altered SWR activity therefore might be the result of network disturbances caused by the mEnt, suggesting that entorhinal signalling might be altered already during the pre-plaque stage of AD in TgF344-AD rats.

The power of slow gamma oscillations increases throughout the whole hippocampus during SWR (25-55 Hz), which is thought to be associated with the quality of spatial memory replay (Carr et al., 2012; Gillespie et al., 2016; Oliva et al., 2018). Previous

studies have observed decreased slow gamma oscillations during SWR in several mouse models of AD (Gillespie et al., 2016; Iaccarino et al., 2018; Stoiljkovic et al., 2019). This decreased slow gamma power has been linked to Aβ induced interneuron dysfunction (Caccavano et al., 2020; Gillespie et al., 2016). However, these studies were performed at late stages of AD, when Aβ plaque pathology was extensive, which could explain the contradiction with the outcomes from the current study. A recent study observed increased gamma power in mild Aβ pathology, which declined as the disease progressed, suggesting an initial increase in gamma power during early stages of AD, similar to what is observed in the current study (Gaubert et al., 2019).

5.5.5 Limitations

The focus of this study was solely on alterations in the hippocampal oscillations. However, it is known that the hippocampus is part of a larger network and receives input from different brain regions like the cortex. Neurodegeneration due to AD doesn't only occur in the hippocampus, it is also found in the basal forebrain for example. Therefore, future research is needed which includes the hippocampal-cortical interactions during memory-demanding tasks. This brings us to another limitation of this study, the OFT is in general more used to study novelty-seeking behavior and is not a memory-demanding maze. Therefore, more research is needed in a more memory-demanding maze during the pre-plaque stage to obtain stronger results for learning impairment in the TgF344-AD rats. Electrophysiological acquisitions during more demanding memory tasks at pre-plaque stages in TgF344-AD rats could be valuable to link the observed alterations in PAC to cognitive impairments.

Electrophysiological measurements are prone to artifacts due to non-biological sources such as electrical interference, which could hamper the detection of SWR and the interpretation of the results (A. A. Liu et al., 2022). The current study was performed in freely moving animals in the absence of a faraday cage. However, the W2100 recording headstages are directly connected to the electrode and a small battery was placed on top of the wireless headstage as a power source, which minimizes noise and therefore, abolishes the need for extra shielding. However, also biological sources of noise such as

excessive movement and scarring of the brain tissue could interfere with the SWR analysis. Two TgF344-AD rats were excluded from the SWR analysis, since we could not detect robust ripples in these animals.

Due to limitations in the experimental setup, the sample size of this study is relatively small (5 animals per group), and it only included male animals. A substantial amount of research has demonstrated sex differences in AD severity and rate of progression, also in the TgF344-AD rats (Bazzigaluppi). Therefore, future studies should be done with larger sample sizes and a combination of male and female animals.

5.6 Conclusion

In the current study we aimed to investigate how hippocampal oscillations were altered during the pre-plaque stage of AD in TgF344-AD rats. We observed state dependent alterations in theta power and decreased theta-gamma modulation. Moreover, SWR characteristics were altered in TgF344-AD rats, with an increased power of the SWR and slow gamma oscillations, together with a decreased duration of SWR. These alterations in hippocampal activity coincided with increased anxiety-like behavior in TgF344-AD rats.

Future research would be valuable to correlate these alterations in hippocampal activity to cognitive deficits by performing electrophysiological experiments during more complex hippocampal-dependent behavioral tasks. Moreover, pharmacological manipulations could unravel pathological mechanisms behind the observed oscillatory alterations, which could be valuable targets for therapeutic treatment.

5.7 Supplementary information

5.7.1 Supplementary Tables

Supplementary table 1: Results of the linear mixed model (LMM) for the power spectral density of different frequency bands

	Delta			*Theta low*			*Theta high*			*Slow gamma*			*Fast gamma*			*HFO*		
	DF	*F-value*	*p*	*DF*	*F-value*	*p*	*DF*	*F-value*	*p*	*DF*	*F-value*	*p*	*DF*	*F-value*	*p*	DF	F-value	p
Genotype	1,8	2.2555	0.1714	1,8	0.1898	0.6745	1,7.3	5.6648	0.0474	1,8	2.2608	0.1711	1,8	0.7627	0.4078	1,7.9	0.0651	0.8051
Trial	1,20.3	0.4927	0.4907	1,22.3	0.0022	0.9632	1,22.7	0.2756	0.6047	1,24	1.1315	0.298	1,22.2	1.1971	0.2856	1,21.9	1.2224	0.2809
State	1,21.0	5.5623	0.0281	1,22.5	10.649	0.0035	1,22.7	5.5354	0.0277	1,24	15.9465	0.0005	1,22	7.4662	0.0121	1,22.2	1.8178	0.1912
*Tr*Gt*	1,20.3	0.0002	0.9884	1,22.3	1.0658	0.313	1,22.7	1.4248	0.2449	1,24	0.2427	0.6267	1,22.2	0.3244	0.5747	1,21.9	6.3981	0.0191
*St*Gt*	1,21.0	2.144	0.158	1,22.5	0.3058	0.5857	1,22.7	1.884	0.1833	1,24	8.0755	0.009	1,22	9.9745	0.0046	1,22.2	0.4426	0.5128
*St*Tr*	1,20.3	0.0004	0.9852	1,22.5	1.1437	0.2962	1,22.7	1.4127	0.2469	1,24	2.0051	0.1696	1,22	4.8906	0.0377	1,21.9	1.5246	0.23
*St*Tr*Gt*	1,20.3	0.038	0.8474	1,22.5	0.0262	0.8729	1,22.7	0.5847	0.4523	1,24	0.6061	0.4439	1,22	0.0334	0.8566	1,21.9	0.8637	0.3628

Statistical results accompanying figure 5-1. DF = degrees of freedom

Supplementary table 2: post-hoc analysis of the power of gamma oscillations

	Slow gamma				*Fast gamma*			
	q-values	*Difference*	*Lower 95%*	*Upper 95%*	*q-values*	*Difference*	*Lower 95%*	*Upper 95%*
WT E – WT QW	0.4235	-0.00088	-0.0031	0.001346	0.8272	0.000045	-0.00026	0.000348
WT E – TG E	0.4235	-0.00356	-0.0124	0.005279	0.8272	-0.00012	-0.00133	0.001092
WT QW – TG QW	0.148	-0.00789	-0.01673	0.000949	0.3449	-0.00079	-0.002	0.000419
TG E – TG QW	<0.0001	-0.00521	-0.00743	-0.00298	0.0021	-0.00063	-0.00095	-0.00031

Statistical results accompanying figure 5-1. FDR corrected p-values (q-value), difference of means and boundaries of the confidence interval of the post hoc tests.

Supplementary table 3: post-hoc analysis of the power of HFO

	q-values	*Difference*	*Lower 95%*	*Upper 95%*
WT trial 1 – WT trial 2	0.0587	-0.00013	-0.00022	-2.7E-05
WT trial 1 – TG trial 1	0.5751	-0.00013	-0.00047	0.000219
WT trial 2 – TG trial 2	0.7506	0.00005	-0.00029	0.000393
TG trial 1 – TG trial 2	0.5751	0.000049	-5.5E-05	0.000153

Statistical results accompanying figure 5-1. FDR corrected p-values (q-value), difference of means and boundaries of the confidence interval of the post hoc tests.

Supplementary table 4: Results of LMM of the PAC for each behavioral state

	Exploration 35-45 Hz			*Exploration 55-90 Hz*			*Wake immobility 60-90 Hz*		
	DF	*F-value*	*p*	*DF*	*F-value*	*p*	*DF*	*F-value*	*p*
Gt	1,8.1	0,4303	0,53	1,8.0	0,9149	0,3659	1,5.6	8,5846	0,0284
Trial	1,7.2	42,4208	0,0003	1,8.2	0,0269	0,8737	1,7.2	0,5439	0,484
*Tr*Gt*	1,7.2	9,2711	0,0181	1,7.4	1,5251	0,2547	1,6.1	5,4318	0,0579

Statistical results accompanying figure 5-2. Gt = Genotype, DF = degrees of freedom

Supplementary table 5: post-hoc analysis of the PAC during exploration (35-45 Hz).

	q-values	*Difference*	*Lower 95%*	*Upper 95%*
WT trial 1 – WT trial 2	0.0009	-0.003981	-0.00537	-0.0026
WT trial 1 – TG trial 1	0.05743	-0.00166	-0.00323	-8.9E-05
WT trial 2 – TG trial 2	0.2497	0.000877	-0.00069	0.002448
TG trial 1 – TG trial 2	0.05743	-0.001445	-0.00283	-5.9E-05

Statistical results accompanying figure 5-2. FDR corrected p-values (q-value), difference of means and boundaries of the confidence interval of the post hoc tests.

Supplementary table 6: Results of the LMM for the Sharp wave ripples per trial.

	PSF SWR			*PSF SG*			*Power SWR*			*Power SG*			*Duration*		
	DF	*F-value*	*p*	*DF*	*F-value*	*p*	*DF*	*F-value*	*p*	*DF*	*F-value*	*p*	*DF*	*F-value*	*p*
Genotype	1,8.2	1.5917	0.2419	1,7.9	1.8032	0.2168	1,7.7	23.9689	0.0013	1,7.8	8.9812	0.0177	1,8.6	0.7627	0.1497
Trial	1,22.5	0.1071	0.7465	1,21.4	5.0894	0.0346	1,7.4	0.0001	0.9914	1,6.3	14.3034	0.0082	1,23.5	1.1971	0.8577
State	1,22.6	122.404	0.002	1,21.4	0.7252	0.4039	1,15	3.3151	0.0887	1,14.1	6.5201	0.0229	1,23.5	7.4662	0.4577
*Tr*Gt*	1,22.7	0.6375	0.433	1,21.4	2.8935	0.1034	1,7.4	0.976	0.3546	1,6.3	0.5822	0.4729	1,23.5	0.3244	0.1275
*St*Gt*	1,22.8	0.6335	0.4344	1,21.4	1.2239	0.2809	1,15	0.1357	0.7177	1,14.1	6.6565	0.0217	1,23.5	9.9745	0.1602
*St*Tr*	1,22.9	2.2521	0.1474	1,21.3	0.0557	0.8158	1,15	0.2619	0.6162	1,14.1	1.1115	0.3095	1,23.5	4.8906	0.8599
*St*Tr*Gt*	1,22.10	3.4823	0.0751	1,21.3	0.0305	0.8631	1,15	0.0774	0.7847	1,14.1	4.7884	0.046	1,23.5	0.0334	0.0286

Statistical results accompanying figure 5-3. DF = degrees of freedom

Supplementary table 7: Results of the LMM for the Sharp wave ripples occurrence rate per trial.

	SWR ratio E/WI		
	DF	*F-value*	*p*
Genotype	1,7.0	0.1823	0.6822
Trial	1,7.0	6.8833	0.0342
*Tr*Gt*	1,7.0	2.3741	0.1673

Statistical results accompanying figure 5-3. DF = degrees of freedom

Supplementary table 8: post-hoc analysis duration SWR

	q-values	*Difference*	*Lower 95%*	*Upper 95%*
WT-E trial 1 – WT-WI trial 1	0.8758	0.7497	-9.0676	10.5669
TG-E trial 1 – TG-WI trial 1	0.9730	-3.5788	-14.0265	6.869
WT-E trial 2 – WT-WI trial 2	0.1884	-11.5697	-22.0174	-1.1219
TG-E trial 2 – TG-WI trial 2	0.3703	6.99	-2.8272	16.8072
WT-E trial 1 – TG-E trial 1	0.9957	2.0681	-7.553	11.6893
WT-WI trial 1 – TG-WI trial 1	1	-2.2603	-12.5375	8.0169
WT-E trial 2 – TG-E trial 2	0.8018	-1.625	-11.2461	7.9962
WT-WI trial 2 – TG-WI trial 2	0.0252	16.9347	6.6575	27.2119
WT-E trial 1 – WT-E trial 2	0.8421	1.8396	-7.9776	11.6568
TG-E trial 1 – TG-E trial 2	0.9328	-1.8535	-11.6707	7.9637
WT-WI trial 1 – WT-WI trial 2	0.1976	-10.4797	-20.9275	-0.032
TG-WI trial 1 – TG-WI trial 2	0.2940	8.7153	-1.7325	19.163

Statistical results accompanying figure 5-3. FDR corrected p-values (q-value), difference of means and boundaries of the confidence interval of the post hoc tests.

Supplementary table 9: post-hoc analysis slow gamma power during SWR

	q-values	*Difference*	*Lower 95%*	*Upper 95%*
WT-E trial 1 – WT-WI trial 1	0.1617	-0.01583	-0.03564	0.003981
TG-E trial 1 – TG-WI trial 1	0.1024	-0.01969	-0.0395	0.000124
WT-E trial 2 – WT-WI trial 2	0.1772	0.016093	-0.00545	0.037636
TG-E trial 2 – TG-WI trial 2	0.0496	-0.03085	-0.05397	-0.00774
WT-E trial 1 – TG-E trial 1	0.1107	-0.01674	-0.03458	0.001094
WT-WI trial 1 – TG-WI trial 1	0.0762	-0.0206	-0.03844	-0.00276
WT-E trial 2 – TG-E trial 2	0.4047	0.00884	-0.01112	0.028796
WT-WI trial 2 – TG-WI trial 2	0.0096	-0.03811	-0.0588	-0.01741
WT-E trial 1 – WT-E trial 2	0.3346	-0.00797	-0.02298	0.007043
TG-E trial 1 – TG-E trial 2	0.1181	0.017616	0.000065	0.035167
WT-WI trial 1 – WT-WI trial 2	0.0488	0.023955	0.006445	0.041466
TG-WI trial 1 – TG-WI trial 2	0.4093	0.006452	-0.0096	0.022503

Statistical results accompanying figure 5-3. FDR corrected p-values (q-value), difference of means and boundaries of the confidence interval of the post hoc tests.

Supplementary table 10: Results of LMM for the behavior during the open field test per trial

	Total distance travelled			*Distance travelled inner area*			*Time spent inner area*			*# Entries inner area*		
	DF	*F-value*	*p*	*DF*	*F-value*	*p*	*DF*	*F-value*	*p*	*DF*	*F-value*	*p*
Genotype	1,8.1	0.0647	0.8055	1,8.5	4.9829	0.0542	1,8.4	9.047	0.0187	1,8.0	1.7344	0.2243
Trial	1,9.2	24.295	0.0008	1,8.8	37.0639	0.0002	1,9.1	30.868	0.0007	1,9.0	19.3489	0.0017
*Tr*Gt*	1,8.3	0.2119	0.6572	1,7.8	0.7627	0.4086	1,8.3	4.2217	0.0729	1,8.0	0.0961	0.7645

Statistical results accompanying figure 5-4. DF = degrees of freedom

Supplementary table 11: Results of LMM for the behavior during the OFT across epochs during trial 1

	Total distance travelled			*Distance travelled inner area*			*Time spent inner area*			*# Entries inner area*		
	DF	*F-value*	*p*	*DF*	*F-value*	*p*	*DF*	*F-value*	*p*	*DF*	*F-value*	*p*
Genotype	1,1	0.1308	0.7251	1,10.2	2.2608	0.1629	1,9.6	37.0991	0.0001	1,9.8	1.0292	0.3348
Epoch	11,111.50	40.7545	0.0001	11,96.4	27.2407	0.0001	11,97.2	20.3168	0.0001	11,108.50	28.9335	0.0001
*Ep*Gt*	11,100.50	1.8695	0.0523	11,96.4	2.8359	0.003	11,97.2	6.1843	0.0001	11,97.5	0.5487	0.8651

Statistical results accompanying figure 5-5 & figure 5-6. DF = degrees of freedom

Supplementary table 12: post-hoc analysis for the time spent in the inner area during the OFT across epochs during trial 1

Genotype-Epoch	*q-values*	*Difference*	*Lower 95%*	*Upper 95%*
WT1 - TG1	0.0012	10.3657	5.2502	15.4812
WT2 - TG2	0.0006	21.237	15.5842	26.8899
WT3 - TG3	0.0087	8.1463	2.8513	13.4413
WT4- TG4	0.3485	3.6553	-2.0057	9.3163
WT5 - TG5	0.2932	-4.0457	-9.5315	1.4401
WT6 - TG6	0.0729	5.863	0.568	11.1579
WT7 - TG7	0.0024	9.4627	4.1685	14.757
WT8 - TG8	1	-0.0394	-5.6929	5.6141
WT9 - TG9	1	-0.1963	-5.8491	5.4565
WT10 - TG10	1	0.0161	-5.2782	5.3103
WT11- TG11	1	0.0161	-5.2782	5.3103
WT12 - TG12	0.9981	0.0063	-5.2887	5.3013

Statistical results accompanying figure 5-5. FDR corrected p-values (q-value), difference of means and boundaries of the confidence interval of the post hoc tests.

Supplementary table 13: post-hoc analysis for the distance travelled in the inner area during the OFT across epochs during trial 1

Genotype-Epoch	*q-values*	*Difference*	*Lower 95%*	*Upper 95%*
WT1 - TG1	0.5328	0.4854	-0.075	1.0458
WT2 - TG2	0.0012	1.5116	0.93259	2.09061
WT3 - TG3	0.9705	0.01117	-0.58698	0.60931
WT4- TG4	1	-0.1909	-0.78905	0.40724
WT5 - TG5	1	-0.18973	-0.80565	0.42619
WT6 - TG6	0.5252	0.4438	-0.13495	1.02254
WT7 - TG7	1	0.20385	-0.41207	0.81978
WT8 - TG8	1	-0.01423	-0.62991	0.60144
WT9 - TG9	1	0.01377	-0.60215	0.62969
WT10 - TG10	1	-0.0114	-0.59041	0.56761
WT11- TG11	1	-0.0114	-0.59041	0.56761
WT12 - TG12	1	-0.02307	-0.60182	0.55568

Statistical results accompanying figure 5-6A. FDR corrected p-values (q-value), difference of means and boundaries of the confidence interval of the post hoc tests.

Supplementary table 14: Results of LMM for the behavior during the OFT across epochs during trial 2

	Total distance travelled			*Distance travelled inner area*			*Time spent inner area*			*# Entries inner area*		
	DF	*F-value*	*p*	*DF*	*F-value*	*p*	*DF*	*F-value*	*p*	*DF*	*F-value*	*p*
Genotype	1,10.1	4.61	0.057	1,9.7	2.2094	0.169	1,9.2	1.445	0.2593	1,9.3	6.9639	0.0263
Epoch	3,32.5	41.9369	0.0001	3,27.7	13.1929	0.0001	3,25.9	7.4003	0.001	3,28.9	7.5719	0.0007
*Ep*Gt*	3,29.4	1.0286	0.3942	3,27.8	1.1961	0.3295	3,25.9	1.7281	0.1859	3,25.3	2.9193	0.0535

Statistical results accompanying figure 5-6. DF = degrees of freedom

6. Effects of circuit specific basal forebrain cholinergic activation on whole-brain functional connectivity

This chapter is based on:

Peeters, L. M., M. van den Berg, R. Hinz, G. Majumdar, I. Pintelon and G. A. Keliris (2020). "Cholinergic Modulation of the Default Mode Like Network in Rats." iScience **23**(9): 101455.

6.1 Abstract

The discovery of the default mode network (DMN), a large-scale brain network which is suppressed during attention demanding tasks, had major impact in neuroscience. This network exhibits an antagonistic relationship with attention related networks. A better understanding of the processes underlying modulation of DMN is imperative, as this network is compromised in several neurological diseases. Cholinergic neuromodulation is one of the major regulatory networks for attention and studies suggest a role in regulation of the DMN. In this study, we unilaterally activated the right basal forebrain cholinergic neurons and observed decreased right intra-hemispheric and interhemispheric FC in the default mode like network (DMLN). Our findings provide critical insights into the interplay between cholinergic neuromodulation and DMLN, demonstrate that differential effects can be exerted between the two hemispheres by unilateral stimulation, and open windows for further studies involving directed modulations of DMN in treatments for diseases demonstrating compromised DMN activity.

6.2 Introduction

An important finding in neuroscience during the last couple of decades was the discovery of the default mode network (DMN), which is a large-scale network of brain areas that are co-activated during passive mental processes and suppressed during externally oriented attention demanding cognitive tasks. This was initially observed by Shulman et al. (1997) in a meta-analysis of nine Positron Emission Tomography (PET) studies. In that study, the authors showed that several brain areas, including the medial prefrontal cortex, posterior cingulate cortex, lateral parietal and temporal cortices, consistently increased their metabolic activity during states of rest or wake immobility (Shulman et al., 1997). Functional imaging studies, which followed, reported that the low frequency activity fluctuations of these areas were highly temporally correlated, forming a set of intrinsically functionally connected brain areas currently known as the default mode network (DMN) (Greicius et al., 2003; Raichle et al., 2001; Raichle & Snyder, 2007). The DMN has been associated with spontaneous internally directed cognitive processes such as mind wandering, self-oriented processes and introspection (Andrews-Hanna, Reidler, Huang, & Buckner, 2010; Buckner & Carroll, 2007). Disruption of DMN functioning has been linked to several neurological disorders including attention deficit hyperactivity disorder (Tian et al., 2006), mood disorders (Greicius et al., 2007), epilepsy (Laufs et al., 2007), Alzheimer's disease (Greicius, Srivastava, Reiss, & Menon, 2004) and others (Broyd et al., 2009). Upon the discovery of the DMN in humans, a default mode like network (DMLN) has been observed in several other mammalian species, such as the macaque monkey (Vincent et al., 2007), rat (Lu et al., 2012) and mouse (Stafford et al., 2014). In rodents, DMLN consists of the following brain regions: orbital cortex, prelimbic cortex, cingulate cortex, auditory/temporal association cortex, posterior parietal cortex, retrosplenial cortex and hippocampus (Lu et al., 2012; Stafford et al., 2014). Multiple studies observed shared features of the DMN in humans and the DMLN in rodents, i.e. its anatomical homology (Lu et al., 2012), its link with brain disorders (Anckaerts et al., 2019; Sforazzini et al., 2016; Shah et al., 2016), its decreased activity during tasks in comparison to rest (Hinz et al., 2019; Rohleder et al., 2016) and

its anti-correlation with task positive networks (Belloy, Naeyaert, et al., 2018; Schwarz et al., 2013).

The DMN has also been described as a "task-negative network" which exhibits anti-correlations with "task-positive networks" (Belloy, Naeyaert, et al., 2018; Fox et al., 2005; Greicius et al., 2003). The antagonistic interaction between the DMN and top-down attentional processes has been observed repeatedly in humans (Buckner & DiNicola, 2019), however, the underlying mechanisms remain poorly understood. A number of previous studies have shown that the extent and the magnitude of the task-induced decreases in BOLD responses within the DMN vary with the difficulty of the cognitive tasks and that task performance is positively correlated with the strength of the DMN suppression (Mayer et al., 2010; Ossandon et al., 2011; Rajan et al., 2019; Singh & Fawcett, 2008; Wen, Liu, Yao, & Ding, 2013). Another important feature of the DMN, demonstrated by several human studies, is decreased functional connectivity (FC) within the network during the performance of cognitive tasks (Fransson, 2006; W. Gao, Gilmore, Alcauter, & Lin, 2013). Interestingly, a recent study in humans demonstrated that the presentation of random flashing checkerboard visual stimuli can induce negative BOLD responses in DMN brain regions (Razlighi, 2018). Similarly, our group evaluated the BOLD responses in the DMLN regions upon the presentation of continuous flickering visual stimuli in sedated rats. We demonstrated that this visual stimulation paradigm could deactivate nodes of the DMLN and decrease the FC assimilating earlier studies in humans (Hinz et al., 2019).

Recent studies have demonstrated that the basal forebrain (BFB) is a key-player in modulating oscillations in the prefrontal cortex during behaviors aligned with DMN activation and de-activation patterns - such as moving from the home cage to an experimental arena where exploration of the environment is enhanced - and suggested these findings are consistent with BFB exerting control of large-scale functional networks such as the DMN (Nair et al., 2018). This hypothesis is also consistent with evidence that cholinergic neurons originating from the BFB are strongly involved in

attentional processes, specifically the projections from the diagonal band of Broca, substantia innominata and the nucleus Basalis of Meynert (NBM) to the cortex (Ballinger, Ananth, Talmage, & Role, 2016; Bloem, Schoppink, et al., 2014; Howe et al., 2017; Parikh, Kozak, Martinez, & Sarter, 2007). These projections induce acute increases of acetylcholine (ACh) in the medial prefrontal cortex which mediate cue detection and are necessary for successful task performance (Gritton et al., 2016; Howe et al., 2017; Parikh et al., 2007). Moreover, ACh enhances visual processing by inducing cortical decorrelation and desynchronization in sensory cortices, which increases the signal to noise ratio (N. Chen, Sugihara, & Sur, 2015; Nguyen, Huppe-Gourgues, & Vaucher, 2015; Pinto et al., 2013). In addition, the BFB has been implicated in cortical network switching between brain states by exerting direct and/or indirect control to the prefrontal cortex (Espinosa, Alonso, Morales, et al., 2019; W. Li et al., 2015).

This evidence suggested an involvement of the BFB cholinergic system in the up- and down-regulation of the DMN and its anti-correlation with task based/attention related networks. Thus, we hypothesized that specific stimulation of cholinergic neurons in the BFB can influence the functional connectivity (FC) in the DMLN of rats as measured with whole-brain measures of activity and connectivity such as resting-state (rs)fMRI, which can directly visualize the complete DMN and task-based networks. Further, inspired by a recent study in rhesus macaques that demonstrated unilateral suppression of cortical fluctuations ipsilateral to pharmacological inactivation in the NBM (Turchi et al., 2018), we hypothesized that unilateral activations of cholinergic neurons in homologous areas in the rat could potentially lead to asymmetric changes to the DMLN that could be beneficial in the treatment of certain neurological syndromes that are thought to stem from hemispheric imbalances in attentional processes such as hemi spatial neglect (Bartolomeo, Thiebaut de Schotten, & Chica, 2012). To this end, we combined functional MRI with designer receptors exclusively activated by designer drugs (DREADDs) to selectively increase the neuronal firing in basal forebrain (BFB) cholinergic neurons and study their effects in whole brain networks with a particular focus on the DMLN. We found that unilateral cholinergic activation in the right BFB resulted in decreased FC in

the DMLN and the effect showed significant laterality in specific connections in the DMLN and task-based networks. The results of this study directly demonstrate the effects of cholinergic neuromodulation in the DMLN in rats and open windows for further studies that could use directed modulations of DMLN in rehabilitation treatments for diseases demonstrating compromised DMN activity.

6.3 Materials and Methods

6.3.1 Animals and ethical statement

In this study, 28 adult ChAT-Cre Long Evans rats were used, of which 14 males and 14 females. Animals were group housed with a 12h light/dark cycle and with controlled temperature (20 – 24°C) and humidity (40%) conditions. Standard food and water were provided ad libitum. All procedures were in accordance with the guidelines approved by the European Ethics Committee (decree 2010/63/EU) and were approved by the Committee on Animal Care and Use at the University of Antwerp, Belgium (approval number: 2015-50).

6.3.2 Intracerebral viral vector injections

The rats were divided in a control group (N = 12) and an experimental group (N = 16) with DREADDs expression. All rats were subjected to a stereotactic surgery targeting the medial nuclei of the right BFB, i.e., the horizontal diagonal band of Broca, nucleus basalis of Meynert and the substantia innominata (AP = -0.5 mm, ML = +2.5mm, DV= -7.5mm from bregma). The stereotactic surgery was performed as follows: rats were anesthetized using 5% isoflurane for induction and 2% for maintenance (Isoflo®, Abbott Laboratories, Ltd., USA) and received a subcutaneous injection of xylocaine (Lidocaine hydrochloride, Astra Zeneca) for local analgesia. The rats received a unilateral injection with a Cre-dependent AAV-virus: AAV8-hSyn-DIO-hM3Dq(Gq)-mCherry (4.8 x 10^{12} GC/mL) for the experimental group and AAV8-hSyn-DIO-mCherry (4.1 x 10^{12} GC/mL) for the control group. Chat-cre transgenic rats were used to specifically express the

DREADDs receptors in all cholinergic neurons in the right BFB. A glass pipette filled with 2.5 µL of the viral vectors was used to inject 2 µL in the brain region of interest at a rate of 46 nL/min using a nano-injector (Nanoject II, Drummond Scientific). At ten minutes after the viral vector injection, the glass pipet was removed from the brain tissue. All MRI procedures started at least two months after viral vector injection to allow full recovery and optimal expression levels of the DREADDs receptors (Urban et al., 2016).

6.3.3 *In vivo* MRI procedures

At the start of the MRI scanning procedures, the rats were anesthetized using isoflurane (5% for induction and 2% for handling procedures). After fixation of the animal in the scanner, the isoflurane was gradually lowered to 0.4 % and an intravenous bolus injection of medetomidine (0.05 mg/kg, Domitor®, Pfizer, Germany) was administered. At 15 minutes after the bolus, the intravenous infusion of medetomidine (0.1 mg/kg/hr) was started. All scans were acquired using a 9.4T Biospec MRI system (Bruker BioSpin, Germany) with Paravision 6 software. Throughout the acquisition of the MRI scans, the physiology of the animals was closely monitored. A pressure-sensitive pad (sampling rate 225 Hz; MR-compatible Small Animal Monitoring and Gating system, SA Instruments, Inc., USA) was used to record the breathing rate and the body temperature of the animal was maintained at (37 ± 0.5) °C using a feedback controlled warm air circuitry (MR-compatible Small Animal Heating System, SA Instruments, Inc., USA). Additionally, a pulse oximeter was used to monitor the blood oxygenation (MR-compatible Small Animal Monitoring and Gating System, SA Instruments, Inc., USA). After the acquisition of all MRI scans, an injection of 0.1 mg/kg atipamezole (Antisedan®, Pfizer, Germany) was administered to counteract the effects of the medetomidine anaesthesia.

6.3.4 MRI scans acquisition

First, three anatomical multi-slice T2 Turbo-RARE scans (echo time (TE): 11 ms, repetition time (TR): 2500 ms, field of view (FOV): (30 x 30) mm2, matrix [256 x 256], 16

slices of 0.8 mm) were acquired to allow flat skull positioning of the coronal slices. Then, a fourth scan was acquired with the above sequence that served as an anatomical reference scan. Magnetic field inhomogeneity was corrected by local shimming in an ellipsoid volume of interest within the brain. Resting state functional MRI (rsfMRI) scans were acquired with geometrical parameters identical to the anatomical reference scan. The rsfMRI scans started at 35 minutes after the medetomidine bolus injection and were acquired using a T2* weighted echo planar imaging (EPI) sequence (TE: 18 ms, TR: 2000ms, FOV: (30 x 30) mm2, matrix [128 x 96], 16 slices of 0.8 mm). First, a 5-minute baseline rsfMRI was acquired. Second, a 20-minute rsfMRI scan was acquired during which the CNO (1mg/kg bodyweight) or vehicle (i.e., saline) was intravenously administered at 5 minutes after the start of the scan. Then, a final 5-minute rsfMRI scan was acquired. These three scans were acquired during one scan session (Figure 6-2A). Two scan sessions were acquired for each animal in the DREADDs-expressing group, during which the effect of either CNO or vehicle was evaluated. One scan session was acquired for each animal in the control group to evaluate the off-target effects of CNO.

6.3.5 MRI data pre-processing

The pre-processing of the rsfMRI data was performed using Matlab R2014a and SPM12 software (Statistical Parametric Mapping, http://www.fil.ion.ucl.ac.uk). First, all images within each session were realigned to the first image. Second, images were normalized to a study-specific mean EPI template using a global 12 parameter affine transformation followed by the estimation of the non-linear deformations. Then, a mask excluding the ventricles and all voxels outside the brain was applied to the images. The head motion estimation parameters were regressed out and the images were smoothed in an isotropic manner, with a Gaussian kernel with full width at half maximum of twice the voxel size (0.624 x 0.624 mm). Afterwards, all images were band pass filtered between 0.01 and 0.2 Hz (Zerbi, Grandjean, Rudin, & Wenderoth, 2015).

6.3.6 MRI data analysis

6.3.6.1 ROI-based analysis

Regions of interest (ROIs) were drawn in brain areas that have been reported to be part of the DMLN in rats, including the cingulate cortex (Cg), orbitofrontal cortex (ORB), prelimbic cortex (PrL), retrosplenial cortex (RSC), parietal association cortex (PtPD) and temporal association cortex (TEA) (Lu et al., 2012; Stafford et al., 2014). In addition, ROIs were drawn in regions belonging to the TPN, namely the primary somatosensory cortex (S1), secondary somatosensory cortex (S2), primary motor cortex (M1), secondary motor cortex (M2) and insula (Ins). Separate ROIs for each hemisphere were used in order to be able to discriminate ipsilateral and contralateral effects of right BFB stimulation. The time series of the ROIs, consisting of 4 voxels, were extracted and Pearson correlation coefficients were calculated between each pair of ROIs. Then, these correlation coefficients were Fisher's z-transformed using an in-house program in Matlab. Mean z-transformed matrices were obtained from the DREADDs expressing group after injection of CNO and vehicle as well as from the sham group after injection of CNO. These z-transformed matrices were used to calculate connectivity laterality indices (CLI) for each pair of ROIs as described in (Di, Kim, Chen, & Biswal, 2014).

6.3.6.2 Seed-based analysis

Seed-based analyses were performed in order to assess alterations in whole-brain FC of brain regions that are part of the DMLN. Mean BOLD signal time series were extracted from seed regions using the REST 1.8 toolbox in Matlab. Consequently, the obtained time series was used in a general linear model analysis to compare it to the time series of all other voxels in the brain. Resulting FC maps represent voxels in the brain that significantly correlate to the temporal signal of the seed region. Mean group FC maps were created for each seed region and these maps were also used to make masks including all significant clusters (family-wise correction (FWE) corrected, $p \leq 0.05$, minimal cluster size = 10 voxels). The union of the masks after CNO and vehicle injection in the DREADDs-expressing group was used to extract mean T-values from each animal.

6.3.6.3 Fractional Amplitude of low frequency fluctuations

The fractional amplitude of low frequency fluctuations (fALFF) has previously been used to reflect spontaneous resting state neural activity (Zou et al., 2008). In this study, we obtained fALFF values using the REST 1.8 Toolbox in order to assess resting state neural activity alterations in the DMLN. The time series of each voxel within a seed-based mask was band-pass filtered between 0.01-0.2Hz and these filtered time series were transformed to a frequency domain using a fast Fourier transformation. Then, the obtained power spectrum was used to calculate the fALFF values which can be defined as the ratio of the power within a frequency range (here 0.01 – 0.2Hz) and the total power of the whole frequency range. The mean fALFF values were compared between the CNO and vehicle injection in the DREADDs-expressing group.

Statistics

A linear mixed model analysis in JMP Pro13 software was performed to evaluate the effect of administration of CNO or vehicle on FC in the DMLN over time in the DREADDs expressing group and the sham group. In this analysis, the FC in the DMLN of the right hemisphere was compared between the baseline scan and at 5-10 minutes, 10-15 minutes, and 15-20 minutes after administration of CNO or vehicle. The subject ID was added in the model as a random variable. Student's T corrections were applied for all multiple comparisons. Further, the FC between ROI pairs in the DMLN and TPN was compared between CNO and vehicle administration in the DREADDs expressing group at 15-20 minutes after injection. A repeated measures Two-way ANOVA with Sidak's multiple comparisons correction was used to evaluate each ROI pair separately. A paired Student's T-test was used to compare the average intra- and inter-hemispheric DMLN FC, the average whole brain FC of seed regions, as well as the fALFF values and CLI after CNO injection or vehicle injection in the DREADDs-expressing animals. An unpaired Student's T-test was used to evaluate intra- and inter-hemispheric DMLN FC alteration between both control groups and between the DREADDs-expressing group and sham group. One-sample Student's T-test were used to make mean seed-based FC maps.

6.3.7 Immunohistochemistry

6.3.7.1 Immunofluorescent staining

After the acquisition of all *in vivo* MRI scans, brain samples were collected from 8 rats to evaluate the expression of the DREADDs. Rats were deeply anesthetized using an intravenous injection with pentobarbital (Dolethal®, Vetoquinol, Belgium). Then, cardiac perfusion was performed, first with an ice-cold PBS solution and afterwards with a 4% paraformaldehyde solution (Merck Millipore, Merck KGaA, Darmstadt, Germany) for fixation of the tissues. Brains were surgically removed and post-fixed in 4% paraformaldehyde solution after which a sucrose gradient (5%, 10% and 20% sucrose) was applied. Brains were snap frozen in liquid nitrogen and stored at -80 °C until further processing. Brains were cut into 12 µm sections using a cryostat (Cryostar NX 70, Thermo Fisher Scientific). For the immunofluorescence stainings, the following primary antibodies were used: Sheep Anti-Choline Acetyltransferase (1:500, Abcam; ab18736) and rabbit Anti-m-cherry (1:500, Abcam; ab167453), as well as the following secondary antibodies: Donkey Anti-Sheep (1:200, Abcam; ab150177) and 1:200 Goat Anti-Rabbit (1:200, Abcam; ab7088). Nuclei were counterstained using DAPI (P369350, Thermofischer Scientific). Stained sections were mounted using Prolonged Gold Antifade.

6.3.7.2 Image acquisition

The overview images were collected from two animals with a CFI Plan Fluo 10X/0.3 objective on an automated Nikon Ti-E inverted microscope (Nikon Instruments Europe, Amsterdam, The Netherlands) equipped with a SPECTRA light engine® solid-state light source (Lumencor, Beaverton, USA) and a Nikon DS-Qi2 digital camera. Nikon NIS-elements software was used to control the image acquisition and stitching. The representative confocal images of 3 animals were taken with a Leica TCS SP8 confocal laser scanning microscope (Leica-microsystems, Wetzlar, Germany). Blue fluorescence was obtained with 405 nm diode laser and PMT detector. A white light laser (excitation wavelength of 488 nm for green fluorescence (Alexa Fluor®488) and 596 nm for red fluorescence (Texas Red®)) and a HyD detector were used to visualize green and red

fluorophores. Z-stacks were acquired with a 0.5 µm interval (HC PL APO CS2 63X/1.20 water). Images were acquired with a resolution of [1024 x 1024] pixels.

6.4 Results

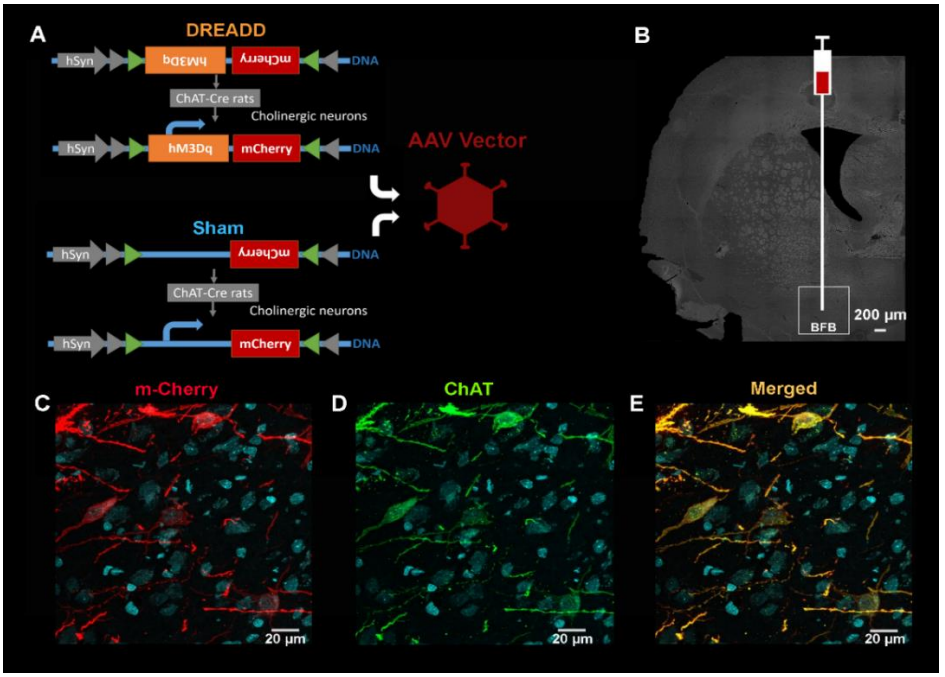

Figure 6-1: Expression of DREADDs in basal forebrain cholinergic neurons. (A, B) Viral vectors containing inverted DNA constructs encoding the DREADDs receptors were injected in the right basal forebrain (BFB) of the experimental group during a stereotactic surgery. Viral vectors with an empty DNA construct were injected in the right BFB of sham treated animals. ChAT-cre transgenic rats were used in both groups. Cre recombinase, only present in cholinergic neurons, is necessary for transcription of the genes, resulting in cell-type specific expression. (C, D, E) Immunohistochemistry was performed on eight animals to check the expression of the DREADDs. Representative maximum intensity projections are shown in which the expression of mCherry is represented in red and cell nuclei in blue. (C) mCherry expression is observed in the cell body and axons of the neurons. (D) ChAT, an enzyme present in cholinergic neurons, is presented in green. (E) Co-localization of mCherry and ChAT in yellow (red + green). Virtually all cholinergic neurons in the target region were transfected and no mCherry was observed in structures other than cholinergic neurons.

6.4.1 DREADDs expression co-localizes with cholinergic neurons in the right basal forebrain

Chemogenetic tools, such as DREADDs, allow to control the activity of selectively targeted neuronal populations (Alexander et al., 2009). In our study, excitatory DREADDs were used to increase the activity of cholinergic neurons in the right BFB. To ensure exclusive DREADDs expression in the cholinergic neurons of the right BFB, we used ChAT-Cre transgenic rats that selectively express Cre-recombinase in all choline acetyltransferase (ChAT) expressing neurons, i.e., cholinergic neurons (Witten et al., 2011). The presence of Cre-recombinase allows the conversion of the inverted DNA constructs, so that gene transcription can take place. Viral vectors containing inverted DNA constructs encoding DREADDs were stereotactically injected in the right BFB (Figure 6-1). Since cholinergic neurons in the anterior medial portion of the BFB have been shown to project to medial and frontal cortex and have been implicated to play a role in attention, these medial nuclei were targeted during the stereotactic surgery (Ballinger et al., 2016; Chaves-Coira et al., 2018). Immunohistochemical experiments were performed on eight animals to validate transfection of cholinergic neurons in the target region. The DREADDs were tagged with a fluorescent label (m-Cherry) which could be observed in the targeted medial nuclei of the basal forebrain (BFB), namely the horizontal diagonal band of Broca, substantia innominata and nucleus basalis of Meynert. Dual visualization of mCherry, and ChAT that is a specific marker for cholinergic neurons via immunohistochemistry, revealed co-localization of mCherry and ChAT in the right BFB (Figure 6-1C-E). These results indicated successful cell-type specific transfection of the cholinergic neurons in the selected regions in the right BFB.

6.4.2 DREADDs-induced neural activity modulation exerts its effects on functional connectivity acutely after administration of clozapine-N-oxide

First, the temporal profile of the DREADDs-induced FC changes within DMLN was evaluated. Regions of interest (ROIs) were drawn in brain regions of the DMLN in rats (Lu et al., 2012; Stafford et al., 2014) and their FC alterations were followed up over time

after administration of clozapine-N-oxide (CNO). Significantly decreased FC in the right DMLN could be observed in the DREADDs-expressing rats starting at 5 – 10 minutes post-CNO injection (1 mg/kg) (p = 0.002, Figure 6-3C). Furthermore, this significantly decreased FC in the DMLN lasted at least until 20 minutes post-CNO injection (10-15 minutes: p = 0.01; 15-20 minutes: p = 0.001, Figure 6-3C). In contrast, CNO injection in the sham group (1 mg/kg) (p = 0.154) or saline injection in the DREADDs-expressing animals (5-10 minutes: p = 0.530; 10-15 minutes: p = 0.871; 15-20 minutes: p = 0.059) did not elicit FC alterations (Figure 6-2).

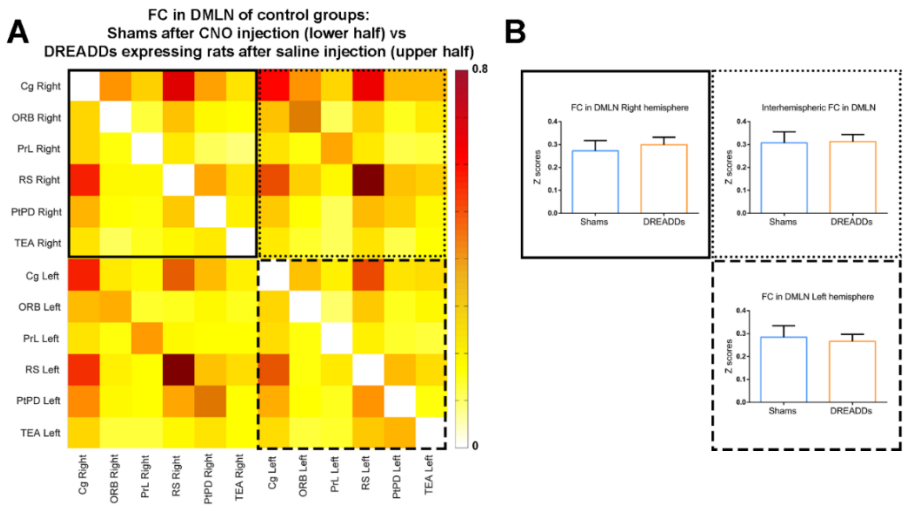

Figure 6-2: DMLN ROI-based analysis in the control groups: sham group after CNO injection and DREADDs expressing rats after saline injection(A) Pairwise z-transformed FC matrix after CNO injection (1 mg/kg) in the sham group (sub-diagonal) and after saline injection in the DREADDs-expressing rats (supra-diagonal). The color bar represents z-scores. (B) Bar-graphs of the average intra-hemispheric FC (z-scores) in the DMLN of the right hemisphere and left hemisphere, as well as the average inter-hemispheric FC of the DMLN. Data are represented as mean +/- SEM. Abbreviations: cingulate cortex (Cg), orbitofrontal cortex (ORB), prelimbic cortex (PrL), retrosplenial cortex (RS), parietal association cortex (PtPD), temporal association cortex (TEA), functional connectivity (FC), default mode-like network (DMLN), clozapine-N-oxide (CNO), designer receptors exclusively activated by designer drugs (DREADDs).

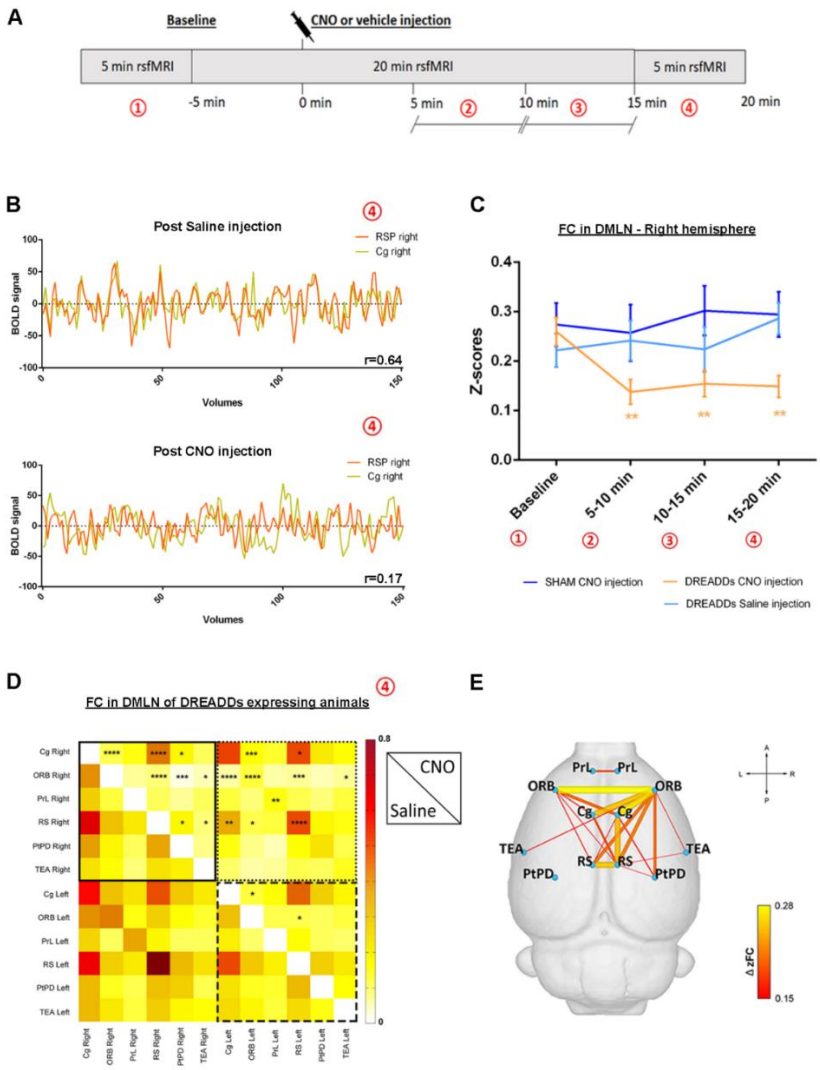

Figure 6-3: DREADDs-induced right basal forebrain (BFB) stimulation alters functional connectivity in the default mode like network (DMLN). (A) Timeline of the acquired rsfMRI scans during one scan session. (B) Example of BOLD signal time courses from the right cingulate and right retrosplenial cortex in one DREADDs-expressing animal after saline (vehicle) and CNO injection. R-values on the lower right corners show the Pearson correlation coefficient of the respective time-courses. (C) FC strength in units of Fischer-z transformed correlation (z-scores), in the right DMLN of the DREADDs-expressing group after CNO injection and saline injection as well as for the sham group after CNO injection. The time development of FC is shown at different time points: baseline, 5-10 minutes, 10-15 minutes, and 15-20 minutes after administration of CNO or

saline (see A). The asterisks indicate significant differences obtained by linear mixed model with Student's T correction for multiple comparisons. (D) Pairwise z-transformed FC matrix after saline injection (sub-diagonal) and after CNO injection (supra-diagonal) in the DREADDs-expressing group. The color bar represents z-scores. The stars indicate significant differences between the saline injection and CNO injection (repeated measures Two-way ANOVA with Sidak's correction for multiple comparisons). (E) Illustration of the significantly decreased FC presented in panel D in a ball and stick diagram overlaid on a 3D anatomical template surface. The lines represent significant differences in the DREADDs group after CNO injection with the color scale representing the actual difference in FC between the two scans (saline vs CNO injection). Yellow indicates larger FC decrease after CNO injection. The z-scores of both groups were statistically compared using a paired Student's T-test. * $p \leq 0.05$, ** $p \leq 0.01$, *** $p \leq 0.001$, **** $p \leq 0.0001$. Abbreviations: cingulate cortex (Cg), orbitofrontal cortex (ORB), prelimbic cortex (PrL), retrosplenial cortex (RS), parietal association cortex (PtPD), temporal association cortex (TEA), functional connectivity (FC), default mode like network (DMLN), clozapine-N-oxide (CNO), designer receptors exclusively activated by designer drugs (DREADDs), minutes (min).

6.4.3 Right basal forebrain stimulation induces decreased intra- and inter-hemispheric functional connectivity in default mode like network

To better understand the effect of right BFB stimulation on bilateral DMLN FC, a ROI-based analysis was performed using DMLN ROIs across the hemispheres. First, the FC of DMLN regions after CNO injection and saline injection was compared in the DREADDs-expressing group. The CNO and saline injections were performed in the same group of animals during different scan sessions. These results demonstrated that CNO-induced stimulation of the right BFB cholinergic system significantly decreased the FC between various DMLN ROI pairs (Figure 6-4D). Additionally, comparing the average intra-hemispheric and inter-hemispheric FC of the DMLN between both groups revealed significantly decreased FC within the right hemisphere ($p = 0.002$) as well as between the hemispheres ($p = 0.007$). Next to the evaluation of the FC within the DMLN, a seed-based analysis was performed for seed regions in the right Cg and right RSP to assess alterations of the FC patterns across the brain. These analyses revealed that right BFB stimulation significantly decreased the FC for both seed regions (Figure 6-4A-D).

Furthermore, comparison of the DMLN FC between the sham group and the saline-injected DREADDs-expressing group showed no significant FC alterations (Figure 6-5 B). Non-specific effect of CNO injection on the intra- and inter-hemispheric FC of the DMLN were evaluated by comparing the sham group with the DREADDs-expressing group after CNO injection. This analysis showed that the average FC in the right hemisphere and between both hemispheres significantly decreased only in the DREADDs-expressing rats (Figure 6-5). These results suggest that CNO injection (1mg/kg) did not induce non-specific effects on FC in the DMLN.

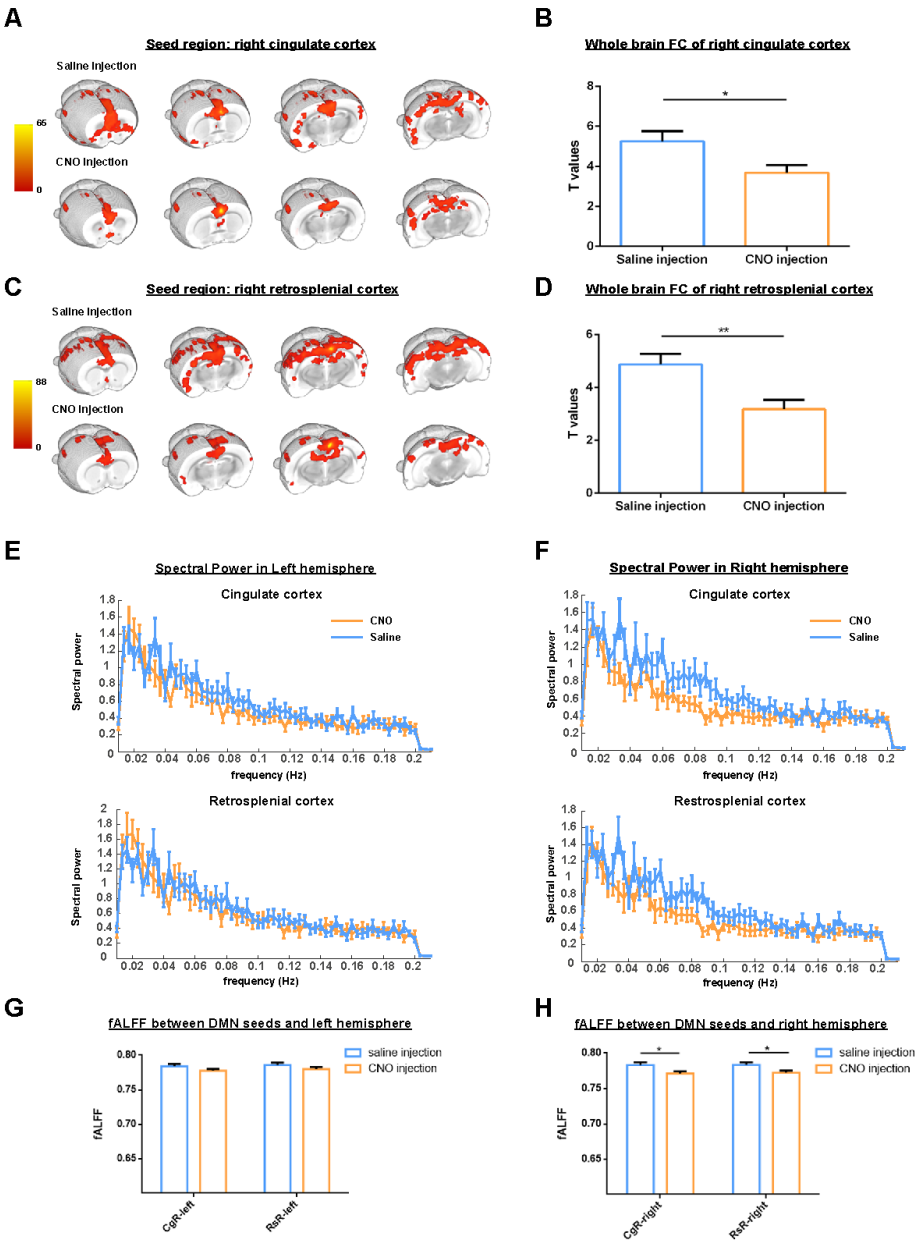

Figure 6-4: Right basal forebrain (BFB) stimulation induces functional connectivity and resting state neural activity decreases in the default mode like network (DMLN). (A, C) Representation of mean seed-based FC maps of the right cingulate cortex (A) and right retrosplenial cortex (C) in the DREADDs-expressing group after injection of saline and CNO (one-sample T-test, FWE corrected p≤0.05, minimal cluster size = 10 voxels). (B, D) Quantification of the FC strength as

mean T-values ± SEM for both seed regions (right cingulate cortex (B) and right retrosplenial cortex (D)). Statistical comparisons were performed using a Paired Student's T-test. (E, F) Group-averaged power-spectra of the seed-based maps of the cingulate and retrosplenial cortex in the left (E) and right (F) hemispheres. Blue curves are the power-spectra after injection of saline, orange curves are the power-spectra after injection of CNO (1mg/kg). (G, H) fALFF values calculated from the seed-based FC maps of the right cingulate cortex and right retrosplenial cortex. fALFF values were extracted from voxels of the left hemisphere (G) and right hemisphere (H), after saline injection (blue) and CNO injection (orange). The bar-graphs present mean fALFF values ± SEM. A Paired Student's T-test was used to statistically compare the mean fALFF values between saline injection and CNO injection within the same group. * $p \leq 0.05$, ** $p \leq 0.01$. Abbreviations: functional connectivity (FC), default mode like network (DMLN), fractional amplitude of low frequency fluctuations (fALFF).

6.4.4 Right BFB stimulation induces resting state neural activity decreases in DMLN

Next to the evaluation of FC alterations in the DMLN, the resting state neural activity alterations in the DMLN were assessed by comparing the fractional amplitude of low frequency fluctuations (fALFF, (Zou et al., 2008)) values upon CNO injection and saline injection in the DREADDs-expressing group. In this analysis, fALFF values were extracted from voxels in a mask consisting of the mean group FC map of seed regions in the right Cg and right RSC (Figure 6-4E-H). These seed regions are key nodes of the DMLN in rats and their FC maps were used as estimated masks of the DMLN FC. The obtained masks were divided into unilateral masks for the ipsilateral right hemisphere and for the contralateral left hemisphere. The extracted fALFF values in the masks of the right DMLN showed significant decreases (Figure 6-4H). Interestingly, no alterations were observed in the fALFF values from the maps in the left hemisphere (Figure 6-4G).

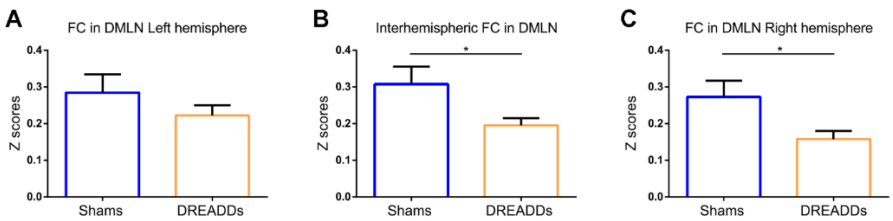

Figure 6-5: FC after injection of CNO in shams and DREADD expressing animals. ROI-based analysis assessing average FC in the DMLN after CNO injection in the sham group and the DREADDs-expressing rats. Panels represent the average intra-hemispheric FC (z-scores) of the DMLN in the left hemisphere (A) and right hemisphere (C), as well as the inter-hemispheric FC (z-scores) of the DMLN (B). The average FC values were statistically compared between both groups using an unpaired Student's T-test. Data are represented as mean +/- SEM.* p≤0.05. Abbreviations: functional connectivity (FC), default mode-like network (DMLN), clozapine-N-oxide (CNO), designer receptors exclusively activated by designer drugs (DREADDs).

6.4.5 Right BFB stimulation does not alter FC and resting state neural activity in the task positive network

To investigate if the changes observed in FC and neural activity observed in the DMLN are also present in other resting state networks (RSNs), we also analysed the task positive network, which in rats includes somatosensory, motor, and insular cortices. No significant differences were observed after injection of saline versus CNO in a ROI-based analysis (Figure 6-6A). Moreover, investigation of the low frequency neural activity using fALFF demonstrates no significant differences in neural activity in the TPN after injection of saline or CNO (Figure 6-6B). These results suggest that the observed changes in FC upon activation of cholinergic neurons in the right BFB are specific to the DMLN.

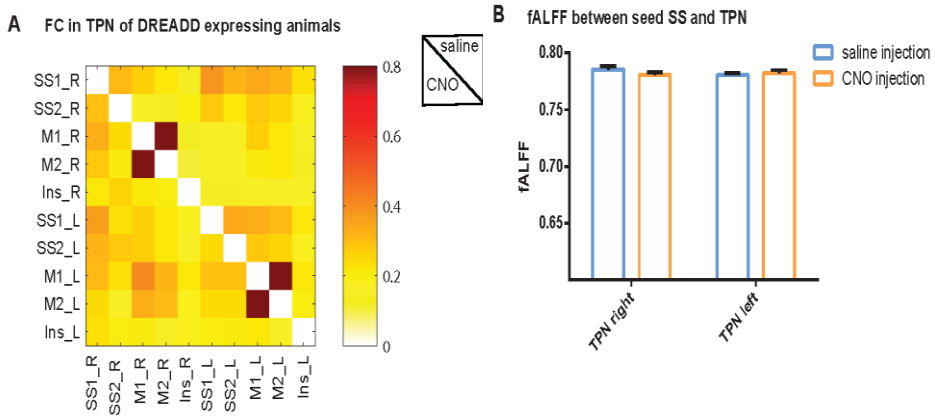

Figure 6-6: DREADDs-induced right basal forebrain (BFB) stimulation does not induce changes in functional connectivity and neural activity in the task-positive network (TPN) A) Pairwise z-transformed FC matrix after saline injection (sub-diagonal) and after CNO injection (supra-diagonal) in the DREADDs-expressing group. The color bar represents z-scores. B) fALFF values calculated from the seed-based FC maps of the left and right primary somatosensory cortex. fALFF values were extracted from voxels of the left hemisphere and right hemisphere, after saline injection (blue) and CNO injection (orange). The bar-graphs present mean fALFF values ± SEM. Abbreviations: primary somatosensory cortex (SS1), secondary somatosensory cortex (SS2), primary motor cortex (M1), secondary motor cortex (M2), insular cortex (Ins), task-positive network (TPN).

6.4.6 Unilateral stimulation of right BFB induces lateralized effects in DMLN and TPN

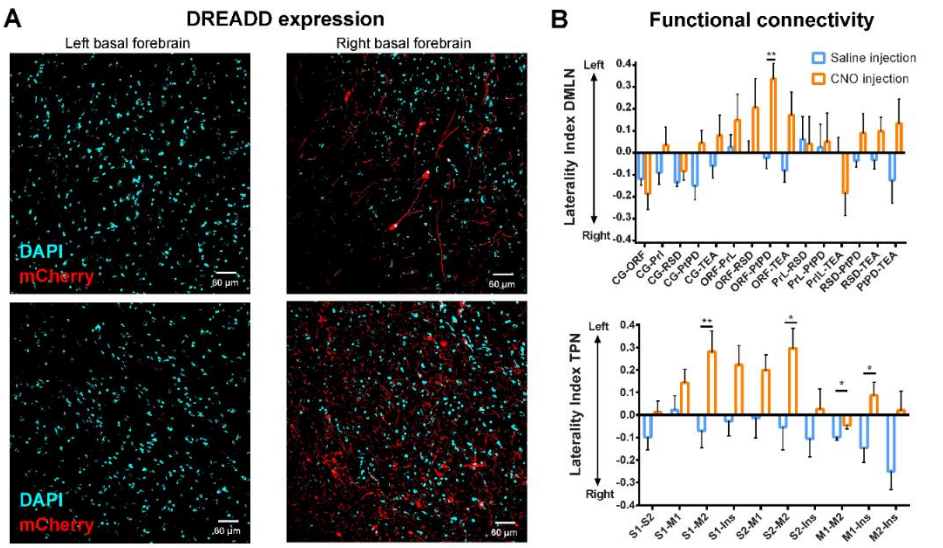

Figure 6-7: Lateralized expression of DREADDs in the basal forebrain induces lateralized changes in FC in DMLN and TPN. A) Maximum-intensity projections of the left and right basal forebrain of two DREADD-expressing animals were obtained and were thresholded, after which the area percentage of m-Cherry and DAPI was calculated. Next, the area percentage and mean intensity of the m-Cherry was normalized to the DAPI, and an expression laterality index (ELI) was calculated. The images demonstrate a highly lateralized expression of m-Cherry, predominantly in the right hemisphere (0.99 top pair, 0.98 bottom pair). B) Connectivity Laterality indices (CLI) were calculated for each ROI-pair in the DMLN (top panel) and TPN (bottom panel). Bar-graphs represent the mean CLI ± SEM, with negative values indicating right hemispheric dominance while positive values indicate left hemispheric dominance. Paired student's T-test was used to statistically compare the mean CLI between saline injection and CNO injection. * p≤0.05, ** p≤0.01. Abbreviations: designer receptors exclusively activated by designer drugs (DREADDs), cingulate cortex (Cg), orbitofrontal cortex (ORB), prelimbic cortex (PrL), retrosplenial cortex (RS), parietal association cortex (PtPD), temporal association cortex (TEA), functional connectivity (FC), default mode like network (DMLN), clozapine-N-oxide (CNO), primary somatosensory cortex (SS1), secondary somatosensory cortex (SS2), primary motor cortex (M1), secondary motor cortex (M2), insular cortex (Ins), task-positive network (TPN).

In the current study, DREADDs were injected in the right BFB during a stereotactic surgery. To evaluate the successful unilateral expression of the DREADDs, histological analysis of the m-Cherry expression in the BFB of both hemispheres was performed in a subset of animals (N=2). The percentage-area of m-Cherry as well as the mean intensities in the maximum-intensity projection were calculated and normalized according to the percentage area and mean intensity of DAPI.

Then, the expression laterality index (ELI) was calculated using ELI=(R-L)/(R+L) for each of the two animals. Figure 6-7A demonstrates that the m-Cherry expression was highly localized to the right BFB, with only minor m-Cherry present in the side contralateral to the injection site leading to expression laterality indices greater than 0.98 for both animals. Then, according to our hypothesis, we investigated if the unilateral stimulation of neurons in the right BFB expressing DREADDS would induce asymmetric and lateralized changes in FC. To evaluate this, connectivity laterality indices (CLI) were calculated based on the ROI-based matrices of the DMLN and TPN, as described previously by (Di et al., 2014). Comparison of the CLI after injection of CNO and saline revealed a significant increase in CLI towards the left hemisphere (as expected from decreased FC in the right hemisphere) for a specific DMN pair and namely the connection between ORF and PtPD (paired t-test, FDR-corrected (0.05); $p = 0.0026$). Interestingly, while no significant changes in global FC were observed in the TPN, analysis of the laterality revealed a shift towards the left hemisphere for some connections upon cholinergic activation (Figure 6-7B).

6.5 Discussion

Chemogenetic-fMRI can provide important information about the effects of particular nodes in the brain on whole brain activity and connectivity within specific networks (Giorgi et al., 2017; Peeters, Hinz, et al., 2020). In this study, excitatory DREADDs were expressed in the right BFB cholinergic neurons of rats, and the effects of DREADDs-induced neural activity alterations were evaluated by means of non-invasive rsfMRI. Several studies have already highlighted that the combination of the DREADDs

technology and *in-vivo* imaging techniques is an emerging powerful tool allowing scientists to advance their knowledge of brain networks in health and disease (reviewed in (Peeters, Missault, Keliris, & Keliris, 2019)). Here, the excitatory DREADDs in the right BFB cholinergic neurons were activated by CNO injection and rsfMRI scans were acquired to evaluate the effect on FC and resting state neural activity in brain regions of the DMLN. We showed that the effects of CNO-induced stimulation of BFB cholinergic neurons appear at 5-10 minutes after administration. The temporal evolution of FC changes we observed is consistent with previous research that demonstrated DREADDs-induced neural activity modulations starting at 5 minutes after administration of its ligand CNO (Alexander et al., 2009; Roelofs et al., 2017). Analysis of the CNO induced functional connectivity and fALFF changes, indicated a general unilateral decrease in FC and fALFF values in the DMLN ipsilateral to the expression cite in the BFB, while changes in other networks were not significant. Notably, significant connectivity laterality changes were found both in the DMN and TPN networks indicating that unilateral BFB cholinergic stimulation can induce brain state changes consistent with a biased attentional processing towards the ipsilateral hemisphere. Importantly, control experiments with CNO injections in sham animals demonstrated the absence of non-specific effects.

The DMN is implicated in higher cognitive functions which are thought to be specific for humans, such as mind wandering and thinking about the past and future. The discovery of a DMLN present in rodents raises questions about the functional homology between these networks. Moreover, the need for anaesthetics and the differences in anatomy between humans and rodents further impede interpretation and translation. Previously, it was shown that visual stimulation decreases FC and deactivates nodes of the DMLN in rats (Hinz et al., 2019), similar to observations in humans (Razlighi, 2018). Several studies have demonstrated that pharmacological stimulation of the human cholinergic system induces a desynchronization in the DMN (reviewed in (Sutherland et al., 2015)), which is analogous with the observations in this study. The aforementioned observations thus suggest shared mechanisms of task induced DMN suppression across species.

The BFB contains prominent groups of cholinergic, GABAergic, and glutamatergic neurons through which it can modulate the entire neocortex. In a recent study, Turchi et al. (2018) investigated how neuronal populations in the BFB contribute to the spontaneous fMRI fluctuations in the cerebral cortex of monkeys. The authors demonstrated that unilateral inactivation of the BFB, in particular the nucleus basalis of Meynert, induced a prominent ipsilateral decrease in the global component of the spontaneous fMRI fluctuations across its cortical projection areas. Furthermore, the spatial extent of commonly observed resting state networks remained unaltered, while significant decreases in ipsilateral network strength could be observed (Turchi et al., 2018). Those results support the neuromodulatory role of the BFB via its control of global spontaneous fluctuations. Advancing further than the above-described results, our study shows that unilateral stimulation specific to the cholinergic BFB system induces mainly ipsilateral FC reductions in the DMLN. Moreover, in our study, selective activation of cholinergic neurons could produce differential effects between the DMN and other networks, suggesting that specificity can play an important role in the surge for therapies targeting specific networks, which provides a specific manipulation tool for both fundamental studies of neuromodulation as well as potential rehabilitation efforts in disorders with lateralized attentional deficits such as hemispatial neglect.

Previous tract tracing studies revealed that the cholinergic BFB neurons collectively project towards a broad range of cortical areas as well as to brain regions of the limbic system and thalamic nuclei (Mesulam, Mufson, Wainer, & Levey, 1983). It has been shown that these cholinergic projection neurons are driven by differential inputs allowing to control the efflux of acetylcholine and its timescale in various brain regions (Gielow & Zaborszky, 2017). This supports the role of the BFB in various networks that are implicated in, for example, attentional processes (Gielow & Zaborszky, 2017; Sarter, Givens, & Bruno, 2001). As such, several behavioral and neuroimaging studies provided evidence suggesting that attentional processes, including “top-down” and “bottom-up” processes, depend on intact BFB cholinergic corticopetal projections (Pinto et al., 2013; Sarter et al., 2001).

The connections between the BFB and PFC have been implicated in the regulation of the DMN (Alves et al., 2019; Nair et al., 2018). In 2018, Nair et al. demonstrated that the BFB exhibits local gamma oscillations that influence gamma-band activity in a hub region of the DMLN, the anterior cingulate cortex, during rest (Nair et al., 2018). In humans, gamma-band activity in DMN areas is elevated during periods of wake immobility and is transiently suppressed during the performance of cognitive tasks (Miller, Weaver, & Ojemann, 2009; Ossandon et al., 2011). It has been suggested that GABAergic cells, in particular somatostatin-expressing cells, or the glutamatergic cells in the BFB mediate the generation and coordination of these gamma oscillations (Espinosa, Alonso, Lara-Vasquez, et al., 2019; Espinosa, Alonso, Morales, et al., 2019; Yang, McKenna, & Brown, 2017). In our study, analysis of the low frequency fluctuations in the BOLD signal revealed decreased FC and resting state neural activity in cortical DMLN region upon stimulation of BFB cholinergic neurons. Interestingly, the low frequency fluctuations in the BOLD signal have been suggested to be related to spontaneous gamma band local field potentials (Leopold, Murayama, & Logothetis, 2003). Therefore, decreases in FC and resting state neural activity (measured by fALFF) might be related to decreased activity in neurons giving rise to gamma oscillations, such as GABAergic and glutamatergic BFB neurons. We suggest that our findings might be mediated through local axonal collaterals from BFB cholinergic neurons that terminate on other BFB cell types (Zaborszky & Duque, 2000). This is in line with other studies showing that the connections between cholinergic neurons and somatostatin cells in the BFB are antagonistic (M. Xu et al., 2015; Zaborszky & Duque, 2000). Additionally, cholinergic stimulation can induce inhibition of the BFB glutamatergic neurons (Yang et al., 2017). The latter is thought to exert its effect on the DMN via the ventral striatum (van der Meer et al., 2010). The interactions between both neuronal populations and the cholinergic neurons might be an underlying mechanism through which the attention networks and DMN exert their antagonism. However, future investigations of the BFB-DMN circuitry have to be performed in order to elucidate the contributions of specific BFB cell types.

In the current study, we did not investigate how chemogenetic activation of basal forebrain cholinergic neurons alters their spiking activity. Cholinergic neurons in the basal forebrain can be divided in two different subtypes, based on their electrophysiological properties, the burst-firing and rhythmic (non-burst) firing neurons. These neuron types have distinct firing properties and are thought to be involved in different cognitive processes taking place at different timescales (Laszlovszky et al., 2020). So far, no study has evaluated how DREADD induced activation alters firing activity of cholinergic neurons in the basal forebrain. However, electrophysiological recordings of mouse striatal cholinergic interneurons demonstrated an tonically increased firing rate after DREADD-induced activation, leading to increased concentrations of ACh. (Unal, Golowasch, & Zaborszky, 2012). Striatal interneurons are known to have a distinct firing pattern of tonic activity interrupted by pauses. DREADD induced activation of these interneurons also occluded these pauses (Aoki et al., 2018). We hypothesize that DREADD induced activation on basal forebrain cholinergic neurons has a similar effect, where spiking activity, of both bursting and rhythmic firing neurons, dramatically increased upon chemogenetic activation, thereby increasing cholinergic tone in the target regions. Increases in cholinergic tone have been observed in rats performing a visual attention task (Parikh et al., 2007). Pinto et al. (2013) showed that enhanced acetylcholine levels, by stimulation of the BFB cholinergic neurons, can improve visual discrimination and sensory processing by inducing desynchronization of cortical activity (Pinto et al., 2013). Recently, research performed in our lab demonstrated that stimulating bottom-up sensory processing in sedated rats induced decreases in FC between different nodes of the DMLN (Hinz et al., 2019). Collectively, these findings might suggest involvement of the BFB cholinergic system in mediating the reduced FC in the DMLN upon stimulation of bottom-up sensory processes.

Previous studies suggested that the BFB is a key player in modulation of cortical networks. In this study, we combined the DREADD technology with *in-vivo* MRI in rats in order to explore the involvement of the BFB cholinergic system in the regulation of the DMLN. As such, excitatory DREADDs were used to selectively activate cholinergic

neurons in the right BFB, and resting state fMRI scans were acquired to evaluate the effect on DMLN FC and resting state neural activity. This is the first study which demonstrates decreased right intra- and interhemispheric FC in the DMLN as well as decreased right intra-hemispheric resting state neural activity upon selective, cholinergic stimulation, in sedated rats. We conjecture that our DREADDs-induced stimulation of the BFB cholinergic neurons mediates decreased DMLN FC through similar pathways as task-related DMLN suppression. To conclude, our findings enrich the current understanding of the DMLN and its underlying mechanisms in rodents and provide a specific tool for future manipulation of activity and connectivity in studies interested in cholinergic neuromodulation both in health and disease.

6.5.1 Limitations of the study

Despite DREADDs being an exquisite tool allowing specific targeting of neuronal populations, their temporal precision is limited due the systemic nature of their application and the mechanisms of action (most via G-protein coupled receptors). In contrast, optogenetics – a technique that allows similar specificity – allows manipulation of cell activities with millisecond precision and recent advancements provide single cell precision, albeit at the cost of more invasive manipulations. Several studies have shown that acute versus tonic cholinergic stimulation induce different effects. Therefore, diverging results could be obtained when combining optogenetics with rsfMRI. Both techniques are still developing and thus some of these limitations are expected to get eliminated in the future. Another, limitation of our study is that although we targeted specifically the cholinergic cells the effects could be mediated through interactions between other neuronal populations in the BFB. More experiments investigating the local interactions of the different neuronal populations in the BFB would be valuable to further elucidate the neuronal mechanisms underlying the neuromodulatory effects of the cholinergic system on the DMLN. To conclude, in the current study, only the right BFB was transfected with DREADDs, resulting in a lateralized decrease in FC in the DMLN. It would be interesting to compare these results to the effects of a bilateral cholinergic stimulation.

7. General Discussion

In this PhD project, we set out to unravel network dysfunction in Alzheimer's Disease (AD). **The overall aims of this PhD project were to evaluate how whole brain network activity and hippocampal oscillatory activity is altered at pre- and early-plaques stages of AD and how this is linked to histopathological AD-related alterations and behavioral disturbances during exploration of a novel environment and during sleep.** For this purpose, we used a multimodal approach where we combined resting state functional MRI (rsfMRI), hippocampal measurements of neuronal activity in freely behaving animals and histological analysis. We investigated pre-plaque and early-plaque stages of AD, using the TgF344-AD rat model, which displays all phenotypical hallmarks of AD. First, we investigated whole brain alterations in network activity using rsfMRI, combined with histology to gain insights into possible disease mechanisms contributing to the changes in network activity. These results are presented in **chapter 3**. In **chapter 4 and 5**, we used hippocampal electrophysiology to evaluate neuronal activity and hippocampal network function during different sleep stages, during wake immobility and during exploration of a novel environment**.** In addition, analysis of the abundance of cholinergic, glutamatergic, and GABAergic synapses was performed to gain insight into synaptic alterations which might contribute to the altered hippocampal activity. **In the next step, we aimed to investigate the effects of modulating cholinergic signaling on the functional connectivity in whole-brain networks**. Therefore, we used designer receptors exclusively activated by designer drugs (DREADDs) to modulate the neuronal activity of basal forebrain (BFB) cholinergic neurons in healthy rats and evaluated the effects on whole brain functional connectivity using rsfMRI in **chapter 6**.

7.1 Recapitulation of research aims and obtained findings

The **first aim** was to evaluate alterations in whole-brain network activity during organized synchronous network events. In chapter 3 we have proven that network function during recurrent patterns of brain activity, so-called quasi periodic patterns

(QPP), is altered during the pre-plaque stage in the TgF344-AD rat model for AD. At this stage soluble amyloid-beta (Aβ) monomers and oligomers were observed in brain homogenates, in the absence of Aβ-plaques and hyperphosphorylated tau (pTau) inclusions. We observed that BOLD activity in the BFB and several regions of the default mode-like network (DMLN) was disrupted in TG rats within 3.6-second long QPPs. Moreover, we observed that in the wild-type (WT) littermates, BFB activity preceded BOLD activity of other regions of the DMLN within 9-second long QPPs. The BFB has been demonstrated to be an important regulator of network activity and has been implicated to regulate DMLN activity and the global signal measured with fMRI (Nair et al., 2018; Turchi et al., 2018). This leading role of the BFB in QPP activity was lost in the TG rats, suggesting altered BFB function during the pre-plaque stage of AD. The altered BFB function coincided with increased astrocyte abundance in the nucleus basalis of Meynert (NBM) and horizontal diagonal band of Broca (HDB), two nuclei of the BFB. This might suggest that astrogliosis severely disrupted BOLD activity in the BFB and, given the role of the BFB in the regulation of the DMLN, might contribute to the changes in BOLD activity within the DMLN. Interestingly, we observed that BOLD activity patterns within short QPPs during the early-plaque stage in TgF344-AD rats was more similar to activity patterns observed in the WT rats, suggesting the action of compensatory mechanisms. Moreover, astrogliosis in the BFB nuclei was not present anymore during the early-plaque stage, whereas Aβ-plaques and pTau accumulations were observed in the brain. **This study provided novel insights into network alterations involving the BFB during the pre-plaque stage of AD, and possible compensatory mechanisms during the early-plaque stage. Moreover, this study shows that resting state functional MRI combined with QPP analysis is a robust method to detect network disturbances in neurological disorders already at early stages (Figure 7-1).**

The **second aim** was to evaluate hippocampal network activity and how behavioral state affects hippocampal function during pre- and early-plaque stages of AD, which could provide insights into the impact of AD on different neuromodulatory systems. In **chapter 4,** we performed 24-hour hippocampal electrophysiological measurements while the

animals were in their home cage, to evaluate circadian rhythmicity, sleep architecture and hippocampal oscillatory activity during sleep. We observed that at pre- and early-plaque stages of AD, circadian rhythmicity was still intact in TgF344-AD rats, and we did not observe significant differences in time spent in REM and NREM states. Moreover, we did not observe signs of sleep fragmentation during NREM sleep. However, we did observe a significantly increased probability for shorter REM bouts, suggestive of REM sleep fragmentation, in TgF344-AD rats at the pre-plaque stage. Interestingly, at the early-plaque stage, REM bout length was not significantly different from WT littermates. When investigating hippocampal oscillatory activity during REM sleep, we observed a significantly decreased fast gamma power in TgF344-AD rats, irrespective of age. In addition, a decreased theta-gamma coupling was observed in the high gamma range at the pre-plaque stage, which was partially compensated in the early-plaque stage. Moreover, theta-gamma coupling in the low gamma range was significantly increased during the pre-plaque stage in TgF344-AD rats but returned to WT levels at the early-plaque stage. These results suggest a partial functional compensation of network activity during early-plaque stage of AD during REM sleep. Interestingly, we observed an increased number of cholinergic synapses in the hippocampus during the early-plaque stage in TgF344-AD rats. This could contribute to the functional compensation we observe during REM sleep, especially since the regulation of REM sleep and theta-gamma coupling are heavily dependent on cholinergic signaling, in the absence of other neuromodulatory inputs. During NREM sleep, we did not observe altered power across different frequency bands, but we did observe a significantly increased duration of sharp wave-ripples (SWR), electrophysiological phenomena closely linked to memory consolidation. These alterations in oscillatory activity during NREM sleep, during which cholinergic modulation is virtually absent, became worse over time in the TgF344-AD rats, which is in contrast to the REM sleep alterations. **These results demonstrate the presence of REM sleep fragmentation already at pre-plaque stages of AD. Moreover, the results of this study in TgF344-AD rats provides strong evidence for hippocampal network disruptions during the pre-plaque stage of AD, and they point towards cholinergic compensatory mechanisms at the early-plaque stage of AD, that improve**

hippocampal network function during sleep. These results are in line with the altered BFB function at the pre-plaque stage of AD, as was observed in chapter 3 since cholinergic projections to the hippocampus originate from the BFB (Figure 7-1).

In **chapter 5,** we evaluated hippocampal network activity while the animals were exploring a novel environment during the pre-plaque stage of AD. High levels of arousal are associated with high noradrenergic signalling, thus alterations which were pronounced during exploration would point towards the impairment of noradrenergic signalling. Moreover, hippocampal function is dependent on behavioral state, thus differences in electrophysiological phenomena during different states could give insights in which hippocampal processes could be affected at early stages of AD. In this study we did observe alterations in hippocampal neuronal activity in 4-month-old TgF344-AD rats. We demonstrated an overall decreased high theta power in TgF344-AD rats, irrespective of behavioral state. In addition, we observed decreased theta-gamma coupling in the high gamma frequencies during wake immobile, similar to what was observed during REM sleep. Interestingly during exploration, an increased coupling strength between consecutive trials was observed during exploration in the slow gamma frequencies in the WT rats, which was less pronounced in the TgF344-AD rats. When investigating sharp wave-ripples during wake immobile and explorative behavior, increased power of SWR was observed in TgF344-AD rats irrespective of behavioral state. In addition, increased slow gamma power during SWR was observed during wake immobile behavior together with a decreased duration of SWR. These alterations in oscillatory activity coincided with increased anxiety-like phenotype, similar to previous behavioral analysis (Pentkowski et al., 2018). **The results of this study confirm that altered hippocampal activity at the pre-plaque stage was also present in awake rats, mainly during the wake immobility behavioral state.** The noradrenergic system is one of the main neuromodulators of explorative behavior and is early affected in AD (Harley & Yuan, 2021; Lima et al., 2019). However, in this study we did observe that hippocampal oscillatory activity shows less alterations when compared to the wake immobile behavioral state, which is shaped by the neuromodulatory input of several wake-promoting systems. This might suggest that

the **noradrenergic system at the pre-plaque stage of AD is relatively spared, which could be explained by the absence of pTau accumulation in the locus coeruleus (LC) at the pre-plaque stage as is observed in chapter 3, which only showed accumulation of pTau in the LC at 6 months of age (Figure 7-1).**

Given the important role of the cholinergic system in AD and the observed involvement of the BFB cholinergic system in compensation of network activity during the early-plaque stage of AD in TgF344-AD rats, we aimed in **the sixth chapter** to investigate the effects of unilateral BFB cholinergic activation on resting state networks. We used chemogenetic tools to selectively activate cholinergic neurons in the NBM of healthy rats and evaluated the effects of cholinergic stimulation on resting state networks using rsfMRI. We observed a lateralized decrease in functional connectivity and decreased amplitude of BOLD fluctuations within the default-mode like network, but not in the lateral cortical network, upon unilateral activation of BFB cholinergic neurons. In addition, we observed increased lateralization of functional connectivity in both the default mode-like network and the lateral cortical network. **This study confirmed that combining resting state functional MRI and chemogenetic tools offers valuable insights into the effects of cell-type specific modulation on brain connectivity. Moreover, this study has shown that the BFB cholinergic system is an important modulator of activity in the default-mode like network and to a lesser extent, lateral cortical network in rodents, which is in line with the results from chapter 3 (Figure 7-1).**

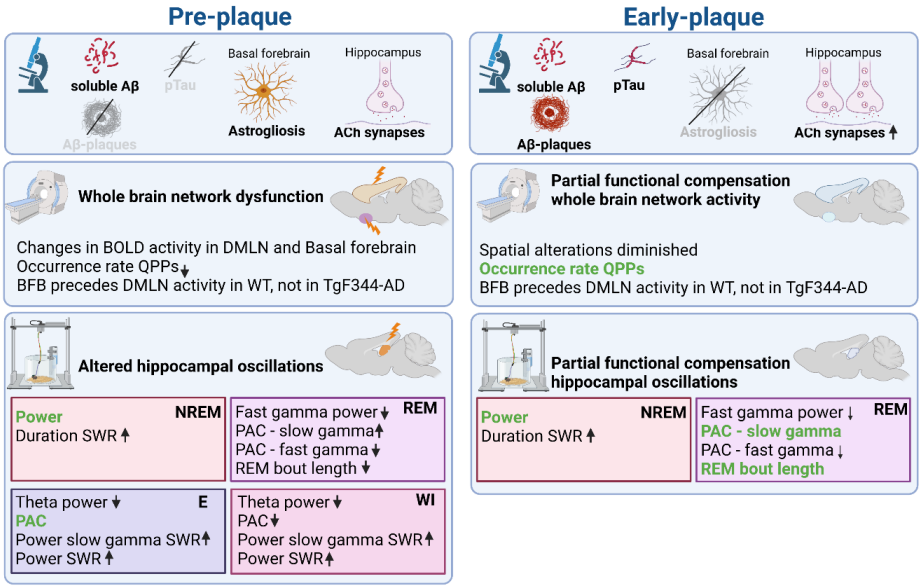

Highlights

- Basal forebrain dysfunction pre-plaque & basal forebrain compensation in animal model of AD
- Hippocampal oscillatory activity altered during pre-plaque stage
- Compensatory increase in cholinergic synapses in hippocampus during early-plaque
- Partial functional recovery of hippocampal oscillatory activity and REM sleep during early-plaque
- Differential impact AD on hippocampal activity during different behavioral states
- RsfMRI + QPPs to detect disconnection BFB and DMLN at early stages of AD
- Stimulation basal forebrain cholinergic network perturbs DMLN, but not LCN connectivity

Figure 7-1: Summary of main findings. Arrows indicate a significant increase or decrease in the parameter in the TgF344-AD rats compared to wild-type littermates. The effect size of the difference is demonstrated by the size of the arrows. Green parameters showed no significant difference between genotypes.

7.2 Quasi-periodic patterns, what are they?

One of the first achievements in this PhD project was the implementation of whole-brain QPP analysis in rats and using QPPs to evaluate network (dys)function in AD. Moreover, we have tried to investigate mechanisms which lead these QPPs and observed for the first time ever that the BFB seems to be an important modulator of whole-brain network activity within QPPs in WT rats. We also demonstrated that QPPs are able to detect

alterations in BFB activity and whole brain network activity, at pre-plaque stages of AD, suggesting that QPPs could be used to detect AD at early stages of AD. Several studies already observed increases in FC, so-called hypersynchrony, during pre-plaque stages of AD in different mouse models (Ben-Nejma et al., 2019; Latif-Hernandez et al., 2019; Shah et al., 2018; Shah et al., 2016). However, the observed changes were not specific to AD, since similar increases in FC in the DMLN and hippocampal network have also been observed in other neurological diseases such as ADHD and temporal lobe epilepsy, therefore limiting the use of these FC changes as biomarker for AD (Haneef et al., 2014; Silberstein, Pipingas, Farrow, Levy, & Stough, 2016; Sun et al., 2012). The altered BFB coactivation and BOLD activity in chapter 3 could be a promising feature to detect AD, since the BFB is one of the first regions affected in AD. However, our findings should be validated in other animal models of AD and in patient populations across the entire AD spectrum. Moreover, the exact meaning of QPPs remains unknown and the biological underpinnings of these recurrent patterns of brain activity remain elusive, limiting the interpretation of the AD related changes. In the next sections we elaborate on possible disease mechanisms underlying these changes in BOLD activity within QPP activity. In addition, we will describe how the QPP propagation observed in chapter 3 relates the functional organization of the brain.

7.2.1 Underpinnings of the BOLD contrast

The BOLD contrast is highly dependent on the hemodynamic response arising from the neurovascular coupling after neuronal activation (Buxton, Wong, & Frank, 1998; van Zijl et al., 1998). Due to this relationship, the BOLD contrast is also heavily influenced by the vascular architecture and reactivity. A vast amount of research is dedicated to disentangle the neuronal and the vascular component in the BOLD signal by acquiring fMRI and simultaneously measure neuronal activity and/or perfusion.

7.2.1.1 Contribution of neuronal subtypes

Early studies which combined fMRI with electrophysiological measurements have demonstrated that the BOLD signal directly reflects an increase in neuronal activity.

BOLD was originally thought to be mainly driven by increased firing rates of excitatory neurons, as increased neuronal activity measured with LFPs strongly correlates with the BOLD signal (Logothetis, Pauls, Augath, Trinath, & Oeltermann, 2001; Silva, Lee, Yang, Iadecola, & Kim, 1999). The direct connection between neuronal activity and BOLD activity has been further demonstrated by recent studies using simultaneous calcium recordings and fMRI which observed that activity of populations of neurons are tightly correlated to the BOLD signal in cortical regions belonging to the DMLN and in the hippocampus in anesthetized and in awake animals (Lake et al., 2020; Z. Ma, Zhang, Tu, & Zhang, 2022; Pais-Roldan et al., 2020).

Excitatory pyramidal neurons have long been thought to be the main driver of positive BOLD activity, while decreased activity of pyramidal neurons was associated with negative BOLD signals. However, pharmacological studies have demonstrated by blocking GABA receptors, that inhibitory interneurons play an important role in positive BOLD activity. Inhibitory neurons can directly alter CBF and BOLD activity, demonstrating that inhibitory neurons are also contributing to the BOLD signal (Han et al., 2019; Howarth, Mishra, & Hall, 2021; Uhlirova et al., 2016). The increased functional connectivity (FC) which is often observed in pre-plaque stages of AD, therefore does not perse mean increased activity of glutamatergic neurons. The hypersynchrony can also be caused by increased inhibitory neuronal activity.

In chapter 3 we observed alterations in BOLD activity in TgF344-AD rats. Interneuron dysfunction is a prominent feature of AD, also at early stages of AD (Caccavano et al., 2020; Hijazi et al., 2020). We observed a decreased ratio between excitatory and inhibitory synapses in the cingulate cortex and retrosplenial cortex, suggesting increases in GABAergic synapses or decreases in glutamatergic synapses. This is in line with observations made during the pre-plaque stage in APP/PS1 mice, which showed hyperexcitability of interneurons (Caccavano et al., 2020; Hijazi et al., 2020). Since inhibitory neurons have been demonstrated to contribute to the BOLD response, we could expect an increase in BOLD signal in TgF344-AD rats. This is in line with what we have observed in chapter 3 within the 3.6-second-long QPP DMLN during the pre-plaque stage, where we observed increased BOLD signal in the cingulate cortex in TgF344-AD

rats (figure 7-2). However, despite the decreased E/I balance observed at the early-plaque stage, we did not observe increased BOLD activity during in 6-month-old TgF344-AD rats, suggesting that besides the impact of interneuronal activity, other contributions to the BOLD signal should be taken into account.

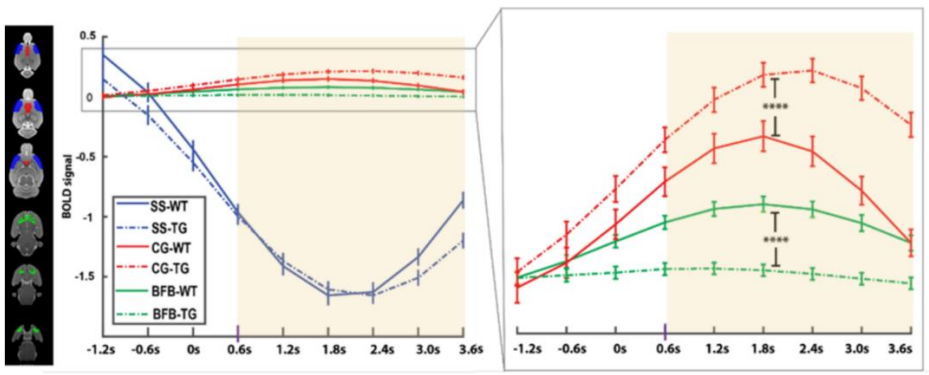

Figure 7-2: Changes in Quasi-periodic patterns in 4M old TgF344-AD rats. BOLD signal before and within the 3.6 second long rQPP DMLN+ (yellow shading) during the pre-plaque stage in TgF344-AD rats in the cingulate cortex (Cg), basal forebrain (BFB), and Somatosensory cortex (SS) were averaged across QPP occurrences. Both graphs show the mean +/- SEM. Stars indicate significant differences in BOLD signal between groups in either the Cg or BFB region between groups. ****p<0.0001

Cortically projecting neuromodulatory neurons have also been implicated to have an impact on neuronal activity and the neurovascular coupling, therefore influencing the BOLD signal (Lecrux & Hamel, 2016; Lecrux et al., 2017; Perrenoud et al., 2012). These neuromodulatory systems can alter the hemodynamic response, independently of activity of excitatory neurons, potentially complicating the interpretation of BOLD signals in diseases in which these systems are affected. It is important to consider if the sensitivity of the vasculature to neuronal activity i.e., cerebrovascular reactivity, is altered by changes in these neuromodulatory systems. Several studies have demonstrated that decreases in cholinergic tone induce a decreased correlation between neuronal activity and the hemodynamic response (Lecrux et al., 2017; Zaldivar, Rauch, Logothetis, & Goense, 2018). Similar changes in neurovascular may contribute to alterations in BOLD signals in AD, because of the cholinergic impairment in AD. In

chapter 3 we observed increased astrocyte abundance in the BFB, which, given the important role of astrocytes in synaptic transmission, could result in a decreased cholinergic innervation of the cortex, which in turn decreases the BOLD activity in cortical regions. When investigating the number of cholinergic synapses in the cortical regions, we did not observe significant differences, so this hypothesis remains speculative. Future experiments should investigate if altered cerebral blood flow and vascular reactivity occurs at pre- and early-plaque stages of AD in the TgF344-AD rats, to improve interpretation of the current findings. In chapter 6 we have increased the cholinergic tone in the cortex by activating cholinergic neurons in the nucleus basalis of Meynert. We observed decreased FC specifically in the DMLN, but not in regions belonging to the LCN (Figure 6-3, Figure 6-6). Cholinergic projections from the NBM innervate regions of the DMLN as well as the LCN such as somatosensory cortices (Bloem, Schoppink, et al., 2014; Chaves-Coira, Barros-Zulaica, Rodrigo-Angulo, & Nunez, 2016; Zaborszky et al., 2015). If neurovascular coupling would be altered by the increased cholinergic tone, one would expect that this effect would be similar in both cortical networks, suggesting neuronal underpinnings to the observed changes in BOLD signal and FC. However, given the aforementioned vascular effect of an increase of acetylcholine, we should consider that altered neurovascular coupling could contribute to the observed changes in FC.

7.2.1.2 Differential contribution of astrocytes

Astrocytes are in close contact with both neurons and vasculature and have been demonstrated to play an important role in supporting neurons in their energy demand through its involvement in the neurovascular coupling (Schummers, Yu, & Sur, 2008; Winship, Plaa, & Murphy, 2007). Neuronal activity evokes a slow increase in intracellular calcium in astrocytes, inducing the release of vasoactive molecules which in turn results in a hemodynamic response. Increases in BOLD signal have been observed after optogenetic stimulation of astrocytes, without altering neuronal activity, further suggesting a role for astrocytes in neurovascular coupling (Takata et al., 2018). However, these slow calcium currents have been criticized as being too slow to explain the

vascular response to neuronal activity (Institoris, Rosenegger, & Gordon, 2015). In contrast, fast calcium signals which occur mainly at the astrocytic end-feet have been increasingly associated with neuronal and/or synaptic activity. These arise shortly after an increase in neuronal activity and potentiate the increase in blood flow in the capillary beds (Di Castro et al., 2011; X. Gu et al., 2018; Otsu et al., 2015). Moreover, these fast calcium signals in response to neuronal activity have been shown to induce increases in the BOLD signal, demonstrating an astrocytic contribution to the resting state signal. Astrogliosis, resulting in increased astroglial reactivity, is a prominent hallmark of AD, which could interfere with neurovascular coupling. In chapter 3 we observe astrogliosis in the BFB at the pre-plaque stage, a region which also showed decreased BOLD activity within recurrent patterns of brain activity. Given the versatile role of astrocytes in neuronal signalling and neurovascular coupling, future experiments aiming to unravel the effects of astrogliosis in the BFB on BOLD activity in the cortex in AD are necessary.

7.2.1.3 Vascular contribution

BOLD activity is, in addition to neuronal and astrocytic signals, shaped by the properties of the vasculature itself (Howarth et al., 2021). The vascular mural cells which are responsible for direct constriction and dilation of blood vessels are the smooth muscle cells, which are present around arterioles, and pericytes, which mainly regulate the flow in the capillary beds (Attwell, Mishra, Hall, O'Farrell, & Dalkara, 2016; C. N. Hall et al., 2014). Pericytes are cells that express smooth muscle actin, and which have been demonstrated to actively constrict and dilate capillaries in response to neuronal activity. Capillary dilatation contributes to 50-80% of the overall change in CBF in response to neuronal activity, whereas arteriole dilation contributes less than 25% to the change in CBF (C. N. Hall et al., 2014). Soluble Aβ-monomers and oligomers have been shown to induce pericyte constriction, whereas intramural Aβ aggregates impair arteriolar reactivity, resulting in vascular impairments in AD (Hill et al., 2015; Kimbrough, Robel, Roberson, & Sontheimer, 2015; Nortley et al., 2019). In chapter 3 we observed differences in BOLD activity in several regions of the brain mainly during the pre-plaque stage in the TgF344-AD rats. Moreover, we observed an increased similarity between

BOLD activity between groups at the early-plaque stage. A similar trend was observed in chapter 5, where alterations in hippocampal neuronal activity were also more pronounced at the pre-plaque stage. These results suggest that the altered BOLD activity has neuronal underpinnings and are therefore, a marker for early synaptic dysfunction in AD. However, we could not exclude vascular contributions, especially since alterations in vascular reactivity are known to occur in AD patients (Alwatban, Murman, & Bashford, 2019; Hutchison et al., 2013). Cerebral amyloid angiopathy and decreased cerebrovascular reactivity in response to hypercapnia have been observed in TgF344-AD rats at 9 months of age (Joo et al., 2017). No studies on cerebrovascular reactivity have been performed at pre- and early-plaque stages of AD in the TgF344-AD rat, therefore we cannot estimate the extend of the vascular contribution to the alterations observed in chapter 3. Currently, several studies in our lab are evaluating cerebrovascular reactivity and cerebral perfusion at the pre-plaque stage of AD in TgF344-AD rats.

7.2.2 Functional gradients in the brain and QPPs

Besides the promising results in this thesis, there is still a lack of knowledge about what QPPs actually are and how they are contributing to the functionality of the brain. A key principle in the topographical structure of the cortex is that it is organized based on cognitive processes (Bernhardt, Smallwood, Keilholz, & Margulies, 2022). Each brain network is characterized by distinct functions. Some are related to primary functions such as auditory or visual perception and movement, while other networks are involved in more general functions such as cognition, attention, and emotional processing. MRI studies in humans, monkeys and rodents have demonstrated that the functional organization of the brain can be captured by two functional gradients (Figure 7-3) (Huntenburg, Yeow, Mandino, & Grandjean, 2021; Margulies et al., 2016; Mesulam, 1998; Tong et al., 2022). The principal gradient or gradient 1, separates unimodal regions (e.g. auditory cortex, motor cortex) from transmodal association regions (e.g. frontal cortex, regions belonging to the DMN). The second gradient separates somatosensory, motor, and auditory cortex from the visual cortex.

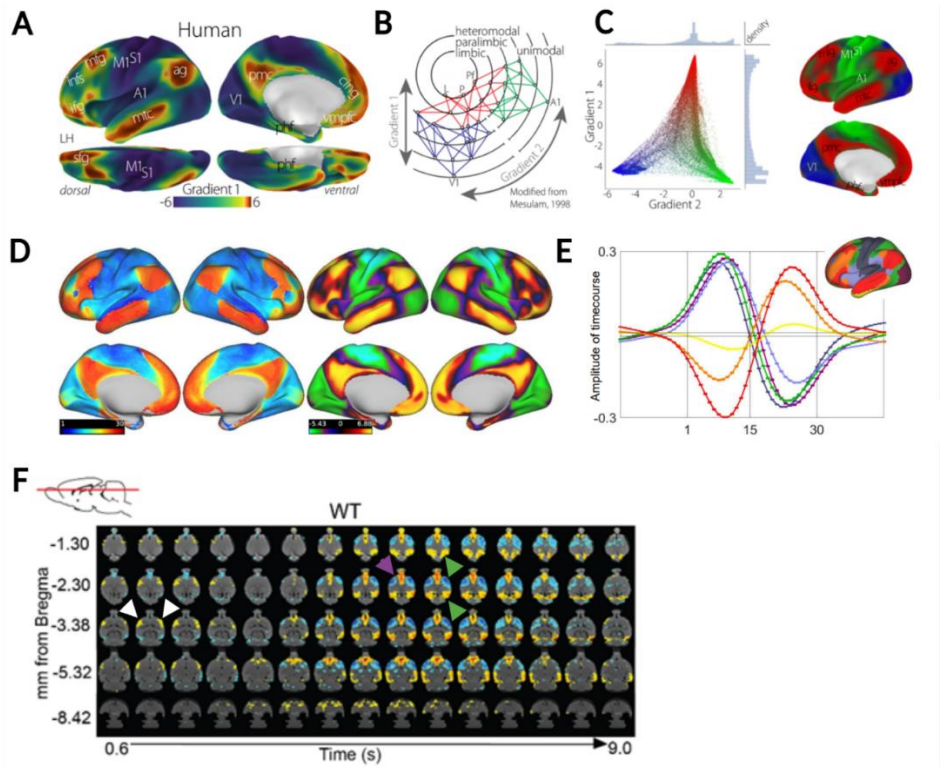

Figure 7-3: functional gradients in the human brain and its relation to propagation of cortical activity within QPPs. The principal gradient of connectivity in both the human and monkey's shows a spectrum between unimodal regions (dark blue) and transmodal regions (sienna). (B) The illustration of connectivity organization suggested by Mesulam (Mesulam, 1998) proposes a hierarchy of processing from distinct unimodal areas to integrative transmodal areas. (C) A scatter plot of the first two connectivity embedding gradients. Gradient 1 extends between primary sensorimotor and transmodal regions (red). Gradient 2 separates somatomotor and auditory cortex (green) from visual cortex (blue). Histograms depicting the distribution of values are presented on the respective axes. Colors from the scatter plot are presented on the cortical surface for anatomical orientation. (D) QPP time peak map (left) vs the primary cortical gradients (Pearson correlation between the maps is 0.91), supporting that the peak activities within QPPs highly resemble the primary cortical gradient. (E) Seven timecourses of the average QPP timecourses across the cortical network (map serves as legend). (F) 9-second long rQPP from wildtype (WT) rats at four months of age. Somatosensory cortex (white arrowheads) activates before the cingulate (purple arrowheads) and visual cortex (green arrowheads). A1, primary auditory; ag, angular gyrus; cing, anterior cingulate cortex; ifg, inferior frontalgyrus; infs,

intermediate frontal sulcus; L, limbic; M1, primary motor; mfg, middle frontal gyrus; mtc, middle temporal cortex; P, parietal; Pf, prefrontal; phf, para-hippocampal formation; pmc, posteromedial cortex;ps, principal sulcus; S1, primary somatosensory; sfg, superior frontal gyrus; V1, primary visual; vmpfc, ventromedial prefrontal cortex. Figure adapted from (Margulies et al., 2016; Yousefi & Keilholz, 2021)

Keilholz et. al investigated if propagation of BOLD activity within QPPs would obey this functional organization (Figure 7-3 D, E). They observed that cortical activity propagates along the primary gradient, where positive BOLD peaks in the somatomotor regions, visual cortex and auditory cortices precede the positive peak activity within the dorsal and ventral attention network, followed by peak activity in the limbic system and DMN (Figure 7-3 E) (Yousefi & Keilholz, 2021). In chapter 3 we tried to investigate how activity propagated during long QPPs. The 9-second long QPPs observed in rats do show an activated LCN, mainly consisting of somatosensory and motor cortices, followed by an activation within the DMLN, similar to the primary functional gradient (Figure 7-3 F). However, the visual cortex peak was lagging behind the peaks in the frontal DMN, which does not follow the primary functional gradient. The second cortical gradient separates auditory, somatosensory, and motor cortices from the visual cortex, so it seems that in anesthetized rats, the QPP activity also propagates along the second gradient.

7.3 The role of sleep in AD

Sleep is a complex behavioural state defined by the complete loss of behavioural control and consciousness. Sleep plays an important role in several physiological functions including synaptic homeostasis and plasticity, brain waste clearance, modulation of immune responses and cognition (Diekelmann & Born, 2010; Zielinski et al., 2016). Research over the past decades demonstrated that physiological changes in circadian rhythm and sleep architecture emerge during the normal aging process (Mander et al., 2017; Romanella et al., 2021). These physiological changes in sleep characteristics are associated with brain changes, such as decreased synaptic plasticity and impaired cognitive function. Sleep alterations are often present during early stages of AD, as reduced total sleep time, sleep fragmentations and a reduced time spent in deep sleep stages have repeatably been observed in MCI patients (Carnicelli et al., 2019; Casagrande et al., 2022). These sleep disturbances exacerbate AD pathology, since Aβ production is increased during wakefulness and clearance of waste products by the glymphatic system is decreased, as NREM time decreases (Duncan et al., 2022; Y. S. Ju et al., 2017; Liguori et al., 2020; Roh et al., 2012).

In chapter 4, we did not observe significant differences in sleep time or circadian rhythmicity. However, we did observe signs of REM sleep fragmentation during the pre-plaque stage of AD. Interestingly, 16-month old TgF344-AD rats display increased fragmentation of both REM and NREM, without differences in time spent in these vigilance states (Kreuzer et al., 2020), suggesting that the alterations in sleep architecture worsen as the disease progresses in TgF344-AD rats, similar to what is observed in human AD (Casagrande et al., 2022; M. Hu et al., 2017; Kang et al., 2017). Animal studies in J20 mice and Tg2576 mice displayed decreased time spent in REM and shorter REM bout length, without alterations in NREM, implying that REM changes precede NREM changes also in other mouse model of AD, similar to what is observed in the TgF344-AD rats (Filon et al., 2020; B. Zhang et al., 2005). REM sleep alterations have also been observed in people with subjective cognitive decline, a patient population at risk of developing AD related dementia (Liguori et al., 2020). In addition, a longitudinal follow up study in patients who converted from MCI to AD-related dementia reported reduced REM sleep (Carnicelli et al., 2019), demonstrating that reduced time spent in REM is associated with a higher risk of developing dementia (Pase et al., 2017). Aforementioned results imply that alterations in REM sleep also occur early in human AD, often in the absence of NREM disturbances which is thought to be the result of degeneration of cholinergic neurons (Kerbler et al., 2015; Romanella et al., 2021). Interestingly, REM sleep seems to be relatively preserved during normal aging.

7.4 Behavioral states, brain states and neurotransmitter systems and AD

In this thesis, we investigated network function using rsfMRI and electrophysiology during different behavioral states; NREM sleep, REM sleep, exploration, wake immobility and under anesthesia. We observed network impairments at the pre-plaque stage mainly during REM sleep, wake immobility and under anesthesia. The network activity during NREM sleep and wake immobility was less affected during the pre-plaque stage. Moreover, hippocampal, and cortical network activity during REM sleep and anesthesia was partially recovered in the early-plaque stage in TgF344-AD rats.

However, we did observe altered hippocampal activity during NREM sleep mainly at the early-plaque stage, suggesting differential effects of behavioral state on network activity. The different states of arousal are tightly controlled by the interplay between neuromodulatory systems. The interplay of the noradrenergic and cholinergic system has been demonstrated to be important for a variety of cognitive functions such as attention, learning and decision making (Slater, Liu, Weiss, Yu, & Wang, 2022). Moreover, these systems have been demonstrated to be affected at early stages of AD.

7.4.1 Integrated and segregated states, different neuromodulatory systems and AD

The brain must integrate a wide range of incoming stimuli from its environment and use this stream of complex information into representations which are used to plan the next action (Shine, 2019). To facilitate this, it is important that several brain regions are connected to each other and work together. But excessive integration, such as during an epileptic seizure when a large number of brain areas activate in synchrony, results in the incapability of the brain to process information in a meaningful way. The capacity for integration is undeniably important for survival, however, the brain must also be able to segregate information into distinct modules, which perform specialized computations. This allows the brain to perform for example difficult cognitive tasks. If there would be no segregation, signals tend to become noisy, limiting the ability of the brain to perform certain cognitive tasks. A proper balance between segregated and integrated brain states is crucial for cognitive function (J. R. Cohen & D'Esposito, 2016). Understanding these dynamics has important clinical implications, as the ability to segregate and/or integrate information is impaired in several neurological disorders, including in AD (Lord, Stevner, Deco, & Kringelbach, 2017; Shappell et al., 2021).

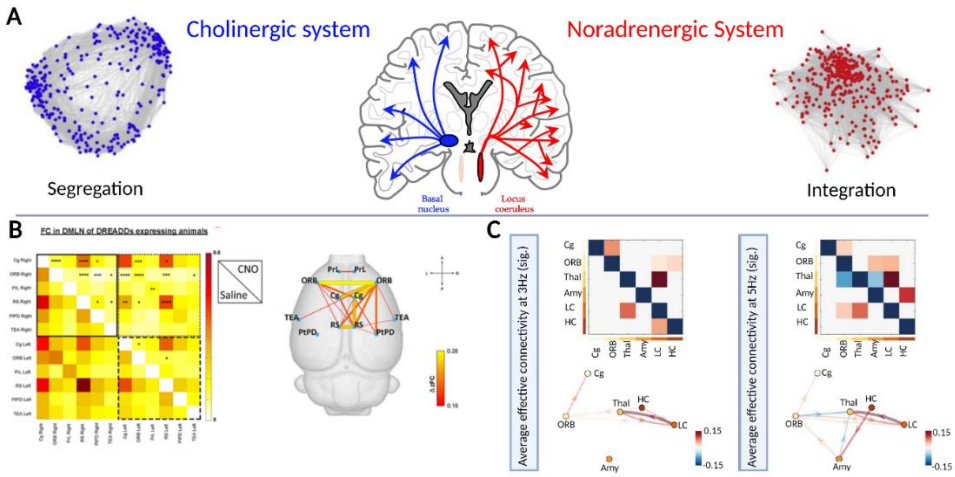

Figure 7-4: The role of the cholinergic system and noradrenergic system in segregation and integration. A) Projections originating from the cholinergic system (blue) demonstrate a high topology and innervate well defined regions with a specific function, suggesting a more segregated structure. On the other hand, the noradrenergic projections (red) from the locus coeruleus (LC) target regions with different functions, promoting integration. B) FC decreased in the DMLN upon activation of basal forebrain cholinergic neurons, supporting the segregating influence of cholinergic activation. C) Effective connectivity, a measure for directed FC, increases upon phasic stimulation of the LC, demonstrating the integrating role of noradrenergic signaling. Cg = cingulate cortex, ORB = orbitofrontal cortex, PrL = prelimbic cortex, TeA = temporary association cortex, PtPD = parietal cortex, Thal = thalamus, Amy = amygdala, HC = hippocampus. Figure adapted from (Grimm et al., 2022; Peeters, van den Berg, et al., 2020; Shine, 2019).

In neuroscience, integration and segregation network measures are primarily based on graph theory metrics, which define a network as a set of nodes and edges between the nodes. In practice, these nodes usually represent EEG electrodes, MEG channels or regions of interest derived from functional or structural MRI scans. Measures of segregation are based on the concepts of clustering coefficients and modularity. The clustering coefficient of a node is determined by the ratio of the number of actual connections with the direct neighbors and the total number of possible connections between the neighbors. A connection is present when there is a significant FC between to nodes. The clustering coefficient provides information about the efficiency of

information transfer which is represented with a high clustering coefficient. Modularity is an important measure for the level of segregation. Modularity is described by the number of connections within groups, minus the expected number of connections in an equivalent network with random connections. High modularity value indicates that each module contains several densely interconnected nodes, but only few connections exist between different modules (M. E. Newman, 2006) (Figure 7-4A). Instead, measuring the integration of a network is commonly based on the average minimum number of connections that link two nodes, the so-called characteristic path length. Short path lengths indicate a high degree of integration. Another measure of high integration is a nodal degree which states the number of edges that is linked to a particular node (Figure 7-4A) (Dai & He, 2014). These metrics have been extensively used to investigate brain function in health and disease.

Recent advances have implicated that the noradrenergic LC and cholinergic BFB regulate the amount of segregation and integration to promote cognitive and attentional function (Grimm et al., 2022; Shine, 2019). High levels of NA have been associated with exploratory behavior and cognitive flexibility when shifting between tasks, while ACh is typically associated with attentional selection and specific cognitive tasks (Aston-Jones & Cohen, 2005; Noudoost & Moore, 2011; Yu & Dayan, 2005). Therefore, researchers hypothesize that NA promotes integration, while ACh promotes segregation. This principle is reflected in the neuroanatomy of the NA and ACh system (Figure 7-4A). Projections from the LC typically cross multisensory boundaries, which allows coordination of activity between otherwise separated regions of the brain (Fuxe et al., 2010). In contrast, the cholinergic neurons in the BFB show a high degree of topology, where specific neurons in the BFB innervate specific cortical regions, promoting segregation (Bloem, Schoppink, et al., 2014; Markello, Spreng, Luh, Anderson, & De Rosa, 2018; Zaborszky et al., 2015). Moreover, the role of the LC in integration is confirmed by a recent study that demonstrated that stimulation of the LC changes the activity and connectivity in neuronal networks. Increased firing in the LC was observed to enhance network integration, demonstrated by increased effective connectivity

between different nodes after phasic LC stimulation (Figure 7-4C) (Grimm et al., 2022). In line with this, we observed in chapter 6 that activation of cholinergic neurons in the BFB promotes segregation as we observed decreased FC in the DMLN (Figure 7-4B) (Peeters, van den Berg, et al., 2020).

AD affects both the noradrenergic as the cholinergic system and is associated with alterations in network function already at early stages of the disease. Recent advances have tried to investigate how the level of integration and segregation in brain networks is affected across the AD spectrum. Early rsfMRI studies in MCI and AD patients observed decreased global network efficiency, demonstrated by increased characteristic path lengths, suggestive of disrupted integration in AD, which progresses with disease severity (Dai & He, 2014; Y. Liu et al., 2014; Z. Liu et al., 2012; Zhao et al., 2012). In addition, two studies showed increased segregation as demonstrated by increased modularity (Z. Liu et al., 2012; Zhao et al., 2012). However, the majority of the studies observed signs of disrupted segregation (Brier, Thomas, Fagan, et al., 2014; G. Chen et al., 2013; J. R. Cohen & D'Esposito, 2016; Y. Li, Qin, Chen, & Li, 2013; Supekar, Menon, Rubin, Musen, & Greicius, 2008). This discrepancy could be explained by differences in AD severity, since the studies that observed increased segregation included patients with a more severely impaired cognition, compared to the studies which observed disrupted segregation (Dai & He, 2014). This discrepancy shows that the network function at different stages of AD shows different characteristics. A recent study investigated these properties in cognitively healthy people carrying the PS1 mutation, which are thought to develop early-onset AD dementia over the next decade. They observed a decreased functional segregation compared to healthy controls without genetic predisposition for AD in the DMN. Moreover, increased integration and functional segregation was observed in regions belonging to the salience network. In turn, they show that a greater tau burden was associated with increased integrated and segregated connectivity in the cingulate cortex and retrosplenial cortex (Guzman-Velez et al., 2022). These results suggest alterations in integration and segregation of functional network occurs already before cognitive symptoms are present. Performing

similar type of analyses to evaluate functional integration and segregation in the TgF344-AD rats would be interesting to identify possible disease mechanisms and to gain further insights into network dysfunction at pre- and early-plaque stages of AD.

7.4.2 The medetomidine-isoflurane anesthetized brain

To limit animal discomfort and motion during MRI scanning procedures, animals are lightly sedated. A variety of anesthesia protocols for laboratory animals are available and several studies have investigated the effects of different anesthetic agents on BOLD activity and functional connectivity (FC). Recent studies have demonstrated that the FC under a combination of 0.4% Isoflurane and medetomidine anesthesia moderately mimics the FC in awake animals and results in high quality rsfMRI scans (Joanes Grandjean et al., 2022; Paasonen et al., 2018; Steiner, Rousseau-Blass, Schroeter, Hartnack, & Bettschart-Wolfensberger, 2021). In both rsfMRI studies described in chapter 3 and 6, this combination of anesthesia was used. Isoflurane is a GABA receptor agonist which are widely distributed in the cerebral cortex, hippocampus, basal ganglia, thalamus, brainstem, and cerebellum. Isoflurane induces anesthesia and a burst suppression like activity pattern, consisting of alternating epochs of silenced cortical activity and periods with high amplitude sharp waves (Ferron, Kroeger, Chever, & Amzica, 2009). Medetomidine is an α2-adrenoreceptor agonist and mediates sedation through activation of these α2-adrenergic receptors which are located throughout the central nervous system. Medetomidine binds to the α2-adrenergic receptors and thereby inhibits the pre-synaptic release of noradrenaline, resulting in sedation and muscle relaxation.

This medetomidine-isoflurane anesthetized state with a low noradrenergic but normal/high cholinergic tone, is very similar to the brain state during REM sleep (Table 1-1). This is further confirmed by the desynchronized cortical and hippocampal EEG/LFP activity which is observed during medetomidine-isoflurane anesthesia, where delta and theta frequencies are dominating (Itamoto et al., 2002; Xi et al., 2018). This could partially explain the high similarity between the QPP findings in chapter 3 and the REM-

sleep disturbances in chapter 4, where we observed altered network activity at the pre-plaque stage and (partial) restoration of network activity during the early-plaque stage, using different experimental techniques that measure neuronal activity.

One major limitation of using medetomidine is the fact that by shutting down the noradrenergic system, you ameliorate the effects of AD related disruptions of noradrenergic signaling on brain activity (Zerbi et al., 2019). This is a severe limitation given the important role of the noradrenergic system in the modulation of cortical activity and its involvement during early stages of AD. We have demonstrated that pTau accumulation was present in the LC of 6-month-old TgF344-AD rats and recent studies observed decreased noradrenergic innervation of the hippocampus and altered noradrenergic signaling at this age (A. M. Goodman et al., 2021). Future studies using anesthetic agents with different mechanisms of action, or studies in awake rats, would be valuable to evaluate the noradrenergic system and its role in network activity in TgF344-AD rats at pre- and early-plaque stages of AD.

7.4.3 Hippocampal function during different behavioral states in AD

One of the aims was to evaluate how hippocampal network function was affected during different behavioral states at the pre- and early-plaque stages of AD. In chapter 5 we evaluated hippocampal activity while the animals were exploring a novel environment. When an animal moves through the environment, pyramidal cells in the hippocampus CA1 area fire in a location-specific manner. The firing sequences of these cells during running behavior are re-expressed at an accelerated rate during subsequent slow-wave sleep (Kudrimoti, Barnes, & McNaughton, 1999; A. K. Lee & Wilson, 2002) or wake immobility (Diba & Buzsaki, 2007). This “replay” of neuronal activity co-occurs with SWR, which are the hallmark of memory replay observed mainly during wake immobility and NREM sleep. We observed decreased duration of SWR during wake immobility. However, in chapter 4 we observed a significantly longer SWR duration in TgF344-AD rats during NREM sleep, irrespective of age. These conflicting results could in part be explained by the influence of behavioral state on SWRs. SWRs appear to have different

functions, dependent on the behavioral state. During wake immobility, SWRs represent the rapid retrieval of previous experiences to aid in memory-guided decision making, while during NREM sleep, SWRs support memory consolidation (Roumis & Frank, 2015). This difference in function is also reflected in differences in generation/regulation of SWRs. Silencing of the CA3 region affects both ripples during wake immobility and during NREM, demonstrating that input from the CA3 is crucial for the generation of SWR, independent of behavioral state (Yamamoto & Tonegawa, 2017). The medial entorhinal cortex (mEnt) is the major input of somatosensory information to the hippocampus (Axmacher et al., 2008; Igarashi et al., 2014). Disruption of entorhinal signalling has been demonstrated to decrease SWR duration during wake immobility, but not during NREM sleep (Oliva et al., 2018; Yamamoto & Tonegawa, 2017), suggesting that entorhinal signalling is not crucial for ripple generation during NREM. Moreover, differences in neuromodulatory systems during wake immobility and NREM sleep could result in apparent conflicting differences in SWR activity.

When animals are moving around and memorizing new locations, theta oscillations are prominently present throughout the hippocampus and have been associated with online spatial memory consolidation (Bland & Oddie, 2001; Buzsaki et al., 2003; Buzsaki & Tingley, 2018; Colgin, 2016). In animals, theta oscillations can be divided into two types, type I, or atropine insensitive theta (8-12 Hz) which are dominant during exploration and type II, or atropine sensitive theta (4-9 Hz), which are dominant during wake immobile (Buzsaki, 2002; Z. Gu & Yakel, 2022; Kramis et al., 1975). In chapter 5 we observed a decreased power of type I theta oscillations, mainly during exploration, in 4-month old TgF344-AD rats, which is in accordance to findings at later stages in the TgF344-AD rats (Stoiljkovic et al., 2019). Several studies have demonstrated that theta rhythm in the CA1 layer of the hippocampus during exploration is partially driven by excitation of CA1 pyramidal cells as a result of excitatory input from the perforant pathway originating from the entorhinal cortex. Inactivation of this pathway has been demonstrated to attenuate the power of the theta rhythm, similar to what is observed in chapter 5, suggesting impairment of the trisynaptic pathway during the pre-plaque stages of AD in

TgF344-AD rats. This is in accordance with findings from another study which showed in TgF344-AD rats at 6 months of age that synaptic transmission between the mEnt and dentate gyrus (DG) was disrupted (Smith et al., 2022; Smith & McMahon, 2018). As described before, we observed shorter SWR duration in TgF344-AD rats during wake immobility, further suggesting impaired entorhinal signalling to the hippocampus. Altogether, the aforementioned result suggest early impairment of the medial perforant pathway during pre-plaque stages of AD in TgF344-AD rats, which alters hippocampal neuronal activity. The cholinergic sprouting during the early-plaque stage observed in chapter 4 could be a compensatory mechanism to counteract the imbalance caused by disruption of the input originating from the medial Ent (Bott et al., 2016), since cholinergic signalling has been shown to be an important modulator of several hippocampal oscillations (Buzsaki & Tingley, 2018; Colgin, 2016).

7.5 Functional compensation in AD

In chapter 4 we observed alterations in REM sleep bout length and several electrophysiological properties of hippocampal local field potentials during the pre-plaque stage of AD (Figure 7-4). At the early-plaque stage, a paradoxical increase in cholinergic synapses was observed (Figure 7-4). This increase in cholinergic synaptic density, so-called cholinergic sprouting, coincided with a restoration of REM bout length, neuronal activity and network function in the hippocampus, phenomena which are under tight control of the cholinergic system. These cholinergic synapses, which partially compensate for AD related network dysfunction, are from neurons originating from the BFB, suggesting an important role of the BFB in compensation of network function during the early-plaque stage of AD.

Cholinergic sprouting is a common phenomenon observed after glutamatergic lesioning of the mEnt, resulting in a loss of glutamatergic input to the hippocampus (Bott et al., 2016; Naumann et al., 1997). This in turn has been demonstrated to induce hyperexcitability in several hippocampal regions, including the DG and CA1 layer (Naumann et al., 1997). Recent studies have demonstrated that the increase in

cholinergic innervation compensates for network hyperactivity, which has been associated with recovery of spatial memory (Bott et al., 2016; Traissard et al., 2007). Interestingly, similar increases in cholinergic synapses in the hippocampus have been observed in MCI patients (DeKosky et al., 2002). The medial Ent is affected by tauopathy and amyloid pathology already at early stages of AD. A study in APOE E4 mice, one of the main known genetic risk factors for AD, has demonstrated that cholinergic sprouting was impaired after glutamatergic lesioning, speeding up disease progression in APOE E4 mice compared to APOE E3 mice (Bott et al., 2016). This suggests that the cholinergic sprouting is an important early compensation mechanism which slows down disease progression, by restoring the network imbalance. However, in AD, network imbalances only worsen during disease progression. Moreover, cholinergic neurons will also be affected at early stages of AD, further hampering the ability to compensate for network imbalances (Bott et al., 2016; L. Hu et al., 2003).

One question that remains is if this basal forebrain compensatory mechanism which partially restored hippocampal function is also, in part, responsible for the restoration of whole brain network activity observed in the QPPs? In chapter 3 we did not observe increased numbers of cholinergic synapses in the cortical regions, however as described in the discussion, this doesn't exclude molecular alterations in cholinergic signaling. It would be interesting to perform an experiment in 4-month old TgF344-AD rats, where cholinergic stimulation is performed, to evaluate if network function is restored upon an increased concentration of ACh. This could provide insights into the disease mechanisms underlying the network alterations at the pre-plaque stage and would strengthen the hypothesis that cholinergic mechanisms are contributing to the restoration of whole brain network activity at the early-plaque stage.

7.6 Modulation of neuronal activity in AD and the role of chemogenetics

In this thesis we prove that network function is already altered at pre-plaque stages of the disease in TgF344-AD rats, and we observed that the basal forebrain cholinergic

system is partially compensating for the observed network disturbances during the early-plaque stage. Several studies have demonstrated that imbalanced neuronal activity is driving AD progression, which in turn has led to the hypothesis that restoring these network imbalances at early stages of the disease would be a valuable therapeutic strategy to slow down or stop the disease progression (Busche et al., 2015; Palop & Mucke, 2016; Styr & Slutsky, 2018). The current therapeutic strategies include pharmacological manipulation of neurotransmitter concentrations in the brain, by using acetylcholinesterase inhibitors which increase cholinergic signaling and NMDA receptor antagonists to reduce glutamatergic signaling. These therapeutics have been demonstrated to alleviate cognitive symptoms and temporarily slow down disease progression, however, only a small number of AD patients benefit from the temporary treatment effects (Arai et al., 2016; Samadi et al., 2013). The severity of AD and the lack of disease-modifying therapeutics have motivated research to develop of non-drug-based therapies to modify neuronal activity.

One of the most successful neuromodulatory approaches is deep brain stimulation (DBS), where an electrode is chronically implanted in a brain region of interest and stimulated by an internal pacemaker to counteract abnormal neuronal activity (Temel & Jahanshahi, 2015). This technique has been successfully used since the 1993 in patients suffering from Parkinson's disease and since then has also been applied in other neurological and psychiatric disorders such as Tourette's syndrome and obsessive-compulsive disorder (Hamani & Temel, 2012). This approach is currently also under investigation in AD, where DBS is applied in the fornix or the NBM. Several preclinical and clinical studies have demonstrated that fornix stimulation improved hippocampus-dependent memory and cognition (for a review (R. Li, Zhang, Rao, & Yuan, 2022). For example, a recent study in aged TgF344-AD rats has demonstrated that chronic fornix stimulation which lasted 5 weeks, reduced amyloidosis, inflammation, and neuronal loss in both the cortex and hippocampus, suggesting a neuroprotective effect of DBS. A relatively large-scale international phase II trial, the Advance I study, confirmed safety of fornix DBS in patients with mild AD. Currently, a large follow up phase IIb/III study is

ongoing to evaluate the long-term effects of DBS on AD related symptoms and neuropathological hallmarks (Jakobs, Lee, & Lozano, 2020; Luo et al., 2021). DBS of the NBM has also demonstrated to have beneficial effects on cognition in animal models for AD and in patients with mild AD (Jafari et al., 2020; Jakobs et al., 2020; Koulousakis, van den Hove, Visser-Vandewalle, & Sesia, 2020; Temel & Jahanshahi, 2015). These results suggest that DBS might be a promising therapeutic strategy to alleviate symptoms and to alter disease progression, however, clinical trials with larger sample sizes are necessary to evaluate efficacy and possible side effects. Moreover, it would be interesting to evaluate the effects of starting DBS at earlier timepoints in the disease, to investigate if the disease progression is effectively altered.

In chapter 6 we have used chemogenetic tools to modulate the activity of specific neuronal populations in the BFB. This technique requires stereotactic intracranial injection of a viral vector containing the gene encoding for DREADDs. This technique offers several advantages with respect to DBS, as it allows targeting of specific neuronal subpopulations. However, in the past and in chapter 6, this neuron-type specificity in animal research was achieved by using transgenic animal lines, which is not possible in humans. Future research should focus on methods or viral vectors that allow neuron-type specific targeting of specific neuronal populations. Another limitation of this technique in the translation to humans is the need to use viral vectors, which could have harmful side effects. Moreover, effects of long-term stimulation of DREADDs has been relatively unexplored, and further research is necessary. But all these considerations regarding translational potential of DREADDs in humans doesn't mean that this technology cannot be beneficial in the development of novel therapeutic strategies. These chemogenetic tools offer opportunities to researchers to enhance their knowledge of the brain in health and in disease. And this new knowledge could eventually drive the progress of future therapies for patients with AD.

7.7 The role of MRI in the detection of presymptomatic AD

As described in the introduction, rsfMRI studies using traditional static FC measures could already detect early alterations in network activity in mouse models of AD, before amyloid plaques were observed in the brain. However, the alterations observed were not specific for AD, as similar observations have been observed in other neurodegenerative diseases. This limited the use of static FC as a biomarker for early synaptic dysfunction in AD. In this thesis, rsfMRI with QPP analysis was performed in a rat model of AD, to investigate network dysfunction at the pre-plaque stage. QPP analysis revealed for the first time in an animal model of AD, a disconnection between the BFB and the DMLN together with a decreased involvement of these regions during recurrent patterns of brain activity. Moreover, the leading role of the BFB in whole brain network activity was lost in TgF344-AD rats, suggesting BFB impairment during early stages of AD in TgF344-AD rats (Figure 7-4). The disconnection between the BFB and DMLN might be specific to AD, since the BFB has been implicated to be affected very early in the disease. However, further validation of these findings in other rodent models of AD and in patient population at risk, for example people with a dominant genetic predisposition who will develop dementia in 10 years, are necessary to evaluate QPPs as an early biomarker for AD.

The question that immediately arises is how can we use rsfMRI QPPs in the diagnosis of presymptomatic AD? Is it feasible to perform regular MRI scans on the entire population above a certain age to detect presymptomatic AD? Currently, scanning time is limited on clinical MRI scanners, suggesting that the feasibility is very low. This does not necessarily mean that the accessibility of MRI will not improve over the next decades, but for now scanning the entire population seems not possible. In a first phase, young people at risk of developing AD, such as carriers of the genetic mutations (e.g., APP mutations), could be included in trials to evaluate the use of QPPs to assess AD related pathology at early, presymptomatic stages. The aim would be to investigate the presence of QPP alterations in people who will develop AD in the next 20 years. The findings proposed in chapter 3 could be very valuable for future clinical trials, as a

therapeutic biomarker, to evaluate the effects of disease modifying therapies. In addition, the findings in chapter 6 support the possible use of MRI as a therapeutic biomarker, as rsfMRI was able to detect the circuit specific effects of cholinergic modulation.

8. References

Abbas, A., Bassil, Y., & Keilholz, S. (2019). Quasi-periodic patterns of brain activity in individuals with attention-deficit/hyperactivity disorder. *Neuroimage Clin, 21*, 101653. doi:10.1016/j.nicl.2019.101653

Abbas, A., Belloy, M., Kashyap, A., Billings, J., Nezafati, M., Schumacher, E. H., & Keilholz, S. (2019). Quasi-periodic patterns contribute to functional connectivity in the brain. *Neuroimage, 191*, 193-204. doi:10.1016/j.neuroimage.2019.01.076

Adamantidis, A. R., Zhang, F., Aravanis, A. M., Deisseroth, K., & de Lecea, L. (2007). Neural substrates of awakening probed with optogenetic control of hypocretin neurons. *Nature, 450*(7168), 420-424. doi:10.1038/nature06310

Aisen, P. S., Cummings, J., Jack, C. R., Jr., Morris, J. C., Sperling, R., Frolich, L., . . . Dubois, B. (2017). On the path to 2025: understanding the Alzheimer's disease continuum. *Alzheimers Res Ther, 9*(1), 60. doi:10.1186/s13195-017-0283-5

Aivar, P., Valero, M., Bellistri, E., & Menendez de la Prida, L. (2014). Extracellular calcium controls the expression of two different forms of ripple-like hippocampal oscillations. *J Neurosci, 34*(8), 2989-3004. doi:10.1523/JNEUROSCI.2826-13.2014

Alexander, G. M., Rogan, S. C., Abbas, A. I., Armbruster, B. N., Pei, Y., Allen, J. A., . . . Roth, B. L. (2009). Remote control of neuronal activity in transgenic mice expressing evolved G protein-coupled receptors. *Neuron, 63*(1), 27-39. doi:10.1016/j.neuron.2009.06.014

Alger, B. E., Nagode, D. A., & Tang, A. H. (2014). Muscarinic cholinergic receptors modulate inhibitory synaptic rhythms in hippocampus and neocortex. *Front Synaptic Neurosci, 6*, 18. doi:10.3389/fnsyn.2014.00018

Allen, E. A., Erhardt, E. B., Damaraju, E., Gruner, W., Segall, J. M., Silva, R. F., . . . Calhoun, V. D. (2011). A baseline for the multivariate comparison of resting-state networks. *Front Syst Neurosci, 5*, 2. doi:10.3389/fnsys.2011.00002

Alves, P. N., Foulon, C., Karolis, V., Bzdok, D., Margulies, D. S., Volle, E., & Thiebaut de Schotten, M. (2019). An improved neuroanatomical model of the default-mode network reconciles previous neuroimaging and neuropathological findings. *Commun Biol, 2*, 370. doi:10.1038/s42003-019-0611-3

Alwatban, M., Murman, D. L., & Bashford, G. (2019). Cerebrovascular Reactivity Impairment in Preclinical Alzheimer's Disease. *J Neuroimaging, 29*(4), 493-498. doi:10.1111/jon.12606

Ammassari-Teule, M. (2020). Neural compensation in presymptomatic hAPP mouse models of Alzheimer's disease. *Learn Mem, 27*(9), 390-394. doi:10.1101/lm.050401.119

Anaclet, C., Pedersen, N. P., Ferrari, L. L., Venner, A., Bass, C. E., Arrigoni, E., & Fuller, P. M. (2015). Basal forebrain control of wakefulness and cortical rhythms. *Nat Commun, 6*, 8744. doi:10.1038/ncomms9744

Anckaerts, C., Blockx, I., Summer, P., Michael, J., Hamaide, J., Kreutzer, C., . . . Van der Linden, A. (2019). Early functional connectivity deficits and progressive microstructural alterations in the TgF344-AD rat model of Alzheimer's Disease:

A longitudinal MRI study. *Neurobiol Dis, 124*, 93-107. doi:10.1016/j.nbd.2018.11.010

Anderson, R. M., Hadjichrysanthou, C., Evans, S., & Wong, M. M. (2017). Why do so many clinical trials of therapies for Alzheimer's disease fail? *Lancet, 390*(10110), 2327-2329. doi:10.1016/S0140-6736(17)32399-1

Andrews-Hanna, J. R., Reidler, J. S., Huang, C., & Buckner, R. L. (2010). Evidence for the default network's role in spontaneous cognition. *J Neurophysiol, 104*(1), 322-335. doi:10.1152/jn.00830.2009

Andrews-Hanna, J. R., Reidler, J. S., Sepulcre, J., Poulin, R., & Buckner, R. L. (2010). Functional-anatomic fractionation of the brain's default network. *Neuron, 65*(4), 550-562. doi:10.1016/j.neuron.2010.02.005

Aoki, S., Liu, A. W., Akamine, Y., Zucca, A., Zucca, S., & Wickens, J. R. (2018). Cholinergic interneurons in the rat striatum modulate substitution of habits. *Eur J Neurosci, 47*(10), 1194-1205. doi:10.1111/ejn.13820

Arai, H., Sumitomo, K., Sakata, Y., Daidoji, K., Takase, T., & Toyoda, T. (2016). Disease state changes and safety of long-term donepezil hydrochloride administration in patients with Alzheimer's disease: interim results from the long-term, large-scale J-GOLD study in Japan. *Psychogeriatrics, 16*(2), 107-115. doi:10.1111/psyg.12130

Aston-Jones, G., & Cohen, J. D. (2005). An integrative theory of locus coeruleus-norepinephrine function: adaptive gain and optimal performance. *Annu Rev Neurosci, 28*, 403-450. doi:10.1146/annurev.neuro.28.061604.135709

Attwell, D., Mishra, A., Hall, C. N., O'Farrell, F. M., & Dalkara, T. (2016). What is a pericyte? *J Cereb Blood Flow Metab, 36*(2), 451-455. doi:10.1177/0271678X15610340

Avery, M. C., & Krichmar, J. L. (2017). Neuromodulatory Systems and Their Interactions: A Review of Models, Theories, and Experiments. *Front Neural Circuits, 11*, 108. doi:10.3389/fncir.2017.00108

Axmacher, N., Elger, C. E., & Fell, J. (2008). Ripples in the medial temporal lobe are relevant for human memory consolidation. *Brain, 131*(Pt 7), 1806-1817. doi:10.1093/brain/awn103

Babiloni, C., Ferri, R., Binetti, G., Vecchio, F., Frisoni, G. B., Lanuzza, B., . . . Rossini, P. M. (2009). Directionality of EEG synchronization in Alzheimer's disease subjects. *Neurobiol Aging, 30*(1), 93-102. doi:10.1016/j.neurobiolaging.2007.05.007

Badhwar, A., Tam, A., Dansereau, C., Orban, P., Hoffstaedter, F., & Bellec, P. (2017). Resting-state network dysfunction in Alzheimer's disease: A systematic review and meta-analysis. *Alzheimers Dement (Amst), 8*, 73-85. doi:10.1016/j.dadm.2017.03.007

Bakker, A., Albert, M. S., Krauss, G., Speck, C. L., & Gallagher, M. (2015). Response of the medial temporal lobe network in amnestic mild cognitive impairment to therapeutic intervention assessed by fMRI and memory task performance. *Neuroimage Clin, 7*, 688-698. doi:10.1016/j.nicl.2015.02.009

Ballinger, E. C., Ananth, M., Talmage, D. A., & Role, L. W. (2016). Basal Forebrain Cholinergic Circuits and Signaling in Cognition and Cognitive Decline. *Neuron, 91*(6), 1199-1218. doi:10.1016/j.neuron.2016.09.006

Bankhead, P., Loughrey, M. B., Fernandez, J. A., Dombrowski, Y., McArt, D. G., Dunne, P. D., . . . Hamilton, P. W. (2017). QuPath: Open source software for digital pathology image analysis. *Sci Rep, 7*(1), 16878. doi:10.1038/s41598-017-17204-5

Bartolomeo, P., Thiebaut de Schotten, M., & Chica, A. B. (2012). Brain networks of visuospatial attention and their disruption in visual neglect. *Front Hum Neurosci, 6*, 110. doi:10.3389/fnhum.2012.00110

Basar, E. (2013). A review of gamma oscillations in healthy subjects and in cognitive impairment. *Int J Psychophysiol, 90*(2), 99-117. doi:10.1016/j.ijpsycho.2013.07.005

Bauer, M., Buckley, M. G., & Bast, T. (2021). Individual differences in theta-band oscillations in a spatial memory network revealed by electroencephalography predict rapid place learning. *Brain and Neuroscience Advances, 5*, 23982128211002725. doi:10.1177/23982128211002725

Bazzigaluppi, P., Beckett, T. L., Koletar, M. M., Lai, A. Y., Joo, I. L., Brown, M. E., . . . Stefanovic, B. (2018). Early-stage attenuation of phase-amplitude coupling in the hippocampus and medial prefrontal cortex in a transgenic rat model of Alzheimer's disease. *J Neurochem, 144*(5), 669-679. doi:10.1111/jnc.14136

Bell, K. F., Bennett, D. A., & Cuello, A. C. (2007). Paradoxical upregulation of glutamatergic presynaptic boutons during mild cognitive impairment. *J Neurosci, 27*(40), 10810-10817. doi:10.1523/JNEUROSCI.3269-07.2007

Belloy, M. E., Billings, J., Abbas, A., Kashyap, A., Pan, W. J., Hinz, R., . . . Keliris, G. A. (2021). Resting Brain Fluctuations Are Intrinsically Coupled to Visual Response Dynamics. *Cereb Cortex, 31*(3), 1511-1522. doi:10.1093/cercor/bhaa305

Belloy, M. E., Naeyaert, M., Abbas, A., Shah, D., Vanreusel, V., van Audekerke, J., . . . Verhoye, M. (2018). Dynamic resting state fMRI analysis in mice reveals a set of Quasi-Periodic Patterns and illustrates their relationship with the global signal. *Neuroimage, 180*(Pt B), 463-484. doi:10.1016/j.neuroimage.2018.01.075

Belloy, M. E., Shah, D., Abbas, A., Kashyap, A., Rossner, S., Van der Linden, A., . . . Verhoye, M. (2018). Quasi-Periodic Patterns of Neural Activity improve Classification of Alzheimer's Disease in Mice. *Sci Rep, 8*(1), 10024. doi:10.1038/s41598-018-28237-9

Belluscio, M. A., Mizuseki, K., Schmidt, R., Kempter, R., & Buzsaki, G. (2012). Cross-frequency phase-phase coupling between theta and gamma oscillations in the hippocampus. *J Neurosci, 32*(2), 423-435. doi:10.1523/JNEUROSCI.4122-11.2012

Ben-Nejma, I. R. H., Keliris, A. J., Daans, J., Ponsaerts, P., Verhoye, M., Van der Linden, A., & Keliris, G. A. (2019). Increased soluble amyloid-beta causes early aberrant brain network hypersynchronisation in a mature-onset mouse model of amyloidosis. *Acta Neuropathol Commun, 7*(1), 180. doi:10.1186/s40478-019-0810-7

Benthem, S. D., Skelin, I., Moseley, S. C., Stimmell, A. C., Dixon, J. R., Melilli, A. S., . . . Wilber, A. A. (2020). Impaired Hippocampal-Cortical Interactions during Sleep

in a Mouse Model of Alzheimer's Disease. *Curr Biol, 30*(13), 2588-2601 e2585. doi:10.1016/j.cub.2020.04.087

Bergmann, T. O., & Born, J. (2018). Phase-Amplitude Coupling: A General Mechanism for Memory Processing and Synaptic Plasticity? *Neuron, 97*(1), 10-13. doi:10.1016/j.neuron.2017.12.023

Berkowitz, L. E., Harvey, R. E., Drake, E., Thompson, S. M., & Clark, B. J. (2018). Progressive impairment of directional and spatially precise trajectories by TgF344-Alzheimer's disease rats in the Morris Water Task. *Sci Rep, 8*(1), 16153. doi:10.1038/s41598-018-34368-w

Bernaud, V. E., Bulen, H. L., Pena, V. L., Koebele, S. V., Northup-Smith, S. N., Manzo, A. A., . . . Bimonte-Nelson, H. A. (2022). Task-dependent learning and memory deficits in the TgF344-AD rat model of Alzheimer's disease: three key timepoints through middle-age in females. *Sci Rep, 12*(1), 14596. doi:10.1038/s41598-022-18415-1

Bernhardt, B. C., Smallwood, J., Keilholz, S., & Margulies, D. S. (2022). Gradients in brain organization. *Neuroimage, 251*, 118987. doi:10.1016/j.neuroimage.2022.118987

Bi, D., Wen, L., Wu, Z., & Shen, Y. (2020). GABAergic dysfunction in excitatory and inhibitory (E/I) imbalance drives the pathogenesis of Alzheimer's disease. *Alzheimers Dement, 16*(9), 1312-1329. doi:10.1002/alz.12088

Bieri, K. W., Bobbitt, K. N., & Colgin, L. L. (2014). Slow and fast gamma rhythms coordinate different spatial coding modes in hippocampal place cells. *Neuron, 82*(3), 670-681. doi:10.1016/j.neuron.2014.03.013

Billings, J. C. W., Medda, A., Shakil, S., Shen, X., Kashyap, A., Chen, S., . . . Keilholz, S. D. (2017). Instantaneous brain dynamics mapped to a continuous state space. *Neuroimage, 162*, 344-352. doi:10.1016/j.neuroimage.2017.08.042

Bishop, G. M., & Robinson, S. R. (2004). The amyloid paradox: amyloid-beta-metal complexes can be neurotoxic and neuroprotective. *Brain Pathol, 14*(4), 448-452. doi:10.1111/j.1750-3639.2004.tb00089.x

Bland, B. H., & Oddie, S. D. (2001). Theta band oscillation and synchrony in the hippocampal formation and associated structures: the case for its role in sensorimotor integration. *Behav Brain Res, 127*(1-2), 119-136. doi:10.1016/s0166-4328(01)00358-8

Bloem, B., Poorthuis, R. B., & Mansvelder, H. D. (2014). Cholinergic modulation of the medial prefrontal cortex: the role of nicotinic receptors in attention and regulation of neuronal activity. *Front Neural Circuits, 8*, 17. doi:10.3389/fncir.2014.00017

Bloem, B., Schoppink, L., Rotaru, D. C., Faiz, A., Hendriks, P., Mansvelder, H. D., . . . Wouterlood, F. G. (2014). Topographic mapping between basal forebrain cholinergic neurons and the medial prefrontal cortex in mice. *J Neurosci, 34*(49), 16234-16246. doi:10.1523/JNEUROSCI.3011-14.2014

Bott, J. B., Heraud, C., Cosquer, B., Herbeaux, K., Aubert, J., Sartori, M., . . . Mathis, C. (2016). APOE-Sensitive Cholinergic Sprouting Compensates for Hippocampal Dysfunctions Due to Reduced Entorhinal Input. *J Neurosci, 36*(40), 10472-10486. doi:10.1523/JNEUROSCI.1174-16.2016

Bourgin, P., Huitron-Resendiz, S., Spier, A. D., Fabre, V., Morte, B., Criado, J. R., . . . de Lecea, L. (2000). Hypocretin-1 modulates rapid eye movement sleep through activation of locus coeruleus neurons. *J Neurosci, 20*(20), 7760-7765. Retrieved from https://www.ncbi.nlm.nih.gov/pubmed/11027239
https://www.ncbi.nlm.nih.gov/pmc/articles/PMC6772862/pdf/ns007760.pdf

Bouwman, F. H., Frisoni, G. B., Johnson, S. C., Chen, X., Engelborghs, S., Ikeuchi, T., . . . Teunissen, C. (2022). Clinical application of CSF biomarkers for Alzheimer's disease: From rationale to ratios. *Alzheimers Dement (Amst), 14*(1), e12314. doi:10.1002/dad2.12314

Braak, H., & Braak, E. (1991). Neuropathological stageing of Alzheimer-related changes. *Acta Neuropathol, 82*(4), 239-259. doi:10.1007/BF00308809

Braak, H., Thal, D. R., Ghebremedhin, E., & Del Tredici, K. (2011). Stages of the pathologic process in Alzheimer disease: age categories from 1 to 100 years. *J Neuropathol Exp Neurol, 70*(11), 960-969. doi:10.1097/NEN.0b013e318232a379

Bragin, A., Jando, G., Nadasdy, Z., Hetke, J., Wise, K., & Buzsaki, G. (1995). Gamma (40-100 Hz) oscillation in the hippocampus of the behaving rat. *J Neurosci, 15*(1 Pt 1), 47-60. Retrieved from https://www.ncbi.nlm.nih.gov/pubmed/7823151

Brayne, C., & Miller, B. (2017). Dementia and aging populations-A global priority for contextualized research and health policy. *PLoS Med, 14*(3), e1002275. doi:10.1371/journal.pmed.1002275

Brier, M. R., Thomas, J. B., & Ances, B. M. (2014). Network dysfunction in Alzheimer's disease: refining the disconnection hypothesis. *Brain Connect, 4*(5), 299-311. doi:10.1089/brain.2014.0236

Brier, M. R., Thomas, J. B., Fagan, A. M., Hassenstab, J., Holtzman, D. M., Benzinger, T. L., . . . Ances, B. M. (2014). Functional connectivity and graph theory in preclinical Alzheimer's disease. *Neurobiol Aging, 35*(4), 757-768. doi:10.1016/j.neurobiolaging.2013.10.081

Brody, D. L., Jiang, H., Wildburger, N., & Esparza, T. J. (2017). Non-canonical soluble amyloid-beta aggregates and plaque buffering: controversies and future directions for target discovery in Alzheimer's disease. *Alzheimers Res Ther, 9*(1), 62. doi:10.1186/s13195-017-0293-3

Brokaw, K., Tishler, W., Manceor, S., Hamilton, K., Gaulden, A., Parr, E., & Wamsley, E. J. (2016). Resting state EEG correlates of memory consolidation. *Neurobiol Learn Mem, 130*, 17-25. doi:10.1016/j.nlm.2016.01.008

Brown, R. E., Basheer, R., McKenna, J. T., Strecker, R. E., & McCarley, R. W. (2012). Control of sleep and wakefulness. *Physiol Rev, 92*(3), 1087-1187. doi:10.1152/physrev.00032.2011

Broyd, S. J., Demanuele, C., Debener, S., Helps, S. K., James, C. J., & Sonuga-Barke, E. J. (2009). Default-mode brain dysfunction in mental disorders: a systematic review. *Neurosci Biobehav Rev, 33*(3), 279-296. doi:10.1016/j.neubiorev.2008.09.002

Brueggen, K., Dyrba, M., Barkhof, F., Hausner, L., Filippi, M., Nestor, P. J., . . . Teipel, S. J. (2015). Basal Forebrain and Hippocampus as Predictors of Conversion to Alzheimer's Disease in Patients with Mild Cognitive Impairment - A Multicenter

DTI and Volumetry Study. *J Alzheimers Dis, 48*(1), 197-204. doi:10.3233/JAD-150063

Bubnys, A., & Tsai, L. H. (2022). Harnessing cerebral organoids for Alzheimer's disease research. *Curr Opin Neurobiol, 72*, 120-130. doi:10.1016/j.conb.2021.10.003

Buckner, R. L., & Carroll, D. C. (2007). Self-projection and the brain. *Trends Cogn Sci, 11*(2), 49-57. doi:10.1016/j.tics.2006.11.004

Buckner, R. L., & DiNicola, L. M. (2019). The brain's default network: updated anatomy, physiology and evolving insights. *Nat Rev Neurosci, 20*(10), 593-608. doi:10.1038/s41583-019-0212-7

Busche, M. A., Chen, X., Henning, H. A., Reichwald, J., Staufenbiel, M., Sakmann, B., & Konnerth, A. (2012). Critical role of soluble amyloid-beta for early hippocampal hyperactivity in a mouse model of Alzheimer's disease. *Proc Natl Acad Sci U S A, 109*(22), 8740-8745. doi:10.1073/pnas.1206171109

Busche, M. A., Kekus, M., Adelsberger, H., Noda, T., Forstl, H., Nelken, I., & Konnerth, A. (2015). Rescue of long-range circuit dysfunction in Alzheimer's disease models. *Nat Neurosci, 18*(11), 1623-1630. doi:10.1038/nn.4137

Busche, M. A., & Konnerth, A. (2015). Neuronal hyperactivity--A key defect in Alzheimer's disease? *Bioessays, 37*(6), 624-632. doi:10.1002/bies.201500004

Buxton, R. B., Wong, E. C., & Frank, L. R. (1998). Dynamics of blood flow and oxygenation changes during brain activation: the balloon model. *Magn Reson Med, 39*(6), 855-864. doi:10.1002/mrm.1910390602

Buzsaki, G. (2002). Theta oscillations in the hippocampus. *Neuron, 33*(3), 325-340. doi:10.1016/s0896-6273(02)00586-x

Buzsaki, G. (2006). *Rhythms of the brain*. Oxford New York: Oxford University Press.

Buzsaki, G. (2015). Hippocampal sharp wave-ripple: A cognitive biomarker for episodic memory and planning. *Hippocampus, 25*(10), 1073-1188. doi:10.1002/hipo.22488

Buzsaki, G., Buhl, D. L., Harris, K. D., Csicsvari, J., Czeh, B., & Morozov, A. (2003). Hippocampal network patterns of activity in the mouse. *Neuroscience, 116*(1), 201-211. doi:10.1016/s0306-4522(02)00669-3

Buzsaki, G., & Tingley, D. (2018). Space and Time: The Hippocampus as a Sequence Generator. *Trends Cogn Sci, 22*(10), 853-869. doi:10.1016/j.tics.2018.07.006

Byron, N., Semenova, A., & Sakata, S. (2021). Mutual Interactions between Brain States and Alzheimer's Disease Pathology: A Focus on Gamma and Slow Oscillations. *Biology (Basel), 10*(8). doi:10.3390/biology10080707

Caccavano, A., Bozzelli, P. L., Forcelli, P. A., Pak, D. T. S., Wu, J. Y., Conant, K., & Vicini, S. (2020). Inhibitory Parvalbumin Basket Cell Activity is Selectively Reduced during Hippocampal Sharp Wave Ripples in a Mouse Model of Familial Alzheimer's Disease. *J Neurosci, 40*(26), 5116-5136. doi:10.1523/JNEUROSCI.0425-20.2020

Canolty, R. T., Edwards, E., Dalal, S. S., Soltani, M., Nagarajan, S. S., Kirsch, H. E., . . . Knight, R. T. (2006). High gamma power is phase-locked to theta oscillations in human neocortex. *Science, 313*(5793), 1626-1628. doi:10.1126/science.1128115

Canolty, R. T., & Knight, R. T. (2010). The functional role of cross-frequency coupling. *Trends Cogn Sci, 14*(11), 506-515. doi:10.1016/j.tics.2010.09.001

Cantero, J. L., Atienza, M., Lage, C., Zaborszky, L., Vilaplana, E., Lopez-Garcia, S., . . . Alzheimer's Disease Neuroimaging, I. (2020). Atrophy of Basal Forebrain Initiates with Tau Pathology in Individuals at Risk for Alzheimer's Disease. *Cereb Cortex, 30*(4), 2083-2098. doi:10.1093/cercor/bhz224

Caravaglios, G., Castro, G., Costanzo, E., Di Maria, G., Mancuso, D., & Muscoso, E. G. (2010). theta power responses in mild Alzheimer's disease during an auditory oddball paradigm: lack of theta enhancement during stimulus processing. *J Neural Transm (Vienna), 117*(10), 1195-1208. doi:10.1007/s00702-010-0488-2

Carnicelli, L., Maestri, M., Di Coscio, E., Tognoni, G., Fabbrini, M., Schirru, A., . . . Bonanni, E. (2019). A longitudinal study of polysomnographic variables in patients with mild cognitive impairment converting to Alzheimer's disease. *J Sleep Res, 28*(5), e12821. doi:10.1111/jsr.12821

Carr, M. F., Jadhav, S. P., & Frank, L. M. (2011). Hippocampal replay in the awake state: a potential substrate for memory consolidation and retrieval. *Nat Neurosci, 14*(2), 147-153. doi:10.1038/nn.2732

Carr, M. F., Karlsson, M. P., & Frank, L. M. (2012). Transient slow gamma synchrony underlies hippocampal memory replay. *Neuron, 75*(4), 700-713. doi:10.1016/j.neuron.2012.06.014

Casagrande, M., Forte, G., Favieri, F., & Corbo, I. (2022). Sleep Quality and Aging: A Systematic Review on Healthy Older People, Mild Cognitive Impairment and Alzheimer's Disease. *Int J Environ Res Public Health, 19*(14). doi:10.3390/ijerph19148457

Chaney, A. M., Lopez-Picon, F. R., Serriere, S., Wang, R., Bochicchio, D., Webb, S. D., . . . Boutin, H. (2021). Prodromal neuroinflammatory, cholinergic and metabolite dysfunction detected by PET and MRS in the TgF344-AD transgenic rat model of AD: a collaborative multi-modal study. *Theranostics, 11*(14), 6644-6667. doi:10.7150/thno.56059

Chaves-Coira, I., Barros-Zulaica, N., Rodrigo-Angulo, M., & Nunez, A. (2016). Modulation of Specific Sensory Cortical Areas by Segregated Basal Forebrain Cholinergic Neurons Demonstrated by Neuronal Tracing and Optogenetic Stimulation in Mice. *Front Neural Circuits, 10*, 28. doi:10.3389/fncir.2016.00028

Chaves-Coira, I., Martin-Cortecero, J., Nunez, A., & Rodrigo-Angulo, M. L. (2018). Basal Forebrain Nuclei Display Distinct Projecting Pathways and Functional Circuits to Sensory Primary and Prefrontal Cortices in the Rat. *Front Neuroanat, 12*, 69. doi:10.3389/fnana.2018.00069

Chen, G., Zhang, H. Y., Xie, C., Chen, G., Zhang, Z. J., Teng, G. J., & Li, S. J. (2013). Modular reorganization of brain resting state networks and its independent validation in Alzheimer's disease patients. *Front Hum Neurosci, 7*, 456. doi:10.3389/fnhum.2013.00456

Chen, N., Sugihara, H., & Sur, M. (2015). An acetylcholine-activated microcircuit drives temporal dynamics of cortical activity. *Nat Neurosci, 18*(6), 892-902. doi:10.1038/nn.4002

Chen, X., Zhang, H., & Shen, D. (2016). Ensemble Hierarchical High-Order Functional Connectivity Networks for MCI Classification. *Med Image Comput Comput Assist Interv, 9901*, 18-25. doi:10.1007/978-3-319-46723-8_3

Chen, X., Zhang, H., Zhang, L., Shen, C., Lee, S. W., & Shen, D. (2017). Extraction of dynamic functional connectivity from brain grey matter and white matter for MCI classification. *Hum Brain Mapp, 38*(10), 5019-5034. doi:10.1002/hbm.23711

Chen, X. Q., & Mobley, W. C. (2019). Exploring the Pathogenesis of Alzheimer Disease in Basal Forebrain Cholinergic Neurons: Converging Insights From Alternative Hypotheses. *Front Neurosci, 13*, 446. doi:10.3389/fnins.2019.00446

Chiesa, P. A., Cavedo, E., Grothe, M. J., Houot, M., Teipel, S. J., Potier, M. C., . . . the Alzheimer Precision Medicine, I. (2019). Relationship between Basal Forebrain Resting-State Functional Connectivity and Brain Amyloid-beta Deposition in Cognitively Intact Older Adults with Subjective Memory Complaints. *Radiology, 290*(1), 167-176. doi:10.1148/radiol.2018180268

Cirrito, J. R., Yamada, K. A., Finn, M. B., Sloviter, R. S., Bales, K. R., May, P. C., . . . Holtzman, D. M. (2005). Synaptic activity regulates interstitial fluid amyloid-beta levels in vivo. *Neuron, 48*(6), 913-922. doi:10.1016/j.neuron.2005.10.028

Cohen, J. R., & D'Esposito, M. (2016). The Segregation and Integration of Distinct Brain Networks and Their Relationship to Cognition. *J Neurosci, 36*(48), 12083-12094. doi:10.1523/JNEUROSCI.2965-15.2016

Cohen, R. M., Rezai-Zadeh, K., Weitz, T. M., Rentsendorj, A., Gate, D., Spivak, I., . . . Town, T. (2013). A transgenic Alzheimer rat with plaques, tau pathology, behavioral impairment, oligomeric abeta, and frank neuronal loss. *J Neurosci, 33*(15), 6245-6256. doi:10.1523/JNEUROSCI.3672-12.2013

Colgin, L. L. (2015). Theta-gamma coupling in the entorhinal-hippocampal system. *Curr Opin Neurobiol, 31*, 45-50. doi:10.1016/j.conb.2014.08.001

Colgin, L. L. (2016). Rhythms of the hippocampal network. *Nat Rev Neurosci, 17*(4), 239-249. doi:10.1038/nrn.2016.21

Colgin, L. L., Denninger, T., Fyhn, M., Hafting, T., Bonnevie, T., Jensen, O., . . . Moser, E. I. (2009). Frequency of gamma oscillations routes flow of information in the hippocampus. *Nature, 462*(7271), 353-357. doi:10.1038/nature08573

Cordova-Palomera, A., Kaufmann, T., Persson, K., Alnaes, D., Doan, N. T., Moberget, T., . . . Westlye, L. T. (2017). Disrupted global metastability and static and dynamic brain connectivity across individuals in the Alzheimer's disease continuum. *Sci Rep, 7*, 40268. doi:10.1038/srep40268

Cuestas Torres, D. M., & Cardenas, F. P. (2020). Synaptic plasticity in Alzheimer's disease and healthy aging. *Rev Neurosci, 31*(3), 245-268. doi:10.1515/revneuro-2019-0058

Dai, Z., & He, Y. (2014). Disrupted structural and functional brain connectomes in mild cognitive impairment and Alzheimer's disease. *Neurosci Bull, 30*(2), 217-232. doi:10.1007/s12264-013-1421-0

Dauwels, J., Srinivasan, K., Ramasubba Reddy, M., Musha, T., Vialatte, F. B., Latchoumane, C., . . . Cichocki, A. (2011). Slowing and Loss of Complexity in Alzheimer's EEG: Two Sides of the Same Coin? *Int J Alzheimers Dis, 2011*, 539621. doi:10.4061/2011/539621

De Roeck, E. E., Engelborghs, S., & Dierckx, E. (2016). Next Generation Brain Health Depends on Early Alzheimer Disease Diagnosis: From a Timely Diagnosis to

Future Population Screening. *J Am Med Dir Assoc, 17*(5), 452-453. doi:10.1016/j.jamda.2016.02.015

DeKosky, S. T., Ikonomovic, M. D., Styren, S. D., Beckett, L., Wisniewski, S., Bennett, D. A., . . . Mufson, E. J. (2002). Upregulation of choline acetyltransferase activity in hippocampus and frontal cortex of elderly subjects with mild cognitive impairment. *Ann Neurol, 51*(2), 145-155. doi:10.1002/ana.10069

Demirtas, M., Falcon, C., Tucholka, A., Gispert, J. D., Molinuevo, J. L., & Deco, G. (2017). A whole-brain computational modeling approach to explain the alterations in resting-state functional connectivity during progression of Alzheimer's disease. *Neuroimage Clin, 16*, 343-354. doi:10.1016/j.nicl.2017.08.006

Deng, W., Aimone, J. B., & Gage, F. H. (2010). New neurons and new memories: how does adult hippocampal neurogenesis affect learning and memory? *Nat Rev Neurosci, 11*(5), 339-350. doi:10.1038/nrn2822

Dhadda, S., Kanekiyo, M., Li, D., Swanson, C. J., Irizarry, M., Berry, S., . . . Berry, D. A. (2022). Consistency of efficacy results across various clinical measures and statistical methods in the lecanemab phase 2 trial of early Alzheimer's disease. *Alzheimers Res Ther, 14*(1), 182. doi:10.1186/s13195-022-01129-x

Di Castro, M. A., Chuquet, J., Liaudet, N., Bhaukaurally, K., Santello, M., Bouvier, D., . . . Volterra, A. (2011). Local Ca2+ detection and modulation of synaptic release by astrocytes. *Nat Neurosci, 14*(10), 1276-1284. doi:10.1038/nn.2929

Di, X., Kim, E. H., Chen, P., & Biswal, B. B. (2014). Lateralized resting-state functional connectivity in the task-positive and task-negative networks. *Brain Connect, 4*(9), 641-648. doi:10.1089/brain.2013.0215

Diba, K., & Buzsaki, G. (2007). Forward and reverse hippocampal place-cell sequences during ripples. *Nat Neurosci, 10*(10), 1241-1242. doi:10.1038/nn1961

Diekelmann, S., & Born, J. (2010). The memory function of sleep. *Nat Rev Neurosci, 11*(2), 114-126. doi:10.1038/nrn2762

Disha Shah, W. G., Jérôme Wahis, Emma S. Luckett, Tarik Jamoulle, Ben Vermaercke, Pranav Preman, Daan Moechars, Véronique Hendrickx, Tom Jaspers, Katleen Craessaerts, Katrien Horré, Leen Wolfs, Mark Fiers, Matthew Holt, Dietmar Rudolf Thal, Zsuzsanna Callaerts-Vegh, Rudi D'Hooge, Rik Vandenberghe, Uwe Himmelreich, Vincent Bonin, Bart De Strooper. (2022). Astrocyte calcium dysfunction causes early network hyperactivity in Alzheimer's Disease. *bioRxiv*. doi:10.1101/2022.04.26.489446

Do Carmo, S., & Cuello, A. C. (2013). Modeling Alzheimer's disease in transgenic rats. *Mol Neurodegener, 8*, 37. doi:10.1186/1750-1326-8-37

Donegan, J. J., Boley, A. M., Yamaguchi, J., Toney, G. M., & Lodge, D. J. (2019). Modulation of extrasynaptic GABAA alpha 5 receptors in the ventral hippocampus normalizes physiological and behavioral deficits in a circuit specific manner. *Nat Commun, 10*(1), 2819. doi:10.1038/s41467-019-10800-1

Dringenberg, H. C. (2000). Alzheimer's disease: more than a 'cholinergic disorder' - evidence that cholinergic-monoaminergic interactions contribute to EEG slowing and dementia. *Behav Brain Res, 115*(2), 235-249. doi:10.1016/s0166-4328(00)00261-8

Drummond, E., & Wisniewski, T. (2017). Alzheimer's disease: experimental models and reality. *Acta Neuropathol, 133*(2), 155-175. doi:10.1007/s00401-016-1662-x

Du, X., Wang, X., & Geng, M. (2018). Alzheimer's disease hypothesis and related therapies. *Transl Neurodegener, 7*, 2. doi:10.1186/s40035-018-0107-y

Du, Y., Fu, Z., & Calhoun, V. D. (2018). Classification and Prediction of Brain Disorders Using Functional Connectivity: Promising but Challenging. *Front Neurosci, 12*, 525. doi:10.3389/fnins.2018.00525

Dubelaar, E. J., Mufson, E. J., ter Meulen, W. G., Van Heerikhuize, J. J., Verwer, R. W., & Swaab, D. F. (2006). Increased metabolic activity in nucleus basalis of Meynert neurons in elderly individuals with mild cognitive impairment as indicated by the size of the Golgi apparatus. *J Neuropathol Exp Neurol, 65*(3), 257-266. doi:10.1097/01.jnen.0000205143.16339.cd

Dubois, B., Feldman, H. H., Jacova, C., Hampel, H., Molinuevo, J. L., Blennow, K., . . . Cummings, J. L. (2014). Advancing research diagnostic criteria for Alzheimer's disease: the IWG-2 criteria. *Lancet Neurol, 13*(6), 614-629. doi:10.1016/S1474-4422(14)70090-0

Duncan, M. J., Farlow, H., Tirumalaraju, C., Yun, D. H., Wang, C., Howard, J. A., . . . Bachstetter, A. D. (2019). Effects of the dual orexin receptor antagonist DORA-22 on sleep in 5XFAD mice. *Alzheimers Dement (N Y), 5*, 70-80. doi:10.1016/j.trci.2019.01.003

Duncan, M. J., Guerriero, L. E., Kohler, K., Beechem, L. E., Gillis, B. D., Salisbury, F., . . . Murphy, M. P. (2022). Chronic Fragmentation of the Daily Sleep-Wake Rhythm Increases Amyloid-beta Levels and Neuroinflammation in the 3xTg-AD Mouse Model of Alzheimer's Disease. *Neuroscience, 481*, 111-122. doi:10.1016/j.neuroscience.2021.11.042

Eban-Rothschild, A., Rothschild, G., Giardino, W. J., Jones, J. R., & de Lecea, L. (2016). VTA dopaminergic neurons regulate ethologically relevant sleep-wake behaviors. *Nat Neurosci, 19*(10), 1356-1366. doi:10.1038/nn.4377

Ego-Stengel, V., & Wilson, M. A. (2010). Disruption of ripple-associated hippocampal activity during rest impairs spatial learning in the rat. *Hippocampus, 20*(1), 1-10. doi:10.1002/hipo.20707

English, D. F., Peyrache, A., Stark, E., Roux, L., Vallentin, D., Long, M. A., & Buzsaki, G. (2014). Excitation and inhibition compete to control spiking during hippocampal ripples: intracellular study in behaving mice. *J Neurosci, 34*(49), 16509-16517. doi:10.1523/JNEUROSCI.2600-14.2014

Espinosa, N., Alonso, A., Lara-Vasquez, A., & Fuentealba, P. (2019). Basal forebrain somatostatin cells differentially regulate local gamma oscillations and functionally segregate motor and cognitive circuits. *Sci Rep, 9*(1), 2570. doi:10.1038/s41598-019-39203-4

Espinosa, N., Alonso, A., Morales, C., Espinosa, P., Chavez, A. E., & Fuentealba, P. (2019). Basal Forebrain Gating by Somatostatin Neurons Drives Prefrontal Cortical Activity. *Cereb Cortex, 29*(1), 42-53. doi:10.1093/cercor/bhx302

Etter, G., van der Veldt, S., Manseau, F., Zarrinkoub, I., Trillaud-Doppia, E., & Williams, S. (2019). Optogenetic gamma stimulation rescues memory impairments in an

Alzheimer's disease mouse model. *Nat Commun, 10*(1), 5322. doi:10.1038/s41467-019-13260-9

Fell, J., & Axmacher, N. (2011). The role of phase synchronization in memory processes. *Nat Rev Neurosci, 12*(2), 105-118. doi:10.1038/nrn2979

Fernandez-Cabello, S., Kronbichler, M., Van Dijk, K. R. A., Goodman, J. A., Spreng, R. N., Schmitz, T. W., & Alzheimer's Disease Neuroimaging, I. (2020). Basal forebrain volume reliably predicts the cortical spread of Alzheimer's degeneration. *Brain, 143*(3), 993-1009. doi:10.1093/brain/awaa012

Fernandez-Ruiz, A., Oliva, A., Fermino de Oliveira, E., Rocha-Almeida, F., Tingley, D., & Buzsaki, G. (2019). Long-duration hippocampal sharp wave ripples improve memory. *Science, 364*(6445), 1082-1086. doi:10.1126/science.aax0758

Ferron, J. F., Kroeger, D., Chever, O., & Amzica, F. (2009). Cortical inhibition during burst suppression induced with isoflurane anesthesia. *J Neurosci, 29*(31), 9850-9860. doi:10.1523/JNEUROSCI.5176-08.2009

Filippi, M., Spinelli, E. G., Cividini, C., & Agosta, F. (2019). Resting State Dynamic Functional Connectivity in Neurodegenerative Conditions: A Review of Magnetic Resonance Imaging Findings. *Front Neurosci, 13*, 657. doi:10.3389/fnins.2019.00657

Filon, M. J., Wallace, E., Wright, S., Douglas, D. J., Steinberg, L. I., Verkuilen, C. L., . . . Westmark, C. J. (2020). Sleep and diurnal rest-activity rhythm disturbances in a mouse model of Alzheimer's disease. *Sleep, 43*(11). doi:10.1093/sleep/zsaa087

Foffani, G., Uzcategui, Y. G., Gal, B., & Menendez de la Prida, L. (2007). Reduced spike-timing reliability correlates with the emergence of fast ripples in the rat epileptic hippocampus. *Neuron, 55*(6), 930-941. doi:10.1016/j.neuron.2007.07.040

Fontanini, A., & Katz, D. B. (2008). Behavioral states, network states, and sensory response variability. *J Neurophysiol, 100*(3), 1160-1168. doi:10.1152/jn.90592.2008

Fowler, C. F., Goerzen, D., Devenyi, G. A., Madularu, D., Chakravarty, M. M., & Near, J. (2022). Neurochemical and cognitive changes precede structural abnormalities in the TgF344-AD rat model. *Brain Communications, 4*(2). doi:ARTN fcac072
10.1093/braincomms/fcac072

Fox, M. D., Snyder, A. Z., Vincent, J. L., Corbetta, M., Van Essen, D. C., & Raichle, M. E. (2005). The human brain is intrinsically organized into dynamic, anticorrelated functional networks. *Proc Natl Acad Sci U S A, 102*(27), 9673-9678. doi:10.1073/pnas.0504136102

Franco-Perez, J., Ballesteros-Zebadua, P., Custodio, V., & Paz, C. (2012). [Major neurotransmitters involved in the regulation of sleep-wake cycle]. *Rev Invest Clin, 64*(2), 182-191. Retrieved from https://www.ncbi.nlm.nih.gov/pubmed/22991780

Fransson, P. (2006). How default is the default mode of brain function? Further evidence from intrinsic BOLD signal fluctuations. *Neuropsychologia, 44*(14), 2836-2845. doi:10.1016/j.neuropsychologia.2006.06.017

Fritz, H. J., Ray, N., Dyrba, M., Sorg, C., Teipel, S., & Grothe, M. J. (2019). The corticotopic organization of the human basal forebrain as revealed by regionally selective

functional connectivity profiles. *Hum Brain Mapp, 40*(3), 868-878. doi:10.1002/hbm.24417

Fullana, N., Gasull-Camos, J., Tarres-Gatius, M., Castane, A., Bortolozzi, A., & Artigas, F. (2020). Astrocyte control of glutamatergic activity: Downstream effects on serotonergic function and emotional behavior. *Neuropharmacology, 166*, 107914. doi:10.1016/j.neuropharm.2019.107914

Fuxe, K., Dahlstrom, A. B., Jonsson, G., Marcellino, D., Guescini, M., Dam, M., . . . Agnati, L. (2010). The discovery of central monoamine neurons gave volume transmission to the wired brain. *Prog Neurobiol, 90*(2), 82-100. doi:10.1016/j.pneurobio.2009.10.012

Gabelle, A., Jaussent, I., Hirtz, C., Vialaret, J., Navucet, S., Grasselli, C., . . . Dauvilliers, Y. (2017). Cerebrospinal fluid levels of orexin-A and histamine, and sleep profile within the Alzheimer process. *Neurobiol Aging, 53*, 59-66. doi:10.1016/j.neurobiolaging.2017.01.011

Gao, F., Liu, T., Tuo, M., & Chi, S. (2021). The role of orexin in Alzheimer disease: From sleep-wake disturbance to therapeutic target. *Neurosci Lett, 765*, 136247. doi:10.1016/j.neulet.2021.136247

Gao, W., Gilmore, J. H., Alcauter, S., & Lin, W. (2013). The dynamic reorganization of the default-mode network during a visual classification task. *Front Syst Neurosci, 7*, 34. doi:10.3389/fnsys.2013.00034

Gaubert, S., Raimondo, F., Houot, M., Corsi, M. C., Naccache, L., Diego Sitt, J., . . . Alzheimer's Disease Neuroimaging, I. (2019). EEG evidence of compensatory mechanisms in preclinical Alzheimer's disease. *Brain, 142*(7), 2096-2112. doi:10.1093/brain/awz150

Gauthier-Umana, C., Munoz-Cabrera, J., Valderrama, M., Munera, A., & Nava-Mesa, M. O. (2020). Acute Effects of Two Different Species of Amyloid-beta on Oscillatory Activity and Synaptic Plasticity in the Commissural CA3-CA1 Circuit of the Hippocampus. *Neural Plast, 2020*, 8869526. doi:10.1155/2020/8869526

Geschwill, P., Kaiser, M. E., Grube, P., Lehmann, N., Thome, C., Draguhn, A., . . . Both, M. (2020). Synchronicity of excitatory inputs drives hippocampal networks to distinct oscillatory patterns. *Hippocampus, 30*(10), 1044-1057. doi:10.1002/hipo.23214

Gielow, M. R., & Zaborszky, L. (2017). The Input-Output Relationship of the Cholinergic Basal Forebrain. *Cell Rep, 18*(7), 1817-1830. doi:10.1016/j.celrep.2017.01.060

Gillespie, A. K., Jones, E. A., Lin, Y. H., Karlsson, M. P., Kay, K., Yoon, S. Y., . . . Huang, Y. (2016). Apolipoprotein E4 Causes Age-Dependent Disruption of Slow Gamma Oscillations during Hippocampal Sharp-Wave Ripples. *Neuron, 90*(4), 740-751. doi:10.1016/j.neuron.2016.04.009

Giorgi, A., Migliarini, S., Galbusera, A., Maddaloni, G., Mereu, M., Margiani, G., . . . Pasqualetti, M. (2017). Brain-wide Mapping of Endogenous Serotonergic Transmission via Chemogenetic fMRI. *Cell Rep, 21*(4), 910-918. doi:10.1016/j.celrep.2017.09.087

Giovannini, M. G., Rakovska, A., Benton, R. S., Pazzagli, M., Bianchi, L., & Pepeu, G. (2001). Effects of novelty and habituation on acetylcholine, GABA, and

glutamate release from the frontal cortex and hippocampus of freely moving rats. *Neuroscience, 106*(1), 43-53. doi:10.1016/s0306-4522(01)00266-4

Girardeau, G., & Zugaro, M. (2011). Hippocampal ripples and memory consolidation. *Curr Opin Neurobiol, 21*(3), 452-459. doi:10.1016/j.conb.2011.02.005

Goerzen, D., Fowler, C., Devenyi, G. A., Germann, J., Madularu, D., Chakravarty, M. M., & Near, J. (2020). An MRI-Derived Neuroanatomical Atlas of the Fischer 344 Rat Brain. *Sci Rep, 10*(1), 6952. doi:10.1038/s41598-020-63965-x

Goodman, A. M., Langner, B. M., Jackson, N., Alex, C., & McMahon, L. L. (2021). Heightened Hippocampal beta-Adrenergic Receptor Function Drives Synaptic Potentiation and Supports Learning and Memory in the TgF344-AD Rat Model during Prodromal Alzheimer's Disease. *J Neurosci, 41*(26), 5747-5761. doi:10.1523/JNEUROSCI.0119-21.2021

Goodman, M. S., Kumar, S., Zomorrodi, R., Ghazala, Z., Cheam, A. S. M., Barr, M. S., . . . Rajji, T. K. (2018). Theta-Gamma Coupling and Working Memory in Alzheimer's Dementia and Mild Cognitive Impairment. *Front Aging Neurosci, 10*, 101. doi:10.3389/fnagi.2018.00101

Gordon, J. A., Lacefield, C. O., Kentros, C. G., & Hen, R. (2005). State-dependent alterations in hippocampal oscillations in serotonin 1A receptor-deficient mice. *J Neurosci, 25*(28), 6509-6519. doi:10.1523/JNEUROSCI.1211-05.2005

Goutagny, R., Gu, N., Cavanagh, C., Jackson, J., Chabot, J. G., Quirion, R., . . . Williams, S. (2013). Alterations in hippocampal network oscillations and theta-gamma coupling arise before Abeta overproduction in a mouse model of Alzheimer's disease. *Eur J Neurosci, 37*(12), 1896-1902. doi:10.1111/ejn.12233

Gozzi, A., & Schwarz, A. J. (2016). Large-scale functional connectivity networks in the rodent brain. *Neuroimage, 127*, 496-509. doi:10.1016/j.neuroimage.2015.12.017

Grandjean, J., Canella, C., Anckaerts, C., Ayranci, G., Bougacha, S., Bienert, T., . . . Gozzi, A. (2020). Common functional networks in the mouse brain revealed by multi-centre resting-state fMRI analysis. *Neuroimage, 205*, 116278. doi:10.1016/j.neuroimage.2019.116278

Grandjean, J., Desrosiers-Gregoire, G., Anckaerts, C., Angeles-Valdez, D., Ayad, F., Barrière, D. A., . . . Hess, A. (2022). StandardRat: A multi-center consensus protocol to enhance functional connectivity specificity in the rat brain. *bioRxiv*, 2022.2004.2027.489658. doi:10.1101/2022.04.27.489658

Greicius, M. D., Flores, B. H., Menon, V., Glover, G. H., Solvason, H. B., Kenna, H., . . . Schatzberg, A. F. (2007). Resting-state functional connectivity in major depression: abnormally increased contributions from subgenual cingulate cortex and thalamus. *Biol Psychiatry, 62*(5), 429-437. doi:10.1016/j.biopsych.2006.09.020

Greicius, M. D., Krasnow, B., Reiss, A. L., & Menon, V. (2003). Functional connectivity in the resting brain: a network analysis of the default mode hypothesis. *Proc Natl Acad Sci U S A, 100*(1), 253-258. doi:10.1073/pnas.0135058100

Greicius, M. D., & Menon, V. (2004). Default-mode activity during a passive sensory task: uncoupled from deactivation but impacting activation. *J Cogn Neurosci, 16*(9), 1484-1492. doi:10.1162/0898929042568532

Greicius, M. D., Srivastava, G., Reiss, A. L., & Menon, V. (2004). Default-mode network activity distinguishes Alzheimer's disease from healthy aging: evidence from functional MRI. *Proc Natl Acad Sci U S A, 101*(13), 4637-4642. doi:10.1073/pnas.0308627101

Grimm, C., Duss, S. N., Privitera, M., Munn, B. R., Frässle, S., Chernysheva, M., . . . Zerbi, V. (2022). Locus Coeruleus firing patterns selectively modulate brain activity and dynamics. *bioRxiv*, 2022.2008.2029.505672. doi:10.1101/2022.08.29.505672

Gritton, H. J., Howe, W. M., Mallory, C. S., Hetrick, V. L., Berke, J. D., & Sarter, M. (2016). Cortical cholinergic signaling controls the detection of cues. *Proc Natl Acad Sci U S A, 113*(8), E1089-1097. doi:10.1073/pnas.1516134113

Grothe, M. J., Ewers, M., Krause, B., Heinsen, H., Teipel, S. J., & Alzheimer's Disease Neuroimaging, I. (2014). Basal forebrain atrophy and cortical amyloid deposition in nondemented elderly subjects. *Alzheimers Dement, 10*(5 Suppl), S344-353. doi:10.1016/j.jalz.2013.09.011

Gu, X., Chen, W., Volkow, N. D., Koretsky, A. P., Du, C., & Pan, Y. (2018). Synchronized Astrocytic Ca(2+) Responses in Neurovascular Coupling during Somatosensory Stimulation and for the Resting State. *Cell Rep, 23*(13), 3878-3890. doi:10.1016/j.celrep.2018.05.091

Gu, Y., Lin, Y., Huang, L., Ma, J., Zhang, J., Xiao, Y., . . . Alzheimer's Disease Neuroimaging, I. (2020). Abnormal dynamic functional connectivity in Alzheimer's disease. *CNS Neurosci Ther, 26*(9), 962-971. doi:10.1111/cns.13387

Gu, Z., & Yakel, J. L. (2022). Cholinergic Regulation of Hippocampal Theta Rhythm. *Biomedicines, 10*(4). doi:10.3390/biomedicines10040745

Gurevicius, K., Lipponen, A., & Tanila, H. (2013). Increased cortical and thalamic excitability in freely moving APPswe/PS1dE9 mice modeling epileptic activity associated with Alzheimer's disease. *Cereb Cortex, 23*(5), 1148-1158. doi:10.1093/cercor/bhs105

Gusnard, D. A., Akbudak, E., Shulman, G. L., & Raichle, M. E. (2001). Medial prefrontal cortex and self-referential mental activity: relation to a default mode of brain function. *Proc Natl Acad Sci U S A, 98*(7), 4259-4264. doi:10.1073/pnas.071043098

Gutierrez-Barragan, D., Basson, M. A., Panzeri, S., & Gozzi, A. (2019). Infraslow State Fluctuations Govern Spontaneous fMRI Network Dynamics. *Curr Biol, 29*(14), 2295-2306 e2295. doi:10.1016/j.cub.2019.06.017

Guzman-Velez, E., Diez, I., Schoemaker, D., Pardilla-Delgado, E., Vila-Castelar, C., Fox-Fuller, J. T., . . . Quiroz, Y. T. (2022). Amyloid-beta and tau pathologies relate to distinctive brain dysconnectomics in preclinical autosomal-dominant Alzheimer's disease. *Proc Natl Acad Sci U S A, 119*(15), e2113641119. doi:10.1073/pnas.2113641119

Hafkemeijer, A., Moller, C., Dopper, E. G., Jiskoot, L. C., van den Berg-Huysmans, A. A., van Swieten, J. C., . . . Rombouts, S. A. (2017). A Longitudinal Study on Resting State Functional Connectivity in Behavioral Variant Frontotemporal Dementia and Alzheimer's Disease. *J Alzheimers Dis, 55*(2), 521-537. doi:10.3233/JAD-150695

Hall, A. M., Moore, R. Y., Lopez, O. L., Kuller, L., & Becker, J. T. (2008). Basal forebrain atrophy is a presymptomatic marker for Alzheimer's disease. *Alzheimers Dement, 4*(4), 271-279. doi:10.1016/j.jalz.2008.04.005

Hall, C. N., Reynell, C., Gesslein, B., Hamilton, N. B., Mishra, A., Sutherland, B. A., . . . Attwell, D. (2014). Capillary pericytes regulate cerebral blood flow in health and disease. *Nature, 508*(7494), 55-60. doi:10.1038/nature13165

Hamani, C., & Temel, Y. (2012). Deep brain stimulation for psychiatric disease: contributions and validity of animal models. *Sci Transl Med, 4*(142), 142rv148. doi:10.1126/scitranslmed.3003722

Han, K., Min, J., Lee, M., Kang, B. M., Park, T., Hahn, J., . . . Suh, M. (2019). Neurovascular Coupling under Chronic Stress Is Modified by Altered GABAergic Interneuron Activity. *J Neurosci, 39*(50), 10081-10095. doi:10.1523/JNEUROSCI.1357-19.2019

Haneef, Z., Lenartowicz, A., Yeh, H. J., Levin, H. S., Engel, J., Jr., & Stern, J. M. (2014). Functional connectivity of hippocampal networks in temporal lobe epilepsy. *Epilepsia, 55*(1), 137-145. doi:10.1111/epi.12476

Hanes, J., Zilka, N., Bartkova, M., Caletkova, M., Dobrota, D., & Novak, M. (2009). Rat tau proteome consists of six tau isoforms: implication for animal models of human tauopathies. *J Neurochem, 108*(5), 1167-1176. doi:10.1111/j.1471-4159.2009.05869.x

Harley, C. W., & Yuan, Q. (2021). Locus Coeruleus Optogenetic Modulation: Lessons Learned from Temporal Patterns. *Brain Sci, 11*(12). doi:10.3390/brainsci11121624

Harrison, B. J., Davey, C. G., Savage, H. S., Jamieson, A. J., Leonards, C. A., Moffat, B. A., . . . Steward, T. (2021). Dynamic Subcortical Modulators of Human Default Mode Network Function. *Cereb Cortex*. doi:10.1093/cercor/bhab487

Hasselmo, M. E. (2006). The role of acetylcholine in learning and memory. *Curr Opin Neurobiol, 16*(6), 710-715. doi:10.1016/j.conb.2006.09.002

Hector, A., & Brouillette, J. (2020). Hyperactivity Induced by Soluble Amyloid-beta Oligomers in the Early Stages of Alzheimer's Disease. *Front Mol Neurosci, 13*, 600084. doi:10.3389/fnmol.2020.600084

Herdick, M., Dyrba, M., Fritz, H. J., Altenstein, S., Ballarini, T., Brosseron, F., . . . Grothe, M. J. (2020). Multimodal MRI analysis of basal forebrain structure and function across the Alzheimer's disease spectrum. *Neuroimage Clin, 28*, 102495. doi:10.1016/j.nicl.2020.102495

Herice, C., Patel, A. A., & Sakata, S. (2019). Circuit mechanisms and computational models of REM sleep. *Neurosci Res, 140*, 77-92. doi:10.1016/j.neures.2018.08.003

Hernandez, A. L. R., Ding, S. L., Simley, A. L., McMahon, L. L., & Carter, C. S. (2021). Modeling AD-related metabolic impairments in the TgF344-AD rat model. *Alzheimers Dement, 17 Suppl 2*, e058576. doi:10.1002/alz.058576

Hernandez, C. M., Jackson, N. L., Hernandez, A. R., & McMahon, L. L. (2022). Impairments in Fear Extinction Memory and Basolateral Amygdala Plasticity in the TgF344-AD Rat Model of Alzheimer's Disease Are Distinct from Nonpathological Aging. *eNeuro, 9*(3). doi:10.1523/ENEURO.0181-22.2022

Hijazi, S., Heistek, T. S., Scheltens, P., Neumann, U., Shimshek, D. R., Mansvelder, H. D., . . . van Kesteren, R. E. (2020). Early restoration of parvalbumin interneuron activity prevents memory loss and network hyperexcitability in a mouse model of Alzheimer's disease. *Mol Psychiatry, 25*(12), 3380-3398. doi:10.1038/s41380-019-0483-4

Hill, R. A., Tong, L., Yuan, P., Murikinati, S., Gupta, S., & Grutzendler, J. (2015). Regional Blood Flow in the Normal and Ischemic Brain Is Controlled by Arteriolar Smooth Muscle Cell Contractility and Not by Capillary Pericytes. *Neuron, 87*(1), 95-110. doi:10.1016/j.neuron.2015.06.001

Hinz, R., Peeters, L. M., Shah, D., Missault, S., Belloy, M., Vanreusel, V., . . . Keliris, G. A. (2019). Bottom-up sensory processing can induce negative BOLD responses and reduce functional connectivity in nodes of the default mode-like network in rats. *Neuroimage, 197*, 167-176. doi:10.1016/j.neuroimage.2019.04.065

Hita-Yanez, E., Atienza, M., Gil-Neciga, E., & Cantero, J. L. (2012). Disturbed sleep patterns in elders with mild cognitive impairment: the role of memory decline and ApoE epsilon4 genotype. *Curr Alzheimer Res, 9*(3), 290-297. doi:10.2174/156720512800107609

Hohenfeld, C., Werner, C. J., & Reetz, K. (2018). Resting-state connectivity in neurodegenerative disorders: Is there potential for an imaging biomarker? *Neuroimage Clin, 18*, 849-870. doi:10.1016/j.nicl.2018.03.013

Howarth, C., Mishra, A., & Hall, C. N. (2021). More than just summed neuronal activity: how multiple cell types shape the BOLD response. *Philos Trans R Soc Lond B Biol Sci, 376*(1815), 20190630. doi:10.1098/rstb.2019.0630

Howe, W. M., Gritton, H. J., Lusk, N. A., Roberts, E. A., Hetrick, V. L., Berke, J. D., & Sarter, M. (2017). Acetylcholine Release in Prefrontal Cortex Promotes Gamma Oscillations and Theta-Gamma Coupling during Cue Detection. *J Neurosci, 37*(12), 3215-3230. doi:10.1523/JNEUROSCI.2737-16.2017

Hoydal, M. A., Wisloff, U., Kemi, O. J., & Ellingsen, O. (2007). Running speed and maximal oxygen uptake in rats and mice: practical implications for exercise training. *Eur J Cardiovasc Prev Rehabil, 14*(6), 753-760. doi:10.1097/HJR.0b013e3281eacef1

Hu, L., Wong, T. P., Cote, S. L., Bell, K. F., & Cuello, A. C. (2003). The impact of Abeta-plaques on cortical cholinergic and non-cholinergic presynaptic boutons in alzheimer's disease-like transgenic mice. *Neuroscience, 121*(2), 421-432. doi:10.1016/s0306-4522(03)00394-4

Hu, M., Zhang, P., Li, C., Tan, Y., Li, G., Xu, D., & Chen, L. (2017). Sleep disturbance in mild cognitive impairment: a systematic review of objective measures. *Neurol Sci, 38*(8), 1363-1371. doi:10.1007/s10072-017-2975-9

Huang, S., Tong, H., Lei, M., Zhou, M., Guo, W., Li, G., . . . Xu, P. (2018). Astrocytic glutamatergic transporters are involved in Abeta-induced synaptic dysfunction. *Brain Res, 1678*, 129-137. doi:10.1016/j.brainres.2017.10.011

Huntenburg, J. M., Yeow, L. Y., Mandino, F., & Grandjean, J. (2021). Gradients of functional connectivity in the mouse cortex reflect neocortical evolution. *Neuroimage, 225*, 117528. doi:10.1016/j.neuroimage.2020.117528

Hutchison, R. M., Womelsdorf, T., Allen, E. A., Bandettini, P. A., Calhoun, V. D., Corbetta, M., . . . Chang, C. (2013). Dynamic functional connectivity: promise, issues, and

interpretations. *Neuroimage, 80*, 360-378. doi:10.1016/j.neuroimage.2013.05.079

Iaccarino, H. F., Singer, A. C., Martorell, A. J., Rudenko, A., Gao, F., Gillingham, T. Z., . . . Tsai, L. H. (2018). Author Correction: Gamma frequency entrainment attenuates amyloid load and modifies microglia. *Nature, 562*(7725), E1. doi:10.1038/s41586-018-0351-4

Igarashi, K. M., Lu, L., Colgin, L. L., Moser, M. B., & Moser, E. I. (2014). Coordination of entorhinal-hippocampal ensemble activity during associative learning. *Nature, 510*(7503), 143-147. doi:10.1038/nature13162

Institoris, A., Rosenegger, D. G., & Gordon, G. R. (2015). Arteriole dilation to synaptic activation that is sub-threshold to astrocyte endfoot Ca2+ transients. *J Cereb Blood Flow Metab, 35*(9), 1411-1415. doi:10.1038/jcbfm.2015.141

Ishii, R., Canuet, L., Aoki, Y., Hata, M., Iwase, M., Ikeda, S., . . . Ikeda, M. (2017). Healthy and Pathological Brain Aging: From the Perspective of Oscillations, Functional Connectivity, and Signal Complexity. *Neuropsychobiology, 75*(4), 151-161. doi:10.1159/000486870

Itamoto, K., Taura, Y., Wada, N., Takuma, T., Une, S., Nakaichi, M., & Hikasa, Y. (2002). Quantitative electroencephalography of medetomidine, medetomidine-midazolam and medetomidine-midazolam-butorphanol in dogs. *J Vet Med A Physiol Pathol Clin Med, 49*(4), 169-172. doi:10.1046/j.1439-0442.2002.00425.x

Izco, M., Pesini, P., Perez-Grijalba, V., Fandos, N., & Sarasa, M. (2013). Optimized protocol for amyloid-beta extraction from the brain. *J Alzheimers Dis, 34*(4), 835-839. doi:10.3233/JAD-121798

Jacob, H. J., & Kwitek, A. E. (2002). Rat genetics: attaching physiology and pharmacology to the genome. *Nat Rev Genet, 3*(1), 33-42. doi:10.1038/nrg702

Jafari, Z., Kolb, B. E., & Mohajerani, M. H. (2020). Neural oscillations and brain stimulation in Alzheimer's disease. *Prog Neurobiol, 194*, 101878. doi:10.1016/j.pneurobio.2020.101878

Jakobs, M., Lee, D. J., & Lozano, A. M. (2020). Modifying the progression of Alzheimer's and Parkinson's disease with deep brain stimulation. *Neuropharmacology, 171*, 107860. doi:10.1016/j.neuropharm.2019.107860

Jalilianhasanpour, R., Beheshtian, E., Sherbaf, G., Sahraian, S., & Sair, H. I. (2019). Functional Connectivity in Neurodegenerative Disorders: Alzheimer's Disease and Frontotemporal Dementia. *Top Magn Reson Imaging, 28*(6), 317-324. doi:10.1097/RMR.0000000000000223

Jalilianhasanpour, R., Ryan, D., Agarwal, S., Beheshtian, E., Gujar, S. K., Pillai, J. J., & Sair, H. I. (2021). Dynamic Brain Connectivity in Resting State Functional MR Imaging. *Neuroimaging Clin N Am, 31*(1), 81-92. doi:10.1016/j.nic.2020.09.004

Jankowsky, J. L., & Zheng, H. (2017). Practical considerations for choosing a mouse model of Alzheimer's disease. *Mol Neurodegener, 12*(1), 89. doi:10.1186/s13024-017-0231-7

Jeong, D. U., Oh, J. H., Lee, J. E., Lee, J., Cho, Z. H., Chang, J. W., & Chang, W. S. (2016). Basal Forebrain Cholinergic Deficits Reduce Glucose Metabolism and Function

of Cholinergic and GABAergic Systems in the Cingulate Cortex. *Yonsei Med J, 57*(1), 165-172. doi:10.3349/ymj.2016.57.1.165

Jones, B. E. (2005). From waking to sleeping: neuronal and chemical substrates. *Trends Pharmacol Sci, 26*(11), 578-586. doi:10.1016/j.tips.2005.09.009

Jones, B. E. (2020). Arousal and sleep circuits. *Neuropsychopharmacology, 45*(1), 6-20. doi:10.1038/s41386-019-0444-2

Jones, D. T., Vemuri, P., Murphy, M. C., Gunter, J. L., Senjem, M. L., Machulda, M. M., . . . Jack, C. R., Jr. (2012). Non-stationarity in the "resting brain's" modular architecture. *PLoS One, 7*(6), e39731. doi:10.1371/journal.pone.0039731

Jones, E. A., Gillespie, A. K., Yoon, S. Y., Frank, L. M., & Huang, Y. (2019). Early Hippocampal Sharp-Wave Ripple Deficits Predict Later Learning and Memory Impairments in an Alzheimer's Disease Mouse Model. *Cell Rep, 29*(8), 2123-2133 e2124. doi:10.1016/j.celrep.2019.10.056

Joo, I. L., Lai, A. Y., Bazzigaluppi, P., Koletar, M. M., Dorr, A., Brown, M. E., . . . Stefanovic, B. (2017). Early neurovascular dysfunction in a transgenic rat model of Alzheimer's disease. *Sci Rep, 7*, 46427. doi:10.1038/srep46427

Ju, Y. E., Lucey, B. P., & Holtzman, D. M. (2014). Sleep and Alzheimer disease pathology--a bidirectional relationship. *Nat Rev Neurol, 10*(2), 115-119. doi:10.1038/nrneurol.2013.269

Ju, Y. S., Ooms, S. J., Sutphen, C., Macauley, S. L., Zangrilli, M. A., Jerome, G., . . . Holtzman, D. M. (2017). Slow wave sleep disruption increases cerebrospinal fluid amyloid-beta levels. *Brain, 140*(8), 2104-2111. doi:10.1093/brain/awx148

Kanbayashi, T., Sugiyama, T., Aizawa, R., Saito, Y., Ogawa, Y., Kitajima, T., . . . Shimizu, T. (2002). Effects of donepezil (Aricept) on the rapid eye movement sleep of normal subjects. *Psychiatry Clin Neurosci, 56*(3), 307-308. doi:10.1046/j.1440-1819.2002.01008.x

Kang, D. W., Lee, C. U., & Lim, H. K. (2017). Role of Sleep Disturbance in the Trajectory of Alzheimer's Disease. *Clin Psychopharmacol Neurosci, 15*(2), 89-99. doi:10.9758/cpn.2017.15.2.89

Kar, S., Slowikowski, S. P., Westaway, D., & Mount, H. T. (2004). Interactions between beta-amyloid and central cholinergic neurons: implications for Alzheimer's disease. *J Psychiatry Neurosci, 29*(6), 427-441. Retrieved from https://www.ncbi.nlm.nih.gov/pubmed/15644984

https://www.jpn.ca/content/jpn/29/6/427.full.pdf

Kay, K., & Frank, L. M. (2019). Three brain states in the hippocampus and cortex. *Hippocampus, 29*(3), 184-238. doi:10.1002/hipo.22956

Kelberman, M. A., Anderson, C. R., Chlan, E., Rorabaugh, J. M., McCann, K. E., & Weinshenker, D. (2022). Consequences of Hyperphosphorylated Tau in the Locus Coeruleus on Behavior and Cognition in a Rat Model of Alzheimer's Disease. *J Alzheimers Dis, 86*(3), 1037-1059. doi:10.3233/JAD-215546

Kelly, S. C., McKay, E. C., Beck, J. S., Collier, T. J., Dorrance, A. M., & Counts, S. E. (2019). Locus Coeruleus Degeneration Induces Forebrain Vascular Pathology in a Transgenic Rat Model of Alzheimer's Disease. *J Alzheimers Dis, 70*(2), 371-388. doi:10.3233/JAD-190090

Kent, B. A., Feldman, H. H., & Nygaard, H. B. (2021). Sleep and its regulation: An emerging pathogenic and treatment frontier in Alzheimer's disease. *Prog Neurobiol, 197*, 101902. doi:10.1016/j.pneurobio.2020.101902

Kent, B. A., Strittmatter, S. M., & Nygaard, H. B. (2018). Sleep and EEG Power Spectral Analysis in Three Transgenic Mouse Models of Alzheimer's Disease: APP/PS1, 3xTgAD, and Tg2576. *J Alzheimers Dis, 64*(4), 1325-1336. doi:10.3233/JAD-180260

Kerbler, G. M., Fripp, J., Rowe, C. C., Villemagne, V. L., Salvado, O., Rose, S., . . . Alzheimer's Disease Neuroimaging, I. (2015). Basal forebrain atrophy correlates with amyloid beta burden in Alzheimer's disease. *Neuroimage Clin, 7*, 105-113. doi:10.1016/j.nicl.2014.11.015

Kilimann, I., Grothe, M., Heinsen, H., Alho, E. J., Grinberg, L., Amaro, E., Jr., . . . Teipel, S. J. (2014). Subregional basal forebrain atrophy in Alzheimer's disease: a multicenter study. *J Alzheimers Dis, 40*(3), 687-700. doi:10.3233/JAD-132345

Killgore, W. D. (2010). Effects of sleep deprivation on cognition. *Prog Brain Res, 185*, 105-129. doi:10.1016/B978-0-444-53702-7.00007-5

Kimbrough, I. F., Robel, S., Roberson, E. D., & Sontheimer, H. (2015). Vascular amyloidosis impairs the gliovascular unit in a mouse model of Alzheimer's disease. *Brain, 138*(Pt 12), 3716-3733. doi:10.1093/brain/awv327

Kincheski, G. C., Valentim, I. S., Clarke, J. R., Cozachenco, D., Castelo-Branco, M. T. L., Ramos-Lobo, A. M., . . . Ferreira, S. T. (2017). Chronic sleep restriction promotes brain inflammation and synapse loss, and potentiates memory impairment induced by amyloid-beta oligomers in mice. *Brain Behav Immun, 64*, 140-151. doi:10.1016/j.bbi.2017.04.007

Kitabatake, Y., Sailor, K. A., Ming, G. L., & Song, H. (2007). Adult neurogenesis and hippocampal memory function: new cells, more plasticity, new memories? *Neurosurg Clin N Am, 18*(1), 105-113, x. doi:10.1016/j.nec.2006.10.008

Kitchigina, V. F. (2018). Alterations of Coherent Theta and Gamma Network Oscillations as an Early Biomarker of Temporal Lobe Epilepsy and Alzheimer's Disease. *Front Integr Neurosci, 12*, 36. doi:10.3389/fnint.2018.00036

Klaassen, A. L., Heiniger, A., Vaca Sanchez, P., Harvey, M. A., & Rainer, G. (2021). Ventral pallidum regulates the default mode network, controlling transitions between internally and externally guided behavior. *Proc Natl Acad Sci U S A, 118*(36). doi:10.1073/pnas.2103642118

Kosten, L., Emmi, S. A., Missault, S., & Keliris, G. A. (2022). Combining magnetic resonance imaging with readout and/or perturbation of neural activity in animal models: Advantages and pitfalls. *Front Neurosci, 16*, 938665. doi:10.3389/fnins.2022.938665

Koulousakis, P., van den Hove, D., Visser-Vandewalle, V., & Sesia, T. (2020). Cognitive Improvements After Intermittent Deep Brain Stimulation of the Nucleus Basalis of Meynert in a Transgenic Rat Model for Alzheimer's Disease: A Preliminary Approach. *J Alzheimers Dis, 73*(2), 461-466. doi:10.3233/JAD-190919

Krajcovicova, L., Marecek, R., Mikl, M., & Rektorova, I. (2014). Disruption of resting functional connectivity in Alzheimer's patients and at-risk subjects. *Curr Neurol Neurosci Rep, 14*(10), 491. doi:10.1007/s11910-014-0491-3

Kramis, R., Vanderwolf, C. H., & Bland, B. H. (1975). Two types of hippocampal rhythmical slow activity in both the rabbit and the rat: relations to behavior and effects of atropine, diethyl ether, urethane, and pentobarbital. *Exp Neurol, 49*(1 Pt 1), 58-85. doi:10.1016/0014-4886(75)90195-8

Kreuzer, M., Keating, G. L., Fenzl, T., Hartner, L., Sinon, C. G., Hajjar, I., . . . Garcia, P. S. (2020). Sleep/Wake Behavior and EEG Signatures of the TgF344-AD Rat Model at the Prodromal Stage. *Int J Mol Sci, 21*(23). doi:10.3390/ijms21239290

Kudrimoti, H. S., Barnes, C. A., & McNaughton, B. L. (1999). Reactivation of hippocampal cell assemblies: effects of behavioral state, experience, and EEG dynamics. *J Neurosci, 19*(10), 4090-4101. doi:10.1523/JNEUROSCI.19-10-04090.1999

Lake, E. M. R., Ge, X., Shen, X., Herman, P., Hyder, F., Cardin, J. A., . . . Constable, R. T. (2020). Simultaneous cortex-wide fluorescence Ca(2+) imaging and whole-brain fMRI. *Nat Methods, 17*(12), 1262-1271. doi:10.1038/s41592-020-00984-6

Laszlovszky, T., Schlingloff, D., Hegedus, P., Freund, T. F., Gulyas, A., Kepecs, A., & Hangya, B. (2020). Distinct synchronization, cortical coupling and behavioral function of two basal forebrain cholinergic neuron types. *Nat Neurosci, 23*(8), 992-1003. doi:10.1038/s41593-020-0648-0

Latif-Hernandez, A., Shah, D., Craessaerts, K., Saido, T., Saito, T., De Strooper, B., . . . D'Hooge, R. (2019). Subtle behavioral changes and increased prefrontal-hippocampal network synchronicity in APP(NL-G-F) mice before prominent plaque deposition. *Behav Brain Res, 364*, 431-441. doi:10.1016/j.bbr.2017.11.017

Lau, P., Bossers, K., Janky, R., Salta, E., Frigerio, C. S., Barbash, S., . . . De Strooper, B. (2013). Alteration of the microRNA network during the progression of Alzheimer's disease. *EMBO Mol Med, 5*(10), 1613-1634. doi:10.1002/emmm.201201974

Laufs, H., Hamandi, K., Salek-Haddadi, A., Kleinschmidt, A. K., Duncan, J. S., & Lemieux, L. (2007). Temporal lobe interictal epileptic discharges affect cerebral activity in "default mode" brain regions. *Hum Brain Mapp, 28*(10), 1023-1032. doi:10.1002/hbm.20323

Lecrux, C., & Hamel, E. (2016). Neuronal networks and mediators of cortical neurovascular coupling responses in normal and altered brain states. *Philos Trans R Soc Lond B Biol Sci, 371*(1705). doi:10.1098/rstb.2015.0350

Lecrux, C., Sandoe, C. H., Neupane, S., Kropf, P., Toussay, X., Tong, X. K., . . . Hamel, E. (2017). Impact of Altered Cholinergic Tones on the Neurovascular Coupling Response to Whisker Stimulation. *J Neurosci, 37*(6), 1518-1531. doi:10.1523/JNEUROSCI.1784-16.2016

Lee, A. K., & Wilson, M. A. (2002). Memory of sequential experience in the hippocampus during slow wave sleep. *Neuron, 36*(6), 1183-1194. doi:10.1016/s0896-6273(02)01096-6

Lee, E., & Chung, W. S. (2019). Glial Control of Synapse Number in Healthy and Diseased Brain. *Front Cell Neurosci, 13*, 42. doi:10.3389/fncel.2019.00042

Lee, J. H., Kim, J. Y., Noh, S., Lee, H., Lee, S. Y., Mun, J. Y., . . . Chung, W. S. (2021). Astrocytes phagocytose adult hippocampal synapses for circuit homeostasis. *Nature, 590*(7847), 612-617. doi:10.1038/s41586-020-03060-3

Leopold, D. A., Murayama, Y., & Logothetis, N. K. (2003). Very slow activity fluctuations in monkey visual cortex: implications for functional brain imaging. *Cereb Cortex, 13*(4), 422-433. doi:10.1093/cercor/13.4.422

Li, H., Jia, X., Qi, Z., Fan, X., Ma, T., Ni, H., . . . Li, K. (2017). Altered Functional Connectivity of the Basal Nucleus of Meynert in Mild Cognitive Impairment: A Resting-State fMRI Study. *Front Aging Neurosci, 9*, 127. doi:10.3389/fnagi.2017.00127

Li, R., Zhang, C., Rao, Y., & Yuan, T. F. (2022). Deep brain stimulation of fornix for memory improvement in Alzheimer's disease: A critical review. *Ageing Res Rev, 79*, 101668. doi:10.1016/j.arr.2022.101668

Li, S., & Selkoe, D. J. (2020). A mechanistic hypothesis for the impairment of synaptic plasticity by soluble Abeta oligomers from Alzheimer's brain. *J Neurochem, 154*(6), 583-597. doi:10.1111/jnc.15007

Li, W., Motelow, J. E., Zhan, Q., Hu, Y. C., Kim, R., Chen, W. C., & Blumenfeld, H. (2015). Cortical network switching: possible role of the lateral septum and cholinergic arousal. *Brain Stimul, 8*(1), 36-41. doi:10.1016/j.brs.2014.09.003

Li, Y., Qin, Y., Chen, X., & Li, W. (2013). Exploring the functional brain network of Alzheimer's disease: based on the computational experiment. *PLoS One, 8*(9), e73186. doi:10.1371/journal.pone.0073186

Liang, L., Yuan, Y., Wei, Y., Yu, B., Mai, W., Duan, G., . . . Deng, D. (2021). Recurrent and concurrent patterns of regional BOLD dynamics and functional connectivity dynamics in cognitive decline. *Alzheimers Res Ther, 13*(1), 28. doi:10.1186/s13195-020-00764-6

Liguori, C., Placidi, F., Izzi, F., Spanetta, M., Mercuri, N. B., & Di Pucchio, A. (2020). Sleep dysregulation, memory impairment, and CSF biomarkers during different levels of neurocognitive functioning in Alzheimer's disease course. *Alzheimers Res Ther, 12*(1), 5. doi:10.1186/s13195-019-0571-3

Lima, K. R., da Silva de Vargas, L., Ramborger, B., Roehrs, R., Sevenster, D., Izquierdo, I., . . . Mello-Carpes, P. B. (2019). Noradrenergic and dopaminergic involvement in novelty modulation of aversive memory generalization of adult rats. *Behav Brain Res, 371*, 111991. doi:10.1016/j.bbr.2019.111991

Lin, S. C., Brown, R. E., Hussain Shuler, M. G., Petersen, C. C., & Kepecs, A. (2015). Optogenetic Dissection of the Basal Forebrain Neuromodulatory Control of Cortical Activation, Plasticity, and Cognition. *J Neurosci, 35*(41), 13896-13903. doi:10.1523/JNEUROSCI.2590-15.2015

Lisgaras, C. P., & Scharfman, H. E. (2023). High-frequency oscillations (250-500 Hz) in animal models of Alzheimer's disease and two animal models of epilepsy. *Epilepsia, 64*(1), 231-246. doi:10.1111/epi.17462

Liska, A., Galbusera, A., Schwarz, A. J., & Gozzi, A. (2015). Functional connectivity hubs of the mouse brain. *Neuroimage, 115*, 281-291. doi:10.1016/j.neuroimage.2015.04.033

Liu, A. A., Henin, S., Abbaspoor, S., Bragin, A., Buffalo, E. A., Farrell, J. S., . . . Buzsaki, G. (2022). A consensus statement on detection of hippocampal sharp wave ripples

and differentiation from other fast oscillations. *Nat Commun, 13*(1), 6000. doi:10.1038/s41467-022-33536-x

Liu, X., Zhang, N., Chang, C., & Duyn, J. H. (2018). Co-activation patterns in resting-state fMRI signals. *Neuroimage, 180*(Pt B), 485-494. doi:10.1016/j.neuroimage.2018.01.041

Liu, Y., Yu, C., Zhang, X., Liu, J., Duan, Y., Alexander-Bloch, A. F., . . . Bullmore, E. (2014). Impaired long distance functional connectivity and weighted network architecture in Alzheimer's disease. *Cereb Cortex, 24*(6), 1422-1435. doi:10.1093/cercor/bhs410

Liu, Z., Wang, F., Tang, M., Zhao, Y., & Wang, X. (2019). Amyloid beta and tau are involved in sleep disorder in Alzheimer's disease by orexin A and adenosine A(1) receptor. *Int J Mol Med, 43*(1), 435-442. doi:10.3892/ijmm.2018.3935

Liu, Z., Zhang, Y., Yan, H., Bai, L., Dai, R., Wei, W., . . . Tian, J. (2012). Altered topological patterns of brain networks in mild cognitive impairment and Alzheimer's disease: a resting-state fMRI study. *Psychiatry Res, 202*(2), 118-125. doi:10.1016/j.pscychresns.2012.03.002

Locatelli, T., Cursi, M., Liberati, D., Franceschi, M., & Comi, G. (1998). EEG coherence in Alzheimer's disease. *Electroencephalogr Clin Neurophysiol, 106*(3), 229-237. doi:10.1016/s0013-4694(97)00129-6

Logothetis, N. K., Pauls, J., Augath, M., Trinath, T., & Oeltermann, A. (2001). Neurophysiological investigation of the basis of the fMRI signal. *Nature, 412*(6843), 150-157. doi:10.1038/35084005

Lord, L. D., Stevner, A. B., Deco, G., & Kringelbach, M. L. (2017). Understanding principles of integration and segregation using whole-brain computational connectomics: implications for neuropsychiatric disorders. *Philos Trans A Math Phys Eng Sci, 375*(2096). doi:10.1098/rsta.2016.0283

Lozano-Montes, L., Dimanico, M., Mazloum, R., Li, W., Nair, J., Kintscher, M., . . . Rainer, G. (2020). Optogenetic Stimulation of Basal Forebrain Parvalbumin Neurons Activates the Default Mode Network and Associated Behaviors. *Cell Rep, 33*(6), 108359. doi:10.1016/j.celrep.2020.108359

Lu, H., Zou, Q., Gu, H., Raichle, M. E., Stein, E. A., & Yang, Y. (2012). Rat brains also have a default mode network. *Proc Natl Acad Sci U S A, 109*(10), 3979-3984. doi:10.1073/pnas.1200506109

Lucey, B. P., & Bateman, R. J. (2014). Amyloid-beta diurnal pattern: possible role of sleep in Alzheimer's disease pathogenesis. *Neurobiol Aging, 35 Suppl 2*, S29-34. doi:10.1016/j.neurobiolaging.2014.03.035

Luo, Y., Sun, Y., Tian, X., Zheng, X., Wang, X., Li, W., . . . Hou, W. (2021). Deep Brain Stimulation for Alzheimer's Disease: Stimulation Parameters and Potential Mechanisms of Action. *Front Aging Neurosci, 13*, 619543. doi:10.3389/fnagi.2021.619543

Ma, T., & Klann, E. (2012). Amyloid beta: linking synaptic plasticity failure to memory disruption in Alzheimer's disease. *J Neurochem, 120 Suppl 1*, 140-148. doi:10.1111/j.1471-4159.2011.07506.x

Ma, Z., Zhang, Q., Tu, W., & Zhang, N. (2022). Gaining insight into the neural basis of resting-state fMRI signal. *Neuroimage, 250*, 118960. doi:10.1016/j.neuroimage.2022.118960

Mably, A. J., Gereke, B. J., Jones, D. T., & Colgin, L. L. (2017). Impairments in spatial representations and rhythmic coordination of place cells in the 3xTg mouse model of Alzheimer's disease. *Hippocampus, 27*(4), 378-392. doi:10.1002/hipo.22697

Maestu, F., de Haan, W., Busche, M. A., & DeFelipe, J. (2021). Neuronal excitation/inhibition imbalance: core element of a translational perspective on Alzheimer pathophysiology. *Ageing Res Rev, 69*, 101372. doi:10.1016/j.arr.2021.101372

Mahase, E. (2023). Alzheimer's disease: FDA approves lecanemab amid cost and safety concerns. *BMJ, 380*, 73. doi:10.1136/bmj.p73

Majeed, W., Magnuson, M., & Keilholz, S. D. (2009). Spatiotemporal dynamics of low frequency fluctuations in BOLD fMRI of the rat. *J Magn Reson Imaging, 30*(2), 384-393. doi:10.1002/jmri.21848

Mander, B. A., Winer, J. R., & Walker, M. P. (2017). Sleep and Human Aging. *Neuron, 94*(1), 19-36. doi:10.1016/j.neuron.2017.02.004

Margulies, D. S., Ghosh, S. S., Goulas, A., Falkiewicz, M., Huntenburg, J. M., Langs, G., . . . Smallwood, J. (2016). Situating the default-mode network along a principal gradient of macroscale cortical organization. *Proc Natl Acad Sci U S A, 113*(44), 12574-12579. doi:10.1073/pnas.1608282113

Markello, R. D., Spreng, R. N., Luh, W. M., Anderson, A. K., & De Rosa, E. (2018). Segregation of the human basal forebrain using resting state functional MRI. *Neuroimage, 173*, 287-297. doi:10.1016/j.neuroimage.2018.02.042

Massimini, M., Huber, R., Ferrarelli, F., Hill, S., & Tononi, G. (2004). The sleep slow oscillation as a traveling wave. *J Neurosci, 24*(31), 6862-6870. doi:10.1523/JNEUROSCI.1318-04.2004

Matsumoto, J. Y., Stead, M., Kucewicz, M. T., Matsumoto, A. J., Peters, P. A., Brinkmann, B. H., . . . Worrell, G. A. (2013). Network oscillations modulate interictal epileptiform spike rate during human memory. *Brain, 136*(Pt 8), 2444-2456. doi:10.1093/brain/awt159

Mayer, J. S., Roebroeck, A., Maurer, K., & Linden, D. E. (2010). Specialization in the default mode: Task-induced brain deactivations dissociate between visual working memory and attention. *Hum Brain Mapp, 31*(1), 126-139. doi:10.1002/hbm.20850

McCormick, D. A., Nestvogel, D. B., & He, B. J. (2020). Neuromodulation of Brain State and Behavior. *Annu Rev Neurosci, 43*, 391-415. doi:10.1146/annurev-neuro-100219-105424

McMillan, P., Korvatska, E., Poorkaj, P., Evstafjeva, Z., Robinson, L., Greenup, L., . . . D'Souza, I. (2008). Tau isoform regulation is region- and cell-specific in mouse brain. *J Comp Neurol, 511*(6), 788-803. doi:10.1002/cne.21867

Mead, S., & Fox, N. C. (2023). Lecanemab slows Alzheimer's disease: hope and challenges. *Lancet Neurol, 22*(2), 106-108. doi:10.1016/S1474-4422(22)00529-4

Mehta, D., Jackson, R., Paul, G., Shi, J., & Sabbagh, M. (2017). Why do trials for Alzheimer's disease drugs keep failing? A discontinued drug perspective for 2010-2015. *Expert Opin Investig Drugs, 26*(6), 735-739. doi:10.1080/13543784.2017.1323868

Merlo, S., Spampinato, S. F., & Sortino, M. A. (2019). Early compensatory responses against neuronal injury: A new therapeutic window of opportunity for Alzheimer's Disease? *CNS Neurosci Ther, 25*(1), 5-13. doi:10.1111/cns.13050

Mesulam, M. M. (1998). From sensation to cognition. *Brain, 121 (Pt 6)*, 1013-1052. doi:10.1093/brain/121.6.1013

Mesulam, M. M., Mufson, E. J., Wainer, B. H., & Levey, A. I. (1983). Central cholinergic pathways in the rat: an overview based on an alternative nomenclature (Ch1-Ch6). *Neuroscience, 10*(4), 1185-1201. doi:10.1016/0306-4522(83)90108-2

Mielke, M. M. (2018). Sex and Gender Differences in Alzheimer's Disease Dementia. *Psychiatr Times, 35*(11), 14-17. Retrieved from https://www.ncbi.nlm.nih.gov/pubmed/30820070
https://www.ncbi.nlm.nih.gov/pmc/articles/PMC6390276/pdf/nihms-1006790.pdf

Miller, K. J., Weaver, K. E., & Ojemann, J. G. (2009). Direct electrophysiological measurement of human default network areas. *Proc Natl Acad Sci U S A, 106*(29), 12174-12177. doi:10.1073/pnas.0902071106

Mitew, S., Kirkcaldie, M. T., Dickson, T. C., & Vickers, J. C. (2013). Altered synapses and gliotransmission in Alzheimer's disease and AD model mice. *Neurobiol Aging, 34*(10), 2341-2351. doi:10.1016/j.neurobiolaging.2013.04.010

Mizuno, S., Kameda, A., Inagaki, T., & Horiguchi, J. (2004). Effects of donepezil on Alzheimer's disease: the relationship between cognitive function and rapid eye movement sleep. *Psychiatry Clin Neurosci, 58*(6), 660-665. doi:10.1111/j.1440-1819.2004.01317.x

Moguilner, S., Garcia, A. M., Perl, Y. S., Tagliazucchi, E., Piguet, O., Kumfor, F., . . . Ibanez, A. (2021). Dynamic brain fluctuations outperform connectivity measures and mirror pathophysiological profiles across dementia subtypes: A multicenter study. *Neuroimage, 225*, 117522. doi:10.1016/j.neuroimage.2020.117522

Molle, M., Yeshenko, O., Marshall, L., Sara, S. J., & Born, J. (2006). Hippocampal sharp wave-ripples linked to slow oscillations in rat slow-wave sleep. *J Neurophysiol, 96*(1), 62-70. doi:10.1152/jn.00014.2006

Mondadori, C. R., Buchmann, A., Mustovic, H., Schmidt, C. F., Boesiger, P., Nitsch, R. M., . . . Henke, K. (2006). Enhanced brain activity may precede the diagnosis of Alzheimer's disease by 30 years. *Brain, 129*(Pt 11), 2908-2922. doi:10.1093/brain/awl266

Mong, J. A., & Cusmano, D. M. (2016). Sex differences in sleep: impact of biological sex and sex steroids. *Philos Trans R Soc Lond B Biol Sci, 371*(1688), 20150110. doi:10.1098/rstb.2015.0110

Monllor, P., Cervera-Ferri, A., Lloret, M. A., Esteve, D., Lopez, B., Leon, J. L., & Lloret, A. (2021). Electroencephalography as a Non-Invasive Biomarker of Alzheimer's Disease: A Forgotten Candidate to Substitute CSF Molecules? *Int J Mol Sci, 22*(19). doi:10.3390/ijms221910889

Moraes Wdos, S., Poyares, D. R., Guilleminault, C., Ramos, L. R., Bertolucci, P. H., & Tufik, S. (2006). The effect of donepezil on sleep and REM sleep EEG in patients with Alzheimer disease: a double-blind placebo-controlled study. *Sleep, 29*(2), 199-205. doi:10.1093/sleep/29.2.199

Mormann, F., Fell, J., Axmacher, N., Weber, B., Lehnertz, K., Elger, C. E., & Fernandez, G. (2005). Phase/amplitude reset and theta-gamma interaction in the human medial temporal lobe during a continuous word recognition memory task. *Hippocampus, 15*(7), 890-900. doi:10.1002/hipo.20117

Morrone, C. D., Lai, A. Y., Bishay, J., Hill, M. E., & McLaurin, J. (2022). Parvalbumin neuroplasticity compensates for somatostatin impairment, maintaining cognitive function in Alzheimer's disease. *Transl Neurodegener, 11*(1), 26. doi:10.1186/s40035-022-00300-6

Muller, U. C., Deller, T., & Korte, M. (2017). Not just amyloid: physiological functions of the amyloid precursor protein family. *Nat Rev Neurosci, 18*(5), 281-298. doi:10.1038/nrn.2017.29

Mungenast, A. E., Siegert, S., & Tsai, L. H. (2016). Modeling Alzheimer's disease with human induced pluripotent stem (iPS) cells. *Mol Cell Neurosci, 73*, 13-31. doi:10.1016/j.mcn.2015.11.010

Munoz-Moreno, E., Simoes, R. V., Tudela, R., Lopez-Gil, X., & Soria, G. (2022). Spatio-temporal metabolic rewiring in the brain of TgF344-AD rat model of Alzheimer's disease. *Sci Rep, 12*(1), 16958. doi:10.1038/s41598-022-20962-6

Musaeus, C. S., Engedal, K., Hogh, P., Jelic, V., Morup, M., Naik, M., . . . Andersen, B. B. (2018). EEG Theta Power Is an Early Marker of Cognitive Decline in Dementia due to Alzheimer's Disease. *J Alzheimers Dis, 64*(4), 1359-1371. doi:10.3233/JAD-180300

Myers, A., & McGonigle, P. (2019). Overview of Transgenic Mouse Models for Alzheimer's Disease. *Curr Protoc Neurosci, 89*(1), e81. doi:10.1002/cpns.81

Nair, J., Klaassen, A. L., Arato, J., Vyssotski, A. L., Harvey, M., & Rainer, G. (2018). Basal forebrain contributes to default mode network regulation. *Proc Natl Acad Sci U S A, 115*(6), 1352-1357. doi:10.1073/pnas.1712431115

Nakazono, T., Jun, H., Blurton-Jones, M., Green, K. N., & Igarashi, K. M. (2018). Gamma oscillations in the entorhinal-hippocampal circuit underlying memory and dementia. *Neurosci Res, 129*, 40-46. doi:10.1016/j.neures.2018.02.002

Naumann, T., Deller, T., Bender, R., & Frotscher, M. (1997). 192 IgG-saporin-induced loss of cholinergic neurons in the septum abolishes cholinergic sprouting after unilateral entorhinal lesion in the rat. *Eur J Neurosci, 9*(6), 1304-1313. doi:10.1111/j.1460-9568.1997.tb01485.x

Neuman, K. M., Molina-Campos, E., Musial, T. F., Price, A. L., Oh, K. J., Wolke, M. L., . . . Nicholson, D. A. (2015). Evidence for Alzheimer's disease-linked synapse loss and compensation in mouse and human hippocampal CA1 pyramidal neurons. *Brain Struct Funct, 220*(6), 3143-3165. doi:10.1007/s00429-014-0848-z

Newman, E. L., Gillet, S. N., Climer, J. R., & Hasselmo, M. E. (2013). Cholinergic blockade reduces theta-gamma phase amplitude coupling and speed modulation of theta frequency consistent with behavioral effects on encoding. *J Neurosci, 33*(50), 19635-19646. doi:10.1523/JNEUROSCI.2586-13.2013

Newman, M. E. (2006). Modularity and community structure in networks. *Proc Natl Acad Sci U S A, 103*(23), 8577-8582. doi:10.1073/pnas.0601602103

Nguyen, H. N., Huppe-Gourgues, F., & Vaucher, E. (2015). Activation of the mouse primary visual cortex by medial prefrontal subregion stimulation is not mediated by cholinergic basalo-cortical projections. *Front Syst Neurosci, 9*, 1. doi:10.3389/fnsys.2015.00001

Nimmrich, V., Draguhn, A., & Axmacher, N. (2015). Neuronal Network Oscillations in Neurodegenerative Diseases. *Neuromolecular Med, 17*(3), 270-284. doi:10.1007/s12017-015-8355-9

Nortley, R., Korte, N., Izquierdo, P., Hirunpattarasilp, C., Mishra, A., Jaunmuktane, Z., . . . Attwell, D. (2019). Amyloid beta oligomers constrict human capillaries in Alzheimer's disease via signaling to pericytes. *Science, 365*(6450). doi:10.1126/science.aav9518

Noudoost, B., & Moore, T. (2011). The role of neuromodulators in selective attention. *Trends Cogn Sci, 15*(12), 585-591. doi:10.1016/j.tics.2011.10.006

O'Brien, R. J., & Wong, P. C. (2011). Amyloid precursor protein processing and Alzheimer's disease. *Annu Rev Neurosci, 34*, 185-204. doi:10.1146/annurev-neuro-061010-113613

Oliva, A., Fernandez-Ruiz, A., Fermino de Oliveira, E., & Buzsaki, G. (2018). Origin of Gamma Frequency Power during Hippocampal Sharp-Wave Ripples. *Cell Rep, 25*(7), 1693-1700 e1694. doi:10.1016/j.celrep.2018.10.066

Oostenveld, R., Fries, P., Maris, E., & Schoffelen, J. M. (2011). FieldTrip: Open source software for advanced analysis of MEG, EEG, and invasive electrophysiological data. *Comput Intell Neurosci, 2011*, 156869. doi:10.1155/2011/156869

Osama Chaudry, K. N., Lei Xie, Peter A. Serrano, Maria E. Figueiredo-Pereira, Patricia Rockwell. (2022). Females outperform males in spatial learning despite increased amyloid plaques and microgliosis in a TgF344-AD rat model of Alzheimer's disease. *bioRxiv*. doi:10.1101/2022.03.27.485975

Osborn, L. M., Kamphuis, W., Wadman, W. J., & Hol, E. M. (2016). Astrogliosis: An integral player in the pathogenesis of Alzheimer's disease. *Prog Neurobiol, 144*, 121-141. doi:10.1016/j.pneurobio.2016.01.001

Ossandon, T., Jerbi, K., Vidal, J. R., Bayle, D. J., Henaff, M. A., Jung, J., . . . Lachaux, J. P. (2011). Transient suppression of broadband gamma power in the default-mode network is correlated with task complexity and subject performance. *J Neurosci, 31*(41), 14521-14530. doi:10.1523/JNEUROSCI.2483-11.2011

Otsu, Y., Couchman, K., Lyons, D. G., Collot, M., Agarwal, A., Mallet, J. M., . . . Charpak, S. (2015). Calcium dynamics in astrocyte processes during neurovascular coupling. *Nat Neurosci, 18*(2), 210-218. doi:10.1038/nn.3906

Ozcan, G. G., Lim, S., Leighton, P., Allison, W. T., & Rihel, J. (2020). Sleep is bi-directionally modified by amyloid beta oligomers. *Elife, 9*. doi:10.7554/eLife.53995

Paasonen, J., Stenroos, P., Salo, R. A., Kiviniemi, V., & Grohn, O. (2018). Functional connectivity under six anesthesia protocols and the awake condition in rat brain. *Neuroimage, 172*, 9-20. doi:10.1016/j.neuroimage.2018.01.014

Pais-Roldan, P., Mateo, C., Pan, W. J., Acland, B., Kleinfeld, D., Snyder, L. H., . . . Keilholz, S. (2021). Contribution of animal models toward understanding resting state

functional connectivity. *Neuroimage, 245*, 118630. doi:10.1016/j.neuroimage.2021.118630

Pais-Roldan, P., Takahashi, K., Sobczak, F., Chen, Y., Zhao, X., Zeng, H., . . . Yu, X. (2020). Indexing brain state-dependent pupil dynamics with simultaneous fMRI and optical fiber calcium recording. *Proc Natl Acad Sci U S A, 117*(12), 6875-6882. doi:10.1073/pnas.1909937117

Palop, J. J., & Mucke, L. (2016). Network abnormalities and interneuron dysfunction in Alzheimer disease. *Nat Rev Neurosci, 17*(12), 777-792. doi:10.1038/nrn.2016.141

Pan, P., Zhu, L., Yu, T., Shi, H., Zhang, B., Qin, R., . . . Xu, Y. (2017). Aberrant spontaneous low-frequency brain activity in amnestic mild cognitive impairment: A meta-analysis of resting-state fMRI studies. *Ageing Res Rev, 35*, 12-21. doi:10.1016/j.arr.2016.12.001

Parikh, V., Kozak, R., Martinez, V., & Sarter, M. (2007). Prefrontal acetylcholine release controls cue detection on multiple timescales. *Neuron, 56*(1), 141-154. doi:10.1016/j.neuron.2007.08.025

Park, K., Lee, J., Jang, H. J., Richards, B. A., Kohl, M. M., & Kwag, J. (2020). Optogenetic activation of parvalbumin and somatostatin interneurons selectively restores theta-nested gamma oscillations and oscillation-induced spike timing-dependent long-term potentiation impaired by amyloid beta oligomers. *BMC Biol, 18*(1), 7. doi:10.1186/s12915-019-0732-7

Pase, M. P., Himali, J. J., Grima, N. A., Beiser, A. S., Satizabal, C. L., Aparicio, H. J., . . . Seshadri, S. (2017). Sleep architecture and the risk of incident dementia in the community. *Neurology, 89*(12), 1244-1250. doi:10.1212/WNL.0000000000004373

Peeters, L. M., Hinz, R., Detrez, J. R., Missault, S., De Vos, W. H., Verhoye, M., . . . Keliris, G. A. (2020). Chemogenetic silencing of neurons in the mouse anterior cingulate area modulates neuronal activity and functional connectivity. *Neuroimage, 220*, 117088. doi:10.1016/j.neuroimage.2020.117088

Peeters, L. M., Missault, S., Keliris, A. J., & Keliris, G. A. (2019). Combining DREADDs and neuroimaging in experimental models: a powerful approach towards neurotheranostic applications. *Br J Pharmacol*. doi:10.1111/bph.14885

Peeters, L. M., Missault, S., Keliris, A. J., & Keliris, G. A. (2020). Combining designer receptors exclusively activated by designer drugs and neuroimaging in experimental models: A powerful approach towards neurotheranostic applications. *Br J Pharmacol, 177*(5), 992-1002. doi:10.1111/bph.14885

Peeters, L. M., van den Berg, M., Hinz, R., Majumdar, G., Pintelon, I., & Keliris, G. A. (2020). Cholinergic Modulation of the Default Mode Like Network in Rats. *iScience, 23*(9), 101455. doi:10.1016/j.isci.2020.101455

Pentkowski, N. S., Berkowitz, L. E., Thompson, S. M., Drake, E. N., Olguin, C. R., & Clark, B. J. (2018). Anxiety-like behavior as an early endophenotype in the TgF344-AD rat model of Alzheimer's disease. *Neurobiol Aging, 61*, 169-176. doi:10.1016/j.neurobiolaging.2017.09.024

Pentkowski, N. S., Bouquin, S. J., Maestas-Olguin, C. R., Villasenor, Z. M., & Clark, B. J. (2022). Differential effects of chronic stress on anxiety-like behavior and

contextual fear conditioning in the TgF344-AD rat model of Alzheimer's disease. *Behav Brain Res, 418*, 113661. doi:10.1016/j.bbr.2021.113661

Perrenoud, Q., Rossier, J., Ferezou, I., Geoffroy, H., Gallopin, T., Vitalis, T., & Rancillac, A. (2012). Activation of cortical 5-HT(3) receptor-expressing interneurons induces NO mediated vasodilatations and NPY mediated vasoconstrictions. *Front Neural Circuits, 6*, 50. doi:10.3389/fncir.2012.00050

Pinto, L., Goard, M. J., Estandian, D., Xu, M., Kwan, A. C., Lee, S. H., . . . Dan, Y. (2013). Fast modulation of visual perception by basal forebrain cholinergic neurons. *Nat Neurosci, 16*(12), 1857-1863. doi:10.1038/nn.3552

Proskauer Pena, S. L., Mallouppas, K., Oliveira, A. M. G., Zitricky, F., Nataraj, A., & Jezek, K. (2021). Early Spatial Memory Impairment in a Double Transgenic Model of Alzheimer's Disease TgF-344 AD. *Brain Sci, 11*(10). doi:10.3390/brainsci11101300

Raichle, M. E. (2015). The brain's default mode network. *Annu Rev Neurosci, 38*, 433-447. doi:10.1146/annurev-neuro-071013-014030

Raichle, M. E., MacLeod, A. M., Snyder, A. Z., Powers, W. J., Gusnard, D. A., & Shulman, G. L. (2001). A default mode of brain function. *Proc Natl Acad Sci U S A, 98*(2), 676-682. doi:10.1073/pnas.98.2.676

Raichle, M. E., & Snyder, A. Z. (2007). A default mode of brain function: a brief history of an evolving idea. *Neuroimage, 37*(4), 1083-1090; discussion 1097-1089. doi:10.1016/j.neuroimage.2007.02.041

Rajan, A., Meyyappan, S., Walker, H., Henry Samuel, I. B., Hu, Z., & Ding, M. (2019). Neural mechanisms of internal distraction suppression in visual attention. *Cortex, 117*, 77-88. doi:10.1016/j.cortex.2019.02.026

Ratner, M. H., Downing, S. S., Guo, O., Odamah, K. E., Stewart, T. M., Kumaresan, V., . . . Farb, D. H. (2021). Prodromal dysfunction of alpha5GABA-A receptor modulated hippocampal ripples occurs prior to neurodegeneration in the TgF344-AD rat model of Alzheimer's disease. *Heliyon, 7*(9), e07895. doi:10.1016/j.heliyon.2021.e07895

Razlighi, Q. R. (2018). Task-Evoked Negative BOLD Response in the Default Mode Network Does Not Alter Its Functional Connectivity. *Front Comput Neurosci, 12*, 67. doi:10.3389/fncom.2018.00067

Roelofs, T. J. M., Verharen, J. P. H., van Tilborg, G. A. F., Boekhoudt, L., van der Toorn, A., de Jong, J. W., . . . Dijkhuizen, R. M. (2017). A novel approach to map induced activation of neuronal networks using chemogenetics and functional neuroimaging in rats: A proof-of-concept study on the mesocorticolimbic system. *Neuroimage, 156*, 109-118. doi:10.1016/j.neuroimage.2017.05.021

Roh, J. H., Huang, Y., Bero, A. W., Kasten, T., Stewart, F. R., Bateman, R. J., & Holtzman, D. M. (2012). Disruption of the sleep-wake cycle and diurnal fluctuation of beta-amyloid in mice with Alzheimer's disease pathology. *Sci Transl Med, 4*(150), 150ra122. doi:10.1126/scitranslmed.3004291

Rohleder, C., Wiedermann, D., Neumaier, B., Drzezga, A., Timmermann, L., Graf, R., . . . Endepols, H. (2016). The Functional Networks of Prepulse Inhibition: Neuronal Connectivity Analysis Based on FDG-PET in Awake and Unrestrained Rats. *Front Behav Neurosci, 10*, 148. doi:10.3389/fnbeh.2016.00148

Romanella, S. M., Roe, D., Tatti, E., Cappon, D., Paciorek, R., Testani, E., . . . Santarnecchi, E. (2021). The Sleep Side of Aging and Alzheimer's Disease. *Sleep Med, 77*, 209-225. doi:10.1016/j.sleep.2020.05.029

Rorabaugh, J. M., Chalermpalanupap, T., Botz-Zapp, C. A., Fu, V. M., Lembeck, N. A., Cohen, R. M., & Weinshenker, D. (2017). Chemogenetic locus coeruleus activation restores reversal learning in a rat model of Alzheimer's disease. *Brain, 140*(11), 3023-3038. doi:10.1093/brain/awx232

Roth, B. L. (2016). DREADDs for Neuroscientists. *Neuron, 89*(4), 683-694. doi:10.1016/j.neuron.2016.01.040

Roumis, D. K., & Frank, L. M. (2015). Hippocampal sharp-wave ripples in waking and sleeping states. *Curr Opin Neurobiol, 35*, 6-12. doi:10.1016/j.conb.2015.05.001

Ruan, Q., D'Onofrio, G., Sancarlo, D., Bao, Z., Greco, A., & Yu, Z. (2016). Potential neuroimaging biomarkers of pathologic brain changes in Mild Cognitive Impairment and Alzheimer's disease: a systematic review. *BMC Geriatr, 16*, 104. doi:10.1186/s12877-016-0281-7

Sabbagh, M., & van Dyck, C. H. (2023). Response to: Multiple Cerebral Hemorrhages in a Patient Receiving Lecanemab and Treated with t-PA for Stroke. *N Engl J Med, 388*(5), 480. doi:10.1056/NEJMc2215907

Sadowski, J. H., Jones, M. W., & Mellor, J. R. (2016). Sharp-Wave Ripples Orchestrate the Induction of Synaptic Plasticity during Reactivation of Place Cell Firing Patterns in the Hippocampus. *Cell Rep, 14*(8), 1916-1929. doi:10.1016/j.celrep.2016.01.061

Samadi, A., de la Fuente Revenga, M., Perez, C., Iriepa, I., Moraleda, I., Rodriguez-Franco, M. I., & Marco-Contelles, J. (2013). Synthesis, pharmacological assessment, and molecular modeling of 6-chloro-pyridonepezils: new dual AChE inhibitors as potential drugs for the treatment of Alzheimer's disease. *Eur J Med Chem, 67*, 64-74. doi:10.1016/j.ejmech.2013.06.021

Samiee, S., & Baillet, S. (2017). Time-resolved phase-amplitude coupling in neural oscillations. *Neuroimage, 159*, 270-279. doi:10.1016/j.neuroimage.2017.07.051

Sanchez-Aguilera, A., & Quintanilla, J. P. (2021). Sharp Wave Ripples in Alzheimer's Disease: In Search of Mechanisms. *J Neurosci, 41*(7), 1366-1370. doi:10.1523/JNEUROSCI.2020-20.2020

Sare, R. M., Cooke, S. K., Krych, L., Zerfas, P. M., Cohen, R. M., & Smith, C. B. (2020). Behavioral Phenotype in the TgF344-AD Rat Model of Alzheimer's Disease. *Front Neurosci, 14*, 601. doi:10.3389/fnins.2020.00601

Sarter, M., Givens, B., & Bruno, J. P. (2001). The cognitive neuroscience of sustained attention: where top-down meets bottom-up. *Brain Res Brain Res Rev, 35*(2), 146-160. Retrieved from https://www.ncbi.nlm.nih.gov/pubmed/11336780

Sasaki, K., Suzuki, M., Mieda, M., Tsujino, N., Roth, B., & Sakurai, T. (2011). Pharmacogenetic modulation of orexin neurons alters sleep/wakefulness states in mice. *PLoS One, 6*(5), e20360. doi:10.1371/journal.pone.0020360

Scammell, T. E., Arrigoni, E., & Lipton, J. O. (2017). Neural Circuitry of Wakefulness and Sleep. *Neuron, 93*(4), 747-765. doi:10.1016/j.neuron.2017.01.014

Scheef, L., Grothe, M. J., Koppara, A., Daamen, M., Boecker, H., Biersack, H., . . . Jessen, F. (2019). Subregional volume reduction of the cholinergic forebrain in subjective cognitive decline (SCD). *Neuroimage Clin, 21*, 101612. doi:10.1016/j.nicl.2018.101612

Schindelin, J., Arganda-Carreras, I., Frise, E., Kaynig, V., Longair, M., Pietzsch, T., . . . Cardona, A. (2012). Fiji: an open-source platform for biological-image analysis. *Nat Methods, 9*(7), 676-682. doi:10.1038/nmeth.2019

Schmitz, T. W., Mur, M., Aghourian, M., Bedard, M. A., Spreng, R. N., & Alzheimer's Disease Neuroimaging, I. (2018). Longitudinal Alzheimer's Degeneration Reflects the Spatial Topography of Cholinergic Basal Forebrain Projections. *Cell Rep, 24*(1), 38-46. doi:10.1016/j.celrep.2018.06.001

Schmitz, T. W., Nathan Spreng, R., & Alzheimer's Disease Neuroimaging, I. (2016). Basal forebrain degeneration precedes and predicts the cortical spread of Alzheimer's pathology. *Nat Commun, 7*, 13249. doi:10.1038/ncomms13249

Schummers, J., Yu, H., & Sur, M. (2008). Tuned responses of astrocytes and their influence on hemodynamic signals in the visual cortex. *Science, 320*(5883), 1638-1643. doi:10.1126/science.1156120

Schwarz, A. J., Gass, N., Sartorius, A., Risterucci, C., Spedding, M., Schenker, E., . . . Weber-Fahr, W. (2013). Anti-correlated cortical networks of intrinsic connectivity in the rat brain. *Brain Connect, 3*(5), 503-511. doi:10.1089/brain.2013.0168

Scimemi, A., Meabon, J. S., Woltjer, R. L., Sullivan, J. M., Diamond, J. S., & Cook, D. G. (2013). Amyloid-beta1-42 slows clearance of synaptically released glutamate by mislocalizing astrocytic GLT-1. *J Neurosci, 33*(12), 5312-5318. doi:10.1523/JNEUROSCI.5274-12.2013

Scott, L., Feng, J., Kiss, T., Needle, E., Atchison, K., Kawabe, T. T., . . . Hajos, M. (2012). Age-dependent disruption in hippocampal theta oscillation in amyloid-beta overproducing transgenic mice. *Neurobiol Aging, 33*(7), 1481 e1413-1423. doi:10.1016/j.neurobiolaging.2011.12.010

Sederberg, P. B., Schulze-Bonhage, A., Madsen, J. R., Bromfield, E. B., Litt, B., Brandt, A., & Kahana, M. J. (2007). Gamma oscillations distinguish true from false memories. *Psychol Sci, 18*(11), 927-932. doi:10.1111/j.1467-9280.2007.02003.x

Sendi, M. S. E., Zendehrouh, E., Fu, Z., Liu, J., Du, Y., Mormino, E., . . . Miller, R. L. (2021). Disrupted Dynamic Functional Network Connectivity Among Cognitive Control Networks in the Progression of Alzheimer's Disease. *Brain Connect*. doi:10.1089/brain.2020.0847

Setti, S. E., Hunsberger, H. C., & Reed, M. N. (2017). Alterations in Hippocampal Activity and Alzheimer's Disease. *Transl Issues Psychol Sci, 3*(4), 348-356. doi:10.1037/tps0000124

Sforazzini, F., Bertero, A., Dodero, L., David, G., Galbusera, A., Scattoni, M. L., . . . Gozzi, A. (2016). Altered functional connectivity networks in acallosal and socially impaired BTBR mice. *Brain Struct Funct, 221*(2), 941-954. doi:10.1007/s00429-014-0948-9

Shah, D., Blockx, I., Guns, P. J., De Deyn, P. P., Van Dam, D., Jonckers, E., . . . Van der Linden, A. (2015). Acute modulation of the cholinergic system in the mouse brain detected by pharmacological resting-state functional MRI. *Neuroimage, 109*, 151-159. doi:10.1016/j.neuroimage.2015.01.009

Shah, D., Jonckers, E., Praet, J., Vanhoutte, G., Delgado, Y. P. R., Bigot, C., . . . Van der Linden, A. (2013). Resting state FMRI reveals diminished functional connectivity in a mouse model of amyloidosis. *PLoS One, 8*(12), e84241. doi:10.1371/journal.pone.0084241

Shah, D., Latif-Hernandez, A., De Strooper, B., Saito, T., Saido, T., Verhoye, M., . . . Van der Linden, A. (2018). Spatial reversal learning defect coincides with hypersynchronous telencephalic BOLD functional connectivity in APP(NL-F/NL-F) knock-in mice. *Sci Rep, 8*(1), 6264. doi:10.1038/s41598-018-24657-9

Shah, D., Praet, J., Latif Hernandez, A., Hofling, C., Anckaerts, C., Bard, F., . . . Van der Linden, A. (2016). Early pathologic amyloid induces hypersynchrony of BOLD resting-state networks in transgenic mice and provides an early therapeutic window before amyloid plaque deposition. *Alzheimers Dement, 12*(9), 964-976. doi:10.1016/j.jalz.2016.03.010

Shakil, S., Lee, C. H., & Keilholz, S. D. (2016). Evaluation of sliding window correlation performance for characterizing dynamic functional connectivity and brain states. *Neuroimage, 133*, 111-128. doi:10.1016/j.neuroimage.2016.02.074

Shappell, H. M., Duffy, K. A., Rosch, K. S., Pekar, J. J., Mostofsky, S. H., Lindquist, M. A., & Cohen, J. R. (2021). Children with attention-deficit/hyperactivity disorder spend more time in hyperconnected network states and less time in segregated network states as revealed by dynamic connectivity analysis. *Neuroimage, 229*, 117753. doi:10.1016/j.neuroimage.2021.117753

Sharif, F., Tayebi, B., Buzsaki, G., Royer, S., & Fernandez-Ruiz, A. (2021). Subcircuits of Deep and Superficial CA1 Place Cells Support Efficient Spatial Coding across Heterogeneous Environments. *Neuron, 109*(2), 363-376 e366. doi:10.1016/j.neuron.2020.10.034

Sharma, N., & Singh, A. N. (2016). Exploring Biomarkers for Alzheimer's Disease. *J Clin Diagn Res, 10*(7), KE01-06. doi:10.7860/JCDR/2016/18828.8166

Sheline, Y. I., Morris, J. C., Snyder, A. Z., Price, J. L., Yan, Z., D'Angelo, G., . . . Mintun, M. A. (2010). APOE4 allele disrupts resting state fMRI connectivity in the absence of amyloid plaques or decreased CSF Abeta42. *J Neurosci, 30*(50), 17035-17040. doi:10.1523/JNEUROSCI.3987-10.2010

Shine, J. M. (2019). Neuromodulatory Influences on Integration and Segregation in the Brain. *Trends Cogn Sci, 23*(7), 572-583. doi:10.1016/j.tics.2019.04.002

Shulman, G. L., Fiez, J. A., Corbetta, M., Buckner, R. L., Miezin, F. M., Raichle, M. E., & Petersen, S. E. (1997). Common Blood Flow Changes across Visual Tasks: II. Decreases in Cerebral Cortex. *J Cogn Neurosci, 9*(5), 648-663. doi:10.1162/jocn.1997.9.5.648

Silberstein, R. B., Pipingas, A., Farrow, M., Levy, F., & Stough, C. K. (2016). Dopaminergic modulation of default mode network brain functional connectivity in attention deficit hyperactivity disorder. *Brain Behav, 6*(12), e00582. doi:10.1002/brb3.582

Silva, A. C., Lee, S. P., Yang, G., Iadecola, C., & Kim, S. G. (1999). Simultaneous blood oxygenation level-dependent and cerebral blood flow functional magnetic resonance imaging during forepaw stimulation in the rat. *J Cereb Blood Flow Metab, 19*(8), 871-879. doi:10.1097/00004647-199908000-00006

Singh, K. D., & Fawcett, I. P. (2008). Transient and linearly graded deactivation of the human default-mode network by a visual detection task. *Neuroimage, 41*(1), 100-112. doi:10.1016/j.neuroimage.2008.01.051

Slanzi, A., Iannoto, G., Rossi, B., Zenaro, E., & Constantin, G. (2020). In vitro Models of Neurodegenerative Diseases. *Front Cell Dev Biol, 8*, 328. doi:10.3389/fcell.2020.00328

Slater, C., Liu, Y., Weiss, E., Yu, K., & Wang, Q. (2022). The Neuromodulatory Role of the Noradrenergic and Cholinergic Systems and Their Interplay in Cognitive Functions: A Focused Review. *Brain Sci, 12*(7). doi:10.3390/brainsci12070890

Small, D. H. (2008). Network dysfunction in Alzheimer's disease: does synaptic scaling drive disease progression? *Trends Mol Med, 14*(3), 103-108. doi:10.1016/j.molmed.2007.12.006

Smith, L. A., Goodman, A. M., & McMahon, L. L. (2022). Dentate Granule Cells Are Hyperexcitable in the TgF344-AD Rat Model of Alzheimer's Disease. *Front Synaptic Neurosci, 14*, 826601. doi:10.3389/fnsyn.2022.826601

Smith, L. A., & McMahon, L. L. (2018). Deficits in synaptic function occur at medial perforant path-dentate granule cell synapses prior to Schaffer collateral-CA1 pyramidal cell synapses in the novel TgF344-Alzheimer's Disease Rat Model. *Neurobiol Dis, 110*, 166-179. doi:10.1016/j.nbd.2017.11.014

Solari, N., & Hangya, B. (2018). Cholinergic modulation of spatial learning, memory and navigation. *Eur J Neurosci, 48*(5), 2199-2230. doi:10.1111/ejn.14089

Solomon, E. A., Kragel, J. E., Sperling, M. R., Sharan, A., Worrell, G., Kucewicz, M., . . . Kahana, M. J. (2017). Widespread theta synchrony and high-frequency desynchronization underlies enhanced cognition. *Nat Commun, 8*(1), 1704. doi:10.1038/s41467-017-01763-2

Somers, C., Goossens, J., Engelborghs, S., & Bjerke, M. (2017). Selecting Abeta isoforms for an Alzheimer's disease cerebrospinal fluid biomarker panel. *Biomark Med, 11*(2), 169-178. doi:10.2217/bmm-2016-0276

Somogyi, P., Katona, L., Klausberger, T., Lasztoczi, B., & Viney, T. J. (2014). Temporal redistribution of inhibition over neuronal subcellular domains underlies state-dependent rhythmic change of excitability in the hippocampus. *Philos Trans R Soc Lond B Biol Sci, 369*(1635), 20120518. doi:10.1098/rstb.2012.0518

Sperling, R. A., Aisen, P. S., Beckett, L. A., Bennett, D. A., Craft, S., Fagan, A. M., . . . Phelps, C. H. (2011). Toward defining the preclinical stages of Alzheimer's disease: recommendations from the National Institute on Aging-Alzheimer's Association workgroups on diagnostic guidelines for Alzheimer's disease. *Alzheimers Dement, 7*(3), 280-292. doi:10.1016/j.jalz.2011.03.003

Stafford, J. M., Jarrett, B. R., Miranda-Dominguez, O., Mills, B. D., Cain, N., Mihalas, S., . . . Fair, D. A. (2014). Large-scale topology and the default mode network in the mouse connectome. *Proc Natl Acad Sci U S A, 111*(52), 18745-18750. doi:10.1073/pnas.1404346111

Stargardt, A., Swaab, D. F., & Bossers, K. (2015). Storm before the quiet: neuronal hyperactivity and Abeta in the presymptomatic stages of Alzheimer's disease. *Neurobiol Aging, 36*(1), 1-11. doi:10.1016/j.neurobiolaging.2014.08.014

Steiner, A. R., Rousseau-Blass, F., Schroeter, A., Hartnack, S., & Bettschart-Wolfensberger, R. (2021). Systematic Review: Anesthetic Protocols and Management as Confounders in Rodent Blood Oxygen Level Dependent Functional Magnetic Resonance Imaging (BOLD fMRI)-Part B: Effects of Anesthetic Agents, Doses and Timing. *Animals (Basel), 11*(1). doi:10.3390/ani11010199

Stoiljkovic, M., Kelley, C., Hajos, G. P., Nagy, D., Koenig, G., Leventhal, L., & Hajos, M. (2016). Hippocampal network dynamics in response to alpha7 nACh receptors activation in amyloid-beta overproducing transgenic mice. *Neurobiol Aging, 45*, 161-168. doi:10.1016/j.neurobiolaging.2016.05.021

Stoiljkovic, M., Kelley, C., Horvath, T. L., & Hajos, M. (2018). Neurophysiological signals as predictive translational biomarkers for Alzheimer's disease treatment: effects of donepezil on neuronal network oscillations in TgF344-AD rats. *Alzheimers Res Ther, 10*(1), 105. doi:10.1186/s13195-018-0433-4

Stoiljkovic, M., Kelley, C., Nagy, D., & Hajos, M. (2015). Modulation of hippocampal neuronal network oscillations by alpha7 nACh receptors. *Biochem Pharmacol, 97*(4), 445-453. doi:10.1016/j.bcp.2015.06.031

Stoiljkovic, M., Kelley, C., Stutz, B., Horvath, T. L., & Hajos, M. (2019). Altered Cortical and Hippocampal Excitability in TgF344-AD Rats Modeling Alzheimer's Disease Pathology. *Cereb Cortex, 29*(6), 2716-2727. doi:10.1093/cercor/bhy140

Strange, B. A., Witter, M. P., Lein, E. S., & Moser, E. I. (2014). Functional organization of the hippocampal longitudinal axis. *Nat Rev Neurosci, 15*(10), 655-669. doi:10.1038/nrn3785

Studart, A. N., & Nitrini, R. (2016). Subjective cognitive decline: The first clinical manifestation of Alzheimer's disease? *Dement Neuropsychol, 10*(3), 170-177. doi:10.1590/S1980-5764-2016DN1003002

Styr, B., & Slutsky, I. (2018). Imbalance between firing homeostasis and synaptic plasticity drives early-phase Alzheimer's disease. *Nat Neurosci, 21*(4), 463-473. doi:10.1038/s41593-018-0080-x

Sun, L., Cao, Q., Long, X., Sui, M., Cao, X., Zhu, C., . . . Wang, Y. (2012). Abnormal functional connectivity between the anterior cingulate and the default mode network in drug-naive boys with attention deficit hyperactivity disorder. *Psychiatry Res, 201*(2), 120-127. doi:10.1016/j.pscychresns.2011.07.001

Supekar, K., Menon, V., Rubin, D., Musen, M., & Greicius, M. D. (2008). Network analysis of intrinsic functional brain connectivity in Alzheimer's disease. *PLoS Comput Biol, 4*(6), e1000100. doi:10.1371/journal.pcbi.1000100

Sutherland, M. T., Ray, K. L., Riedel, M. C., Yanes, J. A., Stein, E. A., & Laird, A. R. (2015). Neurobiological impact of nicotinic acetylcholine receptor agonists: an activation likelihood estimation meta-analysis of pharmacologic neuroimaging studies. *Biol Psychiatry, 78*(10), 711-720. doi:10.1016/j.biopsych.2014.12.021

Tadel, F., Baillet, S., Mosher, J. C., Pantazis, D., & Leahy, R. M. (2011). Brainstorm: a user-friendly application for MEG/EEG analysis. *Comput Intell Neurosci, 2011*, 879716. doi:10.1155/2011/879716

Takata, N., Sugiura, Y., Yoshida, K., Koizumi, M., Hiroshi, N., Honda, K., . . . Tanaka, K. F. (2018). Optogenetic astrocyte activation evokes BOLD fMRI response with oxygen consumption without neuronal activity modulation. *Glia, 66*(9), 2013-2023. doi:10.1002/glia.23454

Tamura, M., Spellman, T. J., Rosen, A. M., Gogos, J. A., & Gordon, J. A. (2017). Hippocampal-prefrontal theta-gamma coupling during performance of a spatial working memory task. *Nat Commun, 8*(1), 2182. doi:10.1038/s41467-017-02108-9

Teipel, S. J., Dyrba, M., Ballarini, T., Brosseron, F., Bruno, D., Buerger, K., . . . Heneka, M. T. (2022). Association of Cholinergic Basal Forebrain Volume and Functional Connectivity with Markers of Inflammatory Response in the Alzheimer's Disease Spectrum. *J Alzheimers Dis, 85*(3), 1267-1282. doi:10.3233/JAD-215196

Teipel, S. J., Fritz, H. C., Grothe, M. J., & Alzheimer's Disease Neuroimaging, I. (2020). Neuropathologic features associated with basal forebrain atrophy in Alzheimer disease. *Neurology, 95*(10), e1301-e1311. doi:10.1212/WNL.0000000000010192

Temel, Y., & Jahanshahi, A. (2015). Neuroscience. Treating brain disorders with neuromodulation. *Science, 347*(6229), 1418-1419. doi:10.1126/science.aaa9610

Thompson, G. J., Pan, W. J., Magnuson, M. E., Jaeger, D., & Keilholz, S. D. (2014). Quasi-periodic patterns (QPP): large-scale dynamics in resting state fMRI that correlate with local infraslow electrical activity. *Neuroimage, 84*, 1018-1031. doi:10.1016/j.neuroimage.2013.09.029

Tian, L., Jiang, T., Wang, Y., Zang, Y., He, Y., Liang, M., . . . Zhuo, Y. (2006). Altered resting-state functional connectivity patterns of anterior cingulate cortex in adolescents with attention deficit hyperactivity disorder. *Neurosci Lett, 400*(1-2), 39-43. doi:10.1016/j.neulet.2006.02.022

Tiraboschi, P., Hansen, L. A., Alford, M., Masliah, E., Thal, L. J., & Corey-Bloom, J. (2000). The decline in synapses and cholinergic activity is asynchronous in Alzheimer's disease. *Neurology, 55*(9), 1278-1283. doi:10.1212/wnl.55.9.1278

Tolar, M., Abushakra, S., & Sabbagh, M. (2020). The path forward in Alzheimer's disease therapeutics: Reevaluating the amyloid cascade hypothesis. *Alzheimers Dement, 16*(11), 1553-1560. doi:10.1016/j.jalz.2019.09.075

Tong, C., Liu, C., Zhang, K., Bo, B., Xia, Y., Yang, H., . . . Liang, Z. (2022). Multimodal analysis demonstrating the shaping of functional gradients in the marmoset brain. *Nat Commun, 13*(1), 6584. doi:10.1038/s41467-022-34371-w

Tononi, G., Edelman, G. M., & Sporns, O. (1998). Complexity and coherency: integrating information in the brain. *Trends Cogn Sci, 2*(12), 474-484. doi:10.1016/s1364-6613(98)01259-5

Tort, A. B., Komorowski, R., Eichenbaum, H., & Kopell, N. (2010). Measuring phase-amplitude coupling between neuronal oscillations of different frequencies. *J Neurophysiol, 104*(2), 1195-1210. doi:10.1152/jn.00106.2010

Tort, A. B., Komorowski, R. W., Manns, J. R., Kopell, N. J., & Eichenbaum, H. (2009). Theta-gamma coupling increases during the learning of item-context associations. *Proc Natl Acad Sci U S A, 106*(49), 20942-20947. doi:10.1073/pnas.0911331106

Tort, A. B., Kramer, M. A., Thorn, C., Gibson, D. J., Kubota, Y., Graybiel, A. M., & Kopell, N. J. (2008). Dynamic cross-frequency couplings of local field potential oscillations in rat striatum and hippocampus during performance of a T-maze task. *Proc Natl Acad Sci U S A, 105*(51), 20517-20522. doi:10.1073/pnas.0810524105

Tournier, B. B., Barca, C., Fall, A. B., Gloria, Y., Meyer, L., Ceyzeriat, K., & Millet, P. (2021). Spatial reference learning deficits in absence of dysfunctional working memory in the TgF344-AD rat model of Alzheimer's disease. *Genes Brain Behav, 20*(5), e12712. doi:10.1111/gbb.12712

Traissard, N., Herbeaux, K., Cosquer, B., Jeltsch, H., Ferry, B., Galani, R., . . . Cassel, J. C. (2007). Combined damage to entorhinal cortex and cholinergic basal forebrain neurons, two early neurodegenerative features accompanying Alzheimer's disease: effects on locomotor activity and memory functions in rats. *Neuropsychopharmacology, 32*(4), 851-871. doi:10.1038/sj.npp.1301116

Trimper, J. B., Galloway, C. R., Jones, A. C., Mandi, K., & Manns, J. R. (2017). Gamma Oscillations in Rat Hippocampal Subregions Dentate Gyrus, CA3, CA1, and Subiculum Underlie Associative Memory Encoding. *Cell Rep, 21*(9), 2419-2432. doi:10.1016/j.celrep.2017.10.123

Tudela, R., Munoz-Moreno, E., Sala-Llonch, R., Lopez-Gil, X., & Soria, G. (2019). Resting State Networks in the TgF344-AD Rat Model of Alzheimer's Disease Are Altered From Early Stages. *Front Aging Neurosci, 11*, 213. doi:10.3389/fnagi.2019.00213

Turchi, J., Chang, C., Ye, F. Q., Russ, B. E., Yu, D. K., Cortes, C. R., . . . Leopold, D. A. (2018). The Basal Forebrain Regulates Global Resting-State fMRI Fluctuations. *Neuron, 97*(4), 940-952 e944. doi:10.1016/j.neuron.2018.01.032

Uhlirova, H., Kilic, K., Tian, P., Thunemann, M., Desjardins, M., Saisan, P. A., . . . Devor, A. (2016). Cell type specificity of neurovascular coupling in cerebral cortex. *Elife, 5*. doi:10.7554/eLife.14315

Unal, C. T., Golowasch, J. P., & Zaborszky, L. (2012). Adult mouse basal forebrain harbors two distinct cholinergic populations defined by their electrophysiology. *Front Behav Neurosci, 6*, 21. doi:10.3389/fnbeh.2012.00021

Urban, D. J., Zhu, H., Marcinkiewcz, C. A., Michaelides, M., Oshibuchi, H., Rhea, D., . . . Roth, B. L. (2016). Elucidation of The Behavioral Program and Neuronal Network Encoded by Dorsal Raphe Serotonergic Neurons. *Neuropsychopharmacology, 41*(5), 1404-1415. doi:10.1038/npp.2015.293

van den Berg, M., Adhikari, M. H., Verschuuren, M., Pintelon, I., Vasilkovska, T., Van Audekerke, J., . . . Verhoye, M. (2022). Altered basal forebrain function during whole-brain network activity at pre- and early-plaque stages of Alzheimer's disease in TgF344-AD rats. *Alzheimers Res Ther, 14*(1), 148. doi:10.1186/s13195-022-01089-2

van der Meer, M. A., Kalenscher, T., Lansink, C. S., Pennartz, C. M., Berke, J. D., & Redish, A. D. (2010). Integrating early results on ventral striatal gamma oscillations in the rat. *Front Neurosci, 4*, 300. doi:10.3389/fnins.2010.00300

Van Egroo, M., Koshmanova, E., Vandewalle, G., & Jacobs, H. I. L. (2022). Importance of the locus coeruleus-norepinephrine system in sleep-wake regulation: Implications for aging and Alzheimer's disease. *Sleep Med Rev, 62*, 101592. doi:10.1016/j.smrv.2022.101592

Van Erum, J., Van Dam, D., & De Deyn, P. P. (2019). Alzheimer's disease: Neurotransmitters of the sleep-wake cycle. *Neurosci Biobehav Rev, 105*, 72-80. doi:10.1016/j.neubiorev.2019.07.019

van Harten, A. C., Mielke, M. M., Swenson-Dravis, D. M., Hagen, C. E., Edwards, K. K., Roberts, R. O., . . . Petersen, R. C. (2018). Subjective cognitive decline and risk of MCI: The Mayo Clinic Study of Aging. *Neurology, 91*(4), e300-e312. doi:10.1212/WNL.0000000000005863

van Zijl, P. C., Eleff, S. M., Ulatowski, J. A., Oja, J. M., Ulug, A. M., Traystman, R. J., & Kauppinen, R. A. (1998). Quantitative assessment of blood flow, blood volume and blood oxygenation effects in functional magnetic resonance imaging. *Nat Med, 4*(2), 159-167. doi:10.1038/nm0298-159

Vazquez, J., & Baghdoyan, H. A. (2001). Basal forebrain acetylcholine release during REM sleep is significantly greater than during waking. *Am J Physiol Regul Integr Comp Physiol, 280*(2), R598-601. doi:10.1152/ajpregu.2001.280.2.R598

Venkataraman, L., Fair, S. R., McElroy, C. A., Hester, M. E., & Fu, H. (2022). Modeling neurodegenerative diseases with cerebral organoids and other three-dimensional culture systems: focus on Alzheimer's disease. *Stem Cell Rev Rep, 18*(2), 696-717. doi:10.1007/s12015-020-10068-9

Verschuuren, M., Verstraelen, P., Garcia-Diaz Barriga, G., Cilissen, I., Coninx, E., Verslegers, M., . . . De Vos, W. H. (2019). High-throughput microscopy exposes a pharmacological window in which dual leucine zipper kinase inhibition preserves neuronal network connectivity. *Acta Neuropathol Commun, 7*(1), 93. doi:10.1186/s40478-019-0741-3

Verstraelen, P., Garcia-Diaz Barriga, G., Verschuuren, M., Asselbergh, B., Nuydens, R., Larsen, P. H., . . . De Vos, W. H. (2020). Systematic Quantification of Synapses in Primary Neuronal Culture. *iScience, 23*(9), 101542. doi:10.1016/j.isci.2020.101542

Vidaurre, D., Smith, S. M., & Woolrich, M. W. (2017). Brain network dynamics are hierarchically organized in time. *Proc Natl Acad Sci U S A, 114*(48), 12827-12832. doi:10.1073/pnas.1705120114

Villette, V., Poindessous-Jazat, F., Simon, A., Lena, C., Roullot, E., Bellessort, B., . . . Stephan, A. (2010). Decreased rhythmic GABAergic septal activity and memory-associated theta oscillations after hippocampal amyloid-beta pathology in the rat. *J Neurosci, 30*(33), 10991-11003. doi:10.1523/JNEUROSCI.6284-09.2010

Vincent, J. L., Patel, G. H., Fox, M. D., Snyder, A. Z., Baker, J. T., Van Essen, D. C., . . . Raichle, M. E. (2007). Intrinsic functional architecture in the anaesthetized monkey brain. *Nature, 447*(7140), 83-86. doi:10.1038/nature05758

Vitiello, M. V., & Borson, S. (2001). Sleep disturbances in patients with Alzheimer's disease: epidemiology, pathophysiology and treatment. *CNS Drugs, 15*(10), 777-796. doi:10.2165/00023210-200115100-00004

Vivekananda, U., Bush, D., Bisby, J. A., Baxendale, S., Rodionov, R., Diehl, B., . . . Burgess, N. (2021). Theta power and theta-gamma coupling support long-term spatial memory retrieval. *Hippocampus, 31*(2), 213-220. doi:10.1002/hipo.23284

W. Boron, E. B. (2016). *Medical Physiology* (Elsevier Ed. 3 ed. Vol. 3): Elsevier.

Wang, D., Zhang, X., Wang, M., Zhou, D., Pan, H., Shu, Q., & Sun, B. (2018). Early Activation of Astrocytes does not Affect Amyloid Plaque Load in an Animal Model of Alzheimer's Disease. *Neurosci Bull, 34*(6), 912-920. doi:10.1007/s12264-018-0262-2

Wang, J., Fang, Y., Wang, X., Yang, H., Yu, X., & Wang, H. (2017). Enhanced Gamma Activity and Cross-Frequency Interaction of Resting-State Electroencephalographic Oscillations in Patients with Alzheimer's Disease. *Front Aging Neurosci, 9*, 243. doi:10.3389/fnagi.2017.00243

Wang, J., Ikonen, S., Gurevicius, K., van Groen, T., & Tanila, H. (2002). Alteration of cortical EEG in mice carrying mutated human APP transgene. *Brain Res, 943*(2), 181-190. doi:10.1016/s0006-8993(02)02617-3

Wang, Y., & Mandelkow, E. (2016). Tau in physiology and pathology. *Nat Rev Neurosci, 17*(1), 5-21. doi:10.1038/nrn.2015.1

Wassing, R., Lakbila-Kamal, O., Ramautar, J. R., Stoffers, D., Schalkwijk, F., & Van Someren, E. J. W. (2019). Restless REM Sleep Impedes Overnight Amygdala Adaptation. *Curr Biol, 29*(14), 2351-2358 e2354. doi:10.1016/j.cub.2019.06.034

Watson, C. J., Baghdoyan, H. A., & Lydic, R. (2012). Neuropharmacology of Sleep and Wakefulness: 2012 Update. *Sleep Med Clin, 7*(3), 469-486. doi:10.1016/j.jsmc.2012.06.010

Weber, F., & Dan, Y. (2016). Circuit-based interrogation of sleep control. *Nature, 538*(7623), 51-59. doi:10.1038/nature19773

Wen, X., Liu, Y., Yao, L., & Ding, M. (2013). Top-down regulation of default mode activity in spatial visual attention. *J Neurosci, 33*(15), 6444-6453. doi:10.1523/JNEUROSCI.4939-12.2013

Wilson, I. A., Ikonen, S., Gallagher, M., Eichenbaum, H., & Tanila, H. (2005). Age-associated alterations of hippocampal place cells are subregion specific. *J Neurosci, 25*(29), 6877-6886. doi:10.1523/JNEUROSCI.1744-05.2005

Winer, J. R., & Mander, B. A. (2018). Waking Up to the Importance of Sleep in the Pathogenesis of Alzheimer Disease. *JAMA Neurol, 75*(6), 654-656. doi:10.1001/jamaneurol.2018.0005

Winship, I. R., Plaa, N., & Murphy, T. H. (2007). Rapid astrocyte calcium signals correlate with neuronal activity and onset of the hemodynamic response in vivo. *J Neurosci, 27*(23), 6268-6272. doi:10.1523/JNEUROSCI.4801-06.2007

Wisor, J. P., Edgar, D. M., Yesavage, J., Ryan, H. S., McCormick, C. M., Lapustea, N., & Murphy, G. M., Jr. (2005). Sleep and circadian abnormalities in a transgenic mouse model of Alzheimer's disease: a role for cholinergic transmission. *Neuroscience, 131*(2), 375-385. doi:10.1016/j.neuroscience.2004.11.018

Witten, I. B., Steinberg, E. E., Lee, S. Y., Davidson, T. J., Zalocusky, K. A., Brodsky, M., . . . Deisseroth, K. (2011). Recombinase-driver rat lines: tools, techniques, and optogenetic application to dopamine-mediated reinforcement. *Neuron, 72*(5), 721-733. doi:10.1016/j.neuron.2011.10.028

Witton, J., Staniaszek, L. E., Bartsch, U., Randall, A. D., Jones, M. W., & Brown, J. T. (2016). Disrupted hippocampal sharp-wave ripple-associated spike dynamics in a transgenic mouse model of dementia. *J Physiol, 594*(16), 4615-4630. doi:10.1113/jphysiol.2014.282889

Xi, C., Sun, S., Pan, C., Ji, F., Cui, X., & Li, T. (2018). Different effects of propofol and dexmedetomidine sedation on electroencephalogram patterns: Wakefulness, moderate sedation, deep sedation and recovery. *PLoS One, 13*(6), e0199120. doi:10.1371/journal.pone.0199120

Xia, Y., Eeles, E., Fripp, J., Pinsker, D., Thomas, P., Latter, M., . . . Rose, S. (2022). Reduced cortical cholinergic innervation measured using [(18)F]-FEOBV PET imaging correlates with cognitive decline in mild cognitive impairment. *Neuroimage Clin, 34*, 102992. doi:10.1016/j.nicl.2022.102992

Xie, L., Kang, H., Xu, Q., Chen, M. J., Liao, Y., Thiyagarajan, M., . . . Nedergaard, M. (2013). Sleep drives metabolite clearance from the adult brain. *Science, 342*(6156), 373-377. doi:10.1126/science.1241224

Xie, Y., Liu, T., Ai, J., Chen, D., Zhuo, Y., Zhao, G., . . . Yan, T. (2019). Changes in Centrality Frequency of the Default Mode Network in Individuals With Subjective Cognitive Decline. *Front Aging Neurosci, 11*, 118. doi:10.3389/fnagi.2019.00118

Xu, M., Chung, S., Zhang, S., Zhong, P., Ma, C., Chang, W. C., . . . Dan, Y. (2015). Basal forebrain circuit for sleep-wake control. *Nat Neurosci, 18*(11), 1641-1647. doi:10.1038/nn.4143

Xu, N., LaGrow, T. J., Anumba, N., Lee, A., Zhang, X., Yousefi, B., . . . Keilholz, S. (2022). Functional Connectivity of the Brain Across Rodents and Humans. *Front Neurosci, 16*, 816331. doi:10.3389/fnins.2022.816331

Xu, Y., Zhao, M., Han, Y., & Zhang, H. (2020). GABAergic Inhibitory Interneuron Deficits in Alzheimer's Disease: Implications for Treatment. *Front Neurosci, 14*, 660. doi:10.3389/fnins.2020.00660

Yamada, T., Hashimoto, R. I., Yahata, N., Ichikawa, N., Yoshihara, Y., Okamoto, Y., . . . Kawato, M. (2017). Resting-State Functional Connectivity-Based Biomarkers and Functional MRI-Based Neurofeedback for Psychiatric Disorders: A Challenge for Developing Theranostic Biomarkers. *Int J Neuropsychopharmacol, 20*(10), 769-781. doi:10.1093/ijnp/pyx059

Yamamoto, J., & Tonegawa, S. (2017). Direct Medial Entorhinal Cortex Input to Hippocampal CA1 Is Crucial for Extended Quiet Awake Replay. *Neuron, 96*(1), 217-227 e214. doi:10.1016/j.neuron.2017.09.017

Yamanaka, A., Beuckmann, C. T., Willie, J. T., Hara, J., Tsujino, N., Mieda, M., . . . Sakurai, T. (2003). Hypothalamic orexin neurons regulate arousal according to energy balance in mice. *Neuron, 38*(5), 701-713. doi:10.1016/s0896-6273(03)00331-3

Yang, C., McKenna, J. T., & Brown, R. E. (2017). Intrinsic membrane properties and cholinergic modulation of mouse basal forebrain glutamatergic neurons in vitro. *Neuroscience, 352*, 249-261. doi:10.1016/j.neuroscience.2017.04.002

Yassa, M. A., Stark, S. M., Bakker, A., Albert, M. S., Gallagher, M., & Stark, C. E. (2010). High-resolution structural and functional MRI of hippocampal CA3 and dentate gyrus in patients with amnestic Mild Cognitive Impairment. *Neuroimage, 51*(3), 1242-1252. doi:10.1016/j.neuroimage.2010.03.040

Yiannopoulou, K. G., Anastasiou, A. I., Zachariou, V., & Pelidou, S. H. (2019). Reasons for Failed Trials of Disease-Modifying Treatments for Alzheimer Disease and Their Contribution in Recent Research. *Biomedicines, 7*(4). doi:10.3390/biomedicines7040097

Yousefi, B., & Keilholz, S. (2021). Propagating patterns of intrinsic activity along macroscale gradients coordinate functional connections across the whole brain. *Neuroimage, 231*, 117827. doi:10.1016/j.neuroimage.2021.117827

Yu, A. J., & Dayan, P. (2005). Uncertainty, neuromodulation, and attention. *Neuron, 46*(4), 681-692. doi:10.1016/j.neuron.2005.04.026

Zaborszky, L., Csordas, A., Mosca, K., Kim, J., Gielow, M. R., Vadasz, C., & Nadasdy, Z. (2015). Neurons in the basal forebrain project to the cortex in a complex topographic organization that reflects corticocortical connectivity patterns: an experimental study based on retrograde tracing and 3D reconstruction. *Cereb Cortex, 25*(1), 118-137. doi:10.1093/cercor/bht210

Zaborszky, L., & Duque, A. (2000). Local synaptic connections of basal forebrain neurons. *Behav Brain Res, 115*(2), 143-158. doi:10.1016/s0166-4328(00)00255-2

Zaborszky, L., Gombkoto, P., Varsanyi, P., Gielow, M. R., Poe, G., Role, L. W., . . . Chiba, A. A. (2018). Specific Basal Forebrain-Cortical Cholinergic Circuits Coordinate Cognitive Operations. *J Neurosci, 38*(44), 9446-9458. doi:10.1523/JNEUROSCI.1676-18.2018

Zaldivar, D., Rauch, A., Logothetis, N. K., & Goense, J. (2018). Two distinct profiles of fMRI and neurophysiological activity elicited by acetylcholine in visual cortex. *Proc Natl Acad Sci U S A, 115*(51), E12073-E12082. doi:10.1073/pnas.1808507115

Zerbi, V., Floriou-Servou, A., Markicevic, M., Vermeiren, Y., Sturman, O., Privitera, M., . . . Bohacek, J. (2019). Rapid Reconfiguration of the Functional Connectome after Chemogenetic Locus Coeruleus Activation. *Neuron, 103*(4), 702-718 e705. doi:10.1016/j.neuron.2019.05.034

Zerbi, V., Grandjean, J., Rudin, M., & Wenderoth, N. (2015). Mapping the mouse brain with rs-fMRI: An optimized pipeline for functional network identification. *Neuroimage, 123*, 11-21. doi:10.1016/j.neuroimage.2015.07.090

Zhang, B., Veasey, S. C., Wood, M. A., Leng, L. Z., Kaminski, C., Leight, S., . . . Trojanowski, J. Q. (2005). Impaired rapid eye movement sleep in the Tg2576 APP murine model of Alzheimer's disease with injury to pedunculopontine cholinergic neurons. *Am J Pathol, 167*(5), 1361-1369. doi:10.1016/S0002-9440(10)61223-0

Zhang, F., Zhong, R., Li, S., Fu, Z., Wang, R., Wang, T., . . . Le, W. (2019). Alteration in sleep architecture and electroencephalogram as an early sign of Alzheimer's

disease preceding the disease pathology and cognitive decline. *Alzheimers Dement, 15*(4), 590-597. doi:10.1016/j.jalz.2018.12.004

Zhao, X., Liu, Y., Wang, X., Liu, B., Xi, Q., Guo, Q., . . . Wang, P. (2012). Disrupted small-world brain networks in moderate Alzheimer's disease: a resting-state FMRI study. *PLoS One, 7*(3), e33540. doi:10.1371/journal.pone.0033540

Zhen, Z. H., Guo, M. R., Li, H. M., Guo, O. Y., Zhen, J. L., Fu, J., & Tan, G. J. (2021). Normal and Abnormal Sharp Wave Ripples in the Hippocampal-Entorhinal Cortex System: Implications for Memory Consolidation, Alzheimer's Disease, and Temporal Lobe Epilepsy. *Front Aging Neurosci, 13*, 683483. doi:10.3389/fnagi.2021.683483

Zhou, F., Yan, X. D., Wang, C., He, Y. X., Li, Y. Y., Zhang, J., . . . Wu, M. N. (2020). Suvorexant ameliorates cognitive impairments and pathology in APP/PS1 transgenic mice. *Neurobiol Aging, 91*, 66-75. doi:10.1016/j.neurobiolaging.2020.02.020

Zielinski, M. R., McKenna, J. T., & McCarley, R. W. (2016). Functions and Mechanisms of Sleep. *AIMS Neurosci, 3*(1), 67-104. doi:10.3934/Neuroscience.2016.1.67

Zou, Q. H., Zhu, C. Z., Yang, Y., Zuo, X. N., Long, X. Y., Cao, Q. J., . . . Zang, Y. F. (2008). An improved approach to detection of amplitude of low-frequency fluctuation (ALFF) for resting-state fMRI: fractional ALFF. *J Neurosci Methods, 172*(1), 137-141. doi:10.1016/j.jneumeth.2008.04.012

9.Academic Curriculum Vitae

9.1 Education

01/09/2018-present **Candidate PhD in Biomedical sciences**
University of Antwerp – Bio-Imaging Lab – Belgium
Focus: PhD programme
Main Topic: Unraveling synaptic and network dysfunction during pre- and early-plaque stages of AD using MRI and local field potentials in a rat model of Alzheimer's Disease
PhD-related courses, trainings, and workshops:
- 'Analysis of grouped and longitudinal data with linear mixed models ' 20 April 2022, StatUA, University of Antwerp
- 'Multivariate statistics: 23 April 2020, StatUA, University of Antwerp
- 'Project Management': 26 March 2019, University of Antwerp
- 'Giving academic presentations in English': 18 Februari-25 March 2019, Linuapolis, University of Antwerp
- 'Academic writing': 10-31 March 2018, University of Antwerp
Responsibilities:
- Animal statistics, 2018 – current
    - Yearly reporting animal statistics
- Local animal welfare officer Bio-imaging lab, 2022 - current
- Chair organizing Committee ISMRM Benelux, 2021 - 2022
    - Organizing one-day international conference
    - 28th of April 2022, MECC Maastricht

Academic assignments:
- Teaching Assistant 2018-2022
    - Integrated Research practicals, 2018 – 2021
      Master Biomedical Sciences
    - Biomedische beeldvorming, 2018-2022
      Bachelor Biomedical sciences
    - Preclinical and clinical imaging, 2018-2021
      Bachelor Biomedical sciences
    - Neurowetenschappen, 2020-2021
      Bachelor Biomedical sciences
    - Integrated Neuroscience practicals, 2022
      Master Biomedical Sciences

-

- Supervision Internships and master theses:
  - Master thesis Stijn de Peuter: 2019-2020, “unravelling hippocampal synaptic dysfunction in a highly translational rat model of Alzheimer’s disease”
  - Bachelor thesis Hasmatullah Froogh: 2019-2020, “Using resting-state fMRI as a readout of pathology in a rat model of Alzheimer’s disease”
  - Bachelor thesis Daniëlle Toen: 2019-2020, “Optimalisatie van het analyse protocol voor local field potential signalen in de hippocampus van een TgF344-AD rat tijdens slaap“
  - Honours college Loran Heymans: 2019-2020, “Invloed van B-amyloïde en p-tau op slaap in vroege stadia van Alzheimer”
  - Bachelor thesis Loran Heymans: 2020-2021, “Invloed van B-amyloïde in de relatie tussen slaap en de ziekte van Alzheimer”
  - Bachelor thesis Noah Verpoorten: 2021-2022, “Verstoringen van hippocampale connectiviteit tijdens vroege stadia van Alzheimer in het TgF344-AD ratmodel”
  - Master thesis Daniëlle Toen: 2021-2022, “Alterations in Sharp-wave ripples and theta-gamma coupling, signs of hippocampal network impairment in TgF344-AD rat model”
  - Master thesis Judith van Rooij: 2021-2022, “Short term effects of resveratrol and caloric restriction on functional connectivity in TgF344-AD rats: a rsfMRI study”

2016-2018 **Master of science in Biomedical sciences: Neuroscience**
Grade: great distinction (75%)
University of Antwerp – Belgium
Focus: advancing level of general scientific knowledge and specialization in molecular imaging.
Main topics: system neuroscience, cellular and molecular neuroscience, clinical neuroscience, neuroimaging, preclinical drug research, protein technology and proteome analysis, genomics and genome analysis, bioethics, advanced data analysis
Thesis: “Alterations in default mode-like network connectivity after activation of basal forebrain cholinergic neurons in rats”
Combining designer receptors exclusively activated by designer drugs (DREADDs) and resting state functional MRI to evaluate the effects of

activation of cholinergic neurons in the nucleus basalis of Meynert whole brain functional connectivity.

Skills: basics of matlab, independent research and teamwork, practical lab experience, performing MRI scans, stereotactic surgery, neuromodulation, data-analysis of pharmacological and functional MRI, thesis writing.

2017 **FELASA type C**

University of Antwerp – Belgium

Focus: knowledge and principles necessary for the humane use and care of animals and for optimum quality of research in laboratory.

Main topics: alternatives for use of animals, ethical aspects, anesthesia and analgesia, humane endpoints, animal physiology and nutrition, study design and protocol preparation.

Skills: practical training in animal handling.

2012-2016 **Bachelor of science in Biomedical sciences**

Grade: Satisfaction (63%)

University of Antwerp – Belgium

Focus: global education in general sciences and sciences applied to humans, as preparation for further studies at Master level.

Main topics: general sciences: physics, chemistry, zoology

Applied sciences: human anatomy, physiology, pathology, pharmacology, neuroscience, molecular biology, and genetics.

Skills: microscopic observation techniques, laboratory skills in chemistry, biochemical analysis, biostatistics, working with cell cultures, teamwork during practical sessions, research, individual work.

Dissertation: "The diverse roles of potassium channels in cancer"

This is a literature study on the role of potassium channels in cancer

9.2 Publications

1. Peeters L.M.*, **van den Berg M.***, Hinz R., Majumdar G., Pintelon I., & Keliris G.A. (2020). "Cholinergic Modulation of the Default Mode Like Network in Rats." iScience, 23(9), 101455. doi:10.1016/j.isci.2020.101455, * Equal contribution
2. **van den Berg, M**., M. H. Adhikari, M. Verschuuren, I. Pintelon, T. Vasilkovska, J. Van Audekerke, S. Missault, L. Heymans, P. Ponsaerts, W. H. De Vos, A. Van der Linden, G. A. Keliris and M. Verhoye (2022). "Altered basal forebrain function during whole-brain network activity at pre- and early-plaque stages of Alzheimer's disease in TgF344-AD rats." Alzheimers Res Ther **14**(1): 148.

3. Grandjean, J., Desrosiers-Gregoire, G., Anckaerts, C., Angeles-Valdez, D., Ayad, F., Barrière, D. A., **van den Berg M.**, . . . Hess, A. (2023). "A consensus protocol for functional connectivity analysis in the rat brain", accepted in Nature Neuroscience Feb 2023.
4. **van den Berg M.**, Toen D., Verhoye M. and Keliris G.A. (2023) Alterations in theta-gamma coupling and sharp wave-ripple, signs of prodromal hippocampal network impairment in the TgF344-AD rat model. Front. Aging Neurosci. 15:1081058. doi: 10.3389/fnagi.2023.1081058

Papers submitted, archived in bioRxiv or in preparation

1. Moradi, F.*, **van den Berg, M**.*, Mirjebreili, M. , Kosten, L.., Verhoye, M., Amiri, M. and Keliris, G. A. (2022). "Early Electrophysiological Aberrations in the Hippocampus of the TgF344-AD Rat Model as a Potential Biomarker for Alzheimer's Disease Prognosis." bioRxiv: 2022.2007.2001.498373 * Equal contribution (submitted to iScience).
2. Sanda, P., Hlinka, J., **van den Berg, M**., Bazhenov, M., Keliris, G. A., & Krishnan, G. (2022). Cholinergic modulation supports DMN suppression during resting state. bioRxiv, 2022.2011.2001.514686. doi:10.1101/2022.11.01.514686 (submitted to iScience).
3. Amiri, S., v**an den Berg, M.**, Nazem-Zadeh, M.R., Verhoye, M., Amiri, M., Keliris, G.A. "Nodal Degree Centrality in the Default Mode Like Network of the Tgf344-Ad Alzheimer's Disease Rat Model as a Measure of Early Network Alterations" (submitted to Journal of Alzheimer's Disease).
4. **Van den Berg, M**., Heymans, L., Verschuuren, M., Pintelon, I., De Vos, Winnok., Verhoye, M., Keliris, G.A. "REM sleep fragmentation, hippocampal network impairment and functional cholinergic compensation at pre- and early-plaque stages of Alzheimer's disease in TgF344-AD rats" (in preparation).

9.3 Abstracts and Conference presentations

9.3.1 Invited Speaker

1. **Van den Berg M.**, Adhikari M.H., Vasilkovska T., de Waegenaere S., Keliris G.A., Van der Linden A., Verhoye M., Dynamic rsfMRI analysis methods to unravel network (dys)function in neurodegenerative disorders. Abstract and oral presentation, BMIC Breakfast session, May 4, 2021
2. **Van den Berg M.**, Imaging synaptic dysfunction and compensation of network activity during pre-plaque and early-plaque stages of AD using dynamic rsfMRI and local field potentials, yESMINAR. Oral presentation, October 19, 2022

9.3.2 Oral presentations

1. **Van den Berg M.**, Keliris A., Ben-Nejma I., Van Audekerke J., Verhoye M., Keliris GA., van der Linden A.: "In vivo assessment of glymphatic clearance - Changes in waste drainage during ageing and AD. Abstract and oral presentation annual Belgian Molecular Imaging Community (BMIC), Brussels Belgium, April 23, 2019
2. **Van den Berg M.**, Peeters L., Hinz R., Keliris G.A., Cholinergic modulation of the default mode-like network in rats. Abstract and oral presentation, EMIM, Thessaloniki, Greece (Virtual), 24th – 28th August 2020
3. **Van den Berg M.,** Adhikari M.H., Keliris G.A., Verhoye M., Spatiotemporal alterations of resting-state quasi-periodic patterns in 4-month-old TgF344-AD rats. Abstract and oral presentation, AD/PD™ 2021, Alzheimer's & Parkinson ‘s Disease Conference, Online, 9-14 March 2021.
4. **Van den Berg M**., Adhikari M.H., Keliris G.A., Verhoye M., Basal forebrain activity altered during recurrent patterns of brain activity in 4-month-old TgF344-AD rats. Abstract & oral presentation, EMIM 2021, Göttingen, 24-27 August 2021
5. De Waegenaere S.*, **van den Berg M.*,** Adhikari M.H., Verhoye M., Spatial Differences in Resting-state Co-activation Patterns in TgF344-AD Rat Model at Pre-plaque Stage, Abstract & Oral presentation, 17th European Molecular Imaging Meeting - EMIM 2022, Thessaloniki, Greece, 15-18 March 2022 - * Equal contribution

9.3.3 Poster presentations

1. **Van den Berg M.,** Keliris A.J., Ben-Nejma I., Van Audekerke J., Verhoye M., Keliris G.A,. van der Linden A.: In vivo assessment of glymphatic clearance – Unraveling the role of the glymphatic system in Alzheimer’s Disease. Abstract and poster presentation at annual Belgian Society for Neuroscience congress (BSN), May 24, 2019
2. **Van den Berg M.,** Peeters L.M., Hinz R., Van Audekerke J., Keliris G.A.: Functional connectivity in the default mode-like network decreases upon activation of basal forebrain cholinergic neurons in rats. Abstract, power pitch and poster presentation at Flanders training network life sciences congress (f-tales), June 7, 2019
3. **Van den Berg M.,** Peeters L.M., Hinz R., Van Audekerke J., Keliris G.A.: Cholinergic modulation of the default mode-like network in rats. Abstract and poster presentation at annual International Society for Magnetic Resonance and Medicine Benelux Chapter (ISMRMB), January 24, 2020

4. Keliris A.J., Ben-Nejma I.R.H., **van den Berg M.**, Vanreusel V., Daans J., Ponsaerts P., Verhoye M., Keliris G.A., Van der Linden A., In vivo assessment of glymphatic system efficacy and dynamics of brain-fluids-circulation during the late-onset of Alzheimer's disease in Tet-Off-APP mice and TgF344-AD rat model, Abstract and poster presentation 15th annual meeting of the European Society for Molecular Imaging, ESMI, in Thessaloniki (Virtual), Greece, 25-28 August 2020.
5. **van den Berg M.**, Adhikari M.H., Keliris G.A., Verhoye M., Spatiotemporal aberrations of resting-state quasi-periodic patterns in 4-month-old TgF344-AD rats. Abstract and poster presentation, ISMRM 2021, International Society of Magnetic Resonance in Medicine, Online, 15-20 May 2021.
6. **van den Berg M.**, Adhikari M.H., Keliris G. A., Verhoye M., Basal forebrain activity altered during recurrent patterns of brain activity in 4-month-old TgF344-AD rats. Abstract and poster presentation, SFN 2021, Chicago, USA + Virtual, 8-12 November 2021
7. **van den Berg M.**, Adhikari M.H., Heymans L., Ponsaerts P., Verhoye M., Keliris G.A., Whole brain and local hippocampal alterations in network function in TgF344-AD rats. Abstract and poster presentation, 17th European Molecular Imaging Meeting - EMIM 2022, Thessaloniki, Greece, 15-18 March 2022
8. Adhikari M.H.*, **van den Berg M.***, Verhoye M., Altered Information Flow from Forebrain to Cortex in A Rat Model of Early Alzheimer's Disease, Abstract and poster presentation, 17th European Molecular Imaging Meeting - EMIM 2022, Thessaloniki, Greece, 15-18 March 2022 - * Equal contribution

9.3.4 Awards

- **Poster award,** Flanders TrAining network LifE Sciences (f-Tales), f-Tales: Neuroplasticity and neuromodulation at different scales, Antwerp, 6-7 June 2019
- **vEMIM 2020 Presentation award,** European society for molecular imaging (ESMI), European molecular imaging meeting 2020 (EMIM), Thessaloniki, Greece (Virtual), 24th – 28th August 2020
- **EMIM 2022 Poster award,** European society for molecular imaging (ESMI), European molecular imaging meeting 2020 (EMIM), Thessaloniki, Greece, 15th – 18th March 2022

9.4 Non-scientific science communication

- "The brain" children's workshop – STEM-academy "Proefkot" to introduce 9–13-year-old children about neuroscience using hands-on activities and games, 20 October 2021

10. Acknowledgements

I've always said that I wanted to study forever, and that's exactly what this PhD has offered me, the opportunity to continue to increase my knowledge on the most fascinating organ of the human body. I've experienced my PhD as a incredibly rewarding and fun ride, but with a lot of obstacles which I needed to overcome. Over the past 4.5 years, I've worked together with great scientists and I have shared my research, and passion with amazing people. In this last chapter of my thesis, I would like to express my gratitude to all the people whom I shared this journey with and everybody who supported me through the most exciting times and through the more difficult times.

First of all, I would like to thank my promotor Marleen Verhoye for her guidance throughout my entire PhD and for the scientific freedom I had. My PhD was a wild ride, and you were always there, ready to take over the steering wheel if that was needed. Your door was always open to discuss finances (me begging for money for electrodes, antibodies etc.), science, issues I ran in to, or just for a chat. Thank you for all the positive feedback throughout the years that have helped me become a (better) scientist. I enjoyed supporting all the practical activities and I learned a lot from watching you prepare practical sessions, interacting with the students etc. Thank you for the opportunity to stay a bit longer in this cozy environment and continue exploring the topic that I love most.

I would also like to thank my former promotor Georgios Keliris. You were always there to motivate me to improve techniques and to implement complementary tools to better understand the brain. You have shown me that stubbornness and determination do pay off, as we succeeded in the implementation of mechanical ventilation and electrophysiology in the lab. You always had nice and interesting ideas to answer our research questions (or to answer 100 other research questions. Thank you also for supporting me through the more difficult times and for shaping me as a neuroscientist.

Annemie, you really are my example. Your never-ending passion for science and your friendly personality are the reason why BIL is where it is now. Thank you for all the scientific input on presentations and teaching me how to create and sell a story. I've learned a lot form our meetings and watching you connect all different outcomes together to solve the puzzle (or raise more interesting questions).

My gratitude also goes to the members of my doctoral committee, Prof. dr. Ir. Peter Delputte, dr. Ir. Arjan den Dekker, Prof. dr. Sebastiaan Engelborghs, Prof. dr. Tommas Ellender, dr. Valerio Zerbi and Prof. dr. Gilles Vandewalle. Thank you for taking the time to read my PhD thesis and providing insightful, valuable feedback.

Starting as a master student many years ago, I was part of the neuromodulation team and of office Uc1.17. I would lke to thank Lore for teaching me everything I know. I still remember the first surgery you taught me (and what you made me do…) and our endless scanning sessions where we tried to fit fat rats into a scanner. Thank you for the guidance during my master thesis and for the fun moments in the office, also during my PhD. Rukun, you were always there with stupid jokes and crazy remarks to light up the spirit in the office. I enjoyed our intubation-trials just after new-year (what a way to start a year). You've taught me the basic principles of coding and image processing and ofcourse I'm grateful for that. I hope we continue meeting together, housewarming in Vremde, BBQ next to the pool in Stabroek, more babyshowers?

Stephan, you were the person who truely understood the difficult situation we both were in, and you could always comfort me (sometimes just by being in the same situation). You've taught me so much regarding experimental designing, work ethic, statistics and what it means to be a scientist. I loved our time in Götingen during EMIM, where we spent more time in the swimming pool and out in the sun than at the conference itself. I enjoyed our talks while you were doing surgeries or scanning and I hope we can meet again soon for some cocktails.

A big thank you to team Holland (Johan, Nick and Joëlle). Johan, you really are the sunshine of the lab, even when you are grumpy. I loved the time when we were corona-buddies (or at least the only 2 people who were always in the lab during COVID). During COVID you have tried to teach me (or push me into) so many practical skills (how to refill scanners, how to check and change gasses, fixing temperature probes, soldering, MRI processing, electrical engineering stuff). I miss starting our mornings with a (too) long coffee break with fresh ginger tea with "lemoen", because we (thougth we) didn't have urgent work. That changed when we got back into our normal routine with everybody back at the lab. Johan, please continue bringing me coffee and ginger tea and enter my office for some nonsense talk (or just scream through the hallway). I can't wait to be back at the MRI scanner again and contact you during the weekend with some Terrorspec issues 😊. This one is for the CHDI part of team Holland – thank you Nick and Joëlle for all the time I've wasted talking to you about everything but work! Nick, I really hope you can finish your PhD soon and be relieved of this burden (you will be a free elf soon!). Joëlle, I never said this, but I am happy that you are now sitting in ~~my~~ our office. Your passion for science is radiating from behind your computer and I'm sure you will have an amazing PhD thesis in some years, but don't foget to put some boundries now and then.

I also want to thank some of the students that helped me with the acquisition and analysis of the data. Stijn, Daniëlle and Loran, thank you for your enthousiasm and hard work. Daniëlle, I've enjoyed working with you and I'm happy that I could show you all the ups-and-downs that come with being a PhD student. I hope you can start a PhD soon at the ministery of defence in Holland, because you deserve it. Loran, you are probably the smartest student I've met and I'm certain that you have a succesful scientific career lying ahead of you. Thank you for all the hours you've spent doing sleep scoring and for the (mental) support when we were doing the ELISA's.

I want to express my gratitude to my fellow Alzheimer team members Sam, Judith and Mohit. Judith, my fellow Faant. Where do I start. I've seen you grow as a scientist. I also

know that you will succesfully defend a PhD, since you are very determined and hard working and definitely not naïve or stupid. Don't forget to have fun girl! Mohit, thank you for teaching me some advanced Matlab skills and a new exciting statistical test (kolmogrothingy?!). I know my coding is still not the most advanced or efficiënt, but it is good enough to give me the output I want. I look forward to more Sunday-afternoon lunches with you, Tara and your wife in Breda. Sam, I envy your advanced computer skills and knowledge about every technology related topic. Thank you for creating the cover of this PhD thesis with me during the Christmas party, I had a lot of fun!

My gratitude also goes to all the other (former) collegues of BIL: Serena, Laia, Maarten, Julie, Aneta, , Gaurav, Garima, Jasmien, Elisabeth, Ignace, Lauren, Leonardo and Claudia. Thank you for the nice time I had at BIL. I could always start a conversation with any of you about science or everything but work.

I would also like to thank my collaborators from the Laboratory of Cell Biology and Histology and the Laboratory of Experimental Hematology., Thank you Isabel Pintelon, Winnok de Vos and Marlies Verschuuren, for performing the histological experiments and helping me with the analysis and interpretation of that. Peter Ponsaerts, thank you for your help during het optimization of the ELISA's and for allowing me to always use your facilities.

Next, I would like to thank my friends, who were determined to make me forget about work and enjoy life. Joyce, José, Marieke, Nadine, Wendy, Yentl, Els, Karen and Ruth, thank you all for listening to the endless stream of scientific concepts which were probably too difficult to understand, and listening to all the struggles I've went through. Marieke and José, we've been friends since forever and besides all the fun we have, we've also supported each other through the most difficult times. Thank you for all the happy moments, dinner parties, sleepover parties and cat-cuddle parties at hotel José (the best hotel in Breda 😊). Yentl, thank you for the thursday pizza nights, all the honest conversations and your never-ending efforts to make me feel better. To my volunteer

friends (you know who you are), thank you for all the sleepover weekends where we played board games, laughed and talked all day and night. These weekends were the perfect way to forget about all the work problems and gave me enough energy to survive the next workweek.

Tamara, I know you've been looking for your name in the collegues section and in the friends section. But you know me, I didn't know to which "group" you belong haha. So there you go, your own section, as you wanted 😉. We have had very different PhD trajectories, but the story is very similar, a lot of ups-and-downs, but also a lot of passion and fun. We've had many wine-nights (or sangria nights), hiking trips and diner dates to discuss all our troubles, the latest gossip and a bit of science. You are always there to remind me that I should step out of my comfort zone, to shape my future career. I admire you for taking giant leaps so easily and I'm grateful for the gentle push you give me. Even with personal issues, I can come to you for advise. You're never scared to tell me I'm wrong and you've changed the way I see things already many times (but Jesus Christ Kovski, BOLD has some neuronal underpinnings!). I wish you all the best in San Francisco and we will meet in Hawaï 😊!

I would like to thank my family-in law, Ada, Kirsten, Alrik, Karin, Wilfred, Mijke, Jelle, Arya and Ravi. You were always there to listen to my stories and were always willing to offer some distraction in the form of wine-nights by the fire with marshmallows, skip-bo competitions, karaoke-nights with bubbles and "game parties" without games but with very tasty home-cooked meals. I love hanging out with Arya and Ravi and we should definitely have more sleepover weekends! I'm really lucky that Rein has such a warm and fun family!

That brings me to the most important people, my family. Mama en papa, thank you for always supporting me with whatever decision I make. I'm very grateful for the financial support for my never-ending study adventures. Mama, you were always there to comfort me and to give me useful advice. Jes and Nick, thank you for distracting me from

work. I immensely enjoy our trips to the zoo, theme parc, disappointing kings day market or just sitting at home gaming for entire weekends (no-life weekends are the best). With you two by my side (surrounded by crazy) its always fun.

Luca, we haven't met that long ago, but you've definitely changed my life. You, kicking inside my tummy, were my main motivation to finish this thesis as soon as possible. I didn't want to worry about my PhD anymore, because I already knew I would rather spent time with you.

And last but not least, thank you Rein. I can't thank you enough for being my safe place, always. You are the only person who can calm my brain down, just by being there next to me, looking at me or holding me. You've sacrificed so much for me already; moving to Belgium, me working way too much and forgetting about you, endless monologs about science and troubles at BIL; and I don't often enough show appreciation for that. Thank you for your patience. I'm excited that I can spent the rest of my life together with you (and our kids).